DIETARY BIOACTIVE COMPONENTS IN INFLAMMATORY BOWEL DISEASE

EDITED BY: Fang Li, Xian Wu, Ce Qi and Yanhui Han

PUBLISHED IN: Frontiers in Nutrition and Frontiers in Immunology

frontiers Research Topics

ISSN 1664-8714
ISBN 978-2-83250-759-9
DOI 10.3389/978-2-83250-759-9

About Frontiers

Frontiers is more than just an open-access publisher of scholarly articles: it is a pioneering approach to the world of academia, radically improving the way scholarly research is managed. The grand vision of Frontiers is a world where all people have an equal opportunity to seek, share and generate knowledge. Frontiers provides immediate and permanent online open access to all its publications, but this alone is not enough to realize our grand goals.

Frontiers Journal Series

The Frontiers Journal Series is a multi-tier and interdisciplinary set of open-access, online journals, promising a paradigm shift from the current review, selection and dissemination processes in academic publishing. All Frontiers journals are driven by researchers for researchers; therefore, they constitute a service to the scholarly community. At the same time, the Frontiers Journal Series operates on a revolutionary invention, the tiered publishing system, initially addressing specific communities of scholars, and gradually climbing up to broader public understanding, thus serving the interests of the lay society, too.

Dedication to Quality

Each Frontiers article is a landmark of the highest quality, thanks to genuinely collaborative interactions between authors and review editors, who include some of the world's best academicians. Research must be certified by peers before entering a stream of knowledge that may eventually reach the public - and shape society; therefore, Frontiers only applies the most rigorous and unbiased reviews.
Frontiers revolutionizes research publishing by freely delivering the most outstanding research, evaluated with no bias from both the academic and social point of view. By applying the most advanced information technologies, Frontiers is catapulting scholarly publishing into a new generation.

What are Frontiers Research Topics?

Frontiers Research Topics are very popular trademarks of the Frontiers Journals Series: they are collections of at least ten articles, all centered on a particular subject. With their unique mix of varied contributions from Original Research to Review Articles, Frontiers Research Topics unify the most influential researchers, the latest key findings and historical advances in a hot research area! Find out more on how to host your own Frontiers Research Topic or contribute to one as an author by contacting the Frontiers Editorial Office: frontiersin.org/about/contact

DIETARY BIOACTIVE COMPONENTS IN INFLAMMATORY BOWEL DISEASE

Topic Editors:
Fang Li, Columbia University Irving Medical Center, United States
Xian Wu, Miami University, United States
Ce Qi, Qingdao University, China
Yanhui Han, University of Massachusetts Amherst, United States

Citation: Li, F., Wu, X., Qi, C., Han, Y., eds. (2022). Dietary Bioactive Components in Inflammatory Bowel Disease. Lausanne: Frontiers Media SA.
doi: 10.3389/978-2-83250-759-9

Table of Contents

frontiers in Nutrition

ORIGINAL RESEARCH
published: 12 October 2021
doi: 10.3389/fnut.2021.748503

Cinnamaldehyde Promotes the Intestinal Barrier Functions and Reshapes Gut Microbiome in Early Weaned Rats

Lili Qi[1], *Haiguang Mao*[1], *Xiaohui Lu*[2], *Tingting Shi*[1] *and Jinbo Wang*[1]*

[1] School of Biological and Chemical Engineering, NingboTech University, Ningbo, China, [2] Ningbo Biomart Lifetech Co. Ltd, Ningbo, China

Cinnamaldehyde is an aromatic aldehyde isolated from the essential oil of cinnamon. It has been proved to possess various bioactivities such as anti-inflammation, anti-bacteria and antihypertensive. Nevertheless, early weaning could lead to intestinal stress, causing a range of intestinal health problems. The aim of this study is to explore the effects of cinnamaldehyde on gut barrier integrity, inflammatory responses, and intestinal microbiome of early weaned rats. In this study, treatment with cinnamaldehyde (100 or 200 mg/kg bodyweight/day) for 2 weeks significantly promoted the production of mucins in the colonic epithelial tissue of rats. Cinnamaldehyde supplementation significantly upregulated the expression of Muc2, TFF3 and the tight junction proteins (ZO-1, claudin-1, and occludin). Hematoxylin and eosin staining results showed that colonic histopathological changes were recovered by cinnamaldehyde supplementation. The mRNA expression of IL-6 and TNF-α were significantly decreased in the cinnamaldehyde groups while the TNF-α protein levels were significantly decreased in the two cinnamaldehyde groups. Cinnamaldehyde treatment obviously attenuated the activation of NF-κB signaling pathway in rat colonic tissue and suppressed the production of inflammatory cytokines. Furthermore, cinnamaldehyde supplementation remodeled the gut microbiome structure, at the genus level, *Akkermansia, Bacteroides, Clostridium III, Psychrobacter, Intestinimonas* were increased, whereas those of *Ruminococcus*, *Escherichia/Shigella* were obviously decreased in the cinnamaldehyde treated groups. These findings indicated that cinnamaldehyde could effectively enhance intestinal barrier integrity, ameliorate inflammatory responses and remodel gut microbiome in early weaned rats.

Keywords: cinnamaldehyde, gut barrier, inflammatory responses, gut microbiota, early weaned rats

OPEN ACCESS

Edited by:
Fang Li,
Columbia University Irving Medical Center, United States

Reviewed by:
Jianan Zhang,
University of Massachusetts Amherst, United States
Daoyuan Ren,
Shaanxi Normal University, China

***Correspondence:**
Jinbo Wang
wjb@nbt.edu.cn

Specialty section:
This article was submitted to Nutritional Immunology, a section of the journal Frontiers in Nutrition

Received: *28 July 2021*
Accepted: *16 September 2021*
Published: *12 October 2021*

Citation:
Qi L, Mao H, Lu X, Shi T and Wang J (2021) Cinnamaldehyde Promotes the Intestinal Barrier Functions and Reshapes Gut Microbiome in Early Weaned Rats. Front. Nutr. 8:748503. doi: 10.3389/fnut.2021.748503

INTRODUCTION

Cinnamaldehyde is the major bioactive component isolated from cinnamon essential oils. Previous studies have shown that cinnamaldehyde exhibits a wide range of biological activities including anti-inflammatory, anti-bacterial, and immune-modulating properties (1–3). As the major component of cinnamon, cinnamaldehyde has been traditionally used as a food additive, and registered as a flavoring agent by the Food and Drug Administration and approved for food use (4).

Gut is an important barrier which protects against the entry of pathogenic bacteria and harmful macromolecules into the body. The immature barrier function plays key roles in the pathogenesis of intestinal inflammatory diseases of newborns and children, such as inflammatory bowel disease (IBD), infectious enteritis, or necrotizing enterocolitis (5). Previous study has suggested that the infant maturation of the intestinal epithelium has lifelong impacts on gut functions and immune homeostasis (6). The suckling-to-weaning dietary transition influences the maturation of gut barrier in mammals. The transition from maternal milk to solid food also results in the remodeling of gut microbiota composition. The intestinal bacterial metabolites were found to be the key intermediates which induced the maturation of gut and formation of intestinal barrier (7).

Many natural bioactive compounds have been found to promote intestinal maturation and modulate the gut microbiota composition (8, 9). Previous investigations suggested that cinnamaldehyde inhibited PLCγ-1 activation in mucosal mast cells, attenuated the inflammatory responses and ameliorated ulcerative colitis in the rat models (10, 11). To our knowledge, the effects of cinnamaldehyde on the gut integrity and mucosal immune functions in juvenile animals have not been explored. Weaning, especially early weaning, is a stressful condition for mammals and negatively affects growth performance by affecting the development of mucosal barrier function in the intestine (12). Early weaning (15- to 21-day weaning age) resulted in sustained impairment in intestinal barrier function, and commonly results in gastrointestinal disorders, inflammation and diarrhea in infants and young animals (13). Therefore, in the current study, we used early weaned rats as the animal model to investigate the effects of cinnamaldehyde on the intestinal barrier, mucosal immune functions and gut microbiota profile in the early weaned rats.

MATERIALS AND METHODS

Materials and Reagents

Cinnamaldehyde was purchased from Sigma-Aldrich (St.Louis, MO, USA). The total RNA Kit and Stool DNA Kit were purchased from OMEGA Bio-Tek (Norcross, GA, USA). One-step qRT-PCR kits were purchased from TOYOBO (Osaka, Japan). Anti-NF-κB p65, anti-phospho-NF-κB p65, anti-TNF, anti-IL-6 and HRP-linked goat anti-rabbit antibody were obtained from Cell Signaling Technology (Beverly, MA, USA). ECL Western Blotting Substrate was supplied by Thermo Fisher (Shanghai, China). RIPA lysis buffer and BCA protein assay kits were obtained from Beyotime (Shanghai, China). Nitrocellulose membranes were purchased from Sigma-Aldrich (St.Louis, MO, USA). AB/PAS staining kits were purchased from Solarbio Life Science (Beijing, China). Enzyme-linked immunosorbent assay (ELISA) kits for estimating TNF-α, and IL-6 levels were obtained from Multisciences Biotech (Hangzhou, China).

Animal Experiment Design

Twenty four early weaned male SPF SD rats (17 days) were purchased from the Laboratory Animal Center of Zhejiang Province (Hangzhou, China). The rats had free access to water and were fed in a temperature-controlled room (23–25°C) under a 12-h dark-light cycle. The experimental procedure was approved by the ethical committee in Zhejiang University, and was decided following the rule of the NIH Guide for the Care and Use of Laboratory Animals (NIH Publication No. 85-23, 1985, revised 1996). The immature rats were removed from their dams at 17 days of age (weaned), following 3 days of adaptive feeding with the diet of rat formula feeds mixed with corn, soybean meal, fish meal, flour, yeast powder, vegetable oil, salt, a variety of vitamins, and mineral elements. The diet contains 18% protein, 4% fat, 5% crude fiber, 1.8% Ca, and 1.2% phosphorus with the energy content of 3.4 kcal/g. The rats were weighed after 3 days (21 days of age) of adaptive feeding, then they were randomly divided into 3 groups with 8 rats per group: control, CIN100 and CIN200. In addition, each mouse was raised separately. The control group was feed with the above formula feeds, and the CIN100 and CIN200 groups were fed with the above formula feeds mixed with the fresh liquid cinnamaldehyde of 100 or 200 mg/kg body weight/d, respectively (the liquid cinnamaldehyde was added directly into formula feeds). The reason why cinnamaldehyde was administered as the amounts of 100–200 mg/kg was the result of the previous pre-test and reference of the previous research reports (14). After 7 days of feeding experiment (28 days of age), euthanasia was carried out by intraperitoneal injection of pentobarbital sodium of 150 mg/kg body weight until the animal stopped breathing, then the abdomen was incised to obtain the colon tissue samples.

Alcian Blue-Periodic Acid Schiff (AB/PAS) Staining

Alcian blue-periodic acid schiff (AB/PAS) staining was conducted to observe the variation of goblet cells. Five millimeter of colonic tissue was immediately fixed in Carnoy's fluid at 4°C for 2 h. Fixed colon tissues were embedded in paraffin and cut into 5 μm sections and subjected to AB/PAS staining. The variation of goblet cells and integrity of mucus were analyzed using a microscope (Nikon E100, Tokyo, Japan). ImageJ software was used for data acquisition and image analysis.

TABLE 1 | Primers used for qRT-PCR.

	Forward primer (5′-3′)	Reverse primer (5′-3′)
MUC2	GCTGACGAGTGGTTGGTGAATG	GATGAGGTGGCAGACAGGAGAC
TFF3	CCGTGGTTGCTGTTTTGAC	GCCTGGACAGCTTCAAAATG
ZO-1	ACCCGAAACTGATGCTGTGGATAG	AAATGGCCGGGCAGAACTTGTGTA
claudin-1	AGCTGCCTGTTCCATGTACT	CTCCCATTTGTCTGCTGCTC
occludin	ACGGACCCTGACCACTATGA	TCAGCAGCAGCCATGTACTC
TNF-α	CCCTCACACTCAGATCATCTTCT	CTACGACGTGGGCTACAG
IL-6	CTCTGGCGGAGCTATTGAGA	AAGTCTCCTGCGTGGAGAAA
GAPDH	GAAGGTGAAGGTCGGAGTCAAC	CATCGCCCCACTTGATTTTGGA

Hematoxylin and Eosin (H&E) Staining

The colonic tissues were fixed in 10% neutral buffered formalin and then transferred to 70% ethanol. Fixed tissues were embedded in paraffin and cut into 4 μm thick slices. Tissues were stained with hematoxylin and eosin (H&E). The histological changes were observed with optical microscopy (Nikon, Tokyo, Japan). Sections were evaluated based on the cell infiltration of inflammatory cells and epithelial damage as previously described.

RT-qPCR

Total RNA was extracted from colonic tissues using the total RNA Kit (OMEGA Bio-Tek). RNA concentrations were determined at 260 nm and purity was assessed by the A260/A280 nm ratio. RT-qPCR was performed using CFX Connect System (Bio-Rad, California, USA) with one-step RT-qPCR Kit (TOYOBO) according to the manufacturer's protocols. The sequences of the primers were listed in **Table 1**. Thermal cycling conditions were as follows: 2 min denaturation at 98°C, followed by 40 cycles at 98°C at 10 s, 10 s at 60°C, 30 s at 68°C. Data were collected and analyzed using the CFX Manager software (Bio-Rad, California, USA). Cycle thresholds were normalized to GAPDH levels and fold changes were calculated to the normalized control of each gene. The relative mRNA levels were examined using the ΔΔCt method. Each sample was treated in triplicate to ensure statistical analysis significance.

Western Blot Analysis

The fresh colon tissue was washed for three times with pre-cooling PBS of 4°C. Filter paper was used to absorb the rest liquid on the tissue surface and then cut the colon tissue into several smaller tissue pieces. Add the tissue pieces into RIPA (Radio Immunoprecipitation Assay) buffer (Beyotime, Shanghai, China) in a ratio of tissue weight (g): lysate (mL) = 1:10, and homogenized using a homogenizer until no obvious tissue mass could be observed, then incubated on ice for 30 min. Centrifuged 10,000 g at 4°C for 10 min, the supernatant was the extracted protein. Fifty microgram of protein samples were separated by either 3–8% Tris-acetate gradient gels for MUC2 detection or 12.5% Tris-glycine gels for detection of other proteins. Then the protein samples were transferred to nitrocellulose membranes (Sigma-Aldrich, St. Louis, MO, USA). The membranes were blocked with 5% skim milk in TBS-T for 2 h and then washed with TBS-T for three times at 4°C. The blocked membranes were incubated in primary antibody at 4°C overnight, followed by incubation with secondary antibody at room temperature for 1 h. ECL Substrate (Thermo Fisher, Shanghai, China) was used to image the protein bands with Chemi Doc XRS system (Bio-Rad, CA, USA). The optical density was analyzed by Quantity one 4.6.2 software. The antibodies used were shown as follows: anti-Claudin-1 (Invitrogen, Cat.37-4900), anti-Occludin (Invitrogen, Cat.33-1500), anti-ZO-1 (Invitrogen, Cat.61-7300), anti-P-NFκB (CST, Cat.3003), anti-NF-κB (CST, Cat.8242), anti-TNF alpha (Abcam, Cat.ab183218), anti-IL6 (Abcam, Cat.ab259341), and anti-β-actin (Abcam, Cat.ab8226).

Enzyme-Linked Immunosorbent Assay (ELISA)

To determine the protein levels of TNF-α and IL-6, the colon tissue was homogenized with cold 10 mM PBS (pH 7.4, containing 1 mM phenylmethylsulfonyl fluoride). After that, the mixture was centrifuged at 10,000×g for 5 min at 4°C. The supernatants were collected and detected by using TNF-α or IL-6 ELISA kits (Multisciences Biotech, Hangzhou, China) according to the manufacturer's instructions. The TNF-α and IL-6 levels were expressed as picograms per gram of tissue protein.

Analysis of Gut Microbiota

The structural changes of gut microbiome were conducted by 16S rRNA sequencing analysis. Total DNA was extracted with the E.Z.N.A. Stool DNA Kit (Omega, Norcross, GA, USA) according to instructions. The collection of feces was carried out in a sterile environment in a super clean table. Fixed the experiment rat and lifted its tail, gently pressed the abdomen with fingers to collect fresh feces and put them into a sterile EP tube, each tube contained 2–3 fecal particles. The bacterial hypervariable V3–V4 region of 16S rRNA was amplified by using

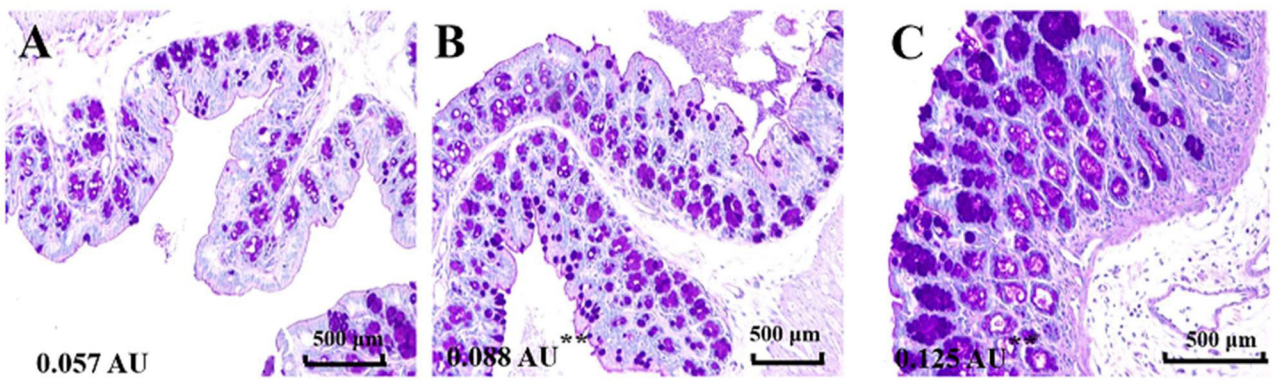

FIGURE 1 | Cinnamaldehyde treatment promoted the production of mucins. The variation of goblet cells in different treatment groups was analyzed by AB/PAS staining (200×, $n = 3$). **(A)** Control. **(B)** CIN100. **(C)** CIN200. The mean fluorescence intensity of each picture is 0.057, 0.088**, 0.125** arbitrary units (AU) using ImageJ software. One-way ANOVA was carried out for each comparison with HSD test.

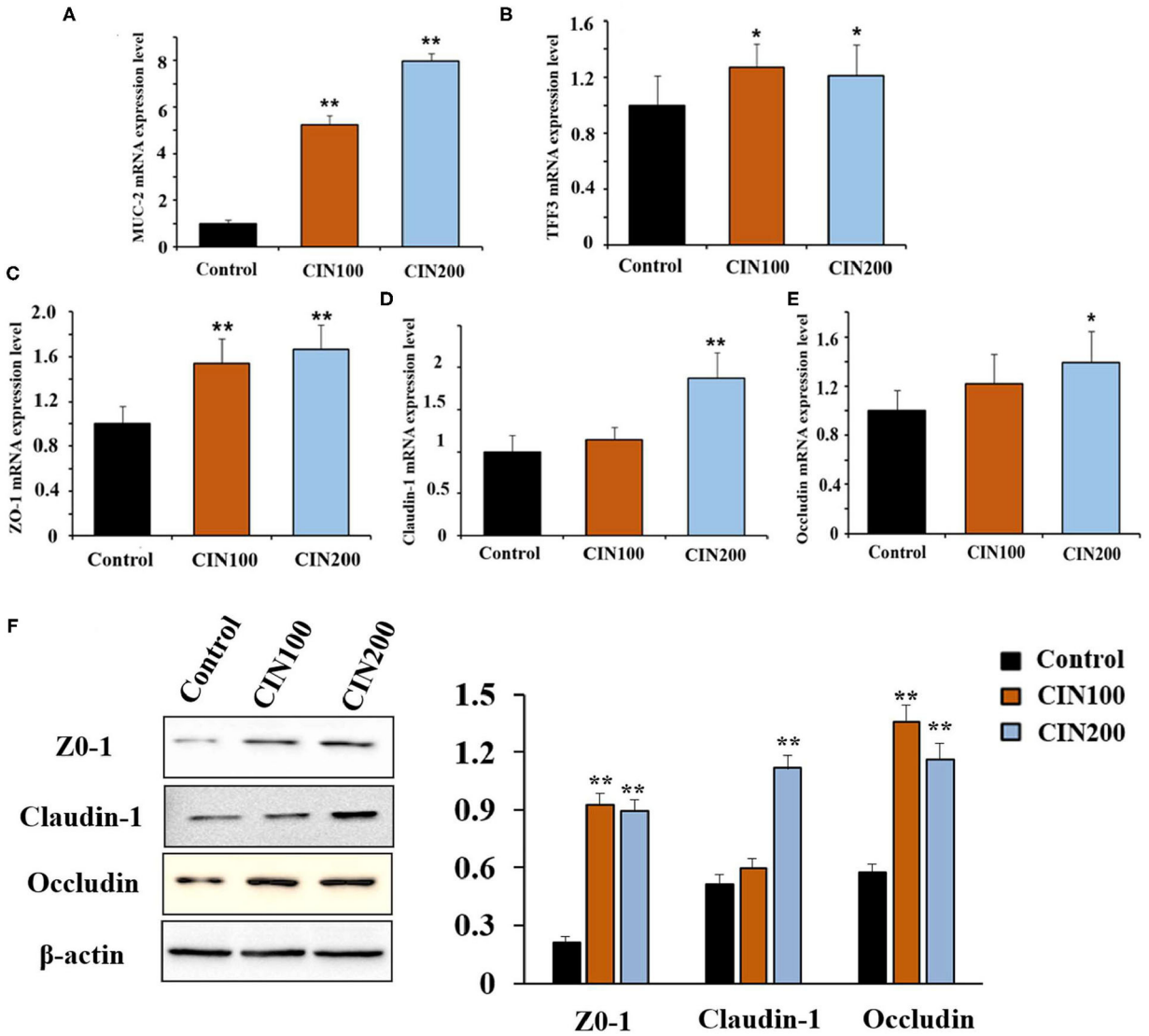

FIGURE 2 | Cinnamaldehyde supplementation promotes the mRNA levels of MUC2, TFF3, TJs, and protein levels of TJs (ZO-1, Claudin-1, and Occludin) in early weaned rats. **(A)** MUC2. **(B)** TFF3. **(C)** ZO-1. **(D)** Claudin-1. **(E)** Occludin. **(F)** Protein levels of TJs. mRNA levels were normalized by GAPDH and protein levels were normalized β-actin. Data are expressed as mean ± SD. $^{*}P < 0.05$, $^{**}P < 0.01$. One-way ANOVA was carried out for each comparison with HSD test.

primer: 341F: CCCTACACGACGCTCTTCCGATCTG and 805R: GACTGG+AGTTCCTTGGCACCCGAGAATTCCA. The validated library was used for sequencing on HiSeq 2500 (Illumina, CA, USA). The high quality paired-end reads were combined to tags based on overlaps by FLASH (Fast Length Adjustment of Short reads, v1.2.11), and then clustered into Operational Taxonomic Units (OTUs) at a similarity cutoff value of 97% using USEARCH (v7.0.1090), and chimeric sequences were compared with Gold database using UCHIME (v4.2.40) to detect. Alpha diversities (Shannon and Simpson) and richness (ACE and Chao1) were obtained using mother (version 1.30.1). Beta diversity was determined using OTUs from each sample. Gut microbiota compositions of the groups at different levels (phylum and genus) were analyzed using MUSCLE software (version 3.8.31). Mothur software and Metastats statistical algorithms were used to compare the relative bacterial abundances at the phylum and genus levels, and significant differences in taxonomic compositions were analyzed via the Kruskal Wallis test. The data was uploaded to SAR with the accession NO. PRJNA761503.

Statistical Analysis

SPSS20.0 (SPSS, Chicago, IL) was used for statistical analysis, a one-way analysis of variance (ANOVA) was carried out for each comparison, followed by *post hoc* analysis to identify differences between specific factor levels using the Tukey's Honest Significant Difference (HSD) test. $P < 0.05$ were regarded as statistically significant.

RESULTS AND DISCUSSION

Cinnamaldehyde Promotes the Production of Colonic Mucin

Mucus is the first mechanical defense in the intestinal barrier, which protects against the invasion of intestinal bacteria and entry of harmful macromolecules (15). Damage of mucus integrity would result in leaky gut, promote the translocation of bacteria and induce intestinal inflammatory responses (16). To investigate the influence of cinnamaldehyde on the intestinal mucus, we visualized the colonic epithelial layer by staining with AB/PAS after 7 days of treatment with

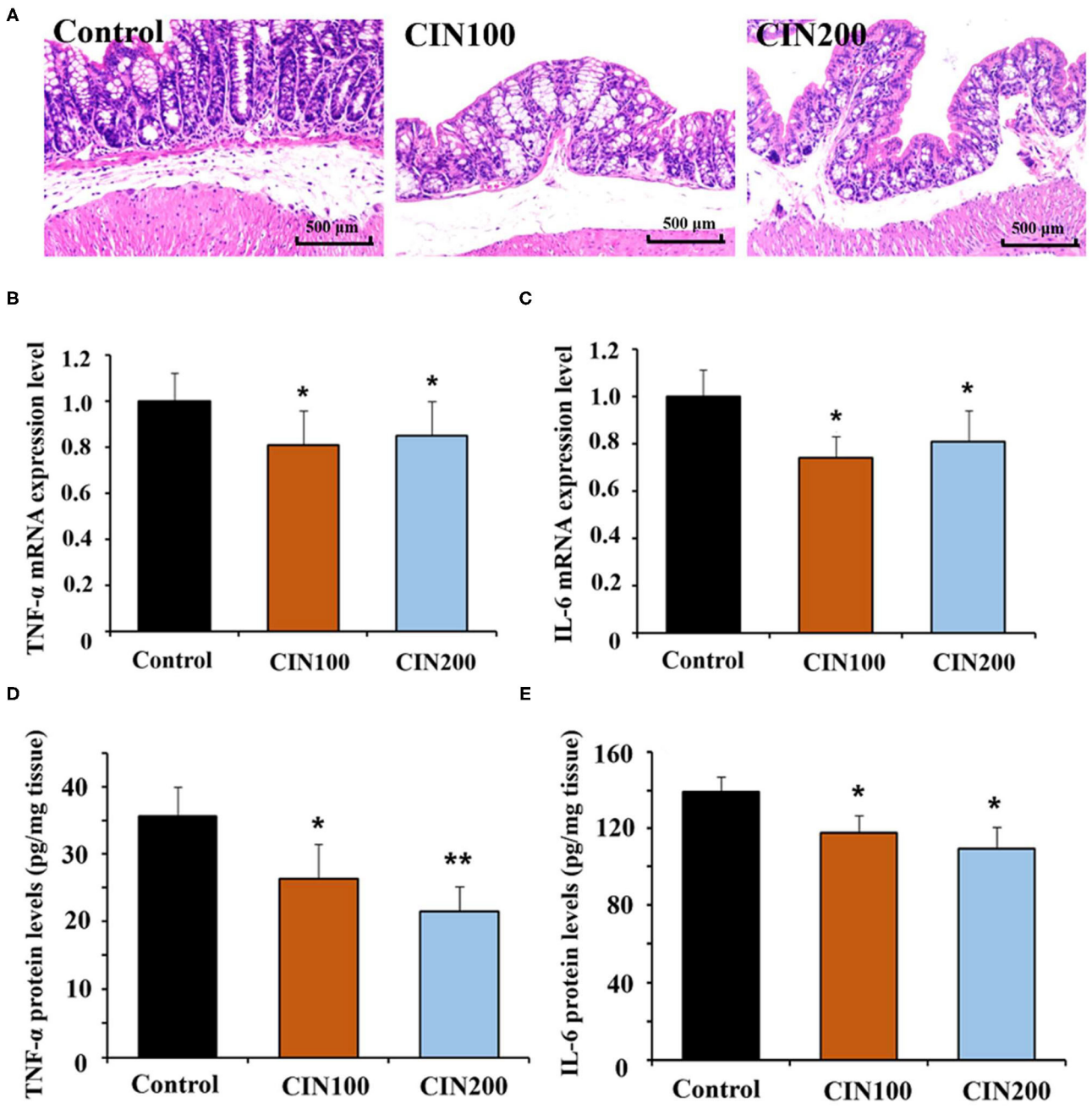

FIGURE 3 | Cinnamaldehyde supplementation attenuates the inflammatory responses in early weaned rat colon. **(A)** H&E stained distal colon sections from untreated and cinnamaldehyde treated rats at day 7 (Original magnification 100×). Inflammation is evident in control group rats. Quantitative RT-PCR was performed to detect the mRNA expression of TNF-α **(B)** and IL-6 **(C)**, normalized by GAPDH. ELISA was conducted to measure the production of TNF-α **(D)** and IL-6 **(E)** in rat colonic tissues. Data are represented as mean ± SD. $^{*}P < 0.05$, $^{**}P < 0.01$. One-way ANOVA was carried out for each comparison with HSD test.

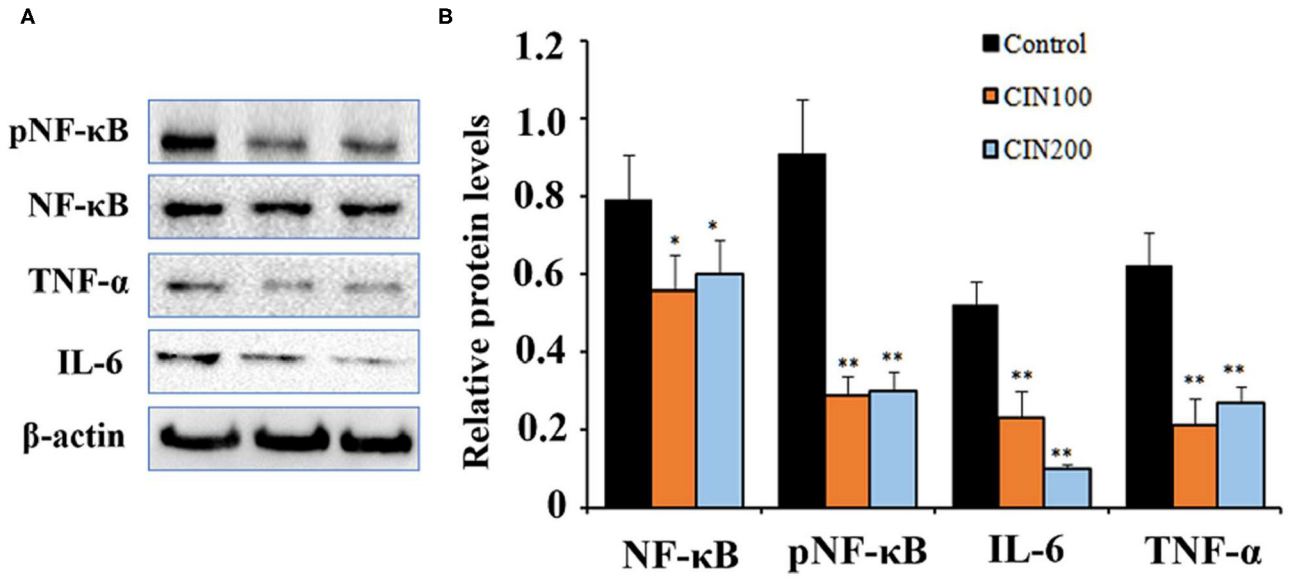

FIGURE 4 | Cinnamaldehyde supplementation inhibits the activation of NF-κB in early weaned rat colon tissues. **(A)** Western blot analysis for NF-κB, pNF-κB and the downstreaming inflammatory cytokines. **(B)** Quantitative analysis for the densitometry of the proteins performed using ImageJ software. Data are expressed as mean ± SD. $^{*}P < 0.05$, $^{**}P < 0.01$. One-way ANOVA was carried out for each comparison with HSD test.

cinnamaldehyde (**Figure 1**). The results showed that treatment with cinnamaldehyde significantly ($P < 0.01$) increased the amount of secretary granules in the colonic epithelial tissues compared to the control (**Figure 1**). This study suggested that cinnamaldehyde might enhance the host defense via promoting the production of mucins.

Cinnamaldehyde Supplementation Improved the Gut Barrier Integrity in Newly Weaned Rats

Increased permeability is thought to be associated with intestinal pathogenesis (17, 18). The intestinal mucus in juvenile animals is immature, which is easy to be infected by intestinal bacteria. In the colon, MUC2 is a predominant secretory mucin expressed in goblet cells (19). Trefoil factor 3 (TFF3) is an important mucosal protective factor which usually enhances the protective properties of the mucus layer in a cooperative manner with MUC2 (20). It has been reported that the expression of MUC2 and TFF3 could be stimulated by phytonutrient such as eugenol, carvacrol, and cinnamaldehyde (21). Here we found that cinnamaldehyde treatment markedly enhanced the mRNA expression of MUC2 and TFF3 in the colon compared with control group (**Figures 2A,B**).

Tight junctions (TJs) also play important roles in the maintenance of intestinal permeability, which is considered to determine selective para-cellular absorption (18). Previous studies have shown that the zonula occludins (ZO), claudin family proteins, and occludin are essential components of TJs in the epithelial barrier (22). The major functions of TJs are to maintain the integrity of the intestinal epithelial barrier. RT-qPCR results showed that treatment with cinnamaldehyde significantly up-regulated the mRNA expression of TJs such as ZO-1 (**Figure 2C**), claudin-1 (**Figure 2D**), and occluding (**Figure 2E**). In the CIN100 group, the mRNA levels of ZO-1, claudin-1, and occludin were elevated by 54, 14, and 22%, respectively, compared with the control group. In the CIN200 group, the mRNA levels of ZO-1, claudin-1, and occludin were elevated by 67, 87, and 39%, respectively. Moreover, WB results also showed that treatment with cinnamaldehyde significantly up-regulated the protein expression levels of TJs such as ZO-1, claudin-1, and occluding (**Figure 2F**). Consistent with these results, a few other phytochemicals, such as flavonoids and polyphenols, have also been indicated to enhance TJ functions and gut integrities (22–24).

Cinnamaldehyde Attenuates the Inflammatory Responses in the Colon Tissues

It has been reported that cinnamaldehyde could play anti-inflammatory activities in infection, injury and autoimmune disease (14, 25). Histological analysis showed clear inflammation in the colon of newly weaned rats, while treatment with cinnamaldehyde markedly ameliorated the histological changes (**Figure 3A**). These results suggested that cinnamaldehyde treatment could attenuate the colonic inflammatory responses of early weaned rats. As cytokines play key roles in the inflammatory responses, the expression and production of cytokines (TNF-α and IL-6) have been determined. The results showed the mRNA expression of IL-6 and TNF-α were significantly decreased in the cinnamaldehyde groups (**Figures 3B,C**). Compared with the control group, TNF-α protein levels were significantly decreased in the two cinnamaldehyde groups. In the control

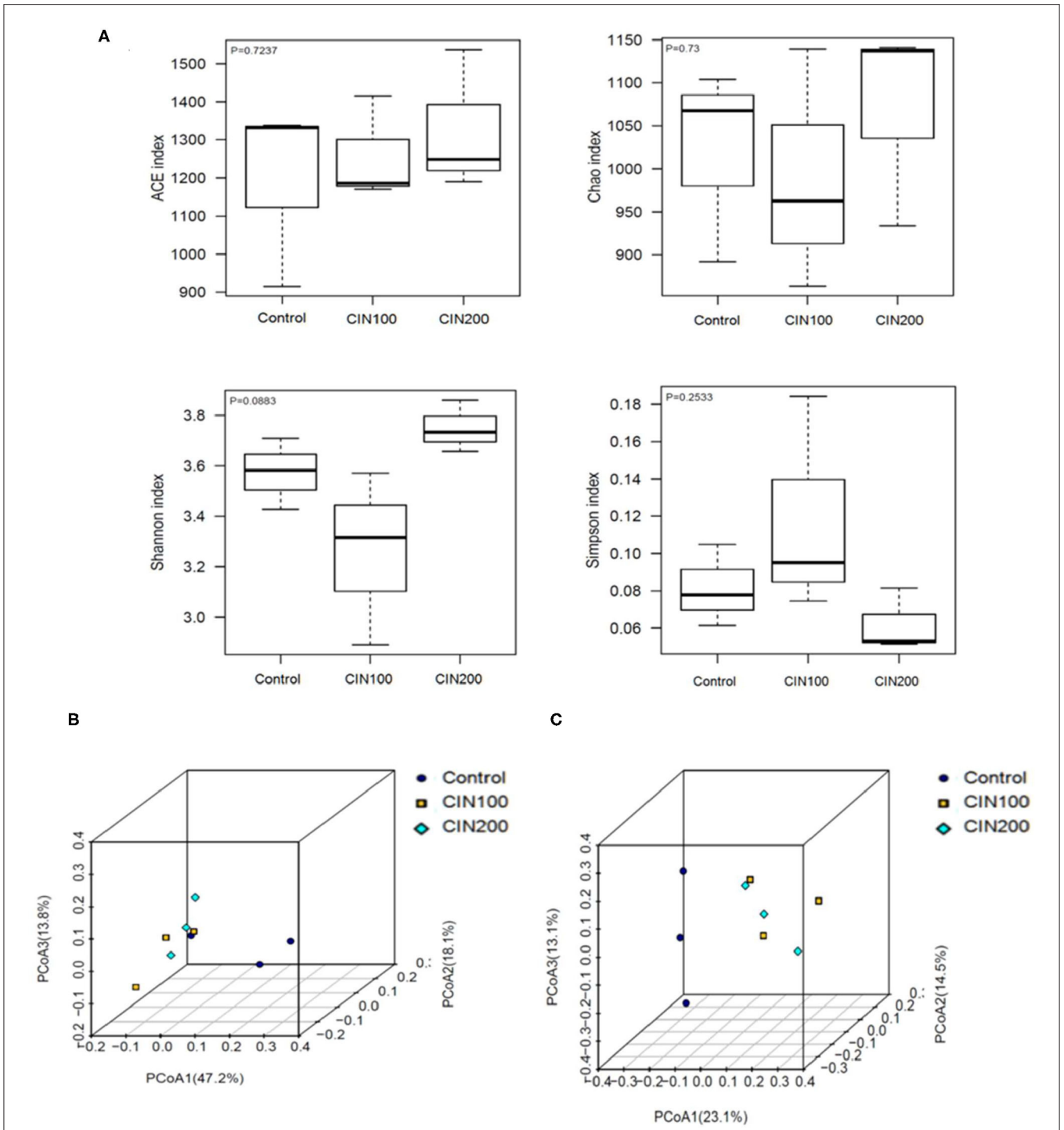

FIGURE 5 | The effects of Cinnamaldehyde supplementation on the α- and β-diversity of gut microbiota communities. **(A)** Alpha diversity metrics for the gut microbiota treated with cinnamaldehyde. **(B)** Beta diversity presented as weighted UniFrac distances. **(C)** Beta diversity presented as unweighted UniFrac distances. One-way ANOVA was carried out for each comparison with HSD test.

group, the concentration of IL-6 was 139.4 ± 7.7 pg/g tissue, while the levels of IL-6 in CIN100 and CIN200 were 117.7 ± 9.3 pg/g tissue and 109.4 ± 11.2 pg/g tissue, respectively (**Figures 3D,E**). Our results demonstrate cinnamaldehyde could attenuate the intestinal inflammatory responses in newly weaned rats. These results are in line with the previous

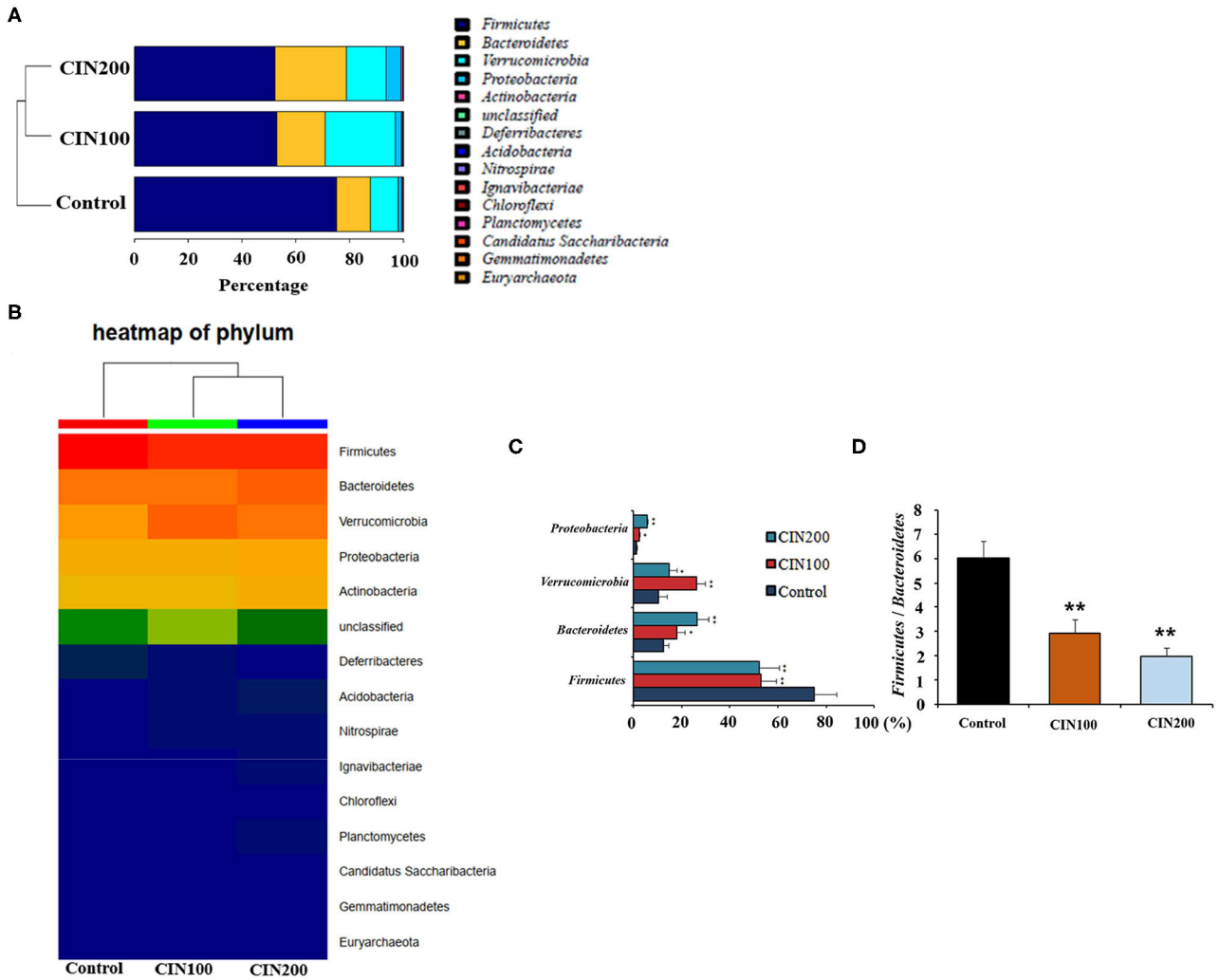

FIGURE 6 | Cinnamaldehyde supplementation remodels the structure of gut microbiota in early weaned rats. **(A)** Composition of gut microbiota at the phylum level analysis. **(B)** Heat map of phylum. **(C)** Relative abundance of the top four phyla. **(D)** Ratio of *Firmicutes* to *Bacteroidetes*. Data are presented as mean ± SEM. $^{*}P < 0.05$ and $^{**}P < 0.01$. One-way ANOVA was carried out for each comparison with HSD test.

study which reported that cinnamaldehyde suppressed the production of TNF-α and IL-6 in ulcerative colitis model mice (11).

Cinnamaldehyde Inhibited the Activation of NF-κB Signaling Pathway in the Colon Tissues

NF-κB signaling pathway play important roles in the inflammatory responses (26). NF-κB exists as an inactive form in the cytoplasm, which is a p50/p65 heterodimer and associated with the inhibitor of nuclear factor-kappa B (IκB). After being stimulated by external stimuli, the p65 is phosphorylated by the protein kinases and then the phosphorylated NF-κB translocates to the nucleus and promotes the expression of downstream inflammatory factors (27). When the signaling pathway is activated, the ratio of pNF-κB/NF-κB is markedly elevated (28). To explore the effects of cinnamaldehyde on NF-κB signaling pathway in colonic tissues of newly weaned rats, western blot analysis was performed to determine the levels of the key proteins. The results showed that when the rats were administrated with 100 or 200 mg cinnamaldehyde/kg body weight, the level of colonic pNF-κB was reduced 54 and 51% (**Figure 4A**), respectively. Compared to the control group, the ratios of pNF-κB/NF-κB were also markedly decreased. The expression levels of TNF-α showed 91% reduction in both cinnamaldehyde groups, while the levels of IL-6 were reduced 44 and 88% (**Figure 4B**), respectively. These results suggested that cinnamaldehyde treatment could attenuate the inflammatory responses through inhibiting the activation of NF-κB signaling pathway. Our results were supported by a previous report that cinnamaldehyde could inhibit the NF-κB activation and attenuate inflammatory responses (16).

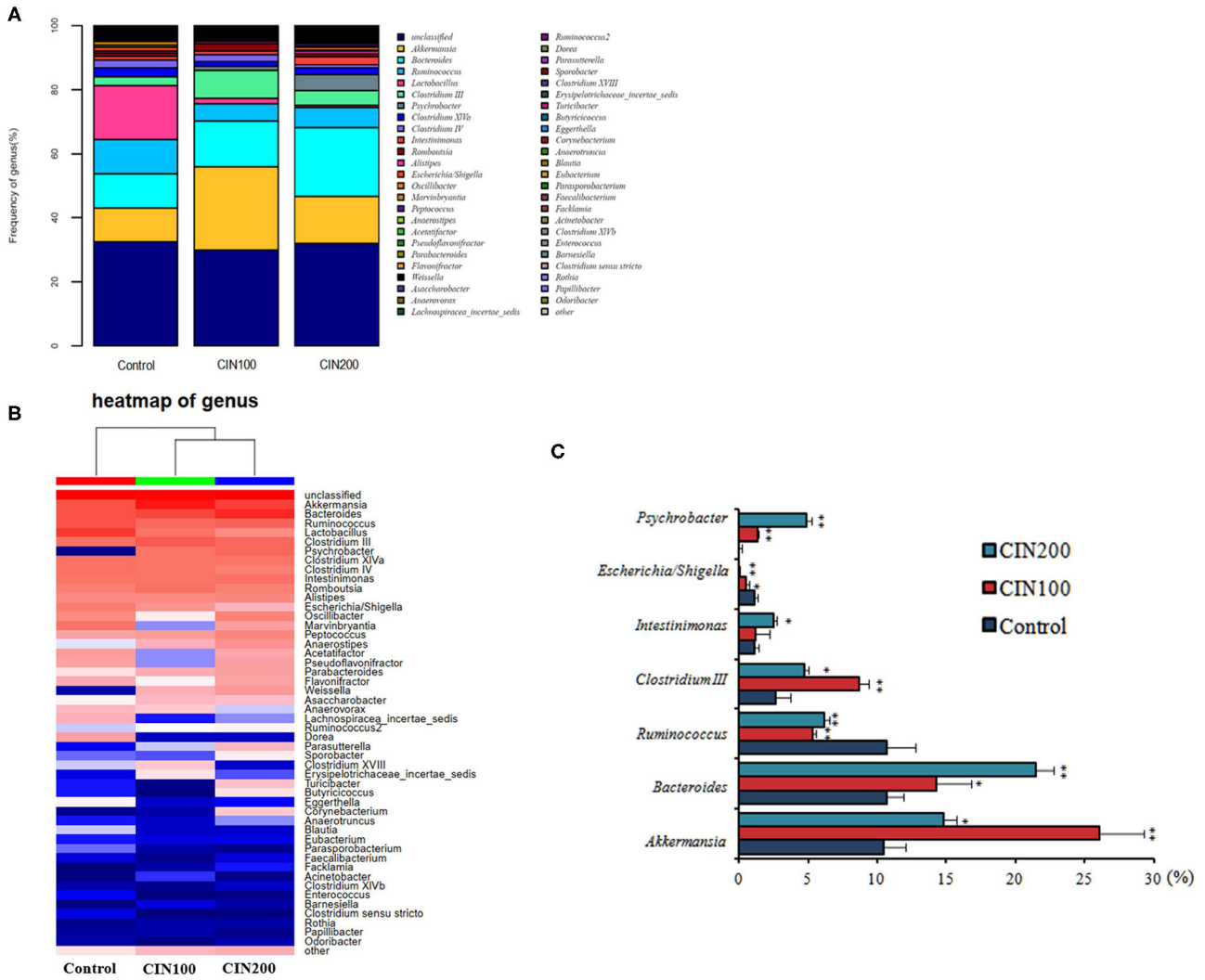

FIGURE 7 | Effects of cinnamaldehyde supplementation on the abundance of intestinal bacteria at genus level. **(A)** The relative abundance of the intestinal bacteria at the genus level. **(B)** Heatmap of genus. **(C)** The relative abundances of the top seven most abundant microbial genera across all samples. $^{*}P < 0.05$ and $^{**}P < 0.01$. One-way ANOVA was carried out for each comparison with HSD test.

Cinnamaldehyde Altered Microbial Composition in Colon of Early Weaned Rats

The impact of cinnamaldehyde on alpha diversity of the gut microbiota community was determined based on ACE Diversity Index, Chao Diversity Index and Shannon's Diversity Index (**Figure 5A**). These measures of diversity were calculated following the creation of a rooted phylogenetic tree using OTUs generated from 16s rRNA sequencing. Species Richness is a measure of the number of different species in each sample. As shown in **Figure 5A**, there was no significant difference between the control and cinnamaldehyde treated groups, a measure of the diversities of the species in each sample exhibited no significant differences between any of the experimental groups. These results showed that cinnamaldehyde couldn't cause a consistent disruption in the alpha diversity of the human gut microbial community. The impact of cinnamaldehyde on the beta diversity of the human gut microbial community was determined using weighted and unweighted UniFrac distance PCoA analysis. The principal coordinates analysis (PCoA) based on the Weighted and Unweighted UniFrac algorithm clearly revealed gut microbial community altered between cinnamaldehyde groups and control group (**Figures 5B,C**). There was no significant difference between the two cinnamaldehyde groups. This suggested the majority members of the microbial community didn't differ dramatically in cinnamaldehyde groups, whereas the composition of the microbial community was distinct from control group.

At the phylum level, *Firmicutes* and *Bacteroidetes* were the most abundant phyla in all groups (**Figures 6A,B**). The

relative abundance of *Firmicutes* in cinnamaldehyde groups was significantly reduced ($P < 0.01$), whereas those of *Bacteroidete, Verrucomicrobia, Proteobacteria* were increased in comparison with the control group ($P < 0.01$).

The *Firmicutes* to *Bacteroidetes* ratio (F/B ratio) has been suggested being highly correlated with many gut diseases. The increase of F/B ratio is an indicator of microbial imbalance, which is associated with intestinal diseases (29, 30). The declined F/B ratiois important for the intervention of intestinal inflammation. The ratio of F/B was 6.0 in the control group, whereas the ratios were 2.9 and 2.0 in the cinnamaldehyde groups (**Figures 6C,D**), respectively. These results suggested that cinnamaldehyde could attenuate the intestinal inflammatory responses via modulating the composition of gut microbiota.

Intestinal microbiota community structure was analyzed by high-throughput sequencing of 16S rRNA. At the genus level, *Akkermansia, Bacteroides, Clostridium III, Psychrobacter, Intestinimonas* were increased, whereas those of *Ruminococcus*, *Escherichia/Shigella*were obviously decreased in the cinnamaldehyde treated groups (**Figures 7A,B**). As shown in **Figure 7C**, the abundance of *Akkermansia muciniphila* increased from 10.48 ± 1.77% in the control group to 26.08 ± 3.15% and 14.79 ± 2.01% in the cinnamaldehyde groups, respectively. Compared with the control group, the abundance of *Ruminococcus* was significantly decreased in CIN100 and CIN200 group. The abundance of *Escherichia/Shigella* was decreased from 1.12 ± 0.09 to 0.55 ± 0.04% and 0.09 ± 0.01%, respectively, in CIN100 and CIN200 groups. It has been reported the *A. muciniphila* is a mucin-degrading bacterium that resides in the mucus layer (31). It has been previously described that *A. muciniphila* population is reduced or depleted in inflammation (32), inflammatory bowel disease and type 2 diabetes (33, 34). The mucolytic properties seem to promote mucus renewal via a positive feedback loop which exists in a symbiotic relationship with the host (35). It has been found that *R.gnavus*can degrade colonic MUC2 (36). High abundance of *R. gnavus* is prevalent in patients with intestinal Crohn's disease and inflammatory bowel disease (37, 38). *Shigella flexneri* could colonize and invade the intestinal epithelium, resulting in severe inflammatory colitis (39). Enterotoxigenic *Escherichia coli* (ETEC) and *Shigella* are most frequently isolated pathogenic bacteria in young children with diarrhea (40). Shigella infection could induce the expression and excretion of cytokines in colonic epithelia. In this study, the expansion of intestinal beneficial bacteria and the reduction of conditional pathogenic bacteria in the cinnamaldehyde groups may be the reasons that the intestinal inflammation was attenuated by cinnamaldehyde treatment.

CONCLUSION

Cinnamaldehyde, an important bioactive component extracted from cinnamonessential oils, has been found to exhibit many biological activities. To our knowledge, this is the first study to investigate the effects of cinnamaldehyde on the intestinal epithelial barrier and the gut micobiome of juvenile rats. Cinnamaldehyde treatment could promote the production of mucins in early weaned rats and upregulate the gene expression of the TJs such as ZO-1, claudin-1, and occludin. The activation of NF-κB signaling pathway was significantly suppressed and the inflammatory responses were attenuated in the colonic tissues of early weaned rats treated with cinnamaldehyde. Treatment with 100 or 200 mg/kg body weight/d of cinnamaldehyde significantly enhanced the phosphorylation of NF-κB, promoted the nuclear translocation of NF-κB, and suppressed the production of cytokines (TNF-α and IL-6). Cinnamaldehyde modulated the gut bacterial microbiota by increasing the abundance of *Bacteroidetes*, *Proteobacteria*, and *Verrucomicrobia* in the colon. In the cinnamaldehyde treated groups, the *Firmicutes* to *Bacteroidetes* ratio was significantly decreased. Moreover, cinnamaldehyde treatment obviously improved the diversity of colonic microbiota in the early weaned rats. These findings suggest that cinnamaldehyde should be considered as a potential drug to prevent or treat the intestinal inflammatory diseases of newborns and children. Clinical trials should be performed to confirm or refute these findings in humans.

DATA AVAILABILITY STATEMENT

The datasets presented in this study can be found in online repositories. The names of the repository/repositories and accession number(s) can be found below: NCBI BioProject, PRJNA761503.

ETHICS STATEMENT

The animal study was reviewed and approved by the Ethical Committee in Zhejiang University.

AUTHOR CONTRIBUTIONS

LQ: investigation, methodology, and writing-original draft. HM: methodology and resources. TS: methodology, investigation, and data curation. XL: formal analysis, data curation, visualization, and software. JW: conceptualization, writing-review and editing, and funding acquisition. All authors contributed to the article and approved the submitted version.

FUNDING

This work was funded by the National Natural Science Foundation of China (No. 31272461), the financial support from Ningbo Science and Technology Bureau Project (No.202003N4305, 2018B10095, and 2017C110017).

REFERENCES

1. Wang F, Pu CH, Zhou P, Wang PJ, Liang DP, Wang QL, et al. Cinnamaldehyde prevents endothelial dysfunction induced by high glucose by activating Nrf2. *Cell Physiol Biochem.* (2015) 36:315–24. doi: 10.1159/000374074
2. Chao LK, Hua KF, Hsu HY, Cheng SS, Lin IF, Chen CJ, et al. Cinnamaldehyde inhibits pro-inflammatory cytokines secretion from monocytes/macrophages through suppression of intracellular signalling. *Food Chem Toxicol.* (2007) 46:220–31. doi: 10.1016/j.fct.2007.07.016
3. Ka SM, Chao LK, Lin JC, Chen ST, Li WT, Lin CN, et al. A low toxicity synthetic cinnamaldehyde derivative ameliorates renal inflammation in mice by inhibiting NLRP3 inflammasome and its related signaling pathways. *Free Radical Bio Med.* (2016) 91:10–24. doi: 10.1016/j.freeradbiomed.2015.12.003
4. Silva AF, Dos Santos AR, Coelho Trevisan DA, Ribeiro AB, Zanetti Campanerut-Sá PA, Kukolj C, et al. Cinnamaldehyde induces changes in the protein profile of *Salmonella Typhimurium* biofilm. *Res Microbiol.* (2018) 169:33–43. doi: 10.1016/j.resmic.2017.09.007
5. Patel RM, Myers LS, Kurundkar AR, Maheshwari A, Nusrat A, Lin PW. Probiotic bacteria induce maturation of intestinal claudin 3 expression and barrier function. *Am J Pathol.* (2012) 180:626–35. doi: 10.1016/j.ajpath.2011.10.025
6. Jain N, Walker WA. Diet and host-microbial crosstalk in postnatal intestinal immune homeostasis. *Nat Rev Gastro Hepat.* (2015) 12:14–25. doi: 10.1038/nrgastro.2014.153
7. Beaumont M, Paës C, Mussard E, Knudsen C, Cauquil L, Aymard P, et al. Gut microbiota derived metabolites contribute to intestinal barrier maturation at the suckling-to-weaning transition. *Gut Microbes.* (2020) 11:1268–86. doi: 10.1080/19490976.2020.1747335
8. Li J, Zhang L, Li Y, Wu Y, Wu T, Feng H, et al. Puerarin improves intestinal barrier function through enhancing goblet cells and mucus barrier. *J Funct Foods.* (2020) 75:104246. doi: 10.1016/j.jff.2020.104246
9. Sandoval-Ramírez A, Catalán Ú, Pedret A, Valls RM, Motilva MJ, Rubió L, et al. Exploring the effects of phenolic compounds to reduce intestinal damage and improve the intestinal barrier integrity: a systematic review of *in vivo* animal studies. *Clin Nutr.* (2020) 40:1719–32. doi: 10.1016/j.clnu.2020.09.027
10. Kageyama-Yahara N, Wang XY, Katagiri T, Wang P, Yamamoto T, Tominaga M, et al. Suppression of phospholipase Cgamma1 phosphorylation by cinnamaldehyde inhibits antigen-induced extracellular calcium influx and degranulation in mucosal mast cells. *Biochem Biophys Res Commun.* (2011) 416:283–8. doi: 10.1016/j.bbrc.2011.11.014
11. Qu S, Shen Y, Wang M, Wang X, Yang Y. Suppression of miR-21 and miR-155 of macrophage by cinnamaldehyde ameliorates ulcerative colitis, *Int Immunopharmacol.* (2019) 67:22–34. doi: 10.1016/j.intimp.2018.11.045
12. Feli S, Jessica EC, Beth LO, Christena CT, Jennifer HH, Jean EFR, et al. Early weaning stress impairs development of mucosal barrier function in the porcine intestine. *Am J Physiol Gastrointest Liver Physiol.* (2010) 298:G352–63. doi: 10.1152/ajpgi.00081.2009
13. Meng Q, Sun S, Luo Z, Shi B, Shan A, Cheng B. Maternal dietary resveratrol alleviates weaning-associated diarrhea and intestinal inflammation in pig offspring by changing intestinal gene expression and microbiota. *Food Funct.* (2019) 10:5626–43. doi: 10.1039/C9FO00637K
14. Liu P, Wang J, Wen W, Pan T, Chen H, Fu Y, et al. Cinnamaldehyde suppresses NLRP3 derived IL-1β via activating succinate/HIF-1 in rheumatoid arthritis rats. *Int Immunopharmacol.* (2020) 84:106570. doi: 10.1016/j.intimp.2020.106570
15. Peterson LW, Artis D. Intestinal epithelial cells: regulators of barrier function and immune homeostasis. *Nat Rev Immunol.* (2014) 14:141–53. doi: 10.1038/nri3608
16. Camilleri M. Leaky gut: mechanisms, measurement and clinical implications in humans. *Gut.* (2019) 68:1516–26. doi: 10.1136/gutjnl-2019-318427
17. Tulyeu J, Kumagai H, Jimbo E, Watanabe S, Yokoyama K, Cui L, et al. Probiotics prevents sensitization to oral antigen and subsequent increases in intestinal tight junction permeability in juvenile–young adult rats. *Microorganisms.* (2019) 7:463. doi: 10.3390/microorganisms7100463
18. Arrieta MC, Bistritz L, Meddings JB. Alterations in intestinal permeability. *Gut.* (2006) 55:1512–20. doi: 10.1136/gut.2005.085373
19. Paturi G, Butts CA, Stoklosinski H, Ansell J. Effects of early dietary intervention with a fermentable fibre on colonic microbiota activity and mucin gene expression in newly weaned rats. *J Funct Foods.* (2012) 4:520–30. doi: 10.1016/j.jff.2012.02.013
20. Wang Y, Liang K, Kong W. Intestinal Trefoil Factor 3 alleviates the intestinal barrier function through reducing the expression of TLR4 in rats with nonalcoholic steatohepatitis. *Arch Med Res.* (2019) 50:2–9. doi: 10.1016/j.arcmed.2019.03.004
21. Wlodarska M, Willing BP, Bravo DM, Finlay BB. Phytonutrient diet supplementation promotes beneficial Clostridia species and intestinal mucus secretion resulting in protection against enteric infection. *Sci Rep.* (2015) 5:9253. doi: 10.1038/srep09253
22. Zhao, Xia B, Li X, Zhang L, Liu X, Shi R, et al. Sesamol supplementation attenuates DSS-induced colitis via mediating gut barrier integrity, inflammatory responses, and reshaping gut microbiome. *J Agric Food Chem.* (2020) 68:10697–708. doi: 10.1021/acs.jafc.0c04370
23. Park HY, Kunitake Y, Hirasaki N, Tanaka M, Matsui T. The aflavins enhance intestinal barrier of Caco-2 cell monolayers through the expression of AMP-activated protein kinase-mediated Occludin, Claudin-1, and ZO-1. *Biosci Biotechnol Biochem.* (2015) 79:130–7. doi: 10.1080/09168451.2014.951027
24. Sharma S, Tripathi P, Sharma J, Dixit A. Flavonoids modulate tight junction barrier functions in hyperglycemic human intestinal Caco-2 cells. *Nutrition.* (2020) 78:110792. doi: 10.1016/j.nut.2020.110792
25. Liu Y, Zhang Y, Zhou Y, Wang T, Deng X, Chu X, et al. Cinnamaldehyde inhibits type three secretion system in *Salmonella enterica* serovar *Typhimurium* by affecting the expression of key effector proteins. *Vet Microbiol.* (2019) 239:108463. doi: 10.1016/j.vetmic.2019.108463
26. Park JS, Park MY, Cho YJ, Lee JH, Yoo CG, Lee CT, et al. Anti-inflammatory effect of erdosteine in lipopolysaccharide-stimulated RAW 264.7 cells. *Inflammation.* (2016) 39:1573–81. doi: 10.1007/s10753-016-0393-4
27. Milanovic M, Kracht M, Schmitz ML. The cytokine-induced conformational switch of nuclear factor κB p65 is mediated by p65 phosphorylation. *Biochem J.* (2014) 457:401–13. doi: 10.1042/BJ20130780
28. Lang L, Xu B, Yuan J, Li S, Lian S, Chen Y, et al. GABA-mediated activated microglia induce neuroinflammation through the NLRP3 NF-κB pathways. *Int Immunopharmacol.* (2020) 89B:106908. doi: 10.1016/j.intimp.2020.106908
29. Chen Q, Liu M, Zhang P, Fan S, Huang J, Yu S, et al. Fucoidan and galactooligosaccharides ameliorate high-fat diet-induced dyslipidemia in rats by modulating the gut microbiota and bile acid metabolism. *Nutrition.* (2019) 65:50–9. doi: 10.1016/j.nut.2019.03.001
30. Vebø HC, Karlsson MK, Avershina E, Finnby L, Rudi K. Bead-beating artefacts in the *Bacteroidetes* to *Firmicutes* ratio of the human stool metagenome. *J Microbiol Methods.* (2016) 129:78–80. doi: 10.1016/j.mimet.2016.08.005
31. Cani PD, de Vos WM Next-generation beneficial Microbes: the case of *Akkermansia muciniphila*. *Front Microbiol.* (2017) 8:1765. doi: 10.3389/fmicb.2017.01765
32. Dao MC, Everard A, Aron-Wisnewsky J, Sokolovska N, Prifti E, Verger EO, et al. *Akkermansia muciniphila* and improved metabolic health during a dietary intervention in obesity: relationship with gut microbiome richness and ecology. *Gut.* (2016) 65:426–36. doi: 10.1136/gutjnl-2014-308778
33. Png CW, Lindén SK, Gilshenan KS, Zoetendal EG, McSweeney CS, Sly LI, et al. Mucolytic bacteria with increased prevalence in IBD mucosa augment in vitro utilization of mucin by other bacteria. *Am J Gastroenterol.* (2010) 105:2420–8. doi: 10.1038/ajg.2010.281
34. Yassour M, Lim MY, Yun HS, Tickle TL, Sung J, Song Y, et al. Sub-clinical detection of gut microbial biomarkers of obesity and type 2 diabetes. *Genome Med.* (2016) 8:17. doi: 10.1186/s13073-016-0271-6
35. Derrien M, Vaughan EE, Plugge CM, Vos WM. *Akkermansia muciniphila* gen. Nov., sp. nov., a human intestinal mucin-degrading bacterium. *Int J Syst Evol Microbiol.* (2004) 54:1469–76. doi: 10.1099/ijs.0.02873-0
36. Chua H, Chou H, Tung Y, Chiang B, Liao C, Liu H, et al. Intestinal dysbiosis featuring abundance of *Ruminococcus gnavus*

associates with allergic diseases in infants. *Gastroenterology*. (2018) 154:154–67. doi: 10.1053/j.gastro.2017.09.006

37. Joossens M, Huys G, Cnockaert M, De Preter V, Verbeke K, Rutgeerts P, et al. Dysbiosis of the faecal microbiota in patients with Crohn's disease and their unaffected relatives. *Gut*. (2011) 60:631–7. doi: 10.1136/gut.2010.223263
38. Willing P, Dicksved J, Halfvarson J, Andersson AF, Lucio M, Zheng Z, et al. A pyrosequencing study in twins shows that gastrointestinal microbial profiles vary with inflammatory bowel disease phenotypes, *Gastroenterology*. (2010) 139:1844–54. doi: 10.1053/j.gastro.2010.08.049
39. Ashida H, Suzuki T, Sasakawa C. *Shigella* infection and host cell death: a double-edged sword for the host and pathogen survival. *Curr Opin Microbiol*. (2021) 59:1–7. doi: 10.1016/j.mib.2020.07.007
40. Mani S, Toapanta FR, McArthur MA, Qadri F, Svennerholm AM, Devriendt B, et al. Role of antigen specific T and B cells in systemic and mucosal immune responses in ETEC and *Shigella* infections, and their potential to serve as correlates of protection in vaccine development. *Vaccine*. (2019) 37:4787–93. doi: 10.1016/j.vaccine.2019.03.040

Conflict of Interest: XL is employed by Ningbo Biomart Lifetech Co. Ltd.

The remaining authors declare that the research was conducted in the absence of any commercial or financial relationships that could be construed as a potential conflict of interest.

frontiers in Nutrition

REVIEW
published: 25 November 2021
doi: 10.3389/fnut.2021.759507

The Functional Role of Lactoferrin in Intestine Mucosal Immune System and Inflammatory Bowel Disease

*Ning Liu[1,2], Gang Feng[3,4], Xiaoying Zhang[3,4], Qingjuan Hu[1,2], Shiqiang Sun[5,6], Jiaqi Sun[3,4], Yanan Sun[1,2], Ran Wang[1,2], Yan Zhang[1,2,7], Pengjie Wang[1,2] and Yixuan Li[1,2]**

[1] Key Laboratory of Precision Nutrition and Food Quality, Ministry of Education, Department of Nutrition and Health, China Agricultural University, Beijing, China, [2] Key Laboratory of Functional Dairy, Ministry of Education, Department of Nutrition and Health, China Agricultural University, Beijing, China, [3] Inner Mongolia Yili Industrial Group, Co., Ltd., Hohhot, China, [4] Yili Maternal & Infant Nutrition Institute, Beijing, China, [5] Department of Gastroenterology and Hepatology, University of Groningen and University Medical Center Groningen, Groningen, Netherlands, [6] Department of Genetics, University of Groningen and University Medical Center Groningen, Groningen, Netherlands, [7] College of Food Science and Engineering, Gansu Agricultural University, Lanzhou, China

Inflammatory bowel disease (IBD), encompassing ulcerative colitis (UC) and Crohn's disease (CD), is one of the main types of intestinal inflammatory diseases with intestine mucosal immune disorder. Intestine mucosal immune system plays a remarkable and important role in the etiology and pathogenesis of IBD. Therefore, understanding the intestine mucosal immune mechanism is a key step to develop therapeutic interventions for IBD. Intestine mucosal immune system and IBD are influenced by various factors, such as inflammation, gut permeability, gut microbiota, and nutrients. Among these factors, emerging evidence show that nutrients play a key role in inflammation activation, integrity of intestinal barrier, and immune cell modulation. Lactoferrin (LF), an iron-binding glycoprotein belonging to transferrin family, is a dietary bioactive component abundantly found in mammalian milk. Notably, LF has been reported to perform diverse biological functions including antibacterial activity, anti-inflammatory activity, intestinal barrier protection, and immune cell modulation, and is involved in maintaining intestine mucosal immune homeostasis. The improved understanding of the properties of LF in intestine mucosal immune system and IBD will facilitate its application in nutrition, clinical medicine, and health. Herein, this review outlines the recent advancements on LF as a potential therapeutic intervention for IBD associated with intestine mucosal immune system dysfunction. We hope this review will provide a reference for future studies and lay a theoretical foundation for LF-based therapeutic interventions for IBD by understanding the particular effects of LF on intestine mucosal immune system.

Keywords: cytokine, intestinal epithelial cells, immunocytes, lactoferrin, inflammatory bowel disease, intestine mucosal immune system

OPEN ACCESS

Edited by:
Xian Wu,
Miami University, United States

Reviewed by:
Maria Elisa Drago-Serrano,
Universidad Autónoma Metropolitana Unidad Xochimilco, Mexico
Xiaoqiong Cao,
University of Massachusetts Amherst, United States

****Correspondence:***
Yixuan Li
liyixuan9735@126.com

Specialty section:
This article was submitted to Nutritional Immunology, a section of the journal Frontiers in Nutrition

Received: *16 August 2021*
Accepted: *18 October 2021*
Published: *25 November 2021*

Citation:
Liu N, Feng G, Zhang X, Hu Q, Sun S, Sun J, Sun Y, Wang R, Zhang Y, Wang P and Li Y (2021) The Functional Role of Lactoferrin in Intestine Mucosal Immune System and Inflammatory Bowel Disease. Front. Nutr. 8:759507. doi: 10.3389/fnut.2021.759507

INTRODUCTION

Lactoferrin (LF), an ∼80 kDa iron-binding glycoprotein present in most biological fluids (saliva, milk, tears, and mucous secretions), was first identified in 1939, and isolated and purified from human and bovine milk in 1960 (1–4). LF is a safe and reliable natural substance, which is widely used in disease prevention, nutritional supplements, food and drug preservation, and cosmetics.

Due to a structure similar to that of serum transferrin (∼60%), LF can reversibly bind with ferric (Fe^{3+}) ion (5, 6). As an iron transporter, LF protects the nervous system by chelating with iron by reducing oxidative stress and improving iron metabolism (7). Additionally, accumulating evidence demonstrated that LF also possesses antimicrobial, anti-inflammatory, immunomodulatory, anti-carcinogenic, and anti-oxidative activities, thereby highlighting the therapeutic values of this multifunctional protein (8–15).

Bacteriostatic effect of LF is attributed to the binding capacity with free iron, which is an essential element for the growth of bacteria (16). The lack of iron suppresses the growth of *Escherichia coli* (*E. coli.*), an iron-dependent bacteria (17). Conversely, LF may serve as an iron donor to support the growth of some bacteria with lower iron demands, such as *Lactobacillus sp.* or *Bifidobacterium sp.*, which is generally considered as a beneficial effect (18, 19). In addition to its antibacterial properties, LF also has both epithelial barrier protection and immunomodulatory properties, which play key roles in the intestine mucosal immune system (20–22). The studies cited above indicate that the physiological functions of LF not only depend on the iron-binding capacity but also on the interaction with molecular and cellular components of both the host and pathogens (23). The intestine mucosal immune system provides a protective barrier against invasion of infectious pathogens and harmful non-self antigens reaching systemic sites within the intestinal tract, and prevents systemic immune responses to commensal bacteria and food antigens (8–10, 13, 14). Inflammatory bowel disease (IBD), mainly divided into ulcerative colitis (UC) and Crohn's disease (CD), is a chronic inflammatory and relapsing disorder of the gastrointestinal tract, in which the interactions among mucosal immune, barrier function, nutrition, and commensal enteric flora are involved (24–28). Accumulating studies report that LF can be considered as a potent anti-inflammatory and immunomodulatory substrate for the prevention and treatment of IBD through regulating intestine mucosal immune response (9, 22, 29, 30). Breakdown of intestinal barrier underpins IBD and other diseases (31). *In vitro* and *in vivo* studies have reported that LF and its derivatives exhibit barrier protection through restoring tight junction (TJ) morphometry, blocking the cleavage of caspase-3, and resuming the drop in transepithelial resistance (TER) in IBD models (30, 32, 33). Furthermore, the LF treatment reduced the secretion and gene expression of tumor necrosis factor alpha (TNF-α), interleukin-8 (IL-8), interleukin-6 (IL-6), and nuclear factor-κB (NF-κB), and signal transducer and activator of transcription 3 (STAT3) signaling pathway activation, both in cultured and Crohn-derived intestinal cells (29, 33–36). It was noted that LF effectively causes dendritic cells (DCs) and macrophages to be tolerogenic phenotype by inhibiting the proliferation of $CD4^+$ T cells and enhancing Treg cell differentiation from $CD4^+$ T cells in the colon, which is key for tissue homeostasis (37, 38).

Accumulating evidence indicate that LF has been reported to enhance intestinal epithelial cell proliferation, cytokines production, and immune cell functions in counteracting inflammatory processes and maintaining immune homeostasis (9, 22, 29, 30). This review aims to outline the intestine mucosal immune system and the functional role of LF (bovine LF, bLF; human LF, hLF; porcine LF, pLF; LF enzymatic hydrolysate; LF peptide-derivatives) on the intestine mucosal immune system and IBD. We hope this review will lay a theoretical foundation for therapeutic interventions of IBD based on molecular basis and intestine mucosal immune mechanism.

INTESTINE MUCOSAL IMMUNE SYSTEM

The intestine mucosal immune system, which is mainly composed of intestinal epithelial cells (IECs) and immunocytes (**Figure 1**), provides a large area for the digestion and absorption of nutrients, serves as a barrier against harmful non-self antigens and infectious pathogens, protects the host against systemic immune responses to commensal bacteria and food antigens, and prevents the trillions of commensal microorganisms living in the gut from reaching systemic sites (39–43). Intestinal epithelial cells not only act as a physical barrier to segregate the intestinal microbiota from the immune cells but also as a coordinator between the intestinal microbiota and immune cells (44). Once the barrier is disrupted, uncontrolled antigens may ingress into the lamina propria (LP) resulting in the release of multiple cytokines, which aggravates the development of inflammation in the intestine (45). Epidemiological observations indeed suggest that patients with IBD have increased intestinal permeability with reduced expression of TJ proteins (46, 47). Additionally, overproduction of proinflammatory cytokines impair the intestinal barrier and induce the accumulation and activation of immune cells, which drive further immune responses and sustain chronic intestinal inflammation in IBD (48, 49). Collectively, IECs and intestinal immunocytes appear of characteristic importance for intestine mucosal immune system and play a key role in pathogenesis of IBD.

Intestinal Epithelial Cells

The IECs lining the gastrointestinal tract in a single-cell form contain multiple cell types including absorptive columnar epithelial cells, goblet cells, Paneth cells, endocrine cells (ECs), microfold (M) cells, cup cells, and tuft cells, which play important roles in the digestion of food, absorption of nutrients, and protection against microbial infection (48, 50, 51). Additionally, IECs participate in immune activities such as immunoglobulin (Ig)A antibody transportation, antigens uptake, and chemokines and cytokines secretion (44, 52–54). Mounting evidence have demonstrated that IECs produce inflammation and chemokines [such as Interleukin (IL)-18, IL-6, TNF-α, and macrophage chemoattractant protein-1 (MCP-1)] in response to stimulation of intestinal bacteria. Inflammation and chemokines play a vital role in the recruitment, proliferation, activation, and immune response of intestinal immune cells (44, 50, 55). Additionally, IECs directly kill bacteria and regulate the homeostasis of intestinal flora through secreting antibacterial substances, such as defensins, cathelicidins, C-type lectins, ribonucleases (RNases),

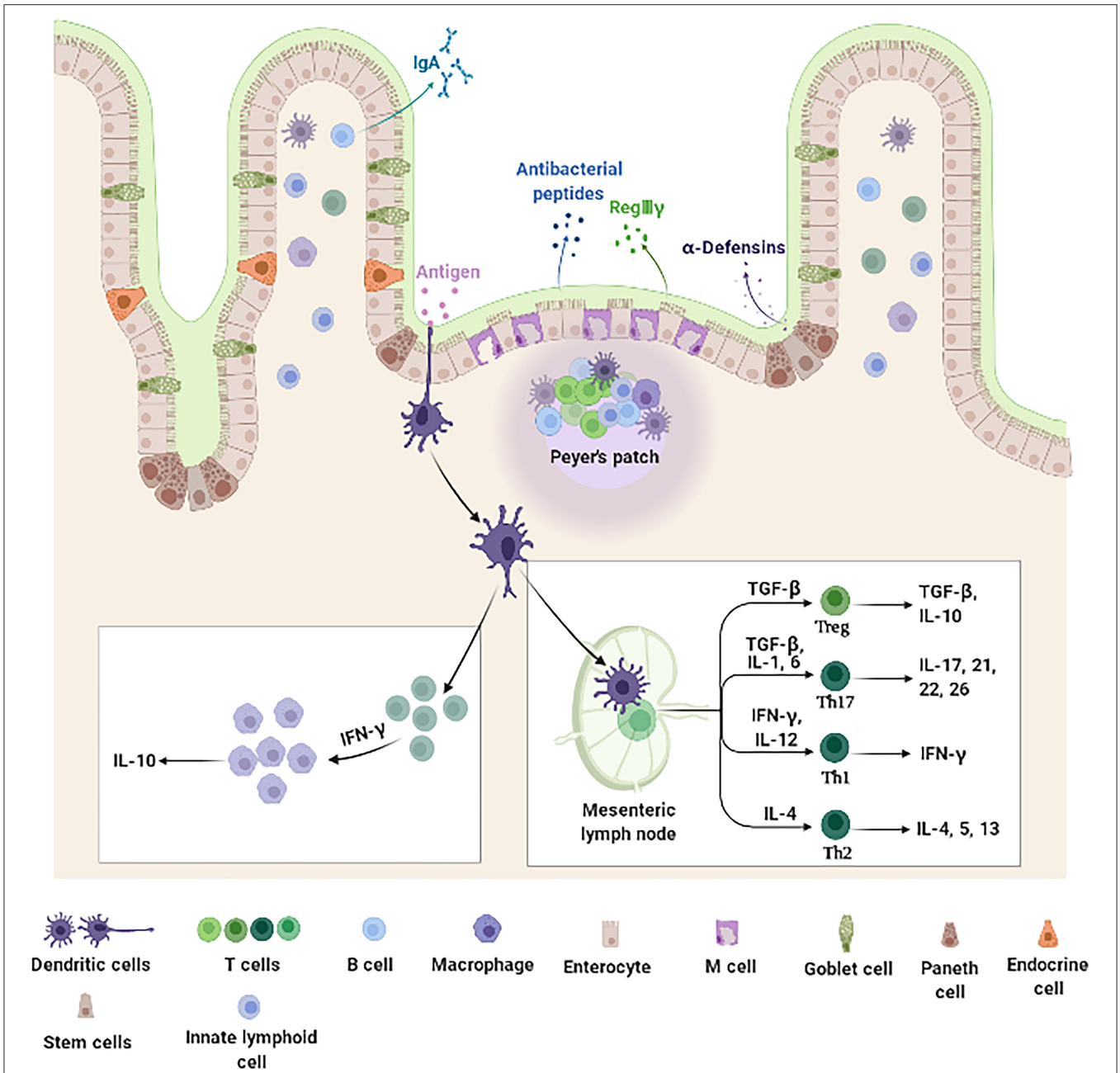

FIGURE 1 | Intestine mucosal immune system landscape. The intestine mucosal immune system is composed of different types of functional cells. Enterocytes, the main functional cells of intestine mucosal immune, are responsible for the absorption of nutrients and water, and also produce antimicrobial peptides (such as RegⅢγ and β-defensin). Paneth cells located at the bottom of the crypt produce amounts of specific antimicrobial peptides (α-defensin). M cells function to sample and transport antigens to immune cells. Goblet cells secrete mucins and promote luminal antigen transfer to DCs. In addition, there are a large number of immune cells distributed in the intestinal epithelium and LP, including DCs, B cells, and T cells. DCs are specialized antigen-presenting cells. After antigens stimulation, they secrete cytokine IFN-γ, which further stimulates monocyte macrophages to secrete IL-10. The DCs that migrate to the MLNs promote the differentiation and maturation of initial T cells. These differentiated and mature T cells can secrete immune factors to participate in intestine mucosal immune system. DCs, dendritic cells; IFN-γ, interferon-γ; IL-10, interleukin-10; LP, lamina propria; M, microfold; MLNs, mesenteric lymph nodes; RegⅢγ, regenerating islet-derived protein Ⅲγ.

and S100 proteins (56). Taken together, IECs serve not only as a physical barrier to prevent intestinal bacteria from invading the intestinal mucosa but also as a bridge between innate and adaptive immune systems.

Intraepithelial Lymphocytes and Lamina Propria Innate Lymphoid Cells

Intestinal innate lymphocytes consist of intestinal intraepithelial lymphocytes (IELs) and LP innate lymphoid cells (ILCs), which

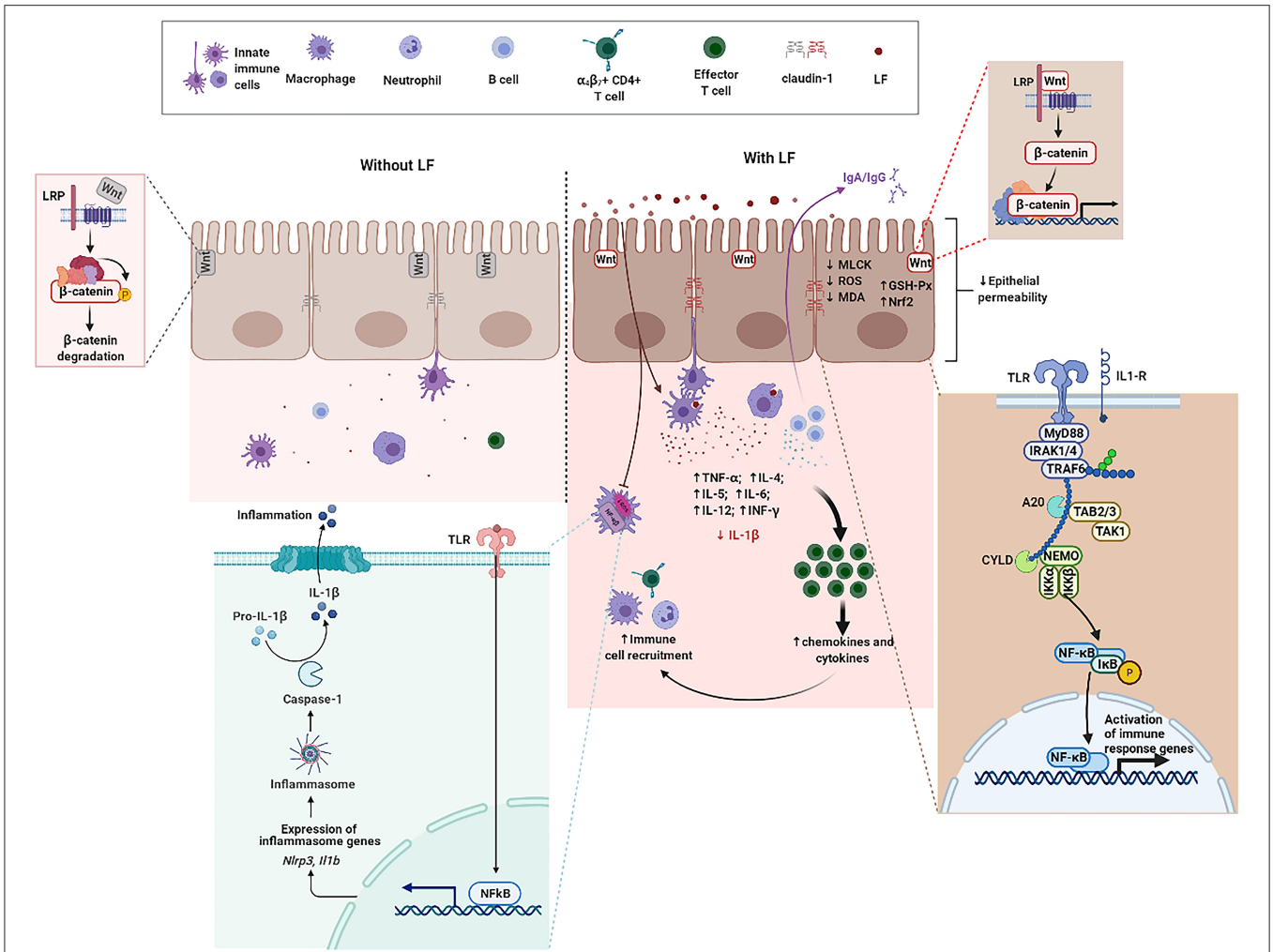

FIGURE 2 | The functional role of LF on intestine mucosal immune system in the context of IBD. Without LF **(Left)**, the intestine mucosal immune system follows the path of autoimmune regulation. The presence of LF **(Right)** promotes TJ between epithelial cells, enhances the expression of β-catenin, and activates the Wnt signaling pathway. LF downregulates the protein abundance of MLCK, reduces the level of ROS and MDA, enhances GSH-Px activity, and upregulates the expression level of Nrf2 in epithelial cells. LF enhances the expression level of TLRs and activates the NF-κB pathway. LF also reduces the secretion and the gene expression of IL-1β, enhances the function of immune cells, promotes the production of cytokines, and promotes the recruitment of immune cells. GSH-Px, glutathione peroxidase; IL-1β, interleukin-1β; LF, lactoferrin; NF-κB, nuclear factor kappa-B; Nrf2, nuclear factor erythroid 2-related factor 2; MDA, malondialdehyde; MLCK, myosin light chain kinase; ROS, reactive oxygen species; TJ, tight junction; TLRs, toll-like receptors.

are the effector compartments of the intestine mucosal immune system (57). IELs represent one of the largest, non-organized lymphocyte population (58) and constitute one of the most abundant T cell populations of barrier immune cells (59–61). Furthermore, IELs with abundant cytoplasmic granules for cytotoxic activity and expression of effector cytokines [interferon-γ (IFN-γ), IL-2, IL-4, or IL-17] play a crucial role in limiting the dissemination of infectious pathogens and malignant cells and control of infiltration of epithelial surfaces by systemic cells (62, 63). ILCs, identified in the recent years as an important subgroup of natural immune cells, have the dual characteristics of natural immune and acquired immune cells (64). ILCs, which lack T cell receptor (TCR) expression, are innate counterparts of T cells involved in host defense against infection, metabolic homeostasis, tissue repair, and chronic inflammatory diseases by secreting effector cytokines and regulating the functions of other innate and adaptive immune cells (64–66). Under the stimulation of intestinal bacteria, ILCs produce large quantities of cytokines, such as TNF-α, IFN-γ, and IL-17, which in turn stimulate the immune response to eliminate pathogens. However, excessive activation of ILCs in the intestine results in intestinal inflammation and IBD (57, 64). It is noteworthy that the phenotype and function of both IELs and ILCs are disrupted under inflammatory conditions, where they help to exacerbate intestine immune responses (65).

Dendritic Cells, T Cells, and B Cells

Dendritic cells that reside in the LP of the intestine are the $CD103^{-}/CX3CR1^{+}$ subgroup, which patrol among enterocytes and extend dendrites toward the lumen to capture antigens,

and then present the antigens to the T cells (67). Additionally, $CD103^+$/CX3CR1 subset of DCs can be further divided into two small subgroups, $CD11b^+/CD8\alpha^-$ and $CD11b^-/CD8\alpha^+$, which can migrate into Peyer's lymph nodes and mesenteric lymph nodes (MLNs) (68). DCs continuously migrate through lymphatics to MLNs where they contribute to initial T cell differentiation, maturation, and immune tolerance which is key for intestine mucosal immune system (68).

Intestinal T cells are widely distributed in the Peyer's lymph nodes, MLNs, LP, and intestinal epithelial tissues (69). According to TCR, intestinal T cells are classified into two major subsets, αβT cells and γδT cells, which play a key role in intestinal immune response (70, 71). Furthermore, studies have shown that γδT cells can produce cytokine IFN-γ in response to the stimulation of *E. coli*, followed by IFN-γ stimulating macrophages to release IL-15 which contribute to the accumulation and activation of γδT cells at the site of infection, and anti-infective immunity (72). Additionally, recent evidence have suggested that γδ T cells can secrete IL-17, which recruit neutrophils, macrophages, and natural killer (NK) cells to resist intestinal bacterial pathogens, especially early in infection (73, 74). T cells in the intestinal tract of healthy individuals play a critical role in the process of intestine mucosal immune and intestinal homeostasis (75). However, T cells in IBD patients are excessively active due to intestine mucosal immune dysfunction. Interestingly, reports have found that T cells in the intestine and peripheral blood of patients with CD and UC are significantly elevated, and those T cells in the inflammatory part of the patients show the characteristics of Th17 and Th1 cells, which can secrete IL-17 and IFN-γ inflammation (76). Correspondingly, the treatment of T cells is of considerable importance for the clinical treatment of intestinal inflammatory diseases.

There are a large number of B cells in the intestine; IgA^+ B cells migrate from Peyer's patches (PPs) to the LP by activation, where they differentiate into IgA-producing plasma cells (77). Under specific immune microenvironment of the intestine, cytokines such as TGF-β and IL-10 are abundant, which promote the differentiation of B cells into secretory IgA plasma cells, and the secreted IgA is transported into the intestinal lumen through IECs to control the invasion of intestinal bacteria by antibody neutralization (78, 79). Therefore, IgA secretory B cells play an extremely important role in the regulation of intestinal flora and the intestinal mucosa defense. Although IgM is the first Ig produced by B cells, the B cells are stimulated by antigens in the germinal center of lymphoid tissues and follicular helper T cells (TFHs), which cause antibody class-switch recombination (CSR) to produce IgG, IgA, and IgE (80).

IMMUNOMODULATORY ROLE OF LACTOFERRIN IN INTESTINE MUCOSAL IMMUNE SYSTEM

Lactoferrin, an ∼80 kDa single polypeptide chain glycoprotein belonging to transferrin family, is widely present in external secretions (milk, seminal fluid, saliva, tears, and mucous secretions) and in some granules of polymorphonuclear leukocytes (20, 81). The presence of disulfide bonds between cysteine residues in LF partly contribute to the secondary structure comprising 33–34% helices and 17–18% strands (82). The three-dimensional structure of LF consists of two highly homologous lobes, the N- and C-lobes (83). Each lobe further consists of two sub-lobes or domains which have high affinity with single Fe^{3+} (84). Accumulating evidence indicate that LF can regulate the proliferation of IECs, development and maturation of immune cells, and production of cytokines to counteract inflammatory processes and maintain intestine mucosal immune homeostasis in the context of IBD (**Figure 2**) (85, 86). Antimicrobial activity, modulation of cytokine production, immune cell migration, and the maturation and growth of immune or epithelial cells are partly due to LF interactions with pathogen-associated microbial patterns (PAMPs), glycosaminoglycans, or iron (86, 87). Thus, the functional role and underlying mechanisms of LF on IECs, immune cell response, and cytokine production are overviewed in **Table 1** and discussed in the ensuing sections.

Lactoferrin Performs Protection of Intestinal Epithelial Cells

Many studies have suggested that LF has anti-inflammatory effects, but the protective effect on small IECs is still poorly understood. Hu et al. took the intestinal porcine epithelial cell line-J2 (IPEC-J2) as the research model to investigate the protective effects and underlying mechanisms of bLF on lipopolysaccharides (LPS)-challenged IPEC-J2 cells *in vitro*. Treatment with bLF resulted in reduced cell permeability, enhanced Claudin-1 protein abundance, and inhibition of myosin light chain kinase (MLCK) protein abundance in LPS-challenged cells (36). Mounting evidence demonstrated that sIgA and the polymeric immunoglobulin receptor (pIgR) play a pivotal role in immune homeostasis by limiting the access of microbial and environmental antigens into the body, maintaining the integrity of the epithelial barrier, and shaping the composition of the commensal microbiota (100–102). bLF supplementation enhances the production of sIgA in small-bowel, supports intestinal barrier integrity by upregulating TJ protein express, and protects intestine from bacterial infections (93). Additionally, previous study reported that formula supplemented with bLF enhanced intestinal crypt proliferation and crypt depth. Furthermore, jejunal crypt cells isolated by using laser capture microdissection (LCM) had enhanced β-catenin mRNA expression, which suggests that the Wnt signaling may partly be involved in cell proliferation induced by bLF (95). Tanaka et al. found that oral administration of bLF protected the mucus barrier overlying the intestinal epithelium against dextran sodium sulfate (DSS)-mediated damage. Notably, bLF supplementation led to the inhibition of cell division in intestinal crypts, which in turn affected carcinogenesis in the colon of LPS-challenged mice (92). Despite mounting basic researches on LF, which is abundant in mammalian colostrum and milk, very little is known about the effects of metal saturation (iron-depleted, iron-saturated, and manganese-saturated forms) of LF

TABLE 1 | An overview of the properties of lactoferrin in the intestine mucosal immune system.

Model	Source	Dose	Time	Findings	References
In vitro, Caco-2 cells/J774A.1 cells	Bovine apo-, native- and holo-LF	5 mg/mL	24 h	Neutralized microbial-derived antigens; Reduced pro-inflammatory effect	(88)
In vitro, IPEC-J2 cells	Bovine native-LF	0.1, 0.25, 0.5, 1.0, 1.5, or 3.0 mg/mL	24 h	Alleviated the LPS-induced cellular inflammation; Reduced NF-κB/MAPK pathways; Maintaining cellular barrier integrity and mitigating oxidative stress; Reduced intracellular reactive oxygen species level and malondialdehyde level; Upregulated the glutathione peroxidase activity and the expression of nuclear factor erythroid 2-related factor 2 (Nrf2) protein; Reduced the IL-1β secretion; Downregulated the phosphorylation levels of NF-κB, IκB, p38, and ERK1/2 in LPS-challenged cells	(36)
In vitro, Caco-2/TC7 cells	Bovine LF	0.5, 1, 2, 5 or 10 mg/mL	24 h	Altered the expression of TLR2, TLR4, and TLR9 receptors; Reduced expression levels of TLR4; Maintaining redox homeostasis	(89)
In vivo, zebrafish	Bovine LF	0, 0.5, 1, or 1.5 g/kg	3 d	Enhanced the neutrophil migration and intestinal mucosal barrier functions related genes expression; Improved performance against bacterial infection	(90)
In vivo, mice	Bovine holo-LF	0, 50, 500, or 5000 μg/day	7 d	Enhanced level of total and specific IgA, protein expression of a-chain and pIgR, mRNA transcripts of a-chain, IL-2 and IL-5, and level of plasma corticosterone	(91)
In vivo, mice	Bovine LF	2.0% bLF in water or diet	84 d	Improved fecal score, lesions in the colon, and body weight loss	(92)
In vivo, rats	Bovine LF	0.5 g/kg/d	18 d	Enhanced small-bowel sIgA concentrations and tight junction proteins expression; Reduced intestinal permeability; Supported intestinal barrier integrity; Protected against bacterial infections	(93)
In vivo, neonatal piglet	Bovine LF	130, 367 or 1300 mg/kg BW/d	14 d	Altered the capacity of MLNs and spleen immune cells; Initiated immune responses in immunologically challenged neonates	(94)
In vivo, piglet	Bovine LF	0.4, 1.0, or 3.6 g/L	14 d	Enhanced intestinal crypt proliferation and crypt depth; Enhanced β-catenin mRNA expression	(95)
In vivo, piglet	Recombinant human LF	2, 11, or 20 mg/g	30 d	Reduced diarrhea; Boosted humoral immunity, Th1, and Th2 cell response; Improved intestinal morphology; Activated the immune-related genes expression	(96)
In vivo, human	Recombinant human LF	1500 mg/d	90 d	Did not reduce inflammation and immune activation	(97)
In vitro, bacteria	Peptide-derived from Bovine LF	0.3-150 mg/mL	16 to 20 h	Attenuated the LPS induced immune disorders; Sustained the balance of $CD3^+$/$CD8^+$ T cells, B cells and NK cells; Activated cellular defense and stimulated B cells to secrete certain IgG	(98)
In vivo, mice	Peptide-derived from Porcine LF	0, 2.5, 5, or 10 mg/kg	7 d	Balanced Th1 and Th2 response; Triggered cellular defense mechanisms and induced B cells to produce antibodies to defend against LPS stimulation	(99)

on intestinal barrier function. For this goal, researchers used Caco-2, a human intestinal epithelial cell line, to investigate the effects of bLF with iron and manganese saturation on the health of the host. Results indicated that no changes of TJ proteins were observed in response to bLF metal saturation status. Notably, different bLF forms markedly suppressed the pro-inflammatory response in macrophage through binding and neutralizing LPS (88). Additionally, LF was also able to neutralize microbial-derived antigens, thereby potentially reducing their pro-inflammatory effect (103). The effect of bLF as a regulator of intestinal innate immunity and oxidative stress on IECs was investigated in a previous study. Innate immune Toll-like receptors (TLRs) mRNA expression, lipid peroxidation, and protein carbonyl levels were determined in enterocyte-like Caco-2/TC7 cells incubated with bLF for 24 h. Results demonstrated that bLF seemed to maintain redox homeostasis and modulate inflammatory response *via* activation of TLRs when exposed to LPS (89). Additionally, LF reduced intracellular ROS level and malondialdehyde (MDA) level as well as upregulated glutathione peroxidase (GSH-Px) activity and the expression of nuclear factor erythroid 2-related factor 2 (Nrf2) protein (36).

Lactoferrin Modulates Immune Cell Function and Cytokine Production

Dietary bLF alters the capacity of MLNs and spleen immune cells in response to stimulation, providing a protective role for LF in the initiation of immune responses in these immunologically challenged neonates (94). It is noted that recombinant human LF (rhLF) secreted by transgenic cattle was used to investigate the immunomodulatory effects of rhLF on the systemic and intestinal immune system in piglets, which are good models widely used in infant nutrition study. Results showed that rhLF milk significantly reduced diarrhea, boosted humoral immunity, Th1 and Th2 cell response, improved intestinal morphology, and activated the transcription of important immune-related genes expression (96). Study on incorporation bLF into soybean meal-based diet demonstrated that 1.5 g/kg bLF supplemented to soybean meal reduced the neutrophils in the intestine when compared with control. Likewise, bLF supplementation enhanced the neutrophil migration and intestinal mucosal barrier functions related to genes expression. These findings suggested that bLF acts as an intestinal anti-inflammatory agent and improves performance against bacterial infection (90). These results indicate a potential role of LF in intestine mucosal immune. Ingestion of soybean meal resulted in intestinal inflammation which is a harmful condition in fish. Interestingly, peptide derived from bLF is also capable of conserving the biological activity (98). LFP-20, a twenty-amino acid antimicrobial peptide in the N terminus of pLF, has been reported to modulate inflammatory response in colitis (99). Pre-treatment with LFP-20 attenuated the LPS-induced immune disorders in ileum and sustained the balance of $CD3^+/CD8^+$ T cells, B cells, and NK cells. Furthermore, LFP-20 facilitated a balanced Th1 and Th2 response. Of note, LFP-20 activated the cellular defense and stimulated the B cells to secrete certain IgG (99). Although mounting researches have focused on exogenous LF, there is little information available regarding the expression of endogenous LF in response to bacterial infection. Previous study indicated that distribution of LF in mice intestine during *E. coli* K88 infection was upregulated in duodenum, ileum, and colon, but reduced in jejunum, by using PCR and immunohistology staining. These data pave the way for a better understanding of the key role of LF in intestine mucosal immune (104). A large number of studies have reported that LF regulates mucosal immune and targets the mechanism that induce inflammation (105). A clinical trial on rhLF conducted with 54 human immunodeficiency virus-infected participants with viral suppression demonstrated that no differences were observed in IL-6, D-dimer levels, monocyte/T-cell activation, mucosal integrity, or intestinal microbiota diversity when compared with controls (97).

Under physiological conditions, bLF supplementation led to the upregulation of sIgA, the protein expression of α-chain and pIgR, and the mRNA expression of α-chain, IL-2, and IL-5 (91). The result suggested that bLF contributed to maintain intestinal homeostasis through an interleukins profile that favored the IgA antibody response (91). Recently, studies indicated that LF was essential for the development of the early stages of B cells in mice by regulating the microenvironment of bone marrow stroma through C-X-C motif chemokine ligand 12 (CXCL12) release (106). Correspondingly, a previous study found that bLF treatment reduced the IL-1β secretion and mRNA expression, and downregulated the phosphorylation levels of NF-κB, IκB, p38, and ERK1/2 in LPS-challenged cells (36). Interestingly, peptide derived from bLF is also capable of conserving the biological activity (98). LFP-20, a twenty-amino acid antimicrobial peptide derived from pLF, has been reported to modulate inflammatory response in colitis (99). Pre-treatment with LFP-20 facilitated a balanced Th1 and Th2 response, which is consistent with the modulation of Th1 cytokines (IL-12p70, IFN-γ, and TNF-α) and Th2 cytokines (IL-4, IL-5, and IL-6) (99).

FUNCTIONAL ROLE OF LACTOFERRIN IN INFLAMMATORY BOWEL DISEASE

IBD, mainly divided into UC and CD, is a chronic inflammatory and relapsing disorder of the gastrointestinal tract in which the interactions among mucosal immune, barrier function, nutrition, and commensal enteric flora are involved (24–28, 107). IBD has become a global disease with rapidly increasing incidence and prevalence, and been diagnosed in developed and developing countries in both men and women (108–111). LF, a multifaceted milk protein, is considered as a potent anti-inflammatory and immunomodulating substrate for protecting mucosa against infections and inflammation (29). Accumulating studies report that LF can be considered as a potential therapy for the prevention and treatment of IBD based on the beneficial effects of LF in inhibiting invasion or adhesion of bacteria or modulating/boosting mucosal immune system (**Figure 2**) (9, 22, 30).

Oral administration offers the most convenient way for supplementing LF, which is considered as a new clinical nutrition strategy for the treatment of IBD (112, 113). As expected, LF ingested through diet, water, or perorally is degraded rapidly by enzymatic hydrolysis in the gastrointestinal tract, which causes undesirable loss of its functional properties (20). Therefore, high amounts, frequent dosing, or an appropriate delivery system may improve its bioavailability (112). Nevertheless, previous study showed that much more undigested LF enters the intestine when it is administered by gavage (20). Two studies that administered LF by gavage to DSS-treated mice found significantly less damage in the colon of the LF groups (34, 114). As matter of fact, antimicrobial peptides such as lactoferricin and lactoferrampin are generated during gastric and intestinal digestion stages (115–119). LF or its derived fragments in high amounts binding to LF receptors in intestinal mucosa and gut-associated lymphatic tissue-related cells would modulate cytokine/chemokine production and immune cells function. Additionally, LF administered to DSS-treated mice *via* intracolonic injection during the DSS treatment period markedly reduced damage in the colon than the controls (120).

Bacteriostatic Properties of Lactoferrin in Inflammatory Bowel Disease

Intestinal microbiota plays a key role in the development and maintenance of IBD (121). Therefore, manipulation of the gut microbiota may represent a target for IBD therapy (122). LF has broad spectrum antibacterial properties against a wide range of pathogenic bacteria including gram-positive bacteria and gram-negative bacteria (116, 123). A previous study was conducted to investigate the ability of bLF to modulate the interactions between the adherent-invasive *E. coli* strain LF82 (ileal Crohn's strain) and Caco-2 cells. Scanning electron microscopy, transmission electron microscopy, and light microscopy revealed that bLF prevents invasion of *E. coli* strain LF82 by binding with the bacteria type 1 pili (29). Recent study reported that bLF-treated DSS-challenged mice turn the *Muribaculaceae*/*Lachnospiraceae* intestinal type into *Akkermansiaceae*/*Bacteroidaceae* intestinal type in colitis mice. This result indicates a direction toward treating colitis by changing the structure and composition of intestinal microbiota. Additionally, metabolomics results demonstrated that bLF changed purine metabolism when compared with DSS-challenged mice (30). However, the underlying mechanisms responsible for the antibacterial properties of LF have not been completely elucidated (124). Accumulating evidence demonstrated that antibacterial activity of LF not only depends on the iron binding capacity but also on serine protease and the permeability of the bacterial cell membrane destruction (17–19, 125–128).

Epithelial Barrier Protection of Lactoferrin in Inflammatory Bowel Disease

The intestinal epithelial barrier integrity is vital to protect the intestinal cells from microbes, and intestinal barrier dysfunction underpins IBD and other diseases (31, 129–131). *In vitro* studies reported that bLF exerts a protective function toward intestinal barrier disorder (32, 33). Hu et al. took TNF-α-challenged HT-29/B6 cells to elucidate the protective properties of bLF on intestinal epithelial barrier and found that bLF restored TJ morphometry and almost completely blocked the cleavage of caspase-3 induced by TNF-α. Additionally, the results of this study demonstrated that bLF treatment resumed the drop in TER and Claudin-8 down-regulation when HT-29/B6 or T84 cells were challenged with *Yersinia enterocolitica* infection (32). In another study conducted by Zhao et al. it was found that bLF significantly enhanced the expression of Claudin-1, Occludin, and ZO-1 at both the mRNA and protein levels (33). Additionally, *in vivo* studies demonstrated that bLF administration ameliorated the severity of DSS or azoxymethane (AOM)-induced colitis as reflected by reduced body weight loss, decreased colon shortening, and reduced myeloperoxidase (MPO) activity (30, 92). Moreover, protein abundance of Claudin-1, Occludin, ZO-1, and regenerating islet-derived protein IIIγ (RegIIIγ) in the colon were enhanced by bLF treatment when compared with the DSS group (30). It was also noted that oral administration of a bovine lactoferricin–lactoferrampin (LFCA)-encoding *Lactococcus lactis* strain prevented DSS-induced colitis through enhancing the protein abundance of ZO-1, E-cadherin, and Claudin-2 (132).

Anti-inflammatory Properties of Lactoferrin in Inflammatory Bowel Disease

In addition to its epithelial barrier protection properties, LF also has anti-inflammatory properties (29, 32, 90, 92, 133). LF affects type 1 interferon expression or immune cell function (13, 134). Growing evidence reported that LF inhibits TNF-α, IL-8, IL-6, and NF-κB signaling pathway activation both in cultured and Crohn-derived intestinal cells (29, 33, 34). In experimental colitis, LF administration leads to a significant reduction in TNF-α, IL-1β, and IL-6, and an increase of IL-4 and IL-10 (35). Furthermore, LF administration ameliorates DSS-induced intestinal inflammation in mice by suppressing NF-κB signaling pathway activation (135). In particular, results from previous study showed that apo-bLF was more efficient than the holo form in decreasing MPO, IL-1β, and TNF-α synthesis in trinitrobenzenesulfonic acid (TNBS)-induced colitis in rats and dextran sulfate (DSS)-induced colitis in mice (34, 38, 136). Moreover, bLF has been considered as a negative regulator for IL-6 production in *in vitro* and *in vivo* studies as well as in clinical trials (133, 137–142). Interestingly, bLF was also found to interfere with STAT3 activation pathways both in IL-6-dependent and IL-6-independent modes (138, 143–145).

Immune Cell Modulation of Lactoferrin in Inflammatory Bowel Disease

Studies have revealed that uncontrolled activation of intestine immune cells and pathogenic immune cells circuits contribute to the onset and development of IBD (48, 146). LF supplementation enhances the expression of CD80, CD83, and CD86, and the production of proinflammatory cytokines of monocyte-derived dendritic cells, which indicate this type of cell maturation (124). Furthermore, LF effectively causes DCs to be tolerogenic by suppressing $CD4^+$ T cells proliferation and enhancing Treg cell differentiation from $CD4^+$ T cells in the colon, when compared with the DSS group (37, 38). Recently, LF has been reported to promote the macrophage shift from inflammatory to tolerogenic phenotype, which is key for tissue homeostasis (133). Consistently, VEN-120, a recombinant human LF, reverses severe inflammation in both the DSS-induced colitis model and the TNFΔARE/+ model of ileitis by increasing Treg cells in LP. *In vitro* study confirmed that $CD4^+$ T cells treated with LF upregulates Treg genes and Treg populations (114). Overall, the studies cited above indicate that LF and LF-derived peptide fraction can be considered as an effective clinical nutrition strategy for the treatment or prevention of IBD.

CONCLUSIONS

The intestine mucosal immune system is a complex network composed of lymph nodes, LP, and epithelial cells, which provides a barrier to separate the intestinal luminal contents from the internal environment, and plays an essential role in a perfect immune response mechanism and a strict immune

regulation mechanism. LF, an iron-binding protein expressed in most biological fluids, has been considered as a potent antimicrobial, anti-inflammatory, and immunomodulatory substrate for modulating/boosting intestine mucosal immune system and protecting the intestine against IBD and other diseases. Owing to the various microbial and host targets of LF, understanding the mechanisms of action of LF in the intestine mucosal immune and IBD is a challenge. Therefore, the underlying mechanisms are still under investigation and further studies are needed. Currently, LF interaction with PAMPs, glycosaminoglycans, or iron as well as nucleus seem to be the most reasonable mechanisms contributing to change in the structure and composition of the intestinal microbiota, maintenance of intestinal epithelial barrier integrity, balance between proinflammatory and anti-inflammatory cytokines production, and immune cell function modulation, which are critical for intestine mucosal immune system and IBD. Therefore, understanding the molecular basis and intestine mucosal immune mechanism is a key step to develop therapeutic interventions, and provides a new target for the treatment of IBD associated with intestine mucosal immune system dysfunction.

AUTHOR CONTRIBUTIONS

Writing—review and editing were carried out by NL, GF, XZ, QH, SS, JS, YS, RW, YZ, and PW. Supervision was done by YL. All authors have read and agreed to the published version of the manuscript.

FUNDING

This work was supported by the National Natural Science Foundation of China (Nos. 31901625, 32130081, 32000082, and 31625025), State Key Laboratory of Animal Nutrition (2004DA125184F1909), Huhhot Science & Technology Plan (No. 2020-Ke Ji Xing Meng-National Innovation Center-3), and the 111 Project (B18053).

REFERENCES

1. Sorensen M, Sorensen S. The proteins in whey. Compte rendu des Travaux du Laboratoire de Carlsberg. *Ser Chim.* (1940) 23:55–99.
2. Groves ML. The isolation of a red protein from Milk2. *J Am Chem Soc.* (1960) 82:3345–50. doi: 10.1021/ja01498a029
3. Montreuil J, Tonnelat J, Mullet S. Preparation and properties of lactosiderophyllin (lactotransferrin) of human milk. *Biochim Biophys Acta.* (1960) 45:413–21. doi: 10.1016/0006-3002(60)91478-5
4. Johanson B. Isolation of an iron-containing red protein from human milk. *Acta Chem Scand.* (1960) 14:510–2. doi: 10.3891/acta.chem.scand.14-0510
5. Baker E. Structure and reactivity of transferrins. *Adv Inorg Chem.* (1994) 41:389–463. doi: 10.1016/S0898-8838(08)60176-2
6. Lambert LA, Perri H, Meehan TJ. Evolution of duplications in the transferrin family of proteins. *Comp Biochem Physiol B Biochem Mol Biol.* (2005) 140:11–25. doi: 10.1016/j.cbpc.2004.09.012
7. Mohamed WA, Salama RM, Schaalan MF. A pilot study on the effect of lactoferrin on Alzheimer's disease pathological sequelae: impact of the p-Akt/PTEN pathway. *Biomed Pharmacother.* (2019) 111:714–23. doi: 10.1016/j.biopha.2018.12.118
8. Actor JK, Hwang SA, Kruzel ML. Lactoferrin as a natural immune modulator. *Curr Pharm Design.* (2009) 15:1956–73. doi: 10.2174/138161209788453202
9. Kanyshkova TG, Buneva VN, Nevinsky GA. Lactoferrin and its biological functions. *Biochemistry (Mosc).* (2001) 66:1–7. doi: 10.1023/A:1002817226110
10. Legrand D, Elass E, Carpentier M, Mazurier J. Lactoferrin: a modulator of immune and inflammatory responses. *Cell Mol Life Sci.* (2005) 62:2549–59. doi: 10.1007/s00018-005-5370-2
11. Wang WP, Iigo M, Sato J, Sekine K, Adachi I, Tsuda H. Activation of intestinal mucosal immunity in tumor-bearing mice by lactoferrin. *Japanese J Cancer Res.* (2000) 91:1022–7. doi: 10.1111/j.1349-7006.2000.tb00880.x
12. Kozu T, Iinuma G, Ohashi Y, Saito Y, Akasu T, Saito D, et al. Effect of orally administered bovine lactoferrin on the growth of adenomatous colorectal polyps in a randomized, placebo-controlled clinical trial. *Cancer Prev Res (Phila).* (2009) 2:975–83. doi: 10.1158/1940-6207.CAPR-08-0208
13. Alexander DB, Iigo M, Hamano H, Kozu T, Saito Y, Saito D, et al. An ancillary study of participants in a randomized, placebo-controlled trial suggests that ingestion of bovine lactoferrin promotes expression of interferon alpha in the human colon. *J Funct Foods.* (2014) 10:305–17. doi: 10.1016/j.jff.2014.06.028
14. Alexander DB, Iigo M, Abdelgied M, Ozeki K, Tanida S, Joh T, et al. Bovine lactoferrin and Crohn's disease: a case study. *Biochem Cell Biol.* (2017) 95:133–41. doi: 10.1139/bcb-2016-0107
15. Iigo M, Alexander DB, Xu J, Futakuchi M, Suzui M, Kozu T, et al. Inhibition of intestinal polyp growth by oral ingestion of bovine lactoferrin and immune cells in the large intestine. *Biometals.* (2014) 27:1017–29. doi: 10.1007/s10534-014-9747-2
16. Arnold RR, Brewer M, Gauthier JJ. Bactericidal activity of human lactoferrin: sensitivity of a variety of microorganisms. *Infect Immun.* 198028:893–8. doi: 10.1128/iai.28.3.893-898.1980
17. Brock JH. Lactoferrin in human milk: its role in iron absorption and protection against enteric infection in the newborn infant. *Arch Dis Child.* (1980) 55:417–21. doi: 10.1136/adc.55.6.417
18. Petschow BW, Talbott RD, Batema RP. Ability of lactoferrin to promote the growth of Bifidobacterium spp. *in vitro* is independent of receptor binding capacity and iron saturation level. *J Med Microbiol.* (1999) 48:541–9. doi: 10.1099/00222615-48-6-541
19. Sherman MP, Bennett SH, Hwang FF Yu C. Neonatal small bowel epithelia: enhancing anti-bacterial defense with lactoferrin and Lactobacillus GG. *Biometals.* (2004) 17:285–9. doi: 10.1023/B:BIOM.0000027706.51112.62
20. Wang B, Timilsena YP, Blanch E, Adhikari B. Lactoferrin: structure, function, denaturation and digestion. *Crit Rev Food Sci Nutr.* (2019) 59:580–96. doi: 10.1080/10408398.2017.1381583
21. Superti F. Lactoferrin from bovine milk: a protective companion for life. *Nutrients.* (2020) 12:2562. doi: 10.3390/nu12092562
22. Cutone A, Ianiro G, Lepanto MS, Rosa L, Valenti P. Bonaccorsi di Patti MC, et al. Lactoferrin in the prevention and treatment of intestinal inflammatory pathologies associated with colorectal cancer development. *Cancers (Basel).* (2020) 12:3806. doi: 10.3390/cancers12123806
23. Latorre D, Puddu P, Valenti P, Gessani S. Reciprocal interactions between lactoferrin and bacterial endotoxins and their role in the regulation of the immune response. *Toxins.* (2010) 2:54–68. doi: 10.3390/toxins2010054
24. Khor B, Gardet A, Xavier RJ. Genetics and pathogenesis of inflammatory bowel disease. *Nature.* (2011) 474:307–17. doi: 10.1038/nature10209
25. Dessein R, Chamaillard M, Danese S. Innate immunity in Crohn's disease: the reverse side of the medal. *J Clin Gastroenterol.* (2008) 42(Suppl. 3) (Pt. 1):S144–7. doi: 10.1097/MCG.0b013e3181662c90
26. Stefanelli T, Malesci A, Repici A, Vetrano S, Danese S. New insights into inflammatory bowel disease pathophysiology: paving the way for novel therapeutic targets. *Curr Drug Targets.* (2008) 9:413–8. doi: 10.2174/138945008784221170

27. Lavelle A, Sokol H. Gut microbiota-derived metabolites as key actors in inflammatory bowel disease. *Nat Rev Gastroenterol Hepatol.* (2020) 17:223–37. doi: 10.1038/s41575-019-0258-z
28. Bouma G, Strober W. The immunological and genetic basis of inflammatory bowel disease. *Nat Rev Immunol.* (2003) 3:521–33. doi: 10.1038/nri1132
29. Bertuccini L, Costanzo M, Iosi F, Tinari A, Terruzzi F, Stronati L, et al. Lactoferrin prevents invasion and inflammatory response following *E. coli* strain LF82 infection in experimental model of Crohn's disease. *Dig Liver Dis.* (2014) 46:496–504. doi: 10.1016/j.dld.2014.02.009
30. Wang S, Zhou J, Xiao D, Shu G, Gu L. Bovine lactoferrin protects dextran sulfate sodium salt mice against inflammation and impairment of colonic epithelial barrier by regulating gut microbial structure and metabolites. *Front Nutr.* (2021) 8:660598. doi: 10.3389/fnut.2021.660598
31. Parikh K, Antanaviciute A, Fawkner-Corbett D, Jagielowicz M, Aulicino A, Lagerholm C, et al. Colonic epithelial cell diversity in health and inflammatory bowel disease. *Nature.* (2019) 567:49–55. doi: 10.1038/s41586-019-0992-y
32. Hering NA, Luettig J, Krug SM, Wiegand S, Gross G, van Tol EA, et al. Lactoferrin protects against intestinal inflammation and bacteria-induced barrier dysfunction in vitro. *Ann N Y Acad Sci.* (2017) 1405:177–88. doi: 10.1111/nyas.13405
33. Zhao X, Xu XX, Liu Y, Xi EZ, An JJ, Tabys D, et al. The *in vitro* protective role of bovine lactoferrin on intestinal epithelial barrier. *Molecules.* (2019) 24:148. doi: 10.3390/molecules24010148
34. Li L, Ren F, Yun Z, An Y, Wang C, Yan X. Determination of the effects of lactoferrin in a preclinical mouse model of experimental colitis. *Mol Med Rep.* (2013) 8:1125–9. doi: 10.3892/mmr.2013.1632
35. Togawa J, Nagase H, Tanaka K, Inamori M, Nakajima A, Ueno N, et al. Oral administration of lactoferrin reduces colitis in rats via modulation of the immune system and correction of cytokine imbalance. *J Gastroenterol Hepatol.* (2002) 17:1291–8. doi: 10.1046/j.1440-1746.2002.02868.x
36. Hu P, Zhao F, Wang J, Zhu W. Lactoferrin attenuates lipopolysaccharide-stimulated inflammatory responses and barrier impairment through the modulation of NF-kappaB/MAPK/Nrf2 pathways in IPEC-J2 cells. *Food Funct.* (2020) 11:8516–26. doi: 10.1039/D0FO01570A
37. Park HW, Park SH, Jo HJ, Kim TG, Lee JH, Kang SG, et al. Lactoferrin induces tolerogenic bone marrow-derived dendritic cells. *Immune Netw.* (2020) 20:e38. doi: 10.4110/in.2020.20.e38
38. Haversen LA, Baltzer L, Dolphin G, Hanson LA, Mattsby-Baltzer I. Anti-inflammatory activities of human lactoferrin in acute dextran sulphate-induced colitis in mice. *Scand J Immunol.* (2003) 57:2–10. doi: 10.1046/j.1365-3083.2003.01162.x
39. Tokuhara D, Kurashima Y, Kamioka M, Nakayama T, Ernst P, Kiyono H, et al. comprehensive understanding of the gut mucosal immune system in allergic inflammation. *Allergol Int.* (2019) 68:17–25. doi: 10.1016/j.alit.2018.09.004
40. Perez-Lopez A, Behnsen J, Nuccio SP, Raffatellu M. Mucosal immunity to pathogenic intestinal bacteria. *Nat Rev Immunol.* (2016) 16:135–48. doi: 10.1038/nri.2015.17
41. Richards JL, Yap YA, McLeod KH, Mackay CR, Marino E. Dietary metabolites and the gut microbiota: an alternative approach to control inflammatory and autoimmune diseases. *Clin Transl Immunology.* (2016) 5:e82. doi: 10.1038/cti.2016.29
42. Shi N, Li N, Duan X, Niu H. Interaction between the gut microbiome and mucosal immune system. *Mil Med Res.* (2017) 4:14. doi: 10.1186/s40779-017-0122-9
43. Maloy KJ, Powrie F. Intestinal homeostasis and its breakdown in inflammatory bowel disease. *Nature.* (2011) 474:298–306. doi: 10.1038/nature10208
44. Allaire JM, Crowley SM, Law HT, Chang SY, Ko HJ, Vallance BA. The intestinal epithelium: central coordinator of mucosal immunity. *Trends Immunol.* (2018) 39:677–96. doi: 10.1016/j.it.2018.04.002
45. Deng F, Peng L, Li Z, Tan G, Liang E, Chen S, et al. YAP triggers the Wnt/beta-catenin signalling pathway and promotes enterocyte self-renewal, regeneration and tumorigenesis after DSS-induced injury. *Cell Death Dis.* (2018) 9:153. doi: 10.1038/s41419-017-0244-8
46. Vancamelbeke M, Vermeire S. The intestinal barrier: a fundamental role in health and disease. *Expert Rev Gastroenterol Hepatol.* (2017) 11:821–34. doi: 10.1080/17474124.2017.1343143
47. Kang JH, Choi S, Jang JE, Ramalingam P, Ko YT, Kim SY, et al. Wasabia japonica is a potential functional food to prevent colitis via inhibiting the NF-kappaB signaling pathway. *Food Funct.* (2017) 8:2865–74. doi: 10.1039/C7FO00576H
48. Neurath MF. Targeting immune cell circuits and trafficking in inflammatory bowel disease. *Nat Immunol.* (2019) 20:970–9. doi: 10.1038/s41590-019-0415-0
49. Carvalho RD, Breyner N, Menezes-Garcia Z, Rodrigues NM, Lemos L, Maioli TU, et al. Secretion of biologically active pancreatitis-associated protein I (PAP) by genetically modified dairy Lactococcus lactis NZ9000 in the prevention of intestinal mucositis. *Microb Cell Fact.* (2017) 16:27. doi: 10.1186/s12934-017-0624-x
50. Soderholm AT, Pedicord VA. Intestinal epithelial cells: at the interface of the microbiota and mucosal immunity. *Immunology.* (2019) 158:267–80. doi: 10.1111/imm.13117
51. Bao C, Liu B, Li B, Chai J, Zhang L, Jiao L, et al. Enhanced transport of shape and rigidity-tuned alpha-Lactalbumin nanotubes across intestinal mucus and cellular barriers. *Nano Lett.* (2020) 20:1352–61. doi: 10.1021/acs.nanolett.9b04841
52. Mabbott NA, Donaldson DS, Ohno H, Williams IR, Mahajan A. Microfold (M) cells: important immunosurveillance posts in the intestinal epithelium. *Mucosal Immunol.* (2013) 6:666–77. doi: 10.1038/mi.2013.30
53. McDole JR, Wheeler LW, McDonald KG, Wang B, Konjufca V, Knoop KA, et al. Goblet cells deliver luminal antigen to CD103+ dendritic cells in the small intestine. *Nature.* (2012) 483:345–9. doi: 10.1038/nature10863
54. Zeuthen LH, Fink LN, Frokiaer H. Epithelial cells prime the immune response to an array of gut-derived commensals towards a tolerogenic phenotype through distinct actions of thymic stromal lymphopoietin and transforming growth factor-β. *Immunology.* (2008) 123:197–208. doi: 10.1111/j.1365-2567.2007.02687.x
55. Wu X, Koh GY, Huang Y, Crott JW, Bronson RT, Mason JB. The combination of curcumin and salsalate is superior to either agent alone in suppressing pro-cancerous molecular pathways and colorectal tumorigenesis in obese mice. *Mol Nutr Food Res.* (2019) 63:e1801097. doi: 10.1002/mnfr.201801097
56. Yue B, Luo XP Yu ZL, Mani S, Wang ZT, Dou W. Inflammatory bowel disease: a potential result from the collusion between gut microbiota and mucosal immune system. *Microorganisms.* (2019) 7:440. doi: 10.3390/microorganisms7100440
57. Montalban-Arques A, Chaparro M, Gisbert JP, Bernardo D. The innate immune system in the gastrointestinal tract: role of intraepithelial lymphocytes and lamina propria innate lymphoid cells in intestinal inflammation. *Inflamm Bowel Dis.* (2018) 24:1649–59. doi: 10.1093/ibd/izy177
58. Eiras P, Leon F, Camarero C, Lombardia M, Roldan E, Bootello A, et al. Intestinal intraepithelial lymphocytes contain a CD3-CD7+ subset expressing natural killer markers and a singular pattern of adhesion molecules. *Scand J Immunol.* (2000) 52:1–6. doi: 10.1046/j.1365-3083.2000.00761.x
59. Hayday A, Theodoridis E, Ramsburg E, Shires J. Intraepithelial lymphocytes: exploring the third way in immunology. *Nat Immunol.* (2001) 2:997–1003. doi: 10.1038/ni1101-997
60. Van Kaer L, Olivares-Villagomez D. Development, homeostasis, and functions of intestinal intraepithelial lymphocytes. *J Immunol.* (2018) 200:2235–44. doi: 10.4049/jimmunol.1701704
61. Sumida H. Dynamics and clinical significance of intestinal intraepithelial lymphocytes. *Immunol Med.* (2019) 42:117–23. doi: 10.1080/25785826.2019.1658516
62. Hu MD, Jia L, Edelblum KL. Policing the intestinal epithelial barrier: innate immune functions of intraepithelial lymphocytes. *Curr Pathobiol Rep.* (2018) 6:35–46. doi: 10.1007/s40139-018-0157-y
63. Ma H, Qiu Y, Yang H. Intestinal intraepithelial lymphocytes: maintainers of intestinal immune tolerance and regulators of intestinal immunity. *J Leukoc Biol.* (2021) 109:339–47. doi: 10.1002/JLB.3RU0220-111
64. Panda SK, Colonna M. Innate lymphoid cells in mucosal immunity. *Front Immunol.* (2019) 10:861. doi: 10.3389/fimmu.2019.00861
65. Olivares-Villagomez D, Van Kaer L. intestinal intraepithelial lymphocytes: sentinels of the mucosal barrier. *Trends Immunol.* (2018) 39:264–75. doi: 10.1016/j.it.2017.11.003

66. Little MC, Bell LV, Cliffe LJ, Else KJ. The characterization of intraepithelial lymphocytes, lamina propria leukocytes, and isolated lymphoid follicles in the large intestine of mice infected with the intestinal nematode parasite Trichuris muris. *J Immunol.* (2005) 175:6713–22. doi: 10.4049/jimmunol.175.10.6713
67. Farache J, Koren I, Milo I, Gurevich I, Kim KW, Zigmond E, et al. Luminal bacteria recruit CD103+ dendritic cells into the intestinal epithelium to sample bacterial antigens for presentation. *Immunity.* (2013) 38:581–95. doi: 10.1016/j.immuni.2013.01.009
68. Ruane DT, Lavelle EC. The role of CD103(+) dendritic cells in the intestinal mucosal immune system. *Front Immunol.* (2011) 2:25. doi: 10.3389/fimmu.2011.00025
69. Macpherson AJ, Smith K. Mesenteric lymph nodes at the center of immune anatomy. *J Exp Med.* (2006) 203:497–500. doi: 10.1084/jem.20060227
70. Ma H, Tao W, Zhu S, T. lymphocytes in the intestinal mucosa: defense and tolerance. *Cell Mol Immunol.* (2019) 16:216–24. doi: 10.1038/s41423-019-0208-2
71. Das D, Anand V, Khandpur S, Sharma VK, Sharma A, T. helper type 1 polarizing gammadelta T cells and scavenger receptors contribute to the pathogenesis of Pemphigus vulgaris. *Immunology.* (2018) 153:97–104. doi: 10.1111/imm.12814
72. McCarthy NE, Eberl M. Human γδ T-cell control of mucosal immunity and inflammation. *Front Immunol.* (2018) 9:985. doi: 10.3389/fimmu.2018.00985
73. Sutton CE, Mielke LA, Mills KH. IL-17-producing γδ T cells and innate lymphoid cells. *Eur J Immunol.* (2012) 42:2221–31. doi: 10.1002/eji.201242569
74. Dieli F, Gebbia N, Poccia F, Caccamo N, Montesano C, Fulfaro F, et al. Induction of gammadelta T-lymphocyte effector functions by bisphosphonate zoledronic acid in cancer patients *in vivo*. *Blood.* (2003) 102:2310–1. doi: 10.1182/blood-2003-05-1655
75. Zheng D, Liwinski T, Elinav E. Interaction between microbiota and immunity in health and disease. *Cell Res.* (2020) 30:492–506. doi: 10.1038/s41422-020-0332-7
76. M'Koma AE. The multifactorial etiopathogeneses interplay of inflammatory bowel disease: an overview. *Gastrointest Disord.* (2019) 1:75–105. doi: 10.3390/gidisord1010007
77. Cerutti A. Location, location, location: B-cell differentiation in the gut lamina propria. *Mucosal Immunol.* (2008) 1:8–10. doi: 10.1038/mi.2007.8
78. Wei HX, Wang B, Li B. IL-10 and IL-22 in mucosal immunity: driving protection and pathology. *Front Immunol.* (2020) 11:1315. doi: 10.3389/fimmu.2020.01315
79. Li Y, Jin L, Chen T. the effects of secretory IgA in the mucosal immune system. *Biomed Res Int.* (2020) 2020:2032057. doi: 10.1155/2020/2032057
80. Roco JA, Mesin L, Binder SC, Nefzger C, Gonzalez-Figueroa P, Canete PF, et al. Class-switch recombination occurs infrequently in germinal centers. *Immunity.* (2019) 51:337–50.e7. doi: 10.1016/j.immuni.2019.07.001
81. Cheng JB, Wang JQ, Bu DP, Liu GL, Zhang CG, Wei HY, et al. Factors affecting the lactoferrin concentration in bovine milk. *J Dairy Sci.* (2008) 91:970–6. doi: 10.3168/jds.2007-0689
82. Moore SA, Anderson BF, Groom CR, Haridas M. Baker EN. Three-dimensional structure of diferric bovine lactoferrin at 28 A resolution. *J Mol Biol.* (1997) 274:222–36. doi: 10.1006/jmbi.1997.1386
83. Steijns JM, van Hooijdonk AC. Occurrence, structure, biochemical properties and technological characteristics of lactoferrin. *Br J Nutr.* (2000) 84(Suppl. 1):S11–7. doi: 10.1017/S0007114500002191
84. Lepanto MS, Rosa L, Paesano R, Valenti P, Cutone A. Lactoferrin in aseptic and septic inflammation. *Molecules.* (2019) 24:1323. doi: 10.3390/molecules24071323
85. Kell DB, Heyden EL, Pretorius E. The biology of lactoferrin, an iron-binding protein that can help defend against viruses and bacteria. *Front Immunol.* (2020) 11:1221. doi: 10.3389/fimmu.2020.01221
86. Legrand D. Overview of lactoferrin as a natural immune modulator. *J Pediatr.* (2016) 173:S10–5. doi: 10.1016/j.jpeds.2016.02.071
87. Legrand D. Lactoferrin, a key molecule in immune and inflammatory processes. *Biochem Cell Biol.* (2012) 90:252–68. doi: 10.1139/o11-056
88. Majka G, Wiecek G, Srottek M, Spiewak K, Brindell M, Koziel J, et al. The impact of lactoferrin with different levels of metal saturation on the intestinal epithelial barrier function and mucosal inflammation. *Biometals.* (2016) 29:1019–33. doi: 10.1007/s10534-016-9973-x
89. Buey B, Belles A, Latorre E, Abad I, Perez MD, Grasa L, et al. Comparative effect of bovine buttermilk, whey, and lactoferrin on the innate immunity receptors and oxidative status of intestinal epithelial cells. *Biochem Cell Biol.* (2021) 99:54–60. doi: 10.1139/bcb-2020-0121
90. Ulloa PE, Solis CJ. De la Paz JF, Alaurent TG, Caruffo M, Hernandez AJ, et al. Lactoferrin decreases the intestinal inflammation triggered by a soybean meal-based diet in zebrafish. *J Immunol Res.* (2016) 2016:1639720. doi: 10.1155/2016/1639720
91. Godinez-Victoria M, Cruz-Hernandez TR, Reyna-Garfias H, Barbosa-Cabrera RE, Drago-Serrano ME, Sanchez-Gomez MC, et al. Modulation by bovine lactoferrin of parameters associated with the IgA response in the proximal and distal small intestine of BALB/c mice. *Immunopharm Immunot.* (2017) 39:66–73. doi: 10.1080/08923973.2017.1282513
92. Tanaka H, Gunasekaran S, Saleh DM, Alexander WT, Alexander DB, Ohara H, et al. Effects of oral bovine lactoferrin on a mouse model of inflammation associated colon cancer. *Biochem Cell Biol.* (2021) 99:159–65. doi: 10.1139/bcb-2020-0087
93. Wu J, Chen J, Wu W, Shi J, Zhong Y, van Tol EA, et al. Enteral supplementation of bovine lactoferrin improves gut barrier function in rats after massive bowel resection. *Br J Nutr.* (2014) 112:486–92. doi: 10.1017/S000711451400107X
94. Comstock SS, Reznikov EA, Contractor N, Donovan SM. Dietary bovine lactoferrin alters mucosal and systemic immune cell responses in neonatal piglets. *J Nutr.* (2014) 144:525–32. doi: 10.3945/jn.113.190264
95. Reznikov EA, Comstock SS Yi C, Contractor N, Donovan SM. Dietary bovine lactoferrin increases intestinal cell proliferation in neonatal piglets. *J Nutr.* (2014) 144:1401–8. doi: 10.3945/jn.114.196568
96. Li Q, Hu W, Zhao J, Wang J, Dai Y, Zhao Y, et al. Supplementation transgenic cow's milk containing recombinant human lactoferrin enhances systematic and intestinal immune responses in piglets. *Mol Biol Rep.* (2014) 41:2119–28. doi: 10.1007/s11033-014-3061-5
97. Sortino O, Hullsiek KH, Richards E, Rupert A, Schminke A, Tetekpor N, et al. The effects of recombinant human lactoferrin on immune activation and the intestinal microbiome among persons living with human immunodeficiency virus and receiving antiretroviral therapy. *J Infect Dis.* (2019) 219:1963–8. doi: 10.1093/infdis/jiz042
98. Bellamy W, Takase M, Wakabayashi H, Kawase K, Tomita M. Antibacterial spectrum of lactoferricin B, a potent bactericidal peptide derived from the N-terminal region of bovine lactoferrin. *J Appl Bacteriol.* (1992) 73:472–9. doi: 10.1111/j.1365-2672.1992.tb05007.x
99. Zong X, Cao X, Wang H, Zhao J, Lu Z, Wang F, et al. Porcine lactoferrin-derived peptide LFP-20 modulates immune homoeostasis to defend lipopolysaccharide-triggered intestinal inflammation in mice. *Br J Nutr.* (2019) 121:1255–63. doi: 10.1017/S0007114519000485
100. Johansen FE, Kaetzel CS. Regulation of the polymeric immunoglobulin receptor and IgA transport: new advances in environmental factors that stimulate pIgR expression and its role in mucosal immunity. *Mucosal Immunol.* (2011) 4:598–602. doi: 10.1038/mi.2011.37
101. Kaetzel CS. Cooperativity among secretory IgA, the polymeric immunoglobulin receptor, and the gut microbiota promotes host-microbial mutualism. *Immunol Lett.* 2014 162(2 Pt A):10–21. doi: 10.1016/j.imlet.2014.05.008
102. Sheng X, Qian X, Tang X, Xing J, Zhan W. Polymeric immunoglobulin receptor mediates immune excretion of mucosal IgM-antigen complexes across intestinal epithelium in flounder *(Paralichthys olivaceus*). *Front Immunol.* (2018) 9:1562. doi: 10.3389/fimmu.2018.01562
103. Belkaid Y, Hand TW. Role of the microbiota in immunity and inflammation. *Cell.* (2014) 157:121–41. doi: 10.1016/j.cell.2014.03.011
104. Liang L, Wang ZJ, Ye G, Tang XY, Zhang YY, Kong JX, et al. Distribution of lactoferrin is related with dynamics of neutrophils in bacterial infected mice intestine. *Molecules.* (2020) 25:1496. doi: 10.3390/molecules 25071496
105. Latorre D, Berlutti F, Valenti P, Gessani S, Puddu P, LF. immunomodulatory strategies: mastering bacterial endotoxin. *Biochem Cell Biol.* (2012) 90:269–78. doi: 10.1139/o11-059

106. Wei LY, Liu C, Wang J, Zheng X, Peng Q, Ye QR, et al. Lactoferrin is required for early B cell development in C57BL/6 mice. *J Hematol Oncol.* (2021) 14:1–6. doi: 10.1186/s13045-021-01074-6
107. Zhou Y, He Y, Liu L, Zhou W, Wang P, Hu H, et al. Alterations in gut microbial communities across anatomical locations in inflammatory bowel diseases. *Front Nutr.* (2021) 8:615064. doi: 10.3389/fnut.2021.615064
108. Ng SC, Shi HY, Hamidi N, Underwood FE, Tang W, Benchimol EI, et al. Worldwide incidence and prevalence of inflammatory bowel disease in the 21st century: a systematic review of population-based studies. *Lancet.* (2017) 390:2769–78. doi: 10.1016/S0140-6736(17)32448-0
109. Scarano A, Butelli E, De Santis S, Cavalcanti E, Hill L, De Angelis M, et al. Combined dietary anthocyanins, flavonols, and stilbenoids alleviate inflammatory bowel disease symptoms in mice. *Front Nutr.* (2017) 4:75. doi: 10.3389/fnut.2017.00075
110. Wu X, Song M, Cai X, Neto C, Tata A, Han Y, et al. Chemopreventive effects of whole cranberry (*Vaccinium macrocarpon*) on colitis-associated colon tumorigenesis. *Mol Nutr Food Res.* (2018) 62:e1800942. doi: 10.1002/mnfr.201800942
111. Li F, Han Y, Cai X, Gu M, Sun J, Qi C, et al. Dietary resveratrol attenuated colitis and modulated gut microbiota in dextran sulfate sodium-treated mice. *Food Funct.* (2020) 11:1063–73. doi: 10.1039/C9FO01519A
112. Onishi H. Lactoferrin delivery systems: approaches for its more effective use. *Expert Opin Drug Deliv.* (2011) 8:1469–79. doi: 10.1517/17425247.2011.615829
113. Yao X, Bunt C, Cornish J, Quek SY, Wen J. Oral delivery of lactoferrin: a review. *Int J Peptide Res Ther.* (2013) 19:125–34. doi: 10.1007/s10989-012-9326-8
114. MacManus CF, Collins CB, Nguyen TT, Alfano RW, Jedlicka P, de Zoeten EF. VEN-120, a recombinant human lactoferrin, promotes a regulatory T cell [Treg] phenotype and drives resolution of inflammation in distinct murine models of inflammatory bowel disease. *J Crohns Colitis.* (2017) 11:1101–12. doi: 10.1093/ecco-jcc/jjx056
115. Bellamy W, Takase M, Yamauchi K, Wakabayashi H, Kawase K, et al. Identification of the bactericidal domain of lactoferrin. *Biochim Biophys Acta.* (1992) 1121:130–6. doi: 10.1016/0167-4838(92)90346-F
116. Lizzi AR, Carnicelli V, Clarkson MM, Nazzicone C, Segatore B, Celenza G, et al. Bovine lactoferrin and its tryptic peptides: antibacterial activity against different species. *Appl Biochem Microbiol.* (2016) 52:435–40. doi: 10.1134/S0003683816040116
117. Furlund CB, Ulleberg EK, Devold TG, Flengsrud R, Jacobsen M, Sekse C, et al. Identification of lactoferrin peptides generated by digestion with human gastrointestinal enzymes. *J Dairy Sci.* (2013) 96:75–88. doi: 10.3168/jds.2012-5946
118. Kuwata H, Yip TT, Tomita M, Hutchens TW. Direct evidence of the generation in human stomach of an antimicrobial peptide domain (lactoferricin) from ingested lactoferrin. *Biochim Biophys Acta.* (1998) 1429:129–41. doi: 10.1016/S0167-4838(98)00224-6
119. Kuwata H, Yip TT, Yip CL, Tomita M, Hutchens TW. Direct detection and quantitative determination of bovine lactoferricin and lactoferrin fragments in human gastric contents by affinity mass spectrometry. *Adv Exp Med Biol.* (1998) 443:23–32. doi: 10.1007/978-1-4757-9068-9_3
120. Hoffman JM, Sideri A, Ruiz JJ, Stavrakis D, Shih DQ, Turner JR, et al. Mesenteric adipose-derived stromal cells from crohn's disease patients induce protective effects in colonic epithelial cells and mice with colitis. *Cell Mol Gastroenterol Hepatol.* (2018) 6:1–16. doi: 10.1016/j.jcmgh.2018.02.001
121. Cader MZ, Kaser A. Recent advances in inflammatory bowel disease: mucosal immune cells in intestinal inflammation. *Gut.* (2013) 62:1653–64. doi: 10.1136/gutjnl-2012-303955
122. Weingarden AR, Vaughn BP. Intestinal microbiota, fecal microbiota transplantation, and inflammatory bowel disease. *Gut Microbes.* (2017) 8:238–52. doi: 10.1080/19490976.2017.1290757
123. Yan M, Dong S, Shen X, Lu C, Ye H, Zhang T. Lactoferrin-thymol complex for the disinfection of gram-positive Staphylococcus aureus and Gram-negative Escherichia coli. *Food Funct.* (2021). doi: 10.1039/D1FO02153B
124. de la Rosa G, Yang D, Tewary P, Varadhachary A, Oppenheim JJ. Lactoferrin acts as an alarmin to promote the recruitment and activation of APCs and antigen-specific immune responses. *J Immunol.* (2008) 180:6868–76. doi: 10.4049/jimmunol.180.10.6868
125. Hendrixson DR, Qiu J, Shewry SC, Fink DL, Petty S, Baker EN, et al. Human milk lactoferrin is a serine protease that cleaves Haemophilus surface proteins at arginine-rich sites. *Mol Microbiol.* (2003) 47:607–17. doi: 10.1046/j.1365-2958.2003.03327.x
126. Gomez HF, Ochoa TJ, Carlin LG, Cleary TG. Human lactoferrin impairs virulence of Shigella flexneri. *J Infect Dis.* (2003) 187:87–95. doi: 10.1086/345875
127. Drago-Serrano ME, de la Garza-Amaya M, Luna JS, Campos-Rodriguez R. Lactoferrin-lipopolysaccharide (LPS) binding as key to antibacterial and antiendotoxic effects. *Int Immunopharmacol.* (2012) 12:1–9. doi: 10.1016/j.intimp.2011.11.002
128. Patras KA, Ha AD, Rooholfada E, Olson J, Ramachandra Rao SP, Lin AE, et al. Augmentation of urinary lactoferrin enhances host innate immune clearance of uropathogenic *Escherichia coli*. *J Innate Immun.* (2019) 11:481–95. doi: 10.1159/000499342
129. Barbara G, Barbaro MR, Fuschi D, Palombo M, Falangone F, Cremon C. et al. Inflammatory and microbiota-related regulation of the intestinal epithelial barrier. *Front Nutr.* (2021) 8:718356. doi: 10.3389/fnut.2021.790387
130. Liu N, Yang Y, Chen J, Jia H, Zhang Y, Jiang D, et al. 3-Acetyldeoxynivalenol induces lysosomal membrane permeabilization-mediated apoptosis and inhibits autophagic flux in macrophages. *Environ Pollut.* (2020) 265(Pt B):114697. doi: 10.1016/j.envpol.2020.114697
131. Liu N, Ma X, Luo X, Zhang Y, He Y, Dai Z, et al. l-Glutamine Attenuates Apoptosis in porcine enterocytes by regulating glutathione-related redox homeostasis. *J Nutr.* (2018) 148:526–34. doi: 10.1093/jn/nxx062
132. Song L, Xie W, Liu Z, Guo D, Zhao D, Qiao X, et al. Oral delivery of a *Lactococcus lactis* strain secreting bovine lactoferricin-lactoferrampin alleviates the development of acute colitis in mice. *Appl Microbiol Biotechnol.* (2019) 103:6169–86. doi: 10.1007/s00253-019-09898-6
133. Cutone A, Rosa L, Lepanto MS, Scotti MJ, Berlutti F. Bonaccorsi di Patti MC, et al. Lactoferrin efficiently counteracts the inflammation-induced changes of the iron homeostasis system in macrophages. *Front Immunol.* (2017) 8:705. doi: 10.3389/fimmu.2017.00705
134. Chatterton DE, Nguyen DN, Bering SB, Sangild PT. Anti-inflammatory mechanisms of bioactive milk proteins in the intestine of newborns. *Int J Biochem Cell Biol.* (2013) 45:1730–47. doi: 10.1016/j.biocel.2013.04.028
135. Spagnuolo PA, Hoffman-Goetz L. Dietary lactoferrin does not prevent dextran sulfate sodium induced murine intestinal lymphocyte death. *Exp Biol Med (Maywood).* (2008) 233:1099–108. doi: 10.3181/0802-RM-53
136. Togawa J, Nagase H, Tanaka K, Inamori M, Umezawa T, Nakajima A, et al. Lactoferrin reduces colitis in rats via modulation of the immune system and correction of cytokine imbalance. *Am J Physiol Gastrointest Liver Physiol.* (2002) 283:G187–95. doi: 10.1152/ajpgi.00331.2001
137. Valenti P, Frioni A, Rossi A, Ranucci S, De Fino I, Cutone A, et al. Aerosolized bovine lactoferrin reduces neutrophils and pro-inflammatory cytokines in mouse models of *Pseudomonas aeruginosa* lung infections. *Biochem Cell Biol.* (2017) 95:41–7. doi: 10.1139/bcb-2016-0050
138. Sessa R, Di Pietro M, Filardo S, Bressan A, Rosa L, Cutone A, et al. Effect of bovine lactoferrin on *Chlamydia trachomatis* infection and inflammation. *Biochem Cell Biol.* (2017) 95:34–40. doi: 10.1139/bcb-2016-0049
139. Cutone A, Frioni A, Berlutti F, Valenti P, Musci G. Bonaccorsi di Patti MC. Lactoferrin prevents LPS-induced decrease of the iron exporter ferroportin in human monocytes/macrophages. *Biometals.* (2014) 27:807–13. doi: 10.1007/s10534-014-9742-7
140. Lepanto MS, Rosa L, Cutone A, Conte MP, Paesano R, Valenti P. Efficacy of lactoferrin oral administration in the treatment of anemia and anemia of inflammation in pregnant and non-pregnant women: an interventional study. *Front Immunol.* (2018) 9:2123. doi: 10.3389/fimmu.2018.02123
141. Paesano R, Pietropaoli M, Berlutti F, Valenti P. Bovine lactoferrin in preventing preterm delivery associated with sterile inflammation. *Biochem Cell Biol.* (2012) 90:468–75. doi: 10.1139/o11-060

142. Paesano R, Pacifici E, Benedetti S, Berlutti F, Frioni A, Polimeni A, et al. Safety and efficacy of lactoferrin versus ferrous sulphate in curing iron deficiency and iron deficiency anaemia in hereditary thrombophilia pregnant women: an interventional study. *Biometals.* (2014) 27:999–1006. doi: 10.1007/s10534-014-9723-x
143. Cutone A, Colella B, Pagliaro A, Rosa L, Lepanto MS. Bonaccorsi di Patti MC, et al. Native and iron-saturated bovine lactoferrin differently hinder migration in a model of human glioblastoma by reverting epithelial-to-mesenchymal transition-like process and inhibiting interleukin-6/STAT3 axis. *Cell Signal.* (2020) 65:109461. doi: 10.1016/j.cellsig.2019.109461
144. Frioni A, Conte MP, Cutone A, Longhi C, Musci G, di Patti MC, et al. Lactoferrin differently modulates the inflammatory response in epithelial models mimicking human inflammatory and infectious diseases. *Biometals.* (2014) 27:843–56. doi: 10.1007/s10534-014-9740-9
145. Chea C, Miyauchi M, Inubushi T, Febriyanti Ayuningtyas N, Subarnbhesaj A, Nguyen PT, et al. Molecular mechanism of inhibitory effects of bovine lactoferrin on the growth of oral squamous cell carcinoma. *PLoS ONE.* (2018) 13:e0191683. doi: 10.1371/journal.pone.0191683
146. Geremia A, Biancheri P, Allan P, Corazza GR, Di Sabatino A. Innate and adaptive immunity in inflammatory bowel disease. *Autoimmun Rev.* (2014) 13:3–10. doi: 10.1016/j.autrev.2013.06.004

Conflict of Interest: GF, XZ, and JS were employed by Inner Mongolia Yili Industrial Group, Co., Ltd.

The remaining authors declare that the research was conducted in the absence of any commercial or financial relationships that could be construed as a potential conflict of interest.

frontiers in Nutrition

ORIGINAL RESEARCH
published: 16 December 2021
doi: 10.3389/fnut.2021.746703

Glutamine Supplementation Enhances the Effects of a Low FODMAP Diet in Irritable Bowel Syndrome Management

*Samira Rastgoo[1], Nasser Ebrahimi-Daryani[2], Shahram Agah[3], Sara Karimi[2], Mohammad Taher[2], Bahram Rashidkhani[1], Ehsan Hejazi[1], Fatemeh Mohseni[1], Mina Ahmadzadeh[1], Amir Sadeghi[4] and Azita Hekmatdoost[1]**

[1] Department of Clinical Nutrition and Dietetics, Faculty of Nutrition and Food Technology, National Nutrition and Food Technology, Research Institute, Shahid Beheshti University of Medical Sciences, Tehran, Iran, [2] Department of Gastroenterology and Hepatology, Tehran University of Medical Sciences, Tehran, Iran, [3] Colorectal Research Center, Iran University of Medical Sciences, Tehran, Iran, [4] Gastroenterology and Liver Diseases Research Center, Research Institute for Gastroenterology and Liver Diseases, Shahid Beheshti University of Medical Sciences, Tehran, Iran

OPEN ACCESS

Edited by:
Xian Wu,
Miami University, United States

Reviewed by:
Xiaoqiong Cao,
University of Massachusetts Amherst, United States
Jianan Zhang,
University of Massachusetts Amherst, United States

***Correspondence:**
Azita Hekmatdoost
a_hekmat2000@yahoo.com

Specialty section:
This article was submitted to Nutritional Immunology, a section of the journal Frontiers in Nutrition

Received: 14 August 2021
Accepted: 18 November 2021
Published: 16 December 2021

Citation:
Rastgoo S, Ebrahimi-Daryani N, Agah S, Karimi S, Taher M, Rashidkhani B, Hejazi E, Mohseni F, Ahmadzadeh M, Sadeghi A and Hekmatdoost A (2021) Glutamine Supplementation Enhances the Effects of a Low FODMAP Diet in Irritable Bowel Syndrome Management. Front. Nutr. 8:746703. doi: 10.3389/fnut.2021.746703

Background and Aims: Although irritable bowel syndrome is one of the most common gastrointestinal disorders presented to gastroenterologists, therapeutic strategies are not yet well-established. Accordingly, we conducted a randomized, double-blind, placebo-controlled, clinical trial to evaluate the possible superiority of adding glutamine supplement to low fermentable oligo- di- monosaccharides and polyols (FODMAP) diet in patients with irritable bowel syndrome (IBS).

Methods: Eligible adults were randomized to receive a low FODMAP diet either with glutamine (15 g/day) or a placebo for 6 weeks. The primary endpoint was a significant reduction in IBS-symptom severity score (IBS-SSS). Secondary endpoints were changes in IBS symptoms, stool frequency, consistency, and quality of life.

Results: The study group enrolled 50 patients, among which 22 participants from each group completed the study protocol. The glutamine group had significant changes in total IBS-severity score, dissatisfaction of bowel habit and interference with community function (58% reduction; $P < 0.001$, 57% reduction; $P < 0.001$, 51% reduction; $P = 0.043$, respectively). Improvement in IBS-severity score of more than 45% was observed in 22 of 25 participants (88%) in the glutamine group, while it was only 15 of 25 participants (60%) in the control group ($p = 0.015$). No serious adverse events were observed.

Conclusions: Our findings indicated the superiority of adding glutamine supplementation to a low FODMAP diet in amelioration of IBS symptoms while confirming the beneficial effects of a low FODMAP diet in IBS management.

Keywords: irritable bowel syndrome (IBS), glutamine, diet, low FODMAP diet, clinical trial

INTRODUCTION

Although irritable bowel syndrome is one of the most prevalent referrals to gastroenterologists, the best method for managing it is still unknown (1, 2). The high prevalence of irritable bowel syndrome (IBS) besides suboptimal medical treatments leads to significant economic costs and psychosocial burden (3–5). The pathophysiology of IBS is multifactorial and the molecular mechanisms underlying the pathophysiology of IBS are not well-understood. However, dietary intolerance, alternation in gut microbiota, and increased intestinal permeability have been suggested as potential risk factors (3, 6, 7). Recent studies have shown that a diet low in fermentable oligosaccharides, disaccharides, monosaccharides, and polyols (FODMAPs) can improve gastrointestinal symptoms in patients with IBS (8–10); however, the patients on low FODMAPs diet are not completely free of symptoms (11). Moreover, the results of previous studies have mainly reported the efficacy of a low FODMAP diet on pain and bloating reduction, with no effect on stool consistency and frequency (8). Thus, it seems that we still need new strategies for IBS management with a special focus on stool consistency and frequency.

Glutamine is a non-essential amino acid that is a preferred energy source for cells with rapid turnover such as lymphocytes and enterocytes. This amino acid promotes enterocyte proliferation, regulates tight junction proteins, and suppresses pro-inflammatory signaling pathways (12). It has been reported that the increased intestinal permeability that occurs in diarrhea-predominant patients with IBS might be due to decreased glutamine synthetase levels (13). Meanwhile; experimental evidence suggests that glutamine supplementation reduces intestinal permeability (14, 15). Furthermore, glutamine supplementation changes the intestinal microenvironment and regulates intestinal bacteria's utilization and metabolism of amino acids, thereby altering the composition of intestinal microbiota (16, 17). Modulation of intestinal microbiota might ameliorate constipation and improve intestinal function (18, 19).

In light of this experimental evidence, we hypothesized that the co-administration of a low FODMAP diet and an oral glutamine supplement would reduce the symptoms and improve the quality of life of patients with IBS more effectively than a low FODMAP diet alone. Thus, the current randomized, double-blind, placebo-controlled trial was conducted to evaluate the effect of a low FODMAP diet with glutamine supplementation on patients with IBS' clinical outcomes and quality of life.

METHODS AND MATERIALS

Participants

This study's participants comprised patients with IBS (as defined by Rome IV criteria) (20) without any other disorders aged between 18 and 70 years old with body mass index (BMI) ranging from 18.5 to 25. Patients were recruited between June 2020 and December 2020 from two gastroenterology clinics in Tehran, Iran. Patients who did not have the following disorders were eligible to participate in the study: any organic intestinal diseases based on colonoscopy over the past 5 years, intestinal infection, history of colorectal disorders, major intestinal surgery, liver, kidney, psychiatric disease, or any GI disease other than IBS.

Patients were excluded from the study if they (a) were taking any medication with antispasmodics, antibiotics, anti-diarrhea or laxative properties, prokinetics, non-steroidal anti-inflammatory, and immunosuppressive agents or (b) were a smoker, pregnant, or breastfeeding. Patients with known allergies to glutamine or whey protein were excluded, as were those who were taking or had taken supplements containing glutamine or whey protein. Patients were also excluded if they had consumed synthetic sweeteners within 2 days before the study or during the study, as such sweeteners can alter intestinal permeability. Finally, any patients unwilling to adhere to the recommended diet were also excluded.

Patients were sub-classified as either having predominant diarrhea (IBS-D), predominant constipation (IBS-C), mixed or alternating bowel habits (IBS-M), or undetermined categories (IBS-U). All patients provided informed written consent to participate in the study after the study protocol was thoroughly explained.

Study Design and Intervention

This study was a randomized, double-blind, placebo-controlled trial. Fifty patients who met the inclusion criteria were randomly assigned to either the experimental (glutamine) or control (placebo) group. Randomization was based on a random table sequence, and all investigators were blind regarding which patients were in which group.

Since receiving 15 g of glutamine or whey does not cause side effects for patients (21), participants received an oral glutamine powder or placebo powder (whey protein) at a dose of 15 g (5 g mixed in water three times per day) for 6 weeks. The powders were similar in color, consistency, and taste. The supplements were concealed as A or B by a third party—for the duration of the study, neither the participants nor investigators knew which group was taking which supplement.

All participants were advised to follow a low FODMAP diet in addition to taking the assigned supplement. Diets were administered by an experienced dietitian according to the guidelines of the National Institute for Health and Care Excellence (NICE) while omitting high FODMAPs foods. All diets contained <5-g FODMAPs per day. Patients' adherence to the diet was evaluated by recording of 3 days (1 weekend and 2 workdays) dietary recalls at week 2 and the end of the study.

Dietary intakes of FODMAPs were assessed using Monash University's low-FODMAP diet database and quantitative reports of FODMAP content in recent studies (22, 23). Patients were followed by phone calls to assess protocol adherence, record any supplement side effects, and answer any study-related questions. Patients' competency was assessed using the measurement of remained supplements.

Study Outcomes

The primary outcome was a significant reduction in IBS-symptom severity score (IBS-SSS). Secondary outcomes were changes in IBS symptoms, quality of life, and stool consistency and frequency. All clinical outcomes were evaluated at baseline

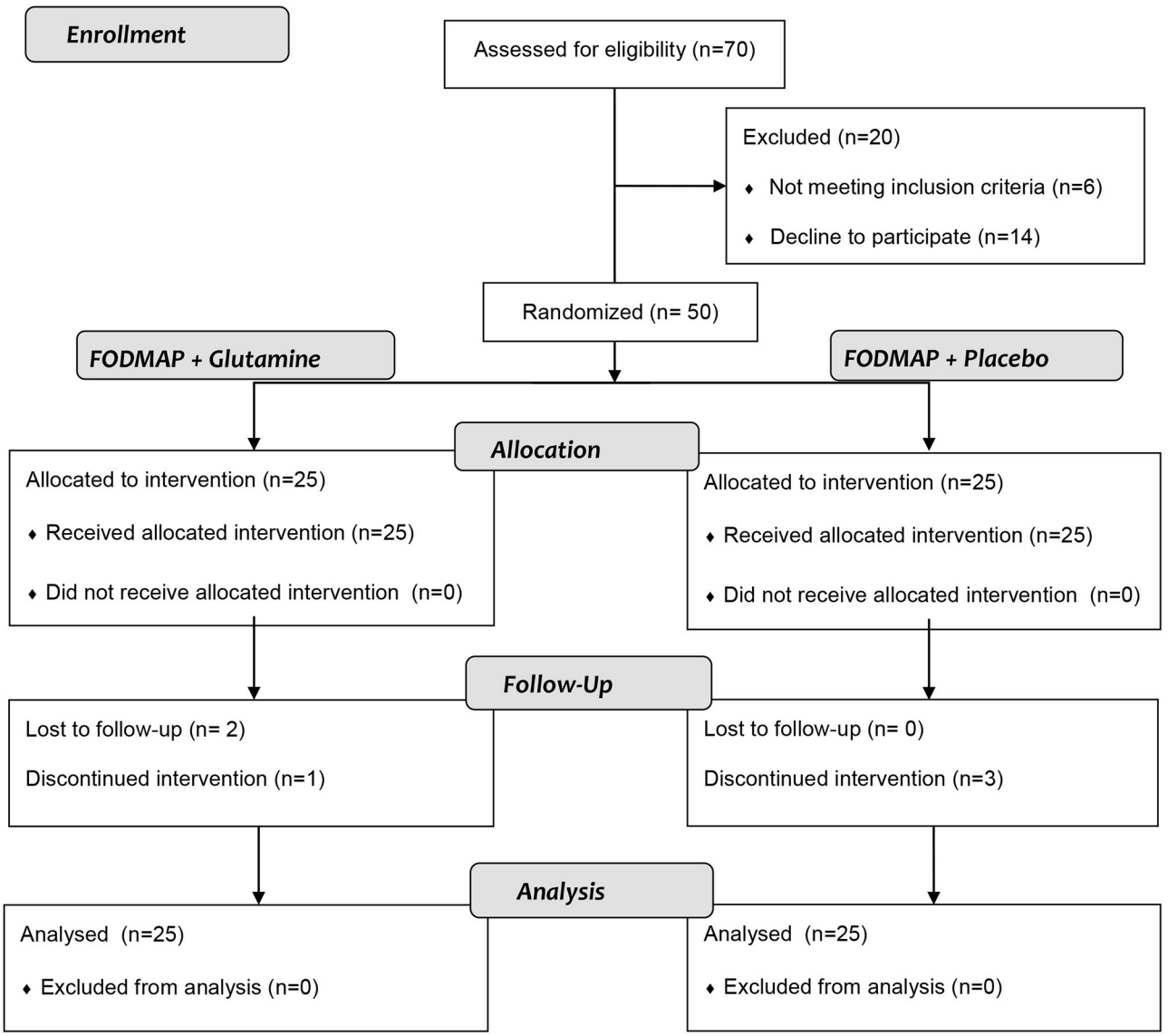

FIGURE 1 | Consort flow chart of the study.

and the end of the study using the IBS-SSSQ (24). This instrument includes five clinically relevant items that determine the severity of abdominal pain, the frequency of pain, abdominal distension, satisfaction with bowel habits, and the interference of IBS with community function as measured on the visual analog scale (VAS) (with an array of 100 mm, with 0 indicating no symptoms and 100 representing extremely severe symptom). The sum of these five items was IBS- symptom severity score (range = 0–500). Scores of 75–175, 175–300, and > 300 indicated mild, moderate, and severe cases, respectively.

Each patient's quality of life (QoL) was assessed at baseline and the end of the study using a 34-item self-report measure specific to IBS (IBS-QoL) (25). Each item was answered on a 5-point Likert scale, and participants' scores were summed to derive the overall score. Scores were subsequently transposed onto a scale from 0 to 100, with higher scores indicating a better quality of life.

Stool consistency was assessed using the validated Bristol Stool Form Scale (BSFS) (26). Stool frequency (i.e., number of stools per day) was recorded at baseline and the end of the study.

Statistical Analysis

The sample size was calculated based on the formula by considering α (type 1 error) = 0.05 and power of 80% according to the published article (11), which was obtained 21. Therefore, according to the formula 21 subjects were needed in each group, considering the probable dropouts, we assigned 25 subjects for each group to meet the adequate power.

TABLE 1 | Characteristics of participants with irritable bowel syndrome at the baseline.

Baseline characteristics	Glutamine ($n = 25$)	Control ($n = 25$)	*P*-value
Age (years)[a]	40.36 ± 15.15	35.09 ± 8.53	0.256
Sex—no. (%)[b]			0.540
Female	14 (56%)	16 (64%)	
Male	11 (44%)	9 (36%)	
Weight (kg)[a]	67.36 ± 8.44	63.09 ± 9.61	0.125
BMI (kg/m^2)[a]	23.48 ± 1.57	22.71 ± 1.62	0.118
IBS subtype—no. (%)[b]			0.215
Constipate	3 (12%)	4 (16%)	
Diarrhea	16 (64%)	14 (56%)	
mixed	6 (24%)	4 (16%)	
Unclassified	0	3 (12%)	
IBS symptoms[a]			
IBS-SSS	308.41 ± 82.44	278.86 ± 47.71	0.155
Abdominal pain intensity	65.91 ± 25.80	56.36 ± 15.44	0.092*
Abdominal pain frequency	52.73 ± 29.14	35 ± 18.71	**0.022***
Abdominal distension	56.14 ± 22.30	66.82 ± 12.20	0.292*
dissatisfaction with bowel habits	64.32 ± 29.93	49.77 ± 20.73	0.068
Interference with life	69.32 ± 22.43	70.91 ± 10.19	0.971*
Stool frequency (no./day)	2.95 ± 2.19	2.68 ± 2.05	0.685*
Stool consistency	5.14 ± 1.70	4.55 ± 1.62	0.240*
Quality of life[a]	63 ± 19.99	65 ± 10.44	0.652

[a]*Data are reported as mean ± SD and compared by independent sample t-test/Mann-Whitney test (*).*
[b]*Data are reported by n (percentage of total); the chi-square test was used.*
Statistically significant values in bold.

All hypothesis tests were 2-tailed, with $P < 0.05$ denoting statistical significance. The Kolmogorov–Smirnov-test with a significance level of 5% was used to test continuous variables for the normality assumption. The chi-square test or Fisher exact-test was used to determine the differences of categorical variables between groups. Comparison between the variables was performed by paired-samples *t*-test/Wilcoxon at the beginning and end of the study in each group. To detect differences in continuous variables between the two groups, independent-samples *t*-test/Mann-Whitney was used. The main effects and interaction effects of the interventions were compared between groups using analysis of covariance (ANCOVA) with baseline measures as a covariate. The data were analyzed according to the intention-to-treat principle. Patients missing the final data were imputed. A multiple imputation procedure was used based on multiple imputations by chained equation. In the multiple imputation procedure, five imputed data sets were generated. The results of the five imputed data sets were pooled to obtain data estimates.

Collected information by food diaries was analyzed in the Nutritionist 4 software modified for Iranian foods (Karen Pharma & Food Supplement Co., Tehran, Iran). Data from the food-record questionnaires were entered and analyzed by an expert dietitian.

Ethics and Approvals

The study protocol was approved by Shahid Beheshti Ethics Committee (IR.SBMU.NNFTRI.REC.1398.083), and it was registered at the Iranian Registry of Clinical Trials, with the registration number IRCT20100524004010N28.

RESULTS

Patient Characteristics

Between June 2020 and December 2020, 70 patients were recruited from two gastroenterology clinics and screened for this trial. From this initial group, 20 patients were excluded and the other 50 were enrolled and underwent the randomization process. Among the 50 included patients, 25 were assigned to the glutamine group and 25 were assigned to the placebo group. One patient was excluded from the glutamine group after discontinuing the study protocol, and two were lost to follow-up issues. Meanwhile, three patients from the control group were excluded due to non-compliance with the recommended diet. Therefore, 22 patients in the glutamine group and 22 patients in the control group completed the study protocol (**Figure 1**).

Table 1 shows the baseline characteristics of participants. The groups were similar in all characteristics except abdominal pain frequency ($p = 0.022$).

Nutritional Data

There was no significant difference in the nutritional compositions of the diet between the two groups (**Table 2**). All participants' dietary recalls demonstrated acceptable adherence to the diet.

TABLE 2 | The mean daily nutrition information during the study in intervention groups.

Parameter	Glutamine group ($n = 25$)		Control group ($n = 25$)			
	Week 2	Week 6	Week 2	Week 6	P^1	P^2
Energy (kcal)	1,799.64 ± 231.60	1,772.05 ± 226.64	1,888.5 ± 302.57	1,885.95 ± 285.05	0.280	0.286
Protein (gr)	73.53 ± 18.86	71.81 ± 22.96	81.30 ± 17.99	77.96 ± 16.64	0.170	0.315
Fat (gr)	67.40 ± 12.99	67.14 ± 14.15	67.08 ± 13.59	65.45 ± 12.29	0.936	0.778
Carbohydrates (gr)	224.61 ± 39.10	223.33 ± 39.33	242.26 ± 35.53	239.70 ± 44.88	0.139	0.205
Dietary fiber (gr)	11.32 ± 3.18	11.12 ± 3.02	12 ± 2.86	11.71 ± 3.64	0.461	0.557
Lactose (gr)	0.822 ± 1	0.622 ± 1.02	0.479 ± 0.69	0.277 ± 0.65	0.285	0.222
Excess fructose (gr)	0.150 ± 0.13	0.143 ± 0.09	0.272 ± 0.26	0.168 ± 0.13	0.051	0.953
Polyols (gr)	0.239 ± 0.33	0.191 ± 0.34	0.327 ± 0.35	0.254 ± 0.41	0.245	0.662
GOS (gr)	0.125 ± 0.09	0.150 ± 0.08	0.131 ± 0.05	0.161 ± 0.08	0.798	0.657
FOS (gr)	0.131 ± 0.08	0.186 ± 0.10	0.138 ± 0.06	0.193 ± 0.08	0.743	0.813
Total fructans (g)	0.475 ± 0.32	0.599 ± 0.28	0.507 ± 0.18	0.644 ± 0.30	0.418	0.613
Total FODMAP(g)	1.81 ± 1.36	1.70 ± 1.15	1.72 ± 0.87	1.50 ± 1.03	0.805	0.489

Data are reported as mean ± SD and compared by sample t-test.
P^1: between group at week 2.
P^2: between group at week 6.
GOS, galaco-oligosaccharide; FOS, fructo-ologosaccharides; FODMAP, fermentable oligo- di- mono- saccharides and polyols. Statistically significant values are bolded.

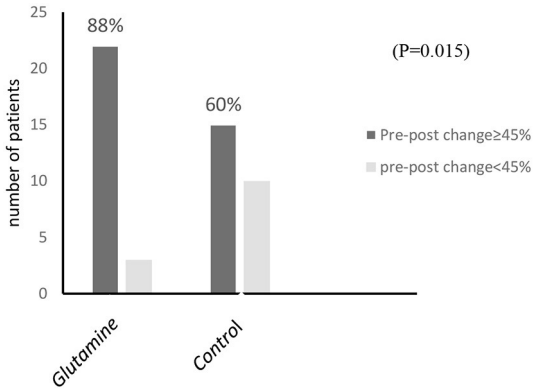

FIGURE 2 | The number of patients in both glutamine and control groups at the end of the study based on the percentage of change in IBS severity score.

Symptoms

Improvement in IBS-severity score of more than 45% was observed in 22 of 25 participants (88%) in the glutamine group, while it was only 15 of 25 participants (60%) in the control group ($P = 0.015$; **Figure 2**). The total scores of IBS-SS and the scores for individual items (abdominal pain intensity, abdominal pain frequency, abdominal distension, dissatisfaction with bowel habits, and interference with life), stool frequency, and consistency are shown in **Table 3**. Significant improvements were observed in these variables in both groups at the end of the study compared with the baseline ($p < 0.001$ for total scores and individual items of IBS-SSS and $P = 0.002$, $P = 0.003$, respectively, for stool frequency and consistency).

Table 4 shows the comparison of pre-post-treatment changes between the glutamine and placebo groups. The glutamine group had significant changes in total IBS-severity score, dissatisfaction of bowel habit and interference with community function (58% reduction; $P < 0.001$, 57% reduction; $P < 0.001$, 51% reduction; $P = 0.043$, respectively). No adverse effect was reported in any group of interventions.

Quality of Life

Baseline quality of life scores was not significantly different between the two groups (**Table 1**). The QOL scores increased in both intervention groups ($+13 \pm 8.12$, $P < 0.001$ in the glutamine group and $+11 \pm 5.12$, $P < 0.001$ in the control group) at the end of the study compared with the baseline (**Table 3**). No significant difference was observed between groups at the end of the study ($P = 0.353$).

DISCUSSION

The present study demonstrated the superiority of adding a glutamine supplement to a low FODMAP diet in amelioration of IBS symptoms while also confirming the beneficial effects of low FODMAPs diets in IBS management (9).

It is well-known that a low FODMAPs diet ameliorates IBS symptoms by reducing luminal distension owing to the osmotic effects of FODMAPs and their rapid fermentation preferentially to hydrogen (1, 10, 27). However, several studies have reported that increased intestinal permeability is another mechanism underlying IBS symptoms (7, 28). Moreover, it has been shown that this disturbance in gut integrity is related to decreased glutamine synthetase levels in patients with IBS (13). This, in turn, results in visceral hypersensitivity, leading to increased gastrointestinal symptoms (7, 13). Experimental evidence has also shown that glutamine improves intestinal permeability (29, 30).

TABLE 3 | Gastrointestinal symptoms and quality of life in patients with irritable bowel syndrome.

Parameter	Glutamine group ($n = 25$)			Control group ($n = 25$)		
	Baseline	Week 6	P^1	Baseline	Week 6	P^2
Total scores of IBS-SSS	308.41 ± 82.44	128.41 ± 41.30	<0.001	278.86 ± 47.71	151.59 ± 32.12	<0.001
Abdominal pain intensity	65.91 ± 25.80	29.09 ± 14.36	<0.001	56.36 ± 15.44	29.55 ± 11.64	<0.001
Abdominal pain frequency	52.73 ± 29.14	20 ± 10.69	<0.001	35 ± 18.71	18.64 ± 8.33	<0.001
Abdominal distension	56.14 ± 22.30	19.55 ± 8.58	<0.001	66.82 ± 12.20	26.14 ± 9.50	<0.001
dissatisfaction of bowel habits	64.32 ± 29.93	26.14 ± 14.63	<0.001	49.77 ± 20.73	35.68 ± 16.49	<0.001
Interference with life	69.32 ± 22.43	33.64 ± 13.64	<0.001	70.91 ± 10.19	41.59 ± 9.31	<0.001
Stool frequency (no./day)	2.95 ± 2.19	1.59 ± 0.796	0.002	2.68 ± 2.06	1.68 ± 0.894	0.002
Stool consistency	5.14 ± 1.70	4.00 ± 0.617	0.003	4.55 ± 1.62	3.82 ± 0.907	0.003
Quality of life	63.23 ± 19.99	76.32 ± 16.74	<0.001	65.41 ± 10.44	76.45 ± 9.86	<0.001

Values are reported as mean ± SD.
P^1: Obtained from the Wilcoxon test for comparison of data between the beginning and end of the study.
P^2: Obtained from the paired samples t-test for comparison of data between the beginning and end of the study.

TABLE 4 | Effects of intervention on studied outcomes.

Parameter	Pre-post change (%)		P^1-value	P^2-value
	Glutamine ($n = 25$)	Control ($n = 25$)		
Total scores of IBS-SSS	58% (–)	46% (–)	**<0.001**	**<0.001**
Abdominal pain intensity	56% (–)	48% (–)	0.072	0.195
Abdominal pain frequency	55% (–)	41% (–)	**0.027**	0.074
Abdominal distension	61% (–)	61% (–)	0.522	0.742
Dissatisfaction of bowel habits	57% (–)	28% (–)	**<0.001**	**<0.001**
Interference with life	51% (–)	41% (–)	**0.002**	**0.043**
Quality of life	27% (+)	18% (+)	0.205	0.327
Stool frequency (no./day)	39% (–)	29% (–)	0.182	0.194
Stool consistency	9% (–)	8% (–)	0.152	0.227

P^1-value: Obtained from two-sample t-test.
P^2-value: Obtained from ANCOVA test adjusted for the baseline values between studied groups. Statistically significant values are bolded.

On the other hand, low-grade inflammation has been observed in the intestinal mucosa of patients with IBS, especially those with increased intestinal permeability (31). Evidence shows that glutamine has anti-inflammatory properties, as it inhibits the activation of nuclear factor κB (NF-κB), signal transducer and activator of transcription (STAT), and inflammatory cytokines such as IL-6, TNF-α, and IL-8 (12).

Zhou et al. (32) reported that the up-regulation of microRNA29 in the colonic mucosa of patients with IBS-D reduces claudin-1 levels, which leads to increased intestinal permeability. Claudin-1 is an integral component of the structure of tight junctions and plays a crucial role in regulating epithelial barrier function (33). Therefore, the alteration of tight junction proteins might initiate IBS and contribute to visceral hypersensitivity (34, 35). Meanwhile, in an *ex-vivo* study evaluating the effects of glutamine on claudin-1 tight junction proteins, colonic biopsies from patients with IBS-D were incubated in cell cultures with glutamine, and the results indicated increased claudin-1 expression (14).

Studies investigating the effects of glutamine supplementation on the severity of gastrointestinal symptoms in patients with IBS are scarce. In line with our study, Zhou et al. (21) found that oral glutamine supplementation normalized intestinal permeability and improved gastrointestinal symptoms in post-infectious IBS. In this study, the patients did not receive dietary advice, so the changes in IBS symptoms were less than our study.

Moreover, recent studies have reported the potential role of intestinal microbiota in the pathophysiology of IBS (36–38). For instance, gut microbiota can affect motor function, hypersensitivity, and immune activity in the gut (resulting in low-grade inflammation), leading to the development of IBS or the exacerbation of gastrointestinal symptoms (37, 39). A recent review of *clinical*, *in vitro*, and *in vivo* studies reported that glutamine affects gut microbiota community and composition through several mechanisms. Therefore, it can be used to manage some conditions such as bacterial translocation, inflammation, and constipation (18). Furthermore, Zhang et al. reported that glutamine supplementation in constipated animals improves intestinal function and ameliorates constipation by modulating gut microbiota through increasing intestinal friendly microbiota levels (19).

The protective and therapeutic roles of glutamine have also been reported in clinical trials for other gastrointestinal diseases (40–42). Glutamine could possibly improve the condition of patients with IBS by regulating intestinal permeability *via* increased tight junction proteins expression, modulating the inflammatory response, oxidative stress, or innate immune response, and also altering intestinal microbiota (29).

This study has some advantages; According to our research, this is the first clinical trial that assessed the superiority of adding glutamine supplement to low FODMAPs in the management of patients with IBS. Preparing individually low FODMAPs diet, assessment of dietary composition, FODMAPs content, and also assessment of dietary adherence during the intervention were other strengths of this study. A limitation of this study was that patients were not followed up after the study ended. Given that national local factors affect the composition of FODMAPs in foods (27), measuring the content of FODMAPs using non-localized data was another limitation of our study.

CONCLUSION

In conclusion, this randomized, double-blind, placebo-controlled trial has shown the superiority of adding glutamine supplementation to a low FODMAPs diet in amelioration of IBS symptoms, while confirming the beneficial effects of a low FODMAPs diet in IBS management. Further studies are needed to find the optimum dosage of glutamine supplementation for IBS management.

DATA AVAILABILITY STATEMENT

The raw data supporting the conclusions of this article will be made available by the authors, without undue reservation.

ETHICS STATEMENT

The studies involving human participants were reviewed and approved by NNFTRI. The patients/participants provided their written informed consent to participate in this study.

AUTHOR CONTRIBUTIONS

SR and AH: conceptualized and designed the study and wrote the manuscript. SR and BR: analyzed the data. SR, NE-D, SA, FM, MA, MT, and SA: collected the data. EH and AH: interpreted the data and provided professional comments. AH: critically revised the manuscript for intellectual content, data accuracy, and had responsibility for the final content. All authors have read and approved the final manuscript.

FUNDING

This study was financially supported by Shahid Beheshti University of Medical Sciences, Tehran, Iran. The funder did not play any role in study design and interference.

REFERENCES

1. Portincasa P, Bonfrate L, de Bari O, Lembo A, Ballou S. Irritable bowel syndrome and diet. *Gastroenterol Rep.* (2017) 5:11–9. doi: 10.1093/gastro/gow047
2. Wilson B, Rossi M, Dimidi E, Whelan K. Prebiotics in irritable bowel syndrome and other functional bowel disorders in adults: a systematic review and meta-analysis of randomized controlled trials. *Am J Clin Nutr.* (2019) 109:1098–111. doi: 10.1093/ajcn/nqy376
3. Defrees DN, Bailey J. Irritable bowel syndrome: epidemiology, pathophysiology, diagnosis, and treatment. *Prim Care.* (2017) 44:655. doi: 10.1016/j.pop.2017.07.009
4. Ford AC, Moayyedi P, Chey WD, Harris LA, Lacy BE, Saito YA, et al. American College of Gastroenterology monograph on management of irritable bowel syndrome. *Am J Gastroenterol.* (2018) 113:1–18. doi: 10.1038/s41395-018-0084-x
5. Peery AF, Dellon ES, Lund J, Crockett SD, McGowan CE, Bulsiewicz WJ, et al. Burden of gastrointestinal disease in the United States: 2012 update. *Gastroenterology.* (2012) 143:1179–87.e3. doi: 10.1053/j.gastro.2012.08.002
6. Gwee KA, Ghoshal UC, Chen M. Irritable bowel syndrome in Asia: pathogenesis, natural history, epidemiology, and management. *J Gastroenterol Hepatol.* (2018) 33:99–110. doi: 10.1111/jgh.13987
7. Zhou Q, Zhang B, Verne GN. Intestinal membrane permeability and hypersensitivity in the irritable bowel syndrome. *Pain.* (2009) 146:41–6. doi: 10.1016/j.pain.2009.06.017
8. Altobelli E, Del Negro V, Angeletti PM, Latella G. Low-FODMAP diet improves irritable bowel syndrome symptoms: a meta-analysis. *Nutrients.* (2017) 9:940. doi: 10.3390/nu9090940
9. Halmos EP, Power VA, Shepherd SJ, Gibson PR, Muir JG. A diet low in FODMAPs reduces symptoms of irritable bowel syndrome. *Gastroenterology.* (2014) 146:67–75.e5. doi: 10.1053/j.gastro.2013.09.046
10. Whelan K, Martin LD, Staudacher HM, Lomer MC. The low FODMAP diet in the management of irritable bowel syndrome: an evidence-based review of FODMAP restriction, reintroduction and personalisation in clinical practice. *J Hum Nutr Diet.* (2018) 31:239–55. doi: 10.1111/jhn.12530
11. Abhari K, Saadati S, Hosseini-Oskouiee F, Yari Z, Hosseini H, Sohrab G, et al. Is Bacillus coagulans supplementation plus low FODMAP diet superior to low FODMAP diet in irritable bowel syndrome management? *Eur J Nutr.* (2020) 59:2111–7. doi: 10.1007/s00394-019-02060-y
12. Kim M-H, Kim H. The roles of glutamine in the intestine and its implication in intestinal diseases. *Int J Mol Sci.* (2017) 18:1051. doi: 10.3390/ijms18051051
13. Zhou Q, Souba WW, Croce CM, Verne GN. MicroRNA-29a regulates intestinal membrane permeability in patients with irritable bowel syndrome. *Gut.* (2010) 59:775–84. doi: 10.1136/gut.2009.181834
14. Bertrand J, Ghouzali I, Guérin C, Bôle-Feysot C, Gouteux M, Déchelotte P, et al. Glutamine restores tight junction protein claudin-1 expression in colonic mucosa of patients with diarrhea-predominant irritable bowel syndrome. *J Parent Enteral Nutr.* (2016) 40:1170–6. doi: 10.1177/0148607115587330
15. Wang W, Qiao S, Li D. Amino acids and gut function. *Amino Acids.* (2009) 37:105–10. doi: 10.1007/s00726-008-0152-4
16. Dai Z-L, Li X-L, Xi P-B, Zhang J, Wu G, Zhu W-Y. L-Glutamine regulates amino acid utilization by intestinal bacteria. *Amino Acids.* (2013) 45:501–12. doi: 10.1007/s00726-012-1264-4
17. Dai Z-L, Wu G, Zhu W-Y. Amino acid metabolism in intestinal bacteria: links between gut ecology and host health. *Front Biosci.* (2011) 16:1768–86. doi: 10.2741/3820
18. Perna S, Alalwan TA, Alaali Z, Alnashaba T, Gasparri C, Infantino V, et al. The role of glutamine in the complex interaction between gut microbiota and health: a narrative review. *Int J Mol Sci.* (2019) 20:5232. doi: 10.3390/ijms20205232
19. Zhang Y, Lu T, Han L, Zhao L, Niu Y, Chen H. L-glutamine supplementation alleviates constipation during late gestation of mini

sows by modifying the microbiota composition in feces. *BioMed Res Int*. (2017). 2017:2861. doi: 10.1155/2017/4862861
20. Drossman DA. Functional gastrointestinal disorders: history, pathophysiology, clinical features, and Rome IV. *Gastroenterology*. (2016) 150:1262–79.e2. doi: 10.1053/j.gastro.2016.02.032
21. Zhou Q, Verne ML, Fields JZ, Lefante JJ, Basra S, Salameh H, et al. Randomised placebo-controlled trial of dietary glutamine supplements for postinfectious irritable bowel syndrome. *Gut*. (2019) 68:996–1002. doi: 10.1136/gutjnl-2017-315136
22. Biesiekierski JR, Rosella O, Rose R, Liels K, Barrett J, Shepherd SJ, et al. Quantification of fructans, galacto-oligosacharides and other short-chain carbohydrates in processed grains and cereals. *J Hum Nutr Diet*. (2011) 24:154–76. doi: 10.1111/j.1365-277X.2010.01139.x
23. Muir JG, Rose R, Rosella O, Liels K, Barrett JS, Shepherd SJ, et al. Measurement of short-chain carbohydrates in common Australian vegetables and fruits by high-performance liquid chromatography (HPLC). *J Agric Food Chem*. (2009) 57:554–65. doi: 10.1021/jf802700e
24. Lembo A, Ameen VZ, Drossman DA. Irritable bowel syndrome: toward an understanding of severity. *Clin Gastroenterol Hepatol*. (2005) 3:717–25. doi: 10.1016/S1542-3565(05)00157-6
25. Gholamrezaei A, Zolfaghari B, Farajzadegan Z, Nemati K, Daghaghzadeh H, Tavakkoli H, et al. Linguistic validation of the irritable bowel syndrome-quality of life questionnaire for Iranian patients. *Acta Med Iran*. (2011) 49:390–5.
26. Blake M, Raker J, Whelan K. Validity and reliability of the Bristol Stool Form Scale in healthy adults and patients with diarrhoea-predominant irritable bowel syndrome. *Aliment Pharmacol Ther*. (2016) 44:693–703. doi: 10.1111/apt.13746
27. Varney J, Barrett J, Scarlata K, Catsos P, Gibson PR, Muir JG. FODMAPs: food composition, defining cutoff values and international application. *J Gastroenterol Hepatol*. (2017) 32:53–61. doi: 10.1111/jgh.13698
28. Dunlop SP, Hebden J, Campbell E, Naesdal J, Olbe L, Perkins AC, et al. Abnormal intestinal permeability in subgroups of diarrhea-predominant irritable bowel syndromes. *Am J Gastroenterol*. (2006) 101:1288–94. doi: 10.1111/j.1572-0241.2006.00672.x
29. Achamrah N, Déchelotte P, Coëffier M. Glutamine and the regulation of intestinal permeability: from bench to bedside. *Curr Opin Clin Nutr Metabolic Care*. (2017) 20:86–91. doi: 10.1097/MCO.0000000000000339
30. dos Santos RdGC, Viana ML, Generoso SV, Arantes RE, Davisson Correia MIT, Cardoso VN. Glutamine supplementation decreases intestinal permeability and preserves gut mucosa integrity in an experimental mouse model. *J Parent Enteral Nutr*. (2010) 34:408–13. doi: 10.1177/0148607110362530
31. Ng QX, Soh AYS, Loke W, Lim DY, Yeo WS. The role of inflammation in irritable bowel syndrome (IBS). *J Inflamm Res*. (2018) 11:345–9. doi: 10.2147/JIR.S174982
32. Zhou Q, Costinean S, Croce CM, Brasier AR, Merwat S, Larson SA, et al. MicroRNA 29 targets nuclear factor-κB–repressing factor and Claudin 1 to increase intestinal permeability. *Gastroenterology*. (2015) 148:158–69.e8. doi: 10.1053/j.gastro.2014.09.037
33. Pope JL, Bhat AA, Sharma A, Ahmad R, Krishnan M, Washington MK, et al. Claudin-1 regulates intestinal epithelial homeostasis through the modulation of Notch-signalling. *Gut*. (2014) 63:622–34. doi: 10.1136/gutjnl-2012-304241
34. Bertiaux-Vandaële N, Youmba SB, Belmonte L, Lecleire S, Antonietti M, Gourcerol G, et al. The expression and the cellular distribution of the tight junction proteins are altered in irritable bowel syndrome patients with differences according to the disease subtype. *Am J Gastroenterol*. (2011) 106:2165–73. doi: 10.1038/ajg.2011.257
35. Martínez C, Vicario M, Ramos L, Lobo B, Mosquera JL, Alonso C, et al. The jejunum of diarrhea-predominant irritable bowel syndrome shows molecular alterations in the tight junction signaling pathway that are associated with mucosal pathobiology and clinical manifestations. *Am J Gastroenterol*. (2012) 107:736–46. doi: 10.1038/ajg.2011.472
36. Collins SM. A role for the gut microbiota in IBS. *Nat Rev Gastroenterol Hepatol*. (2014) 11:497–505. doi: 10.1038/nrgastro.2014.40
37. Dupont H. evidence for the role of gut microbiota in irritable bowel syndrome and its potential influence on therapeutic targets. *Aliment Pharmacol Ther*. (2014) 39:1033–42. doi: 10.1111/apt.12728
38. Lee KN, Lee OY. Intestinal microbiota in pathophysiology and management of irritable bowel syndrome. *World J Gastroenterol*. (2014) 20:8886. doi: 10.3748/wjg.v20.i10.2456
39. Jeffery IB, Quigley EM, Öhman L, Simrén M, O'Toole PW. The microbiota link to irritable bowel syndrome: an emerging story. *Gut Microbes*. (2012) 3:572–6. doi: 10.4161/gmic.21772
40. Benjamin J, Makharia G, Ahuja V, Rajan KA, Kalaivani M, Gupta SD, et al. Glutamine and whey protein improve intestinal permeability and morphology in patients with Crohn's disease: a randomized controlled trial. *Dig Dis Sci*. (2012) 57:1000–12. doi: 10.1007/s10620-011-1947-9
41. Schanuel CM, Dias EN, Ferreira AP. Glutamine as a therapeutic strategy in inflammatory bowel diseases: a systematic review. *Gastroint Hepatol Dig Dis*. (2019) 2:1–6. doi: 10.33425/2639-9334.1033
42. Xue P, Deng L-H, Xia Q, Zhang Z-D, Hu W-M, Yang X-N, et al. Impact of alanyl-glutamine dipeptide on severe acute pancreatitis in early stage. *World J Gastroenterol*. (2008) 14:474. doi: 10.3748/wjg.14.474

Conflict of Interest: The authors declare that the research was conducted in the absence of any commercial or financial relationships that could be construed as a potential conflict of interest.

Publisher's Note: All claims expressed in this article are solely those of the authors and do not necessarily represent those of their affiliated organizations, or those of the publisher, the editors and the reviewers. Any product that may be evaluated in this article, or claim that may be made by its manufacturer, is not guaranteed or endorsed by the publisher.

frontiers in Immunology

ORIGINAL RESEARCH
published: 21 February 2022
doi: 10.3389/fimmu.2022.781934

Effects of Dietary Astragalus Polysaccharide Supplementation on the Th17/Treg Balance and the Gut Microbiota of Broiler Chickens Challenged With Necrotic Enteritis

*Bochen Song[1,2], Peng Li[1], Shaojia Yan[1], Yan Liu[1], Mingkun Gao[1], Huiyuan Lv[1,3], Zengpeng Lv[1] and Yuming Guo[1]**

[1] State Key Laboratory of Animal Nutrition, College of Animal Science and Technology, China Agricultural University, Beijing, China, [2] Department of Animal Science, Shandong Agricultural University, Taian, China, [3] Centre Research Institute, Beijing Centre Biology Co., Ltd., Beijing, China

OPEN ACCESS

Edited by:
Fang Li,
Columbia University Irving Medical Center, United States

Reviewed by:
Wen-Chao Liu,
Guangdong Ocean University, China
Yanhui Han,
University of Massachusetts Amherst, United States

***Correspondence:**
Yuming Guo
guoyum@cau.edu.cn

Specialty section:
This article was submitted to Nutritional Immunology, a section of the journal Frontiers in Immunology

Received: 23 September 2021
Accepted: 31 January 2022
Published: 21 February 2022

Citation:
Song B, Li P, Yan S, Liu Y, Gao M, Lv H, Lv Z and Guo Y (2022) Effects of Dietary Astragalus Polysaccharide Supplementation on the Th17/Treg Balance and the Gut Microbiota of Broiler Chickens Challenged With Necrotic Enteritis. Front. Immunol. 13:781934. doi: 10.3389/fimmu.2022.781934

This study aimed to investigate the effects of dietary astragalus polysaccharide (APS) supplementation on the immune function, gut microbiota and metabolism of broiler chickens challenged with necrotic enteritis (NE). Two hundred forty Arbor Acres broiler chicks (one day old) were randomly assigned using a 2 × 2 factorial arrangement into two groups fed different levels of dietary APS (0 or 200 ppm of diet) and two disease challenge groups (control or NE challenged). The results showed that NE infection significantly increased FCR, mortality rate, Th17/Treg (Th17 cells% in blood and ileum, Th17/Treg, IL-17 and IL-17/IL-10 in blood), NO, lysozyme activity and IL-1β in blood, intestinal immune cell proportion and activity (Tc%, Treg% and monocyte phagocytic activity in ileum), intestinal inflammatory cytokines (TLR2, NF-κB, TNF-α and IL- 6) gene expression levels, and the number of *Clostridium perfringens* in cecum. NE infection significantly reduced body weight gain, thymus index, lymphocyte proliferation activity in blood and ileum, villus height and V/C in jejunum, Th cells% and Mucin2 gene expression in ileum. Dietary APS supplementation significantly increased body weight, feed intake, proportion of immune cells (T cells in blood and Tc, Treg in ileum), lymphocyte proliferation activity, V/C in jejunum, and ZO-1 gene expression in ileum. Dietary APS supplementation significantly reduced FCR and mortality rate, Th17/Treg, Th17%, intestinal pathology scores, intestinal inflammatory cytokine gene expression levels, and the number of *Clostridium perfringens* in cecum. In addition, broilers challenged with NE significantly increased *Staphylococcus* and *Turicibacter* and reduced α diversity of microbiota in ileum. Dietary APS supplementation significantly increased α diversity, *Romboutsia*, *Halomonas*, propionic acid, butyric acid, formononetin, taurine, cholic acid and equol and downregulated uric acid, L-arginine and serotonin in ileum. Spearman's correlation analysis revealed that *Romboutsia, Turicibacter, Staphylocpccus, Halomonas, Streptococcus, Escherichia-Shigella, Prevotella*, uric acid, L-arginine,

jerivne, sodium cholate and cholic acid were related to inflammation and Th17/Treg balance. In conclusion, APS alleviated intestinal inflammation in broilers challenged with NE probably by regulating intestinal immune, Th17/Treg balance, as well as intestinal microbiota and metabolites.

Keywords: necrotic enteritis, astragalus polysaccharide (APS), Th17/Treg, gut microbiota, gut metabolome, broiler chickens

INTRODUCTION

Necrotic enteritis (NE) is an enterotoxic disease caused by type A or type C *Clostridium perfringens*. The mortality rate of necrotizing enteritis is high, and the mortality rate can be as high as 50% when an acute disease occurs, especially when it occurs in chicks, while chronic necrotizing enteritis will significantly reduce the growth performance of chickens, causing intestinal ulcers, erosions, and other adverse effects, seriously affecting the health of poultry and causing serious economic losses to the poultry farming industry (1, 2).

Helper T cells 17 (Th17) and regulatory T cells (Treg) are two closely related T cell types. They play key roles in promoting the immune response and suppressing immunity, respectively. Th17 cells and Tregs coordinate and balance to maintain the normal immune function of animals. Previous studies have found that IL-1β is significantly increased when intestinal inflammation occurs in mice and mediates chronic intestinal inflammation by promoting the accumulation of IL-17A-secreting innate lymphoid cells and Th17 cells (3). Studies have also reported that mice challenged with enterotoxigenic *Escherichia coli* significantly increase the proportions of Th17 and Treg cells in the spleen and intestinal mucosal lymph nodes, upregulate the mRNA and protein expression of RORα in the intestinal mucosal lymph nodes, and downregulate the mRNA and protein expression of Foxp3 (4). In addition, a study found that TNBS- and DSS-induced colitis in mice can significantly increase the level of IL-17 in the intestine (5). Chickens challenged with *coccidia* significantly increase the proportions of Th17 cells in the spleen and caecal tonsils (6). Th17/Treg cells have been widely studied in mammals with ulcerative colitis, but there are no reports about changes in the Th17 cell ratio in broilers challenged with necrotic enteritis.

Chickens with healthy intestines can not only improve the digestion and absorption rate of feed nutrients, but also resist the invasion of intestinal pathogenic bacteria and reduce economic losses caused by disease deaths and complications, which are the key factors to ensure good growth performance of chickens (7). Factors that affect gut health include diet, pathogens, environment, and management. Plant polysaccharides can "escape" the absorption of the small intestine, reach the second half of the intestine and be fermented by the microbiota, and exhibit anti-inflammatory, immune regulation, intestinal barrier protection, antioxidant functions and other activities through a microbiota-dependent or independent mechanism, and thus has become a research hotspot (8–10).

Astragalus polysaccharide (APS) can regulate the immune function of the body. With immune-enhancing and anti-inflammatory properties, it has a unique two-way regulatory ability. Studies have found that the addition of 4 mg/kg APS to the diet has an immunomodulatory effect on broilers challenged by LPS and can reverse the negative effects of LPS. This includes decreases in daily weight gain and feed intake and decreases in the number of intraepithelial lymphocytes and villus height in the jejunum. APS can also reduce the feed conversion rate, serum NO levels and the heterophilic cell/lymphocyte (H: L) ratio (11). Studies in mice have found that APS may effectively alleviate TNBS-induced experimental colitis in rats by restoring the number of Treg cells and inhibiting the level of IL-17 in Pyle's nodes (12). However, the effect of APS on Th17/Treg balance has not been reported in poultry.

According to reports, gut microbiota and metabolites can regulate the ratio of Th17 and Treg cells and the levels of cytokines in animal intestines (13). The molecular weight of APS will be large, and it is difficult for the endogenous enzymes produced in the animal intestine to completely degrade it into monosaccharides; thus, APS can easily reach the back of the intestine, where it is utilized by microorganisms. Therefore, in addition to its similar structure to LPS, APS can directly regulate the immune function of the host and may also indirectly affect the immune function of the host by regulating the gut microbiota and metabolites. Previous studies have found that adding 200 ppm APS to hen diets increases the relative abundance of caecal *Firmicutes* and *Lactobacteriaceae* (14). The addition of γ-irradiated Astragalus polysaccharide (IAPS) to the diet of immunosuppressive broilers significantly increased the caecal microbial α diversity. After adding IAPS to broiler diets, there were lower proportions of *Faecalibacterium*, *Bacteroides*, and

Abbreviations: AhR, Aryl hydrocarbon receptor; APS, Astragalus polysaccharide; BWG, Body weight gain; Con A, Concanavalin A; DTT, 1,4-DL-Dithiothreitol; ELISA, Enzyme-linked immuno sorbent assay; FBS, Fetal bovine serum; FI, Feed intake; Foxp3, Forkhead transcription factor p 3; GAPDH, Glyceraldehyde-3-phosphate dehydrogenase; IFN-γ, Interferon-γ; IgA, Immunoglobulin A; IL-1β, Interleukin-1β; iNOS, inducible nitric oxide synthase; IRAK4, Interleukin-1 receptor associated kinase-4; LPL, Lamina propria lymphocytes; LPS, Lipopolysaccharide; LYZ, Lysozyme; MTT, A 3-(4,5-dimethylthiazol)-2,5-diphenyltetrazolium bromide; NE, Necrotic enteritis; NF-κB, Nuclear factor-κB; NLRP3, NOD-like receptor family proteins 3; NO, Nitrogen Oxide; PBMC, Peripheral blood mononuclear cell; PBS, Phosphate buffered saline; pIgR, Polymeric immunoglobulin receptor; PLS-DA, Partial least squares discrimination analysis; RT-PCR, Reverse transcription-rolymerase chain reaction; sIgA, Secretory immunoglobulin A; Tc cell, Cytotoxic T cell; TGF-β, Transforming growth factor-β; Th cell, Helper T cell; TLR2, Toll-like receptor; TNF-α, Tumor necrosis factor α; Treg cell, Regulatory cell; TSC, Tryptone-sulfite-cycloserine agar medium; V/C, Villi height/crypt depth; ZO-1, Zonula occludens-1.

Butyricicoccus and higher proportions of *Ruminococcaceae UCG-014*, *Negativibacillus*, *Shuttleworthia*, *Sellimonas* and *Lamina RF39_norank* (15). The study found that adding 0.5% crude *Astragalus* to the hen's diet significantly increased *Lactobacillus* in faeces and significantly reduced the relative abundance of *Romboutsia* sp (16).. However, the effects of APS on the ratios of Th17 cells and Tregs in broilers with necrotizing enteritis and the key gut microbes and metabolites that it regulates have not been extensively studied. In view of the ability of APS to regulate the T cell immune response, the importance of T cell immunity in enteritis, and the ability of gut microbiota to regulate T cell subsets, in this study, we explored whether dietary APS supplementation might regulate CD4+ T cell immunity and the gut microbiota and metabolism of broilers with necrotic enteritis. We hypothesize that dietary APS supplementation will regulate the TLRs-NFκB signalling pathway and gut microbiota and metabolism, leading to a dominant position of Tregs, regulating the balance of Th17/Treg, thereby reducing intestinal inflammation and preventing tissue damage.

MATERIALS AND METHODS

Astragalus Polysaccharide

The APS used in this study was purchased from Beijing Centre Biology Co., Ltd. (Beijing). The APS was extracted from the *Astragalus membranaceus* (Fisch.) Bge. var. *mongholicus* (Bge.) Hsiao. The purity of APS is 80%. The molecular weight of APS was determined by LC-MS, ranging from 8 to 160,000 Daltons. According to the best dosage recommended by Beijing Centre Biology Co., Ltd., the added dosage of APS in this study was 200ppm.

Experimental Animals and Diets

Two hundred forty Arbor Acres broiler chicks (one day old) were randomly assigned using a 2 × 2 factorial arrangement into two groups fed different levels of dietary APS (0 or 200 ppm of diet) and two disease challenge groups (control or NE challenged). According to the recommendations of the National Research Council (NRC 2012), drug-free corn-soybean meal diets should be formulated to meet or exceed the nutritional requirements of broilers (**Table 1**). A double-layer, three-dimensional chicken coop was used, and standard management procedures were followed throughout the experiment. The chickens had free access to clean water and feed.

Establishment of the Necrotic Enteritis Model

A broiler subclinical NE model was constructed based on previous research experience (17). The method was as follows: feed was cut 8 hours in advance, and then on the 13th day of age, broiler chickens in the challenge group were orally inoculated with 30 times the dose of attenuated coccidia IV vaccine, 33,000 sporangia per chicken (containing Eimeria acervulina PAHY strain, Eimeria giant PMHY strain, Eimeria tenella PTMZ strain, and Eimeria tenella PNHZ strain Attenuated oocysts, Foshan

TABLE 1 | Ingredients and composition (calculated and analyzed nutrients) of the experimental diets[a] (%, unless otherwise noted, as-fed basis).

Item	d 1 to 21	d 22 to 31
Composition, %		
Corn (7.8% CP)	51.38	60.02
Soybean meal (46% CP)	40.71	25.54
Corn protein flour	0.00	5.66
Soybean oil	3.75	3.32
Wheat flour	0.00	2.00
$CaHPO_3.2H_2O$	1.86	1.33
Stone powder (37%)	1.24	1.14
Sodium chloride	0.35	0.35
DL-Methionine (98%)	0.20	0.070
L-Lysine HCL (98%)	0.00	0.19
Vitamin premix[b]	0.03	0.03
Mineral premix[c]	0.20	0.20
Choline chloride (50%)	0.25	0.16
Sandoquin (Ethoxyquinoline)	0.030	0.00
Calculated nutrient levels[d]		
Metabolizable energy (Kcal/kg)	2928.97	3100.00
Crude protein	21.76	20.00
Calcium	1.01	0.90
Available phosphorus	0.44	0.35
Lysine	1.14	1.00
Methionine	0.54	0.40

[a]*Diets were in mash form.*

[b]*Vitamin premix provided per kg of complete diet: vitamin A(retinylacetate), 9,500 IU; vitamin D3 (cholecalciferol), 2,500 IU; vitamin E(DL-a-tocopherol acetate), 30 IU; vitamin K3 (menadione sodium bisulfate), 2.65 mg; vitamin B12(cyanocobalamin), 0.025 mg; biotin, 0.30 mg; folic acid, 1.25 mg; nicotinic acid, 50 mg; d-pantothenic acid, 12 mg; pyridoxine hydrochloride, 6.0 mg; riboflavin, 6.5 mg; thiamine mononitrate, 3.0 mg.*

[c]*Mineral premix provided per kg of complete diet: iron, 80 mg; copper, 8 mg; manganese, 100 mg; zinc, 80 mg; iodine, 0.35 mg; selenium, 0.15 mg.*

[d]*Calculated value based on the analysis of experimental diets.*

Biotechnology Co., Ltd., Foshan, China). In the control group, 1 mL of sterile PBS was administered orally at the same time. Feed was cut 8 hours in advance, and then at the age of 17 to 23 for seven consecutive days of challenge, all the broiler chickens in the challenge group were orally inoculated with 1 mL of freshly prepared *Clostridium perfringens* CVCC2030 at a concentration of 1×10^9 CFU/mL (China Veterinary Drug Control Center, Beijing, China). Broilers in the control group were force-fed the same volume (1 mL) of sterilized thioglycolate fluid medium (FT, CM801, Beijing Luqiao Technology Co., Ltd.) at the same time point.

Sample Collection and Index Determination

Growth Performance

At 13, 25, and 31 days of age, feed and broilers were weighed in cages to calculate the average daily feed intake (ADFI), average daily gain (ADG), feed conversion rate (FCR) and mortality rate. All chicken coops were checked every day for broiler deaths.

Immune Organ Index

At 2 days and 8 days after infection, namely, 25 and 31 days of age, 6 healthy chickens were randomly selected for each treatment (1 for each replicate). After weighing, the chickens were euthanized by intravenous injection of 50 mg/kg body weight sodium pentobarbital solution under the wings. The thymus, spleen and bursa of fabricius were collected and weighed. Immune organ index (g/kg) = immune organ weight (g)/body weight (kg).

Peripheral Blood Mononuclear Cell Isolation

The isolation of peripheral blood mononuclear cells (PBMC) was conducted as previously described (18) using density gradient centrifugation with Ficoll-Paque Plus following the manufacturer's guidelines. Briefly, six healthy chickens (1 bird per replicate) were randomly selected from each treatment group on d 25 and 31. Heparinized blood samples were collected from the wing vein and then diluted 1:1 with sterile calcium- and magnesium-free Hank's balanced salt solution (CMF-HBSS, Sigma). The diluted samples were placed on ice and then carefully layered into a tube containing an equal volume of Ficoll lymphocyte separation medium (Histopague-1077, Tianjin HaoYang Biological Manufacture Co., Ltd., China) to form a distinct layer above the Ficoll. Following centrifugation at 400 $\times g$ for 30 min at room temperature, the white flocculent material on the interface between the plasma and the lymphocyte separation medium was transferred to a clean tube using a sterile transfer pipette. The lymphocyte suspension was washed 3 times with RPMI 1640 (Invitrogen Corp., Grand Island, NY, USA) incomplete culture medium and then resuspended in 2 mL of RPMI 1640 complete culture medium supplemented with 5% (vol/vol) fetal calf serum, 0.5% penicillin (final concentration, 100 U/mL), 0.5% streptomycin (final concentration, 100 mg/mL), and 1% N-(2-hydroxyethyl)-piperazine-N-2-ethanesulfonic acid (HEPES, final concentration, 24 mmol/L; Amresco 0511, Amresco Inc., Cleveland, OH). The live cells were detected using the Trypan blue dye exclusion technique and a microscope (DM6000B, Leica Microsystems, Wetzla, Germany). The cell suspensions were diluted to a final concentration of 1×10^7 cells/mL in RPMI 1640 medium for subsequent analysis.

Isolation of Ileum Propria Lymphocytes (LPLs)

Separation solution was prepared by adding 5% FBS (Gibco, United States), 1 mmol/L DTT (Biosharp, South Korea) and 10 mmol/L HEPES (Biosharp, South Korea) to D-Hank's solution without calcium magnesium phenol red (HyClone, United States). Digestion solution was prepared by adding 5% FBS (Gibco, USA), 0.25% pancreatin (15090046, Gibco, USA), 0.1% collagenase I (17100, Gibco, USA) and 100 U/mL DNAse I (Thermo Scientific, USA) and incubating at 37° C for 5 min.

For cleaning, 1 g of the anterior ileum (1 cm after the yolk antrum) was cut out. All samples were the same weight. The intestinal tube was cut longitudinally along the mesentery side. The small intestine was turned so that the mucosa faced outward, after which it was rinsed gently in Hank's until the chyme was completely rinsed, and it was then cut into approximately 0.5 cm intestinal tissue fragments laterally. For separation, 5 ml of separation solution was added to a 50-ml centrifuge tube, the tube was placed in a constant temperature shaking box and shaken at 37°C (250 r/min) for 15 minutes and vortexed for 30 seconds, and the intestinal tissue fragments were then filtered through a 200-mesh cell sieve, after which the intestinal tissue fragments were collected in a 50-ml centrifuge tube. To chop the intestinal tissue fragments, they were moved to a petri dish and ophthalmic scissors were used to cut the tissue 100 times into a muddy shape. Five millilitres of digestion solution was then added to a 50-ml centrifuge tube, and the samples were placed in a constant temperature shaking box and shaken (250 r/min) at 37°C for 30–45 minutes. The samples were then vortexed for 30 seconds, the intestinal tissue fragments were filtered through a 300-mesh (48 μm) cell sieve, and the filtrate was collected in a sterile 7 ml centrifuge tube and centrifuges at 4°C (400 x g or 3000 r/min) 10 min (1500–2000 r/min is too low, making it easy to lose many cells, as the enzyme is soluble in water, and there are many washing steps in the differential centrifugation method). The supernatant was discarded, and the pellet was resuspended in 2 ml of RPMI 1640 (or D-Hank's, wash). Samples were then centrifuged (400 x g or 3000 r/min) at 4°C for 10 min, the supernatant was discarded, and the pellet was resuspend in 2 ml of RPMI 1640. The organ tissue lymphocyte separation solution was extracted by differential centrifugation (2500 r/min), washed repeatedly and resuspended, and finally resuspended and cultured with complete RPMI 1640. According to the method of the organ lymphocyte extraction kit, Ficoll-Paque Plus (Histopague-1077, Tianjin HaoYang Biological Manufacture Co., Ltd., China) was used for density gradient centrifugation, and the subsequent method was the same as that of peripheral blood lymphocyte separation.

Ilea Lymphocytes Are Stimulated to Produce Cytokines and Stain Intracellular Cytokines (Th17)

For the intracellular staining of IL-17A, the volume of the isolated ileal lymphocytes was adjusted to 1 ml, and the concentration was adjusted to 2 x 10^6 cells/mL. Two

microliters of cell activation stimulator (423304, Biolegend, San Diego, California, USA), was added (each 100 μL of cell stimulator contains 2.5 mg/ml Brefeldin A, 40.5 μM PMA, 669.3 μM ionomycin), and the cells were incubated in a CO_2 incubator at 37°C for 6 hours. The cells were then centrifuged at 350 x g for 5 minutes, the supernatant was discarded, and the activated cells were collected. Then, 2.5 mL of cell staining buffer (420201, Biolegend, San Diego, California, USA) was added to the cell pellet, mixed by vortexing or pipetting, and centrifuged at 350 x g for 5 minutes. The supernatant was then discarded, and the cells were collected by centrifugation again and resuspended in complete RPMI-1640, after which they were ready for analysis to detect the surface markers or intracellular IL-17 expression of the cells.

Peripheral Blood and Ileum Mononuclear Cell Proliferation

A 3-(4,5-dimethylthiazol)-2,5-diphenyltetrazolium bromide (MTT, Sigma Chemical Co., St. Louis, MO) assay was used to determine the peripheral blood and ileum lymphocyte proliferation response. Briefly, 100 μL of the PBMCs suspension and 100 μL of RPMI 1640 in the absence or presence of 90 μg/mL concanavalin A (Con A; C2613, Sigma Chemical, Co.) or 50 μg/mL lipopolysaccharide (L3129, Sigma Chemical, Co.) were added to a 96-well microtiter plate (Costar 3599, Corning, Inc., Corning, NY). The cultures were set up in triplicate. After a 68-h incubation in a 5% CO_2 incubator (MCO-18AIC CO_2 incubator, Sanyo Electric Biomedical Co. Ltd., Tokyo, Japan) at 39°C, MTT was added to each well at a final concentration of 5 mg/mL. The cells were incubated for an additional 4 h, and then, 100 μL of 10% sodium dodecyl sulfate dissolved in 0.04 mol/L HCl solution was added to each well to lyse the cells and solubilize the MTT crystals. Finally, the absorbance value of each sample was determined using an automated ELISA reader (model 550 Microplate Reader, Bio-Rad Pacific Ltd., Hong Kong, China) at 570 nm. The stimulation index (SI) for each sample was calculated based on the following formula:

$$SI = (\text{Absorbance value of mitogen} - \text{Stimulated cells}) / (\text{Absorbance value of media without mitogen}).$$

Phagocytic Activity of Mononuclear Lymphocytes in Peripheral Blood and Ileum

The phagocytic activity levels of peripheral blood and ileal mononuclear lymphocytes were measured by the neutral red assay method. In short, peripheral blood PBMCs were collected, and the number of cells was adjusted to 2×10^6/ml with RPMI 1640 medium. Then, 100 μL of cell suspension was incubated in a 96-well cell culture plate for 2 hours (with 3 replicate wells), the supernatant was discarded, and 200 μL/well of 0.1% neutral red solution (N299163, Shanghai Aladdin Biochemical Technology Co., Ltd., China) was added, and the cells were further cultured for 2 h. The supernatant was then discarded, and any remaining neutral red was washed away with PBS (3 times). Cell lysate was added at 200 μl/well (ethanol:acetic acid=1:1), kept in the dark at 4°C for 12 h, and the OD value was measured at 550 nm.

Determination of Lymphocyte Subsets in Peripheral Blood and Ileum PBMCs by Flow Cytometry

As mentioned earlier (19, 20), flow cytometry was used to analyze CD3+, CD4+, CD8+, CD25+, IL-17A+ and monocytes/the percentage of macrophage+ cells. In short, primary antibodies against mouse anti-chicken CD45-FITC (8270-02), mouse anti-chicken CD3-Alexa Fluor® 700 (8200-27), mouse anti-chicken CD4-APC (8210-11), mouse anti-chicken CD8α-Pacific Blue™ (8220-26), mouse anti-chicken monocyte/macrophage-PE (8420-09), mouse anti-chicken CD4-Pacific Blue™ (8210-26) (Southern Biotechnology Associates Inc., Birmingham, A), human anti-chicken CD25-Alexa Fluor® 647 (HCA173A647, Bio–Rad Antibodies) and rat anti-mouse IL-17A-PE (506904, Biolegend, San Diego, California, USA) in PBS (pH 7.2) were used. A volume of 100 μL of PBMCs (2×10^6 cells) was added to a 1.0-mL Eppendorf tube, and 25 μL of diluted primary monoclonal antibody (1:100 dilution) and negative isotype control IgG (mouse IgG1κ)-SPRD, mouse IgG1κ-FITC and mouse IgG1κ-R-PE) were used for staining. After incubating for 45 minutes at room temperature, the cells were washed twice with cold PBS and centrifuged at 1,800 x g for 30 minutes to remove unbound primary antibody. A total of 300 μL of haemolysin solution diluted in PBS (1:25) was added to each tube. Finally, the cells were washed twice, and the final volume was 500 μL. Five-color flow cytometry analysis was performed using a Coulter XL (Beckman Coulter Corp., Fullerton, CA) at Xiyuan Hospital of Traditional Chinese Medicine, China Academy of Chinese Medical Sciences. Then, the percentages of CD3+ T, CD4+ T, CD8+ T, CD25+ T, IL-17A+ T and monocyte/macrophage cells in PBMCs and LPL were calculated.

Serum NO, Lysozyme Activity, Cytokine, Immunoglobulin and Mucosal sIgA Contents

A commercial ELISA kit (Genorise Scientific Inc., Paoli, USA) was used to determine the serum levels of IL-1β, IL-4, IL-10, IL-17 and IFN-γ. According to the instructions, a chicken IgG ELISA kit (E30-104, Bethyl Laboratories Inc., Montgomery, TX, USA) was used to determine the level of IgG in the serum. Serum IgG levels were determined using a commercial ELISA kit (IDEXX Laboratories Inc., Westbrook, Maine, USA) according to the protocol recommended by the manufacturer. Serum NO and lysozyme activities were measured using commercial ELISA kits (A013-2-1; A050-1-1, Nanjing Jiancheng Institute of Bioengineering, Nanjing, China). Ileal mucosa sIgA was measured using a commercial ELISA kit (YM-SQ2632, Shanghai Yuan Mu Biotechnology Co., Ltd., Shanghai, China).

Intestinal Lesion Score

According to a method previously described, the intestinal lesion score was determined: the lesions were observed, and the lesion scores were evaluated (21).

Intestinal Tissue Morphology

Fixed intestinal tissue was dehydrated and embedded in paraffin. Tissue sections (thickness of 4 μm) were stained with haematoxylin and eosin (HE, Olympus BX50; Tokyo, Japan). Observed by a Leica microscope (Wetzlar, Germany, ModelDMi8), 10 intact intestinal villi were randomly selected for each slice. Image-ProPlus (version 6.0) software was used to measure the height of each intestinal villus and its corresponding crypt depth and to calculate the ratio of the two. The height of the villi is defined as the vertical distance from the tip of the villi to the villi-crypt junction, and the crypt depth is the vertical distance from the villi-crypt junction to the base of the crypt.

Pathology Score

The fixed jejunum tissue samples were dehydrated and embedded in paraffin. A serial microtome (Leica Microsystems K.K., Tokyo, Japan) was used to slice the embedded tissue into thin slices (4 μm) and mount it on a polylysine-coated glass slide (Boster Corporation, China) following haematoxylin-eosin (HE) staining. Histopathological examination was performed by optical microscopy and a pathological image analysis system (Leica Qwin, Jiangsu, China). The pathology of the jejunum was determined according to the following criteria: (1) inflammation (0~3 points): 0=no inflammatory cell infiltration; 1=mild inflammatory cell infiltration; 2=moderate inflammatory cell infiltration; and 3=severe inflammatory cell infiltration. (2) Damage (0~3 points): 0=no damage; 1=damage to the mucosal layer; 2=damage to the mucosal layer and submucosa; 3=transparent and disappearance of the cell wall. (3) Crypt damage (0~4 points): 0=no damage to crypts; 1 = 1/3 crypts disappeared; 2 = 2/3 crypts disappeared; 3=only the epithelial surface was intact; 4=crypts and all the epithelium on the surface disappeared. The sum of the three scores is the final intestinal pathology score.

Jejunum and Ileum Gene Expression

At 31 days of age, molecular samples of the jejunum and ileum were quick-frozen in liquid nitrogen and then transferred to a -80°C low-temperature freezer to determine the expression levels of immune function-related genes in the spleen and ileum. TRIzol reagent was used to extract total jejunum RNA, and a NanoDrop ultra-micro-calculation protein analyzer was used to determine the quality and concentration of RNA. The reagent kit used in the reverse transcription step was the PrimeScript™ RT reagent Kit with gDNA Eraser (Perfect Real Time) from Takara. The cDNA obtained after reverse transcription was subjected to real-time fluorescent quantitative PCR on an ABI 7500 real-time fluorescent quantitative PCR instrument with the primers shown in **Table 2**. The fluorescence quantification kit was Takara's SYBR® Premix Ex Taq™ II (Tli RNaseH Plus), with GAPDH as the internal reference, and the results are expressed as $2^{(-\triangle\triangle CT)}$.

Caecal Microbial Count

Under aseptic conditions, caecum specimens from broiler chickens 2 and 8 days after infection were collected, quickly frozen in liquid nitrogen and stored at -20°C for caecal bacterial count. The specific method was as follows: the caecum was placed on ice (approximately 4°C) to thaw, and 0.3 g was weighed on a balance on a clean bench and placed in a 5-ml sterile centrifuge tube. Then, 2.7 ml of sterile saline was added for a 10-fold dilution, and the sample was shaken and mixed on a micro shaker and allowed to stand for 10 minutes. Then, 0.3 ml of the supernatant was moved to a sterile centrifuge tube, and sterile saline was used to perform gradient dilutions of 10^2, 10^3, 10^4, 10^5, 10^6, 10^7, 10^8. One hundred microlitres of the solution from each dilution tube was inoculated on the corresponding selective medium, and the plate was spread until the solution was dry on the medium. After culturing under the corresponding conditions, 30–300 colonies were selected for bacterial count. Among them, *Clostridium perfringens* was selected on tryptone-sulfite-cycloserine (TSC) medium (CM138, Beijing Luqiao Technology Co., Ltd., Beijing, China) and cultured under anaerobic conditions at 37°C. Plates were counted after 24 hours. Lactic acid bacteria were counted on MRS agar medium (CM188, Beijing Luqiao Technology Co., Ltd., Beijing, China), and the culture conditions were 5% CO_2 and 37°C for 24 hours. The logarithm of the number of bacteria per gram of caecal content (log10 CFU/g) was used to express the results.

DNA Extraction and High-Throughput Sequencing

Bacterial DNA was extracted from ileal digesta with a QIAamp DNA Stool Mini Kit (Qiagen Inc., V alencia, CA) according to the manufacturer's protocol. The concentrations of DNA extracts were measured on a NanoDrop 2000 spectrophotometer (Thermo Scientific, MA, USA). The V4 region of the bacterial 16S rRNA gene was amplified with the barcoded primer pair 515F/806R (515F: 5′-GTG CCA GCM GCC GCG GTA A-3′, 806R: 5′-GGA CTA CHV GGG TWT CTA AT-3′) according to previously described methods (22). After amplification, PCR products run on a 2% agarose gel and were purified using a QIAquick Gel Extraction Kit (Qiagen, Germany). Pyrosequencing of 16S rDNA was performed on an Illumina HiSeq2500 PE250 platform (Illumina, San Diego, USA) at Novogene Bioinformatics Technology Co. Ltd. (Beijing, China).

Sequence Processing and Bioinformatics Analysis

Raw tags were generated by merging paired-end reads using FLASH software (v1.2.7) (23). Highquality clean tags were obtained by QIIME (v1.7.0) analysis (24), and chimera sequences were removed to obtain effective tags by using the UCHIME algorithm (25). Sequences were analyzed by UPARSE software (v7.0.1001) and clustered into operational taxonomic units (OTUs) at a similarity level of 97% (26). Each OTU was annotated with the Greengenes database (27). Rarefaction curve and Venn diagram were created using R software (v2.15.3). Analysis of microbial alpha diversity was conducted using QIIME software (24) with Python scripts. Beta diversity was evaluated by principal component analysis (PCA) to show the

TABLE 2 | Sequences of the oligonucleotide primers used for quantitative real-time PCR[a].

Gene[b]	Primer sequence[3](5′to3′)[c]	Accession NO.
AhR	F: CACCTACGCCAGTCGCAAGC R: CCTGTGCCTCTTGGATGGATTGG	NM_001323184.1
Caspase1	F: GTGCTGCCGTGGAGACAACATAG R: AGGAGACAGTATCAGGCGTGGAAG	XM_015295935.1
chCD25	F: AAGACAAACCCAAAGCCC R: CTCAGAGAGGCATGTGGGAC	NM_204596
Foxp3	F: GCACACCTCTCAATGCTGCT R: CTAGGTTGCCCAGAGTGGGA	XP_015148603.2
GAPDH	F: AGAACATCATCCCAGCGTCC R: CGGCAGGTCAGGTCAACAAC	NM_204305
IFN-γ	F: AAAGCCGCACATCAAACACA R: GCCATCAGGAAGGTTGTTTTTC	NM_205149.1
IgA	F: ACCACGGCTCTGACTGTACC R: CGATGGTCTCCTTCACATCA	S40610.1
IL-1β	F: TGGGCATCAAGGGCTACA R: CGGCCCACGTAGTAAATGAT	NM_204524.1
IL-4	F: GTGCCCACGCTGTGCTTAC R: AGGAAACCTCTCCCTGGATGTC	NM_001007079.1
IL-6	F: GATCCGGCAGATGGTGATAA R: AGGATGAGGTGCATGGTGAT	NM_204628.1
IL-10	F: CGCTGTCACCGCTTCTTCA R: TCCCGTTCTCATCCATCTTCTC	AJ621614
IL-17A	F: CTCCGATCCCTTATTCTCCTC R: AAGCGGTTGTGGTCCTCAT	AJ493595
IL-17F	F: TGAAGACTGCCTGAACCA R: AGAGACCGATTCCTGATGT	JQ776598
IL-22	F: TGTTGTTGCTGTTTCCCTCTTC R: CACCCCTGTCCCTTTTGGA	AJ617782.1
iNOS	F: GAACAGCCAGCTCATCCGATA R: CCCAAGCTCAATGCACAACTT	U34045
IRAK4	F: TGGTTCGCTGCTTGACAGACTTG R: TGATGCCATTCGCAGTACCTTGAG	XM_015281244.2
Lysozyme C	F: GACGATGTGAGCTGGCAG R: GGATGTTGCACAGGTTCC	NM_205281
Mucin2	F: TTCATGATGCCTGCTCTTGTG R: CCTGAGCCTTGGTACATTCTTGT	XM_421035
NF-kB	F: TGGAGAAGGCTATGCAGCTT R: CATCCTGGACAGCAGTGAGA	NM_205134.1
NLRP3	F: GGTTTACCAGGGGAAATGAGG R: TTGTGCTTCCAGATGCCGT	NM_001348947.1
Occludin	F: AGTTCGACACCGACCTGAAG R: TCCTGGTATTGAGGGCTGTC	NM_205128.1
pIgR	F: ATTTGTCACCACCACAGCCA R: GAGTAGGCGAGGTCAGCATC	NM_001044644
RORα	F: AAATGCCTTGCTGTGGGGATGTC R: GATGATCTCGCTGCTGCTGCTG	NM_001289887.1
TGF-β1	F: GCCGACACGCAGTACACCAAG R: GCAGGCACGGACCACCATATTG	NM_001318456.1
TLR2	F: ACCTTCTGCACTCTGCCATT R: TGTGAATGAAGCACCGGTAA	NM_204278.1
TLR4	F: GATGCATCCCCAGTCCGTG R: CCAGGGTGGTGTTTGGGATT	NM_001030693
TNF-α	F: CCCCTACCCTGTCCCACAA R: TGAGTACTGCGGAGGGTTCAT	AY765397.1
TRIF	F: TCAGCCATTCTCCGTCCTCTTC R: GGTCAGCAGAAGGATAAGGAAAGC	NM_ 496065.1
ZO-1	F: ACAGCTCATCACAGCCTCCT R: TGAAGGGCTTACAGGAATGG	XM_015278981.1

[a]*Primers designed using Primer Express software (Sangon Biotech, Shanghai, China).*

[b]*AhR, aryl hydrocarbon receptor; ChCD25, chicken cluster of differentiation 25; Foxp3, forkhead transcription factor p 3; GAPDH, glyceraldehyde-3-phosphate dehydrogenase; IFN-γ, interferon-γ; IgA, immune globulin A; IL-1β, interleukin-1β; iNOS, inducible nitric oxide synthase; IRAK4, interleukin-1 receptor associated kinase-4; Lyz C, lysozyme C; MUC2, Mucin-2; NF-κB, nuclear factor kappa-β; NLRP3, NOD-like receptor family proteins 3; pIgR, polymeric immunoglobulin receptor; RORα, retinoic acid related-orphan receptors α; TGF-β1, transforming growth factor-β1; TLR2, toll-like receptor 2; TNF-α, tumor necrosis factor α; TRIF, TIR-domain-containing adaptor inducing interferon-β; ZO-1, zonula occludens-1.*

[c]*F, forward; R, reverse.*

differences of bacterial community structures, and the significance of separation was tested *via* ANOSIM using R (v2.15.3). PICRUSt analysis was used to predict the functional potential of bacteria communities (28). OTUs were normalized by copy number, and metagenome prediction was further categorized into Kyoto Encyclopedia of Genes and Genomes (KEGG) at levels 2 and 3 (29).

Short-Chain Fatty Acids of Ileal Contents

Ileal chyme (0.5 g) was weighed in a 10-mL plastic centrifuge tube, 8 ml of deionized water was added, and the samples were ultrasonically shaken for 30 minutes and centrifuged at 8000 rpm at 4°C for 10 minutes. The supernatant was diluted ten times and filtered with a 0.22-μm filter. Twenty-five microlitres of the filtrate was collected, and an ICS-3000 high-performance ion chromatograph (Dionex, USA) was used to detect SCFAs and lactic acid by conductivity. Organic acids were separated under gradient conditions in an AS11 analytical column (250 mm×4 mm) and a AG11 guard column: the gradient used potassium hydroxide as the carrier, 0–5 min, 0.8–1.5 mM; 5–10 min, 1.5–2.5 mM, 10–15 min, 2.5 mM, flow rate 1.0 mL/min.

Detection of Metabolite Composition of Ileal Contents by Non-Targeted Metabolome

The sample detection and data analysis were all completed by Tianjin Nuohe Zhiyuan Technology Co., Ltd. The metabolite extraction process was as follows: (1) To 100 μL of ileum content, 350 μL of extract (methanol: acetonitrile: water volume ratio=2:2:1, methanol and acetonitrile were both chromatographic grade, purchased from Merck) was added, and then 20 μL of internal standard L-2-chlorophenylalanine (CAS#: 103616–89–3, ≥98%; purchased from Shanghai Hengbai Biotechnology Co., Ltd.) was added. The samples were vortexed and mixed for 30 seconds and then sonicated under ice-water bath conditions for 10 min. (2) The samples were incubated at -20°C for 1 h and then centrifuged at 13,000 rpm for 15 min at 4°C. (3) After carefully removing 400μL of supernatant to a 1.5 mL centrifuge tube, the extract was then dried in a vacuum concentrator. (4) Then, 100 μL of extract (equal volume of acetonitrile and water) was added to the dried extract for reconstitution, and the samples were vortexed for 30 s and ultrasonicated for 10 min in an ice water bath. (5) The samples were then centrifuged at 12,000 rpm at 4°C for15 min. (6) Finally, 60 μL of supernatant was carefully removed and placed in a 2-mL injection bottle, and 10 μL of each sample was mixed into a quality control sample, while 60 μL was taken for computer testing.

The system was used to analyze the metabolome components of the ileum content using an Agilent 1290 ultrahigh-performance liquid chromatograph in a series ABSciexTripleTOF6600 high-resolution mass spectrometer. The column used was an ACQUITYUPLCBEHAmide column (1.7 μm2.1*100 mm) purchased from Waters. The mobile phase conditions were 25 mM ammonium acetate and 25 mM ammonia solution (A) and 100% acetonitrile (B). The gradient items for the analysis of the ileal contents sample were: 0–0.5 min, 5%A, 95%B; 0.5–7 min, 5–35%A, 95–65%B; 7–8 min, 35–60%A, 65–40%B; 8–9 min, 60%A, 40%B; 9–9.1 min, 60–5% A, 40–95%B; 9.1–12 min, 5%A, 95%B; the flow rate was 0.5 mL/min, and the injection volume was 2 μL. The mass spectrometry conditions were as follows: AB6600TripleTOF mass spectrometer, which can perform primary and secondary mass spectrometry data based on the IDA function under the control of the software (AnalystTF1.7, ABSciex). In each data acquisition cycle, the strongest signals with greater than 100 molecules are screened out. The ions were collected corresponding to the secondary mass spectrum data. Bombardment energy: 35 eV, 15 secondary spectra every 50 ms. The ESI ion source parameters were set as follows: atomization pressure (GS1): 60 Pa, auxiliary pressure: 60 Pa, air curtain pressure: 30 Pa, temperature: 550°C, and spray voltage: 5500 V (positive ion mode) or -4500 V (negative ion mode). QC samples with RSD<30% were screened, and a feature yield rate>80% was required to ensure good system stability.

The data were first converted to mzXML format using MSconventer, and XCMS (XCMS1.41.0) was used for peak search, peak alignment and other data processing. Then, the data processing and matching of substance identification were performed, and the xcms4dda and xcms4lipid developed by Nuovo Zhiyuan based on XCMS were used. The program and self-built library were processed, minfrac was set to 0.5, and the cut-off was set to 0.8. First, the secondary data were screened. The screening principle is that as long as one forward and one reverse signal is identified, the peak is retained. Second, the peaks of the first- and second-level data are matched, that is, the peaks of the first-level data corresponding to the second-level data are found, and matching is performed according to mztolerance ± 25 ppm. Data analysis included three parts: basic data analysis and personalized data analysis. The goal of basic data analysis is to perform univariate analysis (UVA) and multivariate analysis (MVA) on the qualitative and quantitative results of the metabolome to screen for metabolites with significant differences. Univariate statistical analysis includes data preprocessing (first simulating the missing values in the original data; the numerical simulation method is the minimum one-half method to fill, and then using the total ion current of each sample for normalization), Student's t-test and analysis of variance. Multivariate statistical analysis includes principal component analysis (PCA) and partial least squares regression analysis (Partial Least Squares Discrimination Analysis, PLS-DA), with differential compound screening and identification. Personalized data analysis is a series of bioinformatics analyses on metabolites with significant differences on the basis of basic data analysis, including KEGG annotation analysis of different metabolites and metabolic pathway analysis.

Statistical Analysis

SPSS 20.0 software was used to perform the statistical analysis on each group of data. The GLM process was used for statistical analysis. When the interaction was significant, one-way analysis was used, and Duncan's multiple comparison analysis was used for differences between treatments. $P < 0.05$ was considered

significant, and P values between 0.05 and 0.10 were classified as trends.

The spearman rank correlation coefficient was used for the evaluation of the correlation analysis of the variables and microbes in the broiler chickens.

RESULTS

Growth Performance, Mortality Rate and Immune Organ Index

Figure 1 shows that compared with the unchallenged birds, NE-challenged birds had significantly reduced body weight gain on d 13–25 and mortality on d 13-d 31 ($P < 0.05$) and significantly increased FCR on d 13–25 and d 25–31 ($P < 0.05$). Compared with the control group, dietary APS supplementation alleviated the negative impact of NE on growth performance, significantly reduced the FCR on d 13–25 and the mortality rate on d 13–31 ($P < 0.05$), and significantly increased the average weight on d 31 and the d 25–31 feed intake ($P < 0.05$). There was a tendency to increase body weight gain on d 25–31 ($0.05 < P < 0.1$). Compared with the unchallenged birds, NE-challenged birds had a significantly reduced d 25 thymus index ($P < 0.05$). Compared with the NE group, APS supplementation significantly reduced the spleen index ($P < 0.05$). Compared with the control group, APS supplementation significantly increased the bursa index ($P < 0.05$).

Peripheral Nonspecific Immune Function and Humoral Immune Function

Figure 2 shows that compared with the unchallenged birds, NE-challenged birds had significantly increased d 25 and d 31 serum NO levels and d 25 lysozyme activity ($P < 0.05$). There was a tendency to improve the phagocytic function of monocytes ($0.05 < P < 0.1$). Compared with the unchallenged birds, NE-challenged birds had significantly reduced proliferation activity of B lymphocytes in peripheral blood on d 25 ($P < 0.05$), while dietary APS supplementation increased the proliferation activity of B lymphocytes in peripheral blood on d 25 ($P < 0.05$).

Peripheral Cellular Immune Function

As shown in **Figure 3**, compared with the unchallenged birds, NE-challenged birds significantly increased the proportion of Th17 cells in peripheral blood on d 31 and the proportion of Th17/Treg cells on d 25 and d 31 ($P < 0.05$). There was a tendency to increase the number of d 25 peripheral blood mononuclear macrophages and decrease the proportion of Treg cells ($0.05 < P < 0.1$). Compared with the control group, dietary APS supplementation significantly increased the proportion of T cells in peripheral blood on d 25 ($P < 0.05$) and significantly reduced the Th17/Treg cells at 31 days of age ($P < 0.05$). Compared with the unchallenged birds, NE-challenged birds had significantly reduced proliferation activity of T lymphocytes in peripheral blood on d 25 ($P < 0.05$), while dietary APS supplementation increased the proliferation activity of T lymphocytes in peripheral blood on d 25 ($P < 0.05$). Compared with the unchallenged birds, NE-challenged birds had significantly increased d 25 serum cytokine (IL-1β, IL-4 and IFN-γ) and d 31 serum cytokine (IL-1β, IL-4, IL-17 and IL-17/IL-10) levels ($P < 0.05$). Compared with the control group, dietary APS supplementation significantly reduced d 25 serum cytokines (IL-10, IL-17 and IL17/IL-10) and d 31 IL-17/IL-10 levels ($P < 0.05$) and increased d 31 IL-1β and IL-10 levels ($P < 0.05$). There was a tendency to increase the ratios of d 25 peripheral blood mononuclear macrophages and d 31 Treg cells ($0.05 < P < 0.1$).

Intestinal Lesion Score, Pathology Score and Intestinal Tissue Morphology

Figure 4 shows that compared with the unchallenged birds, NE-challenged birds had significantly increased scores of the duodenum, jejunum, the ileum and total score of the intestine of broilers at d 25 and d 31 ($P < 0.05$). Compared with the control group, dietary APS supplementation significantly reduced the scores of d 25 jejunum and d 31 duodenum, jejunum, and ileum and total score of the intestine ($P < 0.05$). Compared with the unchallenged birds, NE-challenged birds significantly improved the inflammatory cell infiltration and pathological score of the jejunum of d 25 and d 31 broilers and the degree of jejunum injury at d 25 ($P < 0.05$). Compared with the control group, dietary APS supplementation significantly reduced the inflammatory cell infiltration in the jejunum of d 31 broilers and had a tendency to decrease the pathological score of the d 31 jejunum ($P < 0.05$). Compared with the unchallenged birds, NE-challenged birds had significantly reduced d 25 jejunum villus height and d 31 V/C ($P < 0.05$) and a significantly increased d 31 jejunal crypt depth ($P < 0.05$). Compared with the control group, dietary APS supplementation significantly reduced the depth of jejunal crypts in broilers at d 31 ($P < 0.05$) and significantly increased the V/C ($P < 0.05$). Compared with the control group, dietary APS supplementation significantly increased the mRNA expression of ZO-1 in ileum on d 31 ($P < 0.05$).

Intestinal Nonspecific Immune Function and Humoral Immune Function

As shown in **Figure 5**, compared with unchallenged birds, NE-challenged birds had significantly improved the phagocytic function of monocytes at d 25. Compared with the unchallenged birds, NE-challenged birds had significantly increased *iNOS*, *IgA* and *pIgR* mRNA levels ($P < 0.05$) and significantly reduced *Mucin-2* mRNA levels in jejunum and ileum at d 31 ($P < 0.05$). Compared with unchallenged birds, NE-challenged birds had significantly reduced proliferation activity of B lymphocytes in the ileum at d 25 ($P < 0.05$) and significantly improved the phagocytic function of monocytes at d 25 ($P < 0.05$). Compared with the control group, dietary APS supplementation improved the proliferation activity of B lymphocytes in the ileum at d 25 ($P < 0.05$). Compared with the unchallenged birds, NE-challenged birds had significantly reduced sIgA levels in the ileal mucosa on d 25 ($P < 0.05$).

Intestinal Cellular Immune Function

As shown in **Figure 6**, compared with the control group, NE-challenged broilers significantly increased the proportions of d

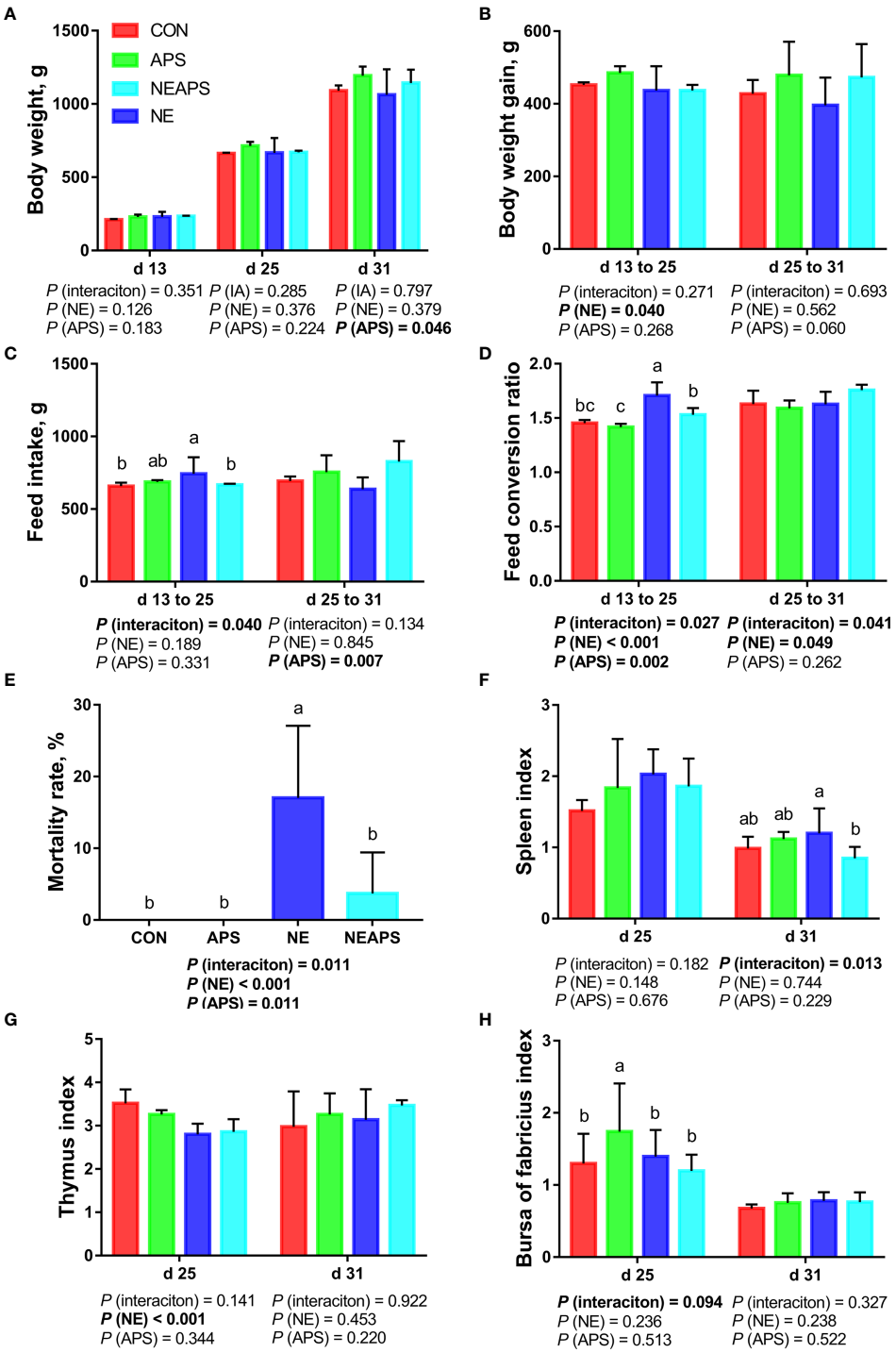

FIGURE 1 | Effects of dietary astragalus polysaccharides supplementation on growth performance, mortality rate and immune organ index of broiler chickens challenged with necrotic enteritis. The body weight **(A)**, body weight gain **(B)**, feed intake **(C)** and feed conversion ratio **(D)** were analyzed by weighted. The mortality rate **(E)** was calculated as the ratio of the number of broilers that died in each cage to the total number of broilers on d 13 to 31. The spleen index **(F)**, thymus index **(G)** and bursa of fabricius index **(H)** were analyzed by weighted. All graphs are presented as mean, with the standard deviation (SD) shown *via* the whiskers. The main effect and interaction effects were analyzed using the general linear model (GLM) procedure, with the *P* values for the main effects written out below each plot. The one-way ANOVA and multiple comparisons were performed when interactive effects differed significantly. The lowercase letters on the bar charts indicate significant differences ($P < 0.05$). CON, control group; APS, APS group; NE, NE infection group; NEAPS, APS infected with NE group.

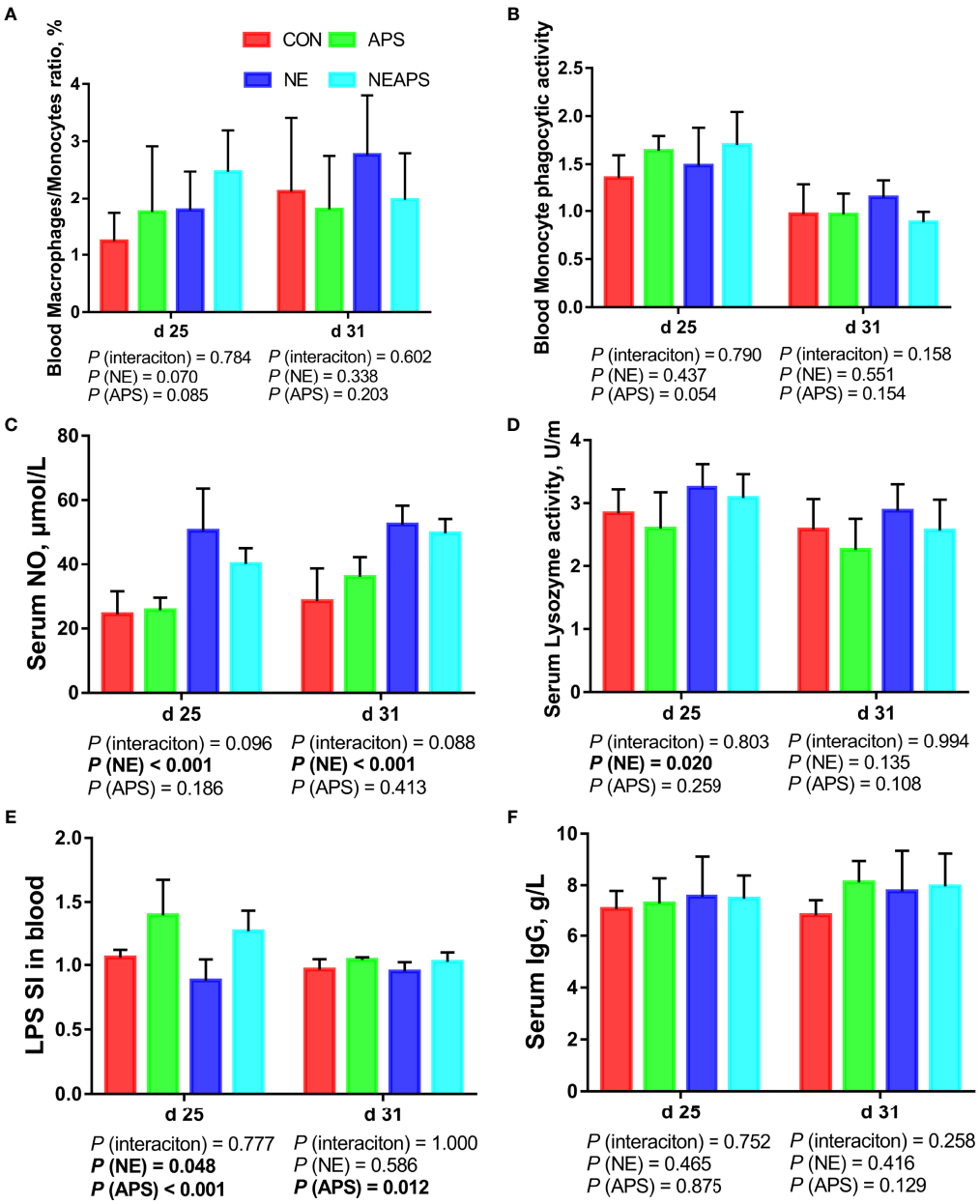

FIGURE 2 | Effects of dietary astragalus polysaccharides supplementation on peripheral nonspecific immune function and humoral immune function of broiler chickens challenged with necrotic enteritis. The frequencies of Mononuclear/Macrophage **(A)** of peripheral blood lymphocytes were analyzed by flow cytometry. The phagocytic activity of Monocytes **(B)** was analyzed by neutral red method. The levels of NO **(C)**, lysozyme activity **(D)**, and IgG **(F)** were analyzed by ELISA kit. Peripheral blood lymphocytes were stimulated with lipopolysaccharide (LPS) **(E)**, and the stimulation index (SI) was calculated as described in the Materials and Methods section. All graphs are presented as mean, with the standard deviation (SD) shown *via* the whiskers. The main effect and interaction effects were analyzed using the general linear model (GLM) procedure, with the *P* values for the main effects written out below each plot. The one-way ANOVA and multiple comparisons were performed when interactive effects differed significantly. CON, control group; APS, APS group; NE, NE infection group; NEAPS, APS infected with NE group.

25 ileum Tc and Treg cells and the proportion of d 31 Th17/Treg cells ($P < 0.05$) and significantly reduced the proportion of d 25 Th cells ($P < 0.05$). There was a tendency to increase the proportion of d 25 Th17 cells ($0.05 < P < 0.1$). Compared with the control group, dietary APS supplementation significantly reduced the proportion of Th17 cells in the ileum at d 25 ($P < 0.05$) and significantly increased the proportion of Tc and Treg cells in the ileum at d 31 ($P < 0.05$). There was a tendency to decrease Th17/Treg cells in the ileum at d 25 ($0.05 < P < 0.1$). Compared with unchallenged birds, NE-challenged birds had

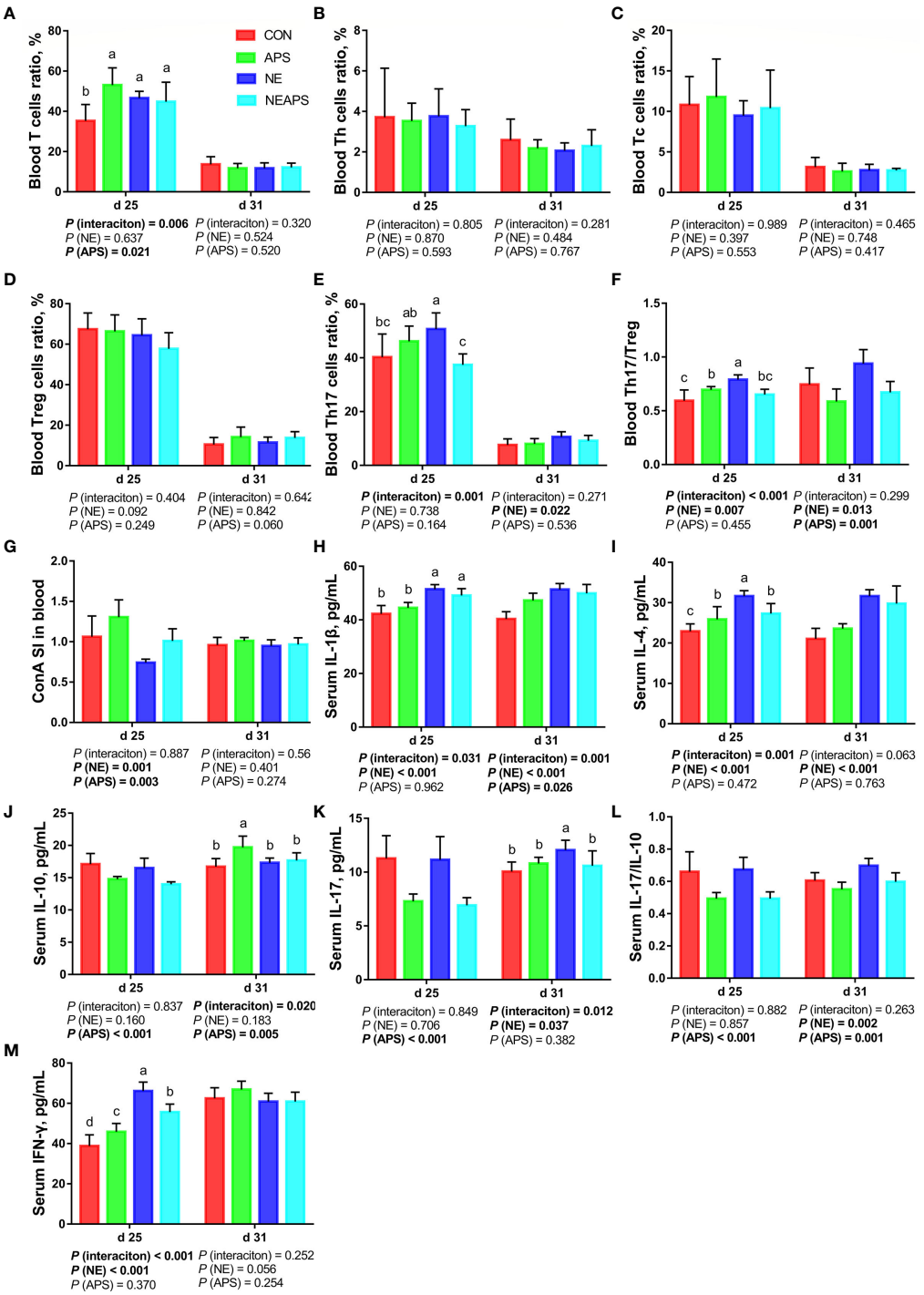

FIGURE 3 | Effects of dietary astragalus polysaccharides supplementation on peripheral cellular immune function of broiler chickens challenged with necrotic enteritis. The frequencies of T **(A)**, Th **(B)**, Tc **(C)**, Treg **(D)** and Th17 **(E)** of peripheral blood lymphocytes were analyzed by flow cytometry. The Th17/Treg **(F)** of peripheral blood lymphocytes was calculated by dividing the proportion of Th17 cells by the proportion of Treg cells. Peripheral blood lymphocytes were stimulated with concanavalin A (ConA) **(G)**, and the stimulation index (SI) was calculated as described in the Materials and Methods section. The levels of IL-1β **(H)**, IL-4 **(I)**, IL-10 **(J)**, IL-17 **(K)**, IL-17/IL-10 **(L)** and IFN-γ **(M)** in serum were analyzed by ELISA kit. All graphs are presented as mean, with the standard deviation (SD) shown *via* the whiskers. The main effect and interaction effects were analyzed using the general linear model (GLM) procedure, with the *P* values for the main effects written out below each plot. The one-way ANOVA and multiple comparisons were performed when interactive effects differed significantly. The lowercase letters on the bar charts indicate significant differences ($P < 0.05$). CON, control group; APS, APS group; NE, NE infection group; NEAPS, APS infected with NE group.

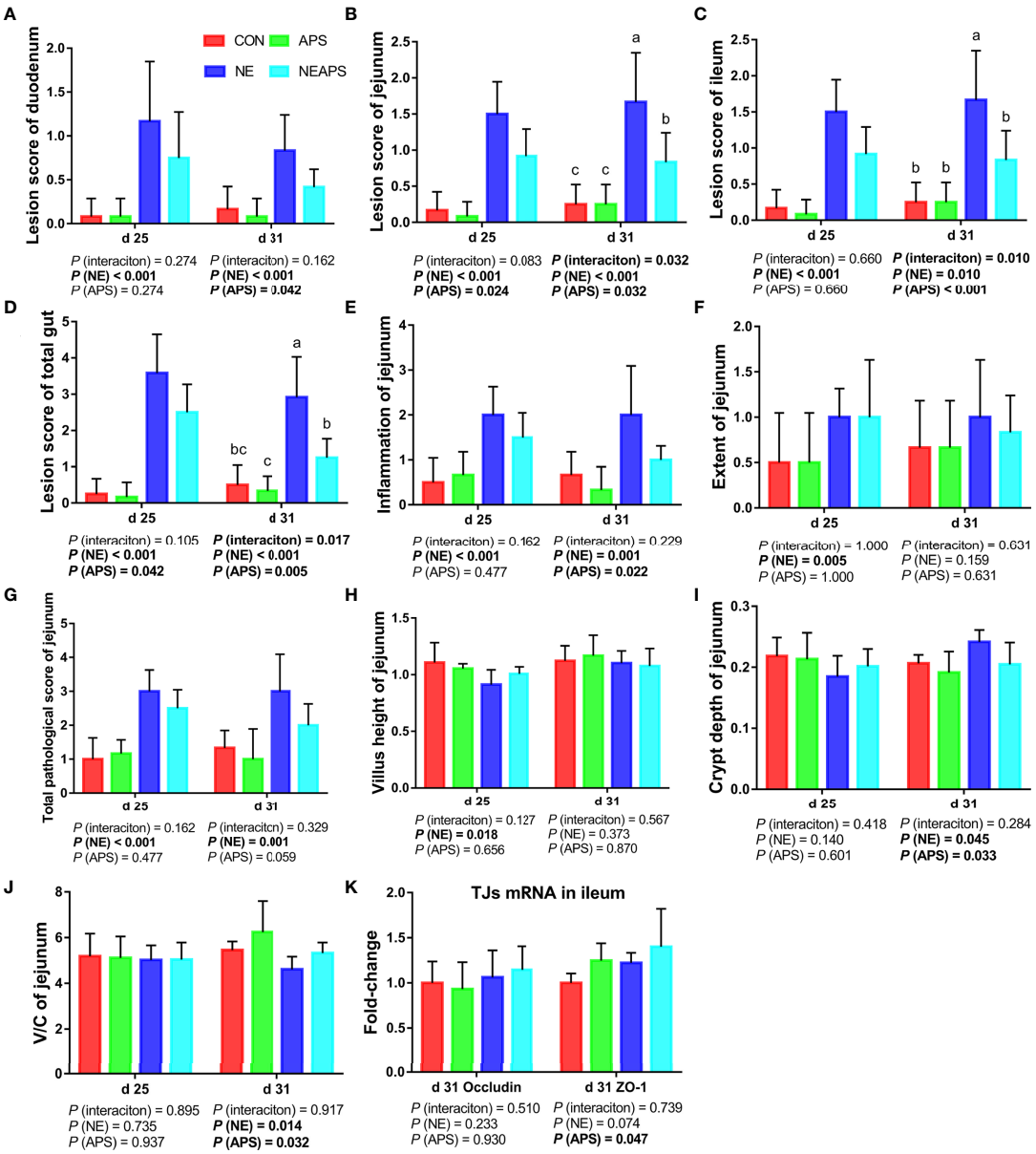

FIGURE 4 | Effects of astragalus polysaccharide supplementation on intestinal lesion score, pathology score and intestinal tissue morphology of broiler chickens challenged with necrotic enteritis. The lesion scores of duodenum **(A)**, jejunum **(B)**, ileum **(C)** and total gut **(D)** were analyzed as described in the Materials and Methods section. The inflammation of jejunum **(E)**, extent of jejunum **(F)** and total pathological score of jejunum **(G)** were analyzed as described in the Materials and Methods section. The villus height of jejunum **(H)** and crypt depth **(I)** of jejunum were analyzed by HE staining. The V/C of jejunum **(J)** was calculated by dividing the villus height by the crypt depth. The mRNA levels of *Occludin* and *ZO-1* in ileum **(K)** were analyzed by RT-PCR. All graphs are presented as mean, with the standard deviation (SD) shown *via* the whiskers. The main effect and interaction effects were analyzed using the general linear model (GLM) procedure, with the *P* values for the main effects written out below each plot. The one-way ANOVA and multiple comparisons were performed when interactive effects differed significantly. The lowercase letters on the bar charts indicate significant differences ($P < 0.05$). CON, control group; APS, APS group; NE, NE infection group; NEAPS, APS infected with NE group.

significantly reduced proliferation activity of T lymphocytes in the ileum at d 25 ($P < 0.05$) at d 25. Compared with the control group, dietary APS supplementation improved the proliferation activity of T lymphocytes in the ileum at d 25 ($P < 0.05$). Compared with the unchallenged birds, NE-challenged birds had significantly increased *TLR2, IRAK4, NF-κB, IFN-γ, TNF-α, TGF-β1, IL-6, IL-10, RORα and Foxp3* mRNA levels ($P < 0.05$) in jejunum on d 31. There was a tendency to increase *IL-17F and IL-17F/IL-10* expression ($0.05 < P < 0.1$) in jejunum. Compared with the control group, dietary APS supplementation significantly reduced the mRNA levels of *TNF-α, IL-17F, and Foxp3* ($P < 0.05$) in jejunum. There was a tendency to downregulate *IL-6 and RORα*

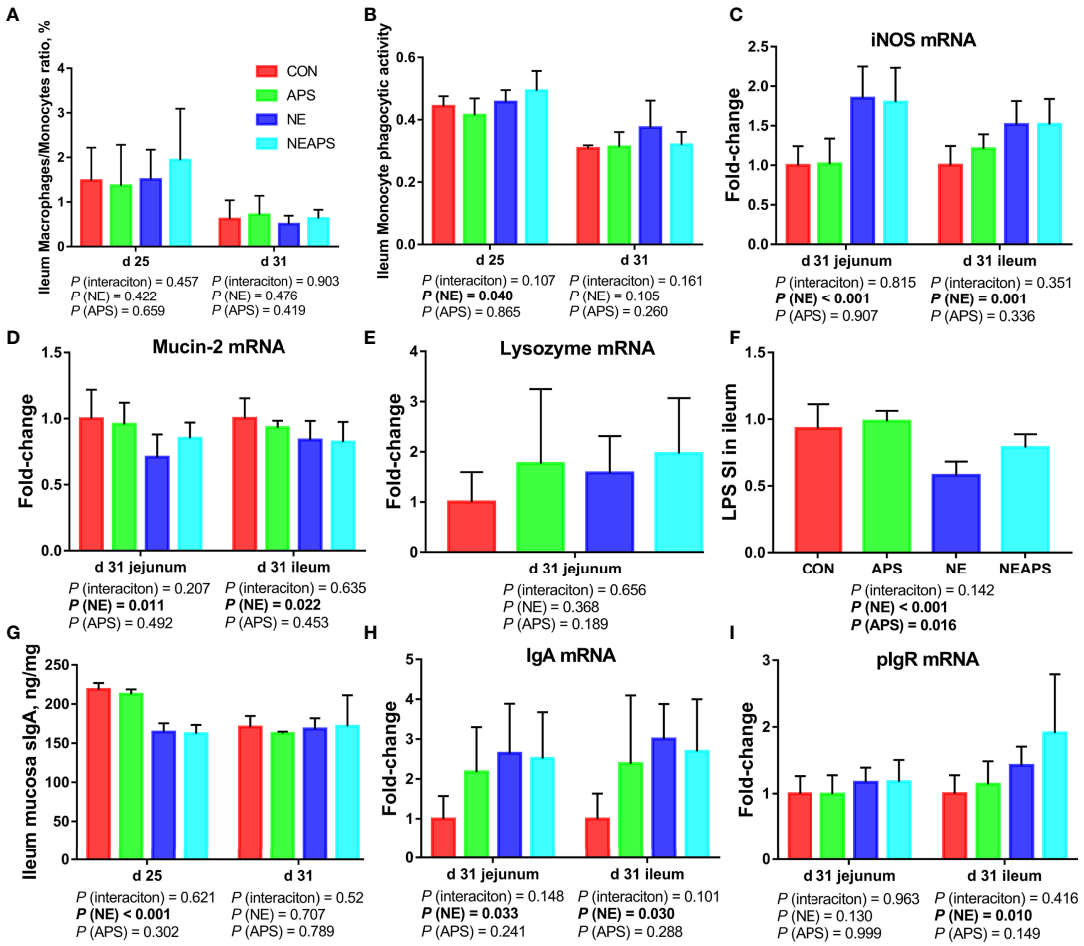

FIGURE 5 | Effects of dietary astragalus polysaccharides supplementation on intestinal nonspecific immune function and humoral immune function of broiler chickens challenged with necrotic enteritis. The frequencies of Mononuclear/Macrophage **(A)** of ileum lymphocytes were analyzed by flow cytometry. The phagocytic activity of Monocytes **(B)** was analyzed by neutral red method. The mRNA levels of *iNOS* **(C)**, *Mucin-2* **(D)**, *lysozyme* **(E)**, *IgA* **(H)** and *pIgR* **(I)** in jejunum and ileum were analyzed by RT-PCR. Ileum lymphocytes were stimulated with lipopolysaccharide (LPS) **(F)**, and the stimulation index (SI) was calculated as described in the Materials and Methods section. The level of sIgA of ileum mucosa **(G)** was analyzed by ELISA kit. All graphs are presented as mean, with the standard deviation (SD) shown *via* the whiskers. The main effect and interaction effects were analyzed using the general linear model (GLM) procedure, with the *P* values for the main effects written out below each plot. The one-way ANOVA and multiple comparisons were performed when interactive effects differed significantly. CON, control group; APS, APS group; NE, NE infection group; NEAPS, APS infected with NE group.

(0.05 <*P* <0.1) in jejunum. A strong interaction between dietary APS and NE infection was observed in relation to *TLR2, IFN-γ, TNF-α, IL-6, IL-10, RORα and Foxp3* ($P < 0.05$) in jejunum. Compared with the unchallenged birds, NE-challenged birds had significantly increased *NLRP3, TLR2, IRAK4, NF-κB and IFN-γ* mRNA levels ($P < 0.05$) in ileum on d 31. There was a tendency to increase *RORα* ($0.05 < P < 0.1$) in ileum. Compared with the control group, dietary APS supplementation significantly reduced mRNA levels of *IL-4* and *IL-17F/IL-10* ($P < 0.05$) and significantly increased *AhR and ZO-1* mRNA levels ($P < 0.05$) in ileum on d 31. There was a tendency to increase *Foxp3* and decrease *IL-17F* ($0.05 < P < 0.1$) in ileum. A strong interaction between dietary APS and NE infection was observed in relation to *IFN-γ, IL-17F* and *IL-22* ($P < 0.05$) in ileum.

Ileum Microbiota

β Diversity

As shown in **Figures 7A, B**, the four groups of CC, CA, CN and CNA on d 25 and d 31 could be separated well, demonstrating that the addition of APS in broiler diets on d 25 and d 31 and infection with necrotic enteritis could cause a significant influence on ileal microbial composition.

Alpha Diversity

Figures 7C, D shows that compared with the unchallenged birds, NE-challenged birds significantly reduced the observed_species, Shannon, Simpson and Chao1 indices at d 25 and significantly reduced the observed_species and Chao1 indices at d 31 ($P < 0.05$). Dietary APS supplementation significantly increased

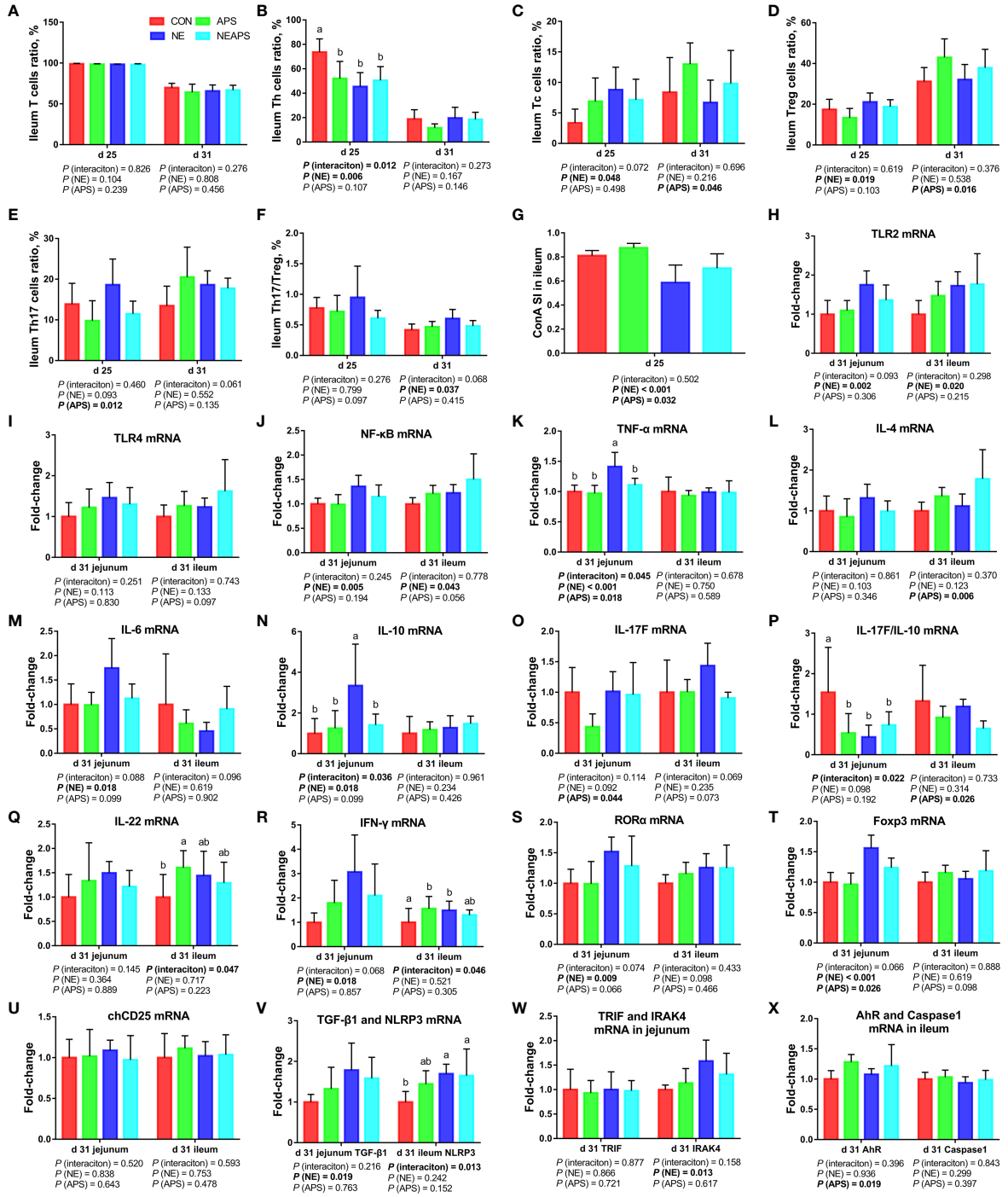

FIGURE 6 | Effects of dietary astragalus polysaccharides supplementation on intestinal cellular immune function of broiler chickens challenged with necrotic enteritis. The frequencies of T **(A)**, Th **(B)**, Tc **(C)**, Treg **(D)** and Th17 **(E)** of ileum lymphocytes were analyzed by flow cytometry. The Th17/Treg **(F)** of ileum lymphocytes was calculated by dividing the proportion of Th17 cells by the proportion of Treg cells. Ileum lymphocytes were stimulated with concanavalin A (ConA) **(G)**, and the stimulation index (SI) was calculated as described in the Materials and Methods section. The mRNA levels of *TLR2* **(H)**, *TLR4* **(I)**, *NF-κB* **(J)**, *TNF-α* **(K)**, *IL-4* **(L)**, *IL-6* **(M)**, *IL-10* **(N)**, *IL-17F* **(O)**, *IL-17F/IL-10* **(P)**, *IL-22* **(Q)**, *IFN-γ* **(R)**, *RORα* **(S)**, *Foxp3* **(T)**, *chCD25* **(U)**, *TGF-β1* **(V)**, *NLRP3* **(V)**, *TRIF* **(W)**, *IRAK4* **(W)**, *AhR* **(X)** and *Caspase1* **(X)** in jejunum and ileum were analyzed by RT-PCR. All graphs are presented as mean, with the standard deviation (SD) shown *via* the whiskers. The main effect and interaction effects were analyzed using the general linear model (GLM) procedure, with the *P* values for the main effects written out below each plot. The one-way ANOVA and multiple comparisons were performed when interactive effects differed significantly. The lowercase letters on the bar charts indicate significant differences ($P < 0.05$). CON, control group; APS, APS group; NE, NE infection group; NEAPS, APS infected with NE group.

the observed_species at d 25 ($P < 0.05$). NE and APS supplementation had significant interaction effects on the d 31 Shannon and Simpson indices ($P < 0.05$). Dietary APS supplementation significantly increased the alpha diversity of unchallenged broilers but had no significant effect on NE-challenged broilers.

Top Ten Microorganisms in the Ileum

Figures 7E, F shows that broiler infection with necrotic enteritis increased the relative abundance of d 25 *Lactobacillus* and d 25 *Staphylococcus* and decreased the relative abundance of d 25 *Escherichia-Shigella*, d 25 *Prevotella*, d 25 *Halomonas*, and d 31 *Escherichia-Shigella*.

Dietary APS supplementation increased the relative abundance of d 25 *Escherichia-Shigella*, d 25 *Streptococcus*, d 25 *Staphylococcus*, d 25 *Halomonas*, d 31 *Escherichia-Shigella*, d 31 *Romboutsia* and d 31 *Streptococcus* and decreased the relative abundance of d 25 and d 31 *Lactobacillus*.

T-Test Test for Different Microorganisms

As shown in **Figures 7G–K**, broiler infection with necrotic enteritis significantly increased d 25 *Lactobacillus* and d 31 *Turicibacter* ($P < 0.05$). The addition of APS to broiler diets significantly increased d 25 *Staphylococcus*, d 25 *Halomonas* and d 31 *Romboutsia* ($P < 0.05$) and significantly reduced d 25 *Lactobacillus* and d 31 *Lactobacillus* ($P < 0.05$).

Caecal Microbiota

Figure 7L shows that compared with the unchallenged birds, NE-challenged birds had significantly increased *Clostridium perfringens* numbers in the caecum at d 31 ($P < 0.05$). Compared with the control group, dietary APS supplementation significantly reduced the number of *Clostridium perfringens* in the caecum at d 31 ($P < 0.05$).

Non-Targeted Metabolome Analysis of Ileum Contents

Data Quality Assessment and Comparison of Differences Between Groups

To ensure the reliability of the data, the influence of factors such as the sample preparation process and instrument instability must be minimized. In the process of detection and analysis, three QC samples are used to monitor and ensure the stability of the instrument, after which the missing values are simulated in the original data to standardize the data. After obtaining the sorted data, we perform partial least squares discrimination analysis (PLS-DA). Orthogonal partial least squares-discriminant analysis was performed on the data, and the PLS-DA model of the APS supplementation group versus the control group was obtained. As shown in **Figures 8A, B**, compared with the control group CC, in the CA ileum content of the APS supplementation group, the middle metabolites changed significantly, and there were significant differences between the two treatment groups. The results of the permutation test of the PLS-DA model are shown in **Figure 8C** (intercept R2 = 0.91, Q2 = -0.59). Thus, it can be seen that the PLS-DA model does not have an overfitting phenomenon, and the model has good robustness.

Differential Metabolite Screening Between Groups

According to the relative molecular mass and the secondary mass spectrometry data combined with the HMDB, PubChem and KEGG databases, a comparison search was conducted to analyze the potential differential metabolites. According to the condition that the variable importance in the projection (VIP) of the first principal component of the PLS-DA model was greater than 1 and $P < 0.05$, 35 different metabolites were identified in positive ion mode (**Table 3**). There were 14 types in negative ion mode (**Table 4**). Compared with the blank control group, the metabolites that were increased in the ileal content of broiler diets with APS were mainly formononetin, bile acid, taurine and bile acid intermediates, equol, glycitein and 20 other kinds, while serotonin (5-HT), uric acid, L-arginine, DL-lysine, indole-derived salt, cystine, 4-pyruvate, L-tianmen 29 kinds of aspartic acid, thymine, and protoporphyrin IX were downregulated. As shown in **Figures 8D, E**, the screening of differential metabolites was visualized in the form of a volcano map.

Differential Metabolite KEGG Analysis

Table 5 shows that the differential metabolites between groups were mapped to 23 metabolic pathways in the KEGG database: gap junction, pyrimidine metabolism, neuroactive ligand-receptor interaction, purine metabolism, tryptophan metabolism, metabolic pathways, primary bile acid biosynthesis, histidine metabolism, taurine and hypotaurine metabolism, nicotinamide and nicotinamide metabolism, neuroactive ligand-receptor interaction, metabolic pathways, arginine biosynthesis, alanine, aspartate and glutamate metabolism, glycine, serine and threonine metabolism, cysteine and methionine metabolism, beta-alanine metabolism, vitamin B6 metabolism, vitamin B6 metabolism pantothenate and CoA biosynthesis, porphyrin and chlorophyll metabolism, sulfur metabolism, aminoacyl-tRNA biosynthesis, and ABC transporters.

Enrichment Analysis of Metabolic Pathways of Differential Metabolites

The metabolites of differences between groups were entered into MetaboAnalyst, the database corresponding to chickens was used to perform enrichment analysis on metabolic pathways, and the corresponding P values were calculated. Through topological and enrichment analyses of the metabolic pathways where the differential metabolites are located, the metabolic pathways are screened in depth to identify the metabolic pathways that are more relevant to the experimental treatment. The screening conditions were $P < 0.05$ in the enrichment analysis and an influence value greater than 0.1 in the topological analysis. As shown in **Figures 8F, G**, through enrichment analysis of differential metabolites combined with topological analysis, the metabolic pathways significantly enhanced by APS supplementation mainly included primary

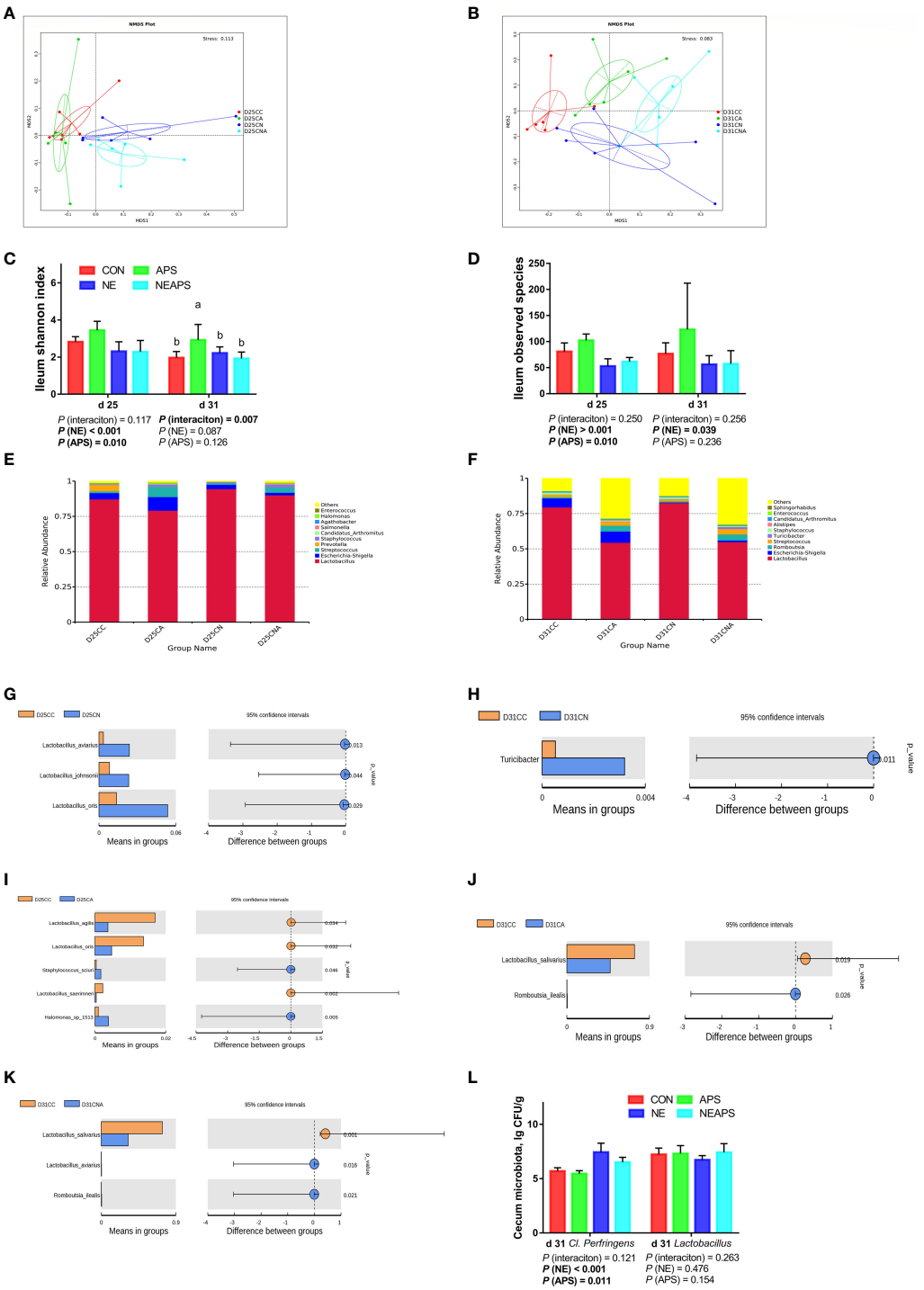

FIGURE 7 | Effects of dietary supplementation of astragalus polysaccharides on the gut microbiota of broiler chickens challenged with necrotic enteritis. The beta diversity **(A, B)** of ileum microbiota of broiler chickens was analyzed by non-metric multidimensional scaling (NMDS). The alpha diversity of ileum microbiota of broiler chickens was analyzed by shannon index **(C)** and observed species **(D)**. Top ten microbiota at the genus level in ileum of broiler chickens on d 25 **(E)** and d 31**(F)**. Differential microbes in ileum of broiler chickens by T-test **(G–K)**. The numbers of *Clostridium perfringens* and *Lactobacillus* **(L)** in cecum were detected by culture count method. All graphs are presented as mean, with the standard deviation (SD) shown *via* the whiskers. The main effect and interaction effects were analyzed using the general linear model (GLM) procedure, with the *P* values for the main effects written out below each plot. The one-way ANOVA and multiple comparisons were performed when interactive effects differed significantly. The lowercase letters on the bar charts indicate significant differences ($P < 0.05$). CC/CON, control group; CA/APS, APS group; CN/NE, NE infection group; CNA/NEAPS, APS infected with NE group.

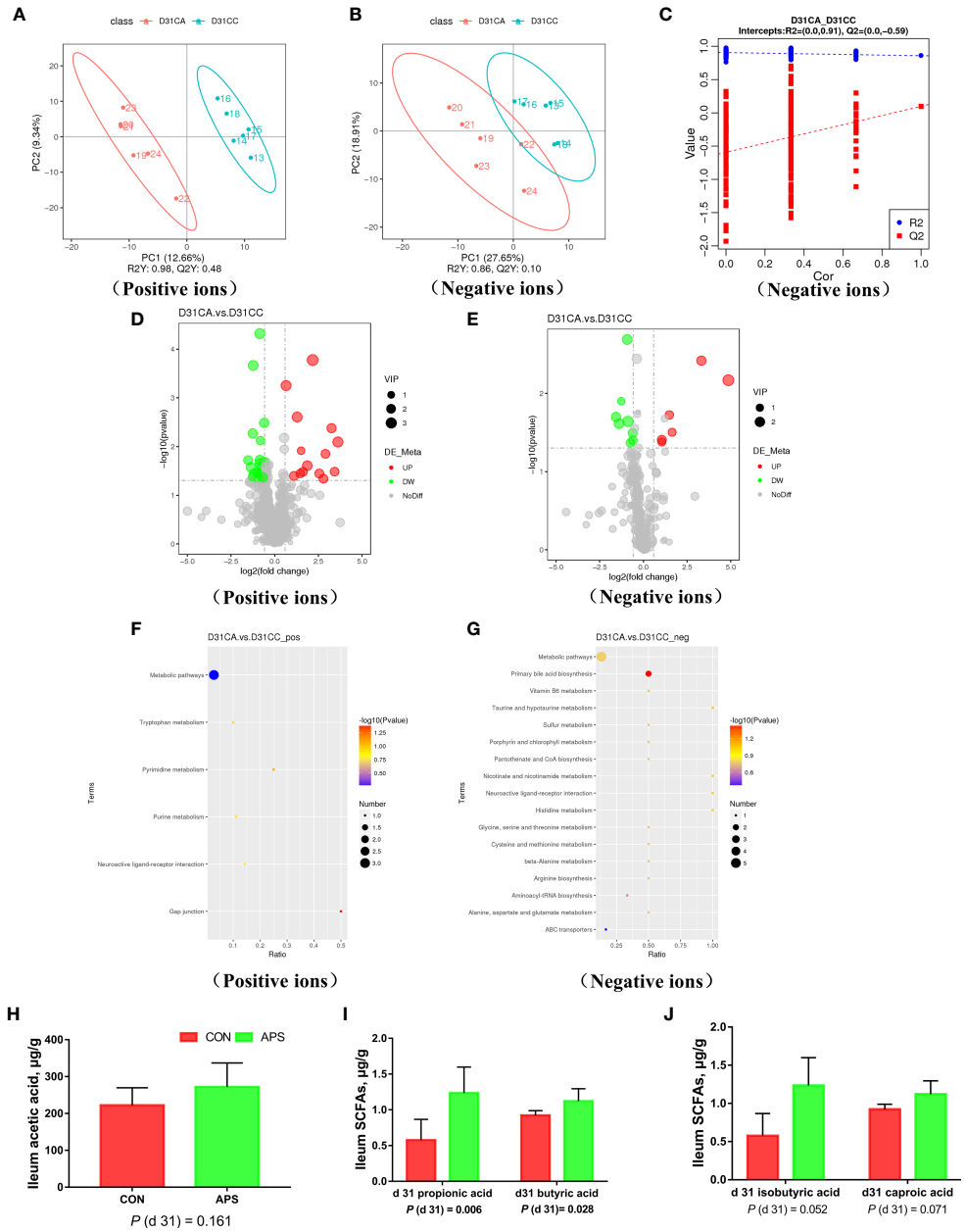

FIGURE 8 | Effects of dietary supplementation of astragalus polysaccharides on ileal metabolome and short-chain fatty acids of broiler chickens. PLS-DA scatter plot for group CA group vs. CC group **(A, B)**. Permutation test **(C)** of PLS-DA model for group CA versus CC (negative ion mode). Volcano plot for group CA versus CC **(D, E)**. Each point in the mountain chart represents a metabolite, the abscissa represents the fold change (take the log 2 logarithm) of each substance in the group, and the ordinate represents the P-value of the T test (take the log 10 logarithm). The size of the scatter points represents the VIP value of the PLS-DA model, and the larger the scatter point, the greater the VIP value. Scattered colors represent the final screening results. Significantly up-regulated metabolites are shown in red, significantly down-regulated metabolites are shown in green, and non-significantly different metabolites are shown in grey. CA group versus CC group KEGG pathway enrichment analysis bubble chart **(F, G)**. According to the results of KEGG enrichment, select the top 20 pathways sorted by P-values from small to large to draw a bubble chart. The abscissa is x/y (the number of differential metabolites in the corresponding metabolic pathway / the total number of metabolites identified in the pathway), the larger the value, the higher the enrichment of differential metabolites in the pathway, and the ordinate is the KEGG pathway name. The ordinate and color of the bubble indicate the P-values of the enrichment analysis (take the negative common logarithm, ie -log 10 P-values). The redder the color, the smaller the P-values, indicating that the degree of enrichment is more significant, the reliability of the test is greater and the difference in statistics is more significant. The size of the dot represents the number of different metabolites in the corresponding pathway. The larger the dot, the more differential metabolites in the pathway. The levels of short-chain fatty acids **(H–J)** in the ileal contents of broiler chickens were analyzed by high performance liquid chromatography (Dionex, USA). All graphs are presented as mean, with the standard deviation (SD) shown via the whiskers. Statistical differences were determined by one-way ANOVA, with the P values for the main effects written out below each plot. P-values represent the effect of the APS. CA, dietary APS supplementation group; CC, control group.

TABLE 3 | Up-regulated and down-regulated metabolites in ileum from group CA[a] vs CC[b] (Positive ions).

Items	Name	Fold Change	*P*-values[c]	VIP[d]	Molecular Weight
Up-regulated metabolites					
1	Tetranor-12(S)-HETE	4.52	<0.001	3.62	271.1
2	N4-(2,6-dimethoxy-3-pyridyl)-3,5-dimethyl-4-isoxazolesulfonamide	1.57	<0.001	2.94	313.1
3	4-[2-(4-chlorophenyl) diaz-1-enyl]-2-methyl-6-(piperidinomethyl)phenol	2.44	<0.001	2.85	343.1
4	MAG (18:3)	9.54	<0.001	2.28	352.3
5	(S)-Equol	12.29	0.010	3.00	242.1
6	N-(1,3-benzodioxol-5-ylmethyl)-6-morpholinonicotinamide	2.85	0.010	1.35	341.1
7	Jervine	7.48	0.010	2.03	425.3
8	Sodium cholate	3.65	0.020	2.67	430.3
9	FMH	10.77	0.030	1.99	433.2
10	Formononetin	3.07	0.030	2.02	268.1
11	Glycitein	2.75	0.040	1.87	284.1
12	Milbemycin A4 oxime	5.87	0.040	2.14	555.3
13	diethyl 2-[(4-benzhydrylpiperidino) methylidene] malonate	2.15	0.040	2.19	443.2
14	7-Ketodeoxycholic acid	6.92	0.050	2.04	406.3
Down-regulated metabolites					
1	EMH	0.55	<0.001	2.97	397.1
2	Uric Acid	0.43	<0.001	2.84	168.0
3	Taurocholic acid sodium salt hydrate	0.66	<0.001	2.36	538.3
4	NPK	0.42	0.010	2.44	714.4
5	Thymine	0.57	0.010	1.81	126.0
6	L-arginine	0.56	0.020	2.68	174.1
7	15-Deoxy-Δ12,14-prostaglandin J2-2-glycerol ester	0.35	0.020	2.16	408.2
8	Serotonin	0.65	0.020	2.41	176.1
9	FRH	0.55	0.020	2.43	480.2
10	ACar 10:1	0.39	0.030	2.42	313.2
11	1,3-diazaspiro [4.5] decane-2,4-dione	0.58	0.030	2.12	168.1
12	LPC 22:6	0.62	0.030	1.60	567.3
13	DL-Lysine	0.59	0.030	2.09	129.1
14	5,6-diphenyl-2,3-dihydropyrazine	0.50	0.030	2.11	234.1
15	PC (18:5e/2:0)	0.43	0.040	1.78	541.3
16	2-Hydroxycinnamic acid	0.54	0.040	1.94	164.0
17	PC (18:4e/2:0)	0.42	0.040	1.90	543.3
18	Gly-Val	0.63	0.040	2.11	174.1
19	Loxoprofen	0.62	0.040	2.22	246.1
20	2-Hydroxyphenylalanine	0.52	0.050	1.87	181.1
21	3-Methylcrotonylglycine	0.64	0.050	1.72	140.0

[a]*CA, astragalus polysaccharide group;*
[b]*CC, control group;*
[c]*P-values represent the effect of the APS;*
[d]*VIP, variable importance in projection.*

TABLE 4 | Up-regulated and down-regulated metabolites in ileum from group CA[a] vs CC[b] (Negative ions).

Items	Name	Fold Change	*P*-values[c]	VIP[d]	Molecular Weight
Up-regulated metabolites					
1	Cholic acid	9.98	<0.001	1.91	408.3
2	Equol	29.12	0.010	2.86	242.1
3	Glycoursodeoxycholic acid	2.80	0.020	1.49	449.3
4	Cholesteryl sulfate	3.13	0.030	1.32	466.3
5	Taurine	2.08	0.040	1.75	125.0
6	Dihydroroseoside	2.08	0.040	1.34	388.2
Down-regulated metabolites					
1	DL-4-Hydroxyphenyllactic acid	0.53	<0.001	2.19	182.1
2	Protoporphyrin IX	0.42	0.010	1.05	562.3
3	Cystine	0.34	0.020	1.89	240.0
4	4-Pyridoxic acid	0.54	0.020	2.47	183.1
5	Mestranol	0.38	0.020	2.24	310.2
6	N-Acetylalanine	0.65	0.030	1.75	131.1
7	L-Aspartic acid	0.66	0.040	1.60	133.0
8	3-Indoxyl sulphate	0.60	0.040	1.55	213.0

[a]*CA, astragalus polysaccharide group;*
[b]*CC, control group;*
[c]*P-values represent the effect of the APS;*
[d]*VIP, variable importance in projection.*

TABLE 5 | Annotation of KEGG[a] pathways.

Items	Map Title	*P*-values[b]	Meta IDs
Positive ions			
1	Gap junction	0.04	Serotonin
2	Pyrimidine metabolism	0.08	Thymine
3	Neuroactive ligand-receptor interaction	0.14	Serotonin
4	Purine metabolism	0.17	Uric Acid
5	Tryptophan metabolism	0.19	Serotonin
6	Metabolic pathways	0.56	Thymine, Serotonin, Uric Acid
Negative ions			
1	Primary bile acid biosynthesis	0.04	Taurine, Cholic acid
2	Histidine metabolism	0.09	L-Aspartic acid
3	Taurine and hypotaurine metabolism	0.09	Taurine
4	Nicotinate and nicotinamide metabolism	0.09	L-Aspartic acid
5	Neuroactive ligand-receptor interaction	0.09	Taurine
6	Metabolic pathways	0.16	Taurine, Protoporphyrin IX, 4-Pyridoxic acid, Cholic acid, L-Aspartic acid
7	Arginine biosynthesis	0.17	L-Aspartic acid
8	Alanine, aspartate and glutamate metabolism	0.17	L-Aspartic acid
9	Glycine, serine and threonine metabolism	0.17	L-Aspartic acid
10	Cysteine and methionine metabolism	0.17	L-Aspartic acid
11	beta-Alanine metabolism	0.17	L-Aspartic acid
12	Vitamin B6 metabolism	0.17	4-Pyridoxic acid
13	Pantothenate and CoA biosynthesis	0.17	L-Aspartic acid
14	Porphyrin and chlorophyll metabolism	0.17	Protoporphyrin IX
15	Sulfur metabolism	0.17	Taurine
16	Aminoacyl-tRNA biosynthesis	0.25	L-Aspartic acid
17	ABC transporters	0.45	Taurine

*The order of enriched pathways was displayed based on hits and pathway impact. * Only those pathways with hits > 2 and adjust P-values < 0.05 were considered significantly enriched.*
[a]*KEGG, kyoto encyclopedia of genes and genomes;*
[b]*P-values represent the effect of the APS.*

bile acid biosynthesis, tryptophan metabolism, histidine metabolism, taurine and hypotaurine metabolism, nicotinate and nicotinamide metabolism, gap junctions, neuroactive ligand-receptor interactions, pyrimidine metabolism and purine metabolism.

Short-Chain Fatty Acids in Ileal Contents

Figures 8H–J shows that compared with the blank control group, the addition of APS to the broiler diet significantly increased the levels of propionic acid and butyric acid in the ileal content ($P < 0.05$). There was a tendency to increase isobutyric acid and caproic acid ($0.05 < P < 0.1$).

Correlation Heat Map

To explore the relationships between the intestinal microbiota, intestinal metabolites and apparent immune indicators in broiler chickens, based on the abovementioned ileal microbiome and metabolomics data, we subsequently performed a spearman correlation analysis (**Figure 9**) to determine the microbes and metabolites related to the immunomodulatory effect of APS.

As shown in **Figure 9A**, production performance was positively correlated with *Turicibacter*, *Romboutsia*, propionic acid, butyric acid, formononetin, S-equol, and cholic acid and was negatively correlated with *Lactobacillus*, *Halomonas*, *Prevotella*, uric acid, and L-arginine ($P < 0.05$). The proportion of Th17 cells in peripheral blood was positively correlated with *Lactobacillus*, *Halomonas*, *Prevotella*, Jerrivne, sodium cholate and cholic acid and negatively correlated with *Turicibacter* and *Romboutsia* ($P < 0.05$). The proportion of Treg cells in peripheral blood was positively correlated with *Lactobacillus*, jervine, sodium cholate, 7-ketodeoxycholic acid and cholic acid and negatively correlated with *Turicibacter* and *Romboutsia* ($P < 0.05$). The peripheral blood Th17/Treg ratio was positively correlated with uric acid and L-arginine ($P < 0.05$) and negatively correlated with 7-ketodeoxycholic acid, glycoursodeoxycholic acid and taurine ($P < 0.05$). Serum IL-1β was positively correlated with propionic acid, formononetin, jervine, sodium cholate, 7-ketodeoxycholic acid, cholic acid, glycoursodeoxycholic acid, taurine and milbemycin A4 oxime ($P < 0.05$) and negatively correlated with *Escherichia-Shigella*, *Prevotella*, uric acid and L-arginine ($P < 0.05$). Serum IL-17 was positively correlated with *Turicibacter*, *Romboutsia*, propionic acid, 7-ketodeoxycholic acid, glycoursodeoxycholic acid and milbemycin A4 oxime ($P < 0.05$) and negatively correlated with *Staphylococcus*, *Halomonas*, *Streptococcus*, uric acid and L-arginine ($P < 0.05$). Serum IL-17/IL-10 was positively correlated with *Romboutsia* and equol ($P < 0.05$) and negatively correlated with *Staphylococcus*, *Halomonas* and *Streptococcus* ($P < 0.05$). Peripheral blood T cell proliferation activity was positively correlated with *Halomonas*, *Escherichia-Shigella*, *Prevotella* and milbemycin A4 oxime ($P < 0.05$) and negatively correlated with *Lactobacillus* ($P < 0.05$). Peripheral blood B cell proliferation activity was positively correlated with *Halomonas*, *Prevotella* and milbemycin A4 oxime ($P < 0.05$) and negatively correlated with *Turicibacter* and uric acid ($P < 0.05$). *Lactobacillus* was positively correlated with serotonin and negatively correlated with propionic acid and S-equol ($P < 0.05$). As shown in **Figure 9B**, jejunal inflammatory cell infiltration was negatively correlated with *Romboutsia* ($P < 0.05$). The depth of jejunal crypts was positively correlated with equol ($P < 0.05$). Jejunal

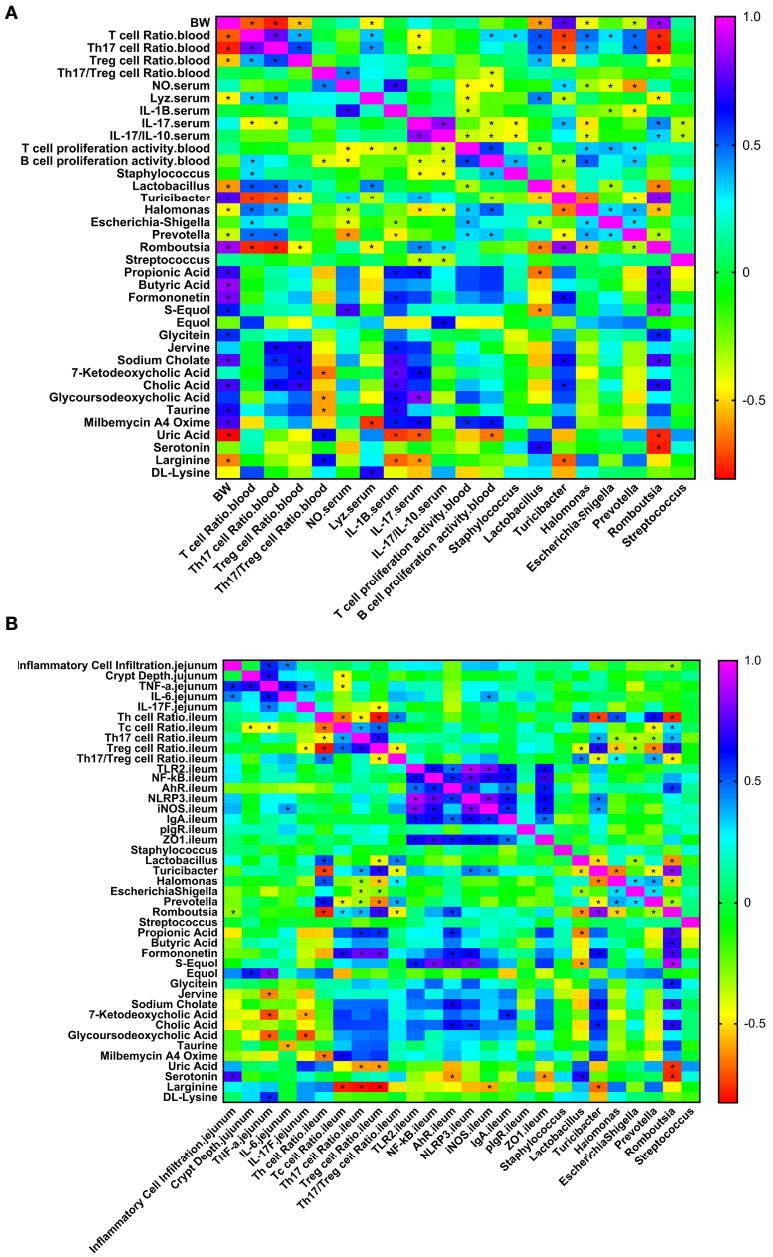

FIGURE 9 | Correlation heat map of ileum differential bacteria and differential immune function of broiler chickens. Spearman's correlations were calculated for all significantly different peripheral **(A)** and intestinal **(B)** immune indexes and different ileal microbes on genus level. Colors of squares represent r values of spearman's correlation coefficient. *$P < 0.05$.

TNF-α gene expression was positively correlated with equol and DL-lysine and negatively correlated with jervine, 7-ketodeoxycholic acid and glycoursodeoxycholic acid ($P < 0.05$). The expression of the *IL-6* gene in the jejunum was negatively correlated with taurine ($P < 0.05$). The expression of the *IL-17F* gene in the jejunum was negatively correlated with 7-ketodeoxycholic acid and glycoursodeoxycholic acid ($P < 0.05$). The proportion of Th cells in the ileum was positively correlated with *Lactobacillus*, *Halomonas* and *Prevotella* ($P < 0.05$) and negatively correlated with *Turicibacter*, *Romboutsia* and milbemycin A4 oxime ($P < 0.05$). The proportion of Tc cells in the ileum was positively correlated with *Romboutsia*, formononetin and milbemycin A4 oxime ($P < 0.05$) and negatively correlated with *Prevotella* and L-arginine ($P < 0.05$). The proportion of Th17 cells in the ileum was positively correlated with *Turicibacter*, *Romboutsia*, propionic acid and formononetin ($P < 0.05$) and negatively correlated with *Halomonas*, *Escherichia-Shigella*, *Prevotella*, uric acid and L-arginine ($P < 0.05$). The proportion of Treg cells in the ileum

was positively correlated with *Turicibacter*, *Romboutsia*, propionic acid and formononetin ($P < 0.05$) and negatively correlated with *Lactobacillus*, *Halomonas*, *Escherichia-Shigella*, *Prevotella*, uric acid and L-arginine ($P < 0.05$). The ratio of Th17/Treg cells in the ileum was positively correlated with *Lactobacillus*, *Halomonas*, and *Prevotella* ($P < 0.05$) and negatively correlated with *Turicibacter* and *Romboutsia* ($P < 0.05$). The expression of *TLR2* and *NF-κB* genes in the ileum was positively correlated with S-equol ($P < 0.05$). The expression of the *iNOS* gene in the ileum was positively correlated with *Turicibacter* and negatively correlated with L-arginine ($P < 0.05$). *IgA* gene expression in the ileum was positively correlated with 7-ketodeoxycholic acid ($P < 0.05$). Ileal *ZO-1* gene expression was negatively correlated with serotonin ($P < 0.05$). In addition, *Lactobacillus* was positively correlated with serotonin and negatively correlated with propionic acid and S-equol ($P < 0.05$). *Turicibacter* was positively correlated with formononetin, sodium cholate and cholic acid ($P < 0.05$) and negatively correlated with L-arginine ($P < 0.05$). *Romboutsia* was positively correlated with propionic acid, butyric acid, formononetin, S-equol, glycitein, sodium cholate and cholic acid ($P < 0.05$) and negatively correlated with uric acid and serotonin ($P < 0.05$). The results show that the immunomodulatory effect of APS is associated with a specifically altered microbe-metabolic axis.

DISCUSSION

Necrotic enteritis (NE) is an enterotoxic disease caused by *Clostridium perfringens*. This disease often occurs in broilers at 2–5 weeks of age, with a mortality rate of approximately 2%-10%, with a maximum of 50%. Geier et al. (30) showed that necrotic enteritis can increase the broiler feed-to-meat ratio, mortality and intestinal disease and reduce body weight. The main reason for the decline in growth performance is that coccidia cause proteins (including plasma) to leak into the intestinal lumen, which promotes the rapid reproduction and pathogenicity of toxin-producing *Clostridium perfringens*, resulting in a decrease in the digestion and absorption capacity of the small intestine (1). It is estimated that the poultry industry loses up to US$2 billion each year (2). Consistent with previous studies (17, 31), this experiment also observed that NE infection has a significant negative impact on broiler body weight and body weight gain. Supplementation with APS can effectively improve the decline in growth performance caused by NE infection. APS improves the growth performance of chickens (32, 33) but has a positive effect on animal growth in other animals, such as pigs (34, 35). APS alleviates the decline in growth performance caused by NE, which may be due to the direct bacteriostasis of APS, which reduces the number of *Clostridium perfringens*, or it may regulate the host immune function to sterilize and achieve indirect bacteriostasis, thereby reducing intestinal damage and the loss of growth performance. Therefore, the next step is to test the immune function of broilers.

First, we tested the systemic immune response and found that NE infection reduced the broiler thymus index, increased peripheral blood NO levels and lysozyme activity, increased the Th17 cell ratio and Th17/Treg cell ratio, and increased the production of the proinflammatory cytokines IL-17 and Th17/IL-10. At the same time, other inflammatory cytokines, such as IL-1β and IFN-γ, and the anti-inflammatory cytokine IL-4 were increased, reducing the proliferation capacities of T and B lymphocytes in the preinfection period, indicating that NE Infection of broilers caused systemic inflammation and simultaneously suppressed systemic cellular immune function. Previous studies have found that NE-challenged broilers significantly upregulate the expression of splenic inflammatory cytokine genes, causing systemic inflammation (36, 37). It has been reported that enterotoxigenic E. coli-challenged mice significantly upregulate the proportions of Th17 and Treg cells in the spleen and intestinal mucosal lymph nodes, upregulate the mRNA and protein expression of RORα in the intestinal mucosal lymph nodes, and downregulate the mRNA and protein expression of Foxp3 (4). Another study found that coccidia infection significantly increased the proportion of Th17 cells in the spleen and caecal tonsils (6), which is consistent with the findings of this study. We speculate that the reason for the more serious systemic inflammatory response caused by NE may be that strong intestinal inflammation leads to damage to the intestinal barrier. Pathogens and proinflammatory cytokines enter the blood through intestinal epithelial cells, stimulate peripheral immune organs and cause systemic inflammation. Dietary APS supplementation can increase the ratio of Treg cells and the IL-10 levels in peripheral blood, reduce the ratio of Th17/Treg cells and Th17/IL-10 cytokines, and alleviate the systemic inflammation caused by NE. Liu et al. found that APS can alleviate the immune stress response of chickens induced by LPS mainly by reducing the transcription of genes such as TLR4 and NF-κB (38). In a mouse study, it was found that intraperitoneal injection of APS downregulated the ratio of Th2 and Th17 cells in the peripheral blood of mice challenged with bacterial sepsis (39), consistent with the results of this study, indicating that dietary APS supplementation can alleviate the systemic inflammation caused by NE. We speculate that this may be due to APS alleviating intestinal inflammation and improving the intestinal barrier, thereby indirectly alleviating systemic inflammation.

The more serious systemic inflammatory response in broilers after NE infection may be related to intestinal inflammation and the impaired intestinal barrier (40). The damage to the intestinal tract is caused by pathogenic bacteria and dietary supplemented APS. As the intestine is the first target organ of action, we also need to pay attention to the situation of intestinal inflammation. In view of the characteristics of NE infection, intestinal health and function were also the focus of this trial. The scores of intestinal lesions, histopathology scores, intestinal tissue morphology and the number of caecal pathogens are important indicators for assessing intestinal health, functional integrity and disease recovery. In this trial, NE infection caused bleeding points in the jejunum and ileum, and the degree of jejunum lesions was stronger than that of the ileum. The score of intestinal lesions, histopathological scores of the jejunum and the number of *Clostridium perfringens* in the caecum were significantly increased, and the structure of the jejunum was severely damaged. The decrease in sIgA in the ileal mucosa indicated that the NE model was successfully established, the intestinal mucosa

had a strong inflammatory response and some mucosal immune functions were impaired. These results are consistent with previous studies, indicating that NE infection causes inflammation of the intestinal mucosa inflammatory response and simultaneously damages the intestinal barrier structure and increases the permeability of the intestine. Pathogens and proinflammatory cytokines pass through the intestinal barrier and into the blood, which induces the occurrence of systemic inflammation (17, 31, 41). However, dietary APS supplementation reduced intestinal lesion scores and pathological scores, increased jejunum V/C values, and reduced crypt depth. Therefore, we inferred that dietary APS supplementation alleviated the intestinal damage caused by NE and prevented pathogenic bacteria from entering the bloodstream, which alleviated the systemic immune response.

To clarify the mechanism of dietary APS supplementation in intestinal inflammation and intestinal health, we further evaluated the ratio and proliferation activity of Th17/Treg cells in the ileum and the changes in the expression profiles of related immune signalling pathways and related downstream target genes in the intestine. Th17 and Treg cells in the body are related to each other developmentally, and they transform into each other under the control of a variety of factors. Th17 cells play an important role in the development of autoimmunity and inflammation and are key in the immune response; Treg cells regulate the systemic immune response by regulating the activity of effector T cells and maintaining peripheral immune tolerance. The transcription factors Foxp3+ and RORγt are specific transcription factors of Treg cells and Th17 cells, respectively, and are closely related to the differentiation of the two. Regulating the balance of Foxp3+ and RORγt can indirectly correct the imbalance of Th17/Treg cells. The results of this study found that NE infection resulted in the upregulation of the ratios of Tc and Th17 cells and Th17/Treg cells in the ileum, the decrease of the ratio of Tc cells, the activation of TLR2-NF-κB signals in the jejunum and ileum, and upregulation of the expression of the Th17 cell-related genes RORα, IL-6, TGF-β1. These results indicate that NE infection differentially regulates the expression of intestinal immune-related genes, and the Th17/Treg cell ratio is unbalanced, leading to aggravation of the intestinal immune inflammatory response. Studies have found that large amounts of STAT-3, IL-1β, IL-6 and IL-17 are produced in caecal intraepithelial lymphocytes in broiler chickens challenged by *E. coli* (42). Coccidia infection in broilers significantly increases the proportions of Th17 cells in the spleen and caecal tonsils (6). Previous studies on mouse colitis have found that IL-1β is significantly increased when intestinal inflammation occurs, which mediates chronic intestinal inflammation by promoting the accumulation of IL-17A-secreting innate lymphoid cells and Th17 cells (3). It has been reported that enterotoxigenic *E. coli*-challenged mice significantly upregulate the proportion of Th17 and Treg cells in the spleen and intestinal mucosal lymph nodes, upregulate the mRNA and protein expression of RORα in the intestinal mucosal lymph nodes, and downregulate the mRNA and protein expression of Foxp3 (4). Other studies have found that TNBS-induced colitis and DSS-induced colitis show significant increases in intestinal IL-17 (5), consistent with the findings of this study. Dietary APS supplementation can decrease intestinal RORα, IL-17F, and IL-17F/IL-10 levels, increase ileal IL-4 mRNA levels, reduce the ileal Th17 and Th17/Treg cell ratios, increase ileal T and B cell proliferation activity, increase the expression of the IL-4 gene in the ileum, and simultaneously increase ZO-1 to improve the damage to the intestinal barrier caused by NE, reduce the intestinal lesion score and pathological score, and alleviate the intestinal inflammation caused by NE. Other scholars have pointed out that the addition of APS can reduce the overexpression of proinflammatory cytokines caused by LPS by inhibiting the TLR-NF-κB signalling pathway (43). Studies have also found that dietary supplementation with 400 ppm APS can significantly reduce IL-17 levels and RORα expression in the colon of mice with TNBS-induced colitis and increase the proportion of Treg cells in the colon (12), consistent with the results of this study. Therefore, these results demonstrate that the addition of APS not only enhances the body's innate immune defence response to pathogen infection by regulating the TLR signalling pathway but also balances the proinflammatory/anti-inflammatory responses of intestinal Th17/Treg cells to avoid excessive inflammation and maintain immune homeostasis. This effect is achieved by downregulating the proportions of proinflammatory Th17 cells and their cytokines and upregulating the expression levels of anti-inflammatory Tregs and their cytokines.

According to the scores of intestinal lesions and pathological scores, ileal lesions are higher than those in the jejunum, and the abundance of microorganisms in the ileum of broilers is significantly higher than that in the jejunum (44); therefore, the interaction effect between microorganisms and the host may be more important in the ileum. strong. Combined with previous research reports, the segmented filamentous bacteria *Helicobacter* and *Clostridium* and the SCFAs produced by intestinal microbes can regulate the differentiation of intestinal Th17 and Treg cells (13). This study also found that dietary APS can increase the abundance of segmented filamentous bacteria and *Romboutsia* that can produce SCFAs. To clarify whether APS can regulate mucosal immune function and alleviate mucosal immune function by improving the gut microbiota through the mechanism of intestinal inflammation, we evaluated the microbiota, SCFAs and metabolome of ileum. We found that NE infection in broilers significantly increased the number of *Clostridium perfringens* in the caecum and the relative abundance of *Lactobacillus*, *Staphylococcus* and *Turicibacter* in the ileum. *Lactobacillus* is mostly beneficial bacteria, and NE infection increases its abundance. We speculate that the reason may be that *Lactobacillus* itself is the dominant ileum genus, and the abundance remains above 80%, while NE infection leads to the living environment of intestinal microbes. The changes in the ileum reduce the diversity of ileal microbial species α, which is specifically reflected in the reduction of the abundance of *Escherichia-Shigella*, the second most common bacterium in the control group, and provides a living space for the increase in the abundance of *Lactobacillus*. Regarding *Staphylococcus*, studies have found that most species pathogenic bacteria, among which *Staphylococcus*

aureus can cause serious animal diseases, such as mastitis, purulent disease, arthritis and urinary tract infections (45, 46). It has been reported that the abundance of *Turicibacter* in the colon of mice with acute dextran sulfate (DSS)-induced colitis increases and is significantly positively correlated with DSS treatment (47), which is consistent with the findings of this study. These findings indicate that NE infection can reduce the ileal microbial alpha diversity and increase the abundance of the harmful bacteria *Staphylococcus* and *Turicibacter* associated with DSS enteritis. However, dietary APS supplementation significantly reduced the number of *Clostridium perfringens* in the caecum, significantly increased the abundance of *Romboutsia*, *Staphylococcus*, and *Halomonas* in the ileum, and decreased the abundance of *Lactobacillus*. According to reports, *Romboutsia* is a gram-positive coccus that is more common in healthy human mucosa and may be related to host health (48). *Romboutsia* mainly uses monosaccharides and disaccharides to form acetic acid, formic acid and lactic acid (49). *Lactobacillus* is the dominant genus of the ileum, and the increase in the abundance of other microorganisms will inevitably reduce its abundance. The results showed that APS supplementation improved the ileal microbiota and increased the abundance of the SCFA-producing bacteria *Romboutsia*. Therefore, the level of microbial metabolite SCFAs in the ileum may also increase.

Changes in microbiota lead to changes in microbes and host metabolism. By targeting the metabolome, we found that APS supplementation significantly increased the levels of propionic acid and butyric acid in the ileal contents of d 31 broilers, and there was a tendency to increase isobutyric acid and caproic acid levels. Short-chain fatty acids (SCFAs) play an important role in intestinal physiology. According to reports, SCFAs, especially butyrate, can be used as an energy source for colonic epithelial cells (50). In addition, SCFAs have a negative impact on the expression of virulence factors of bacterial pathogens (51). Studies have also found that in mice, the SCFA butyrate produced by the fermentation of symbiotic microorganisms in the starch in the back half of the intestine helps the thymus to produce Treg cells, and the produced propionic acid can inhibit histone deacetylase. (HDAC), which enhances the production of new Treg cells in peripheral blood (52), consistent with the results in the peripheral blood and ileum in this study. The results indicated that dietary APS supplementation may increase the levels of propionic acid and butyric acid by increasing the abundance of *Romboutsia* in the ileum, protecting intestinal epithelial cells, and increasing the proportion of Treg cells in the peripheral blood to alleviate inflammatory damage caused by NE.

We measured the nontarget metabolome of the ileal content and found that dietary APS supplementation increased formononetin, bile acid, taurine and bile acid intermediates, equol, and glycitein and reduced 5-HT, uric acid, an indole-derived salts in the ileal content. Through enrichment analysis of differential metabolites combined with topological analysis, the metabolic pathways significantly enhanced by APS supplementation mainly included primary bile acid biosynthesis, tryptophan metabolism, histidine metabolism, taurine metabolism, nicotinate and nicotinamide metabolism, gap junctions, neuroactive ligand-receptor interactions, pyrimidine metabolism and purine metabolism. Previous studies have found that formononetin is a flavonoid compound that has anti-inflammatory, antioxidant, lipid metabolism, and antitumor activities in Astragalus, Spatholobi and other plants (53). These results indicate that in addition to directly regulating the immune function of the host, APS may also be metabolized by intestinal microorganisms to produce formononetin to regulate the mucosal immune function of broilers. Studies have also found that intraperitoneal injection of formononetin can slow DSS-induced colitis by inhibiting NLRP3 inflammasomes (54). It has been reported that bile acids can promote the differentiation and activity of Th17 cells and Tregs involved in regulating inflammation and can regulate the differentiation and activity of Th17 cells and Tregs associated with intestinal inflammatory diseases (55, 56). Taurine is a sulfur-containing amino acid in animals that has biological effects such as improving immune function, antioxidation, and lowering blood sugar (57, 58). The composition of murine intestinal commensal bacteria (*Bacteroides polymorpha*, *Bacteroides fragilis*) in the murine intestinal bile acid pool regulates the number of RORγ+ regulatory T cells in the colon. In SPF mice with insufficient diet and nutrition, the intestinal bile acid pool was restored (replenishing a specific combination of primary or secondary bile acids), colon RORγ+ Tregs were increased through the bile acid-VDR axis, and the susceptibility to colitis was reduced (59). S-equol and glycitein are derived from soybeans, have oestrogenic and antiestrogenic properties, and have anti-inflammatory and antioxidant effects (60, 61). Equol is an important product formed by the microbial metabolism of soybean isoflavones, a secondary metabolite formed during the growth of soybeans (62) and possibly a metabolite of the active ingredients of soybean meal produced by ileal microorganisms. Jervine comes from the Veratrum plant and is a steroidal alkaloid. It has anti-inflammatory, antioxidant and antihypertensive effects (63). According to reports, uric acid may be a danger signal released by damaged cells, which can stimulate the NFκB signalling pathway of dendritic cells to promote the release of cytokines related to Th17 differentiation and then induce inflammation and a strong immune response (64). Arginine is an essential amino acid in poultry, and poultry lack carbamoyl phosphate synthase and dihydropyrrole-5-carboxylic acid synthase, which are necessary to synthesize arginine. However, some studies have found that excessive L-arginine may cause inflammatory episodes such as pancreatitis in animals (65, 66). Through spearman correlation analysis, we found that the ratio of Th17/Treg cells was mainly positively correlated with *Lactobacillus*, *Halomonas*, *Prevotella*, uric acid and L-arginine and negatively correlated with *Romboutsia* and *Turicibacter*. *Romboutsia* was positively correlated with propionic acid, butyric acid, formononetin, S-equol, glycitein, sodium cholate and cholic acid and negatively correlated with uric acid and serotonin. Correlation analysis results indicate that *Romboutsia* may upregulate formononetin and equol by producing enzymes to degrade substrates such as APS and soybean meal and downregulate metabolites such as uric acid to regulate Th17/Treg balance and host immune function, thereby producing beneficial effects.

CONCLUSION

Taken together, dietary APS supplementation improved the production performance and immune function of broilers challenged with NE and regulated the Th17/Treg balance. Further microbiome and metabolomics studies demonstrated that APS induced structural rearrangement of gut microbiota, mediating alterations in a wide range of metabolites. With clustering and correlation analysis, the immunoregulatory effect of APS was highly correlated with an increased abundance of *Romboutsia*, which was linked to the upregulation and downregulation of a range of metabolites, such as formononetin, propionic acid, butyric acid, sodium cholate, bile acid, S-equol, glycitein, uric acid, and L-arginine. The specific alterations within the microbe-metabolic axis may play an important role in the immunoregulation of APS. The results provide new insights into the regulatory effect of APS on the immune system of broiler chickens challenged with NE.

DATA AVAILABILITY STATEMENT

The 16S rRNA gene amplicon sequencing results were submitted to the Sequence Read Archive of the NCBI (accession number: PRJNA766165). This data can be found here: https://www.ncbi.nlm.nih.gov/bioproject/766165.

ETHICS STATEMENT

The animal study was reviewed and approved by China Agricultural University Animal Care and Use Committee (Beijing, China).

AUTHOR CONTRIBUTIONS

BS designed and performed experiments, analyzed data, and wrote the paper. PL and SY performed some experiments, and analyzed some data. YL and MG analyzed some 16SrRNA sequencing data. HL analyzed some metabolome data. ZL performed some experiments. YG initiated the study, designed animal experiments, analyzed data, and wrote the paper. All authors contributed to the article and approved the submitted version.

FUNDING

This study was funded by the China Agriculture Research System program (CARS-41-G11).

REFERENCES

1. Van Immerseel F, De Buck J, Pasmans F, Huyghebaert G, Haesebrouck F, Ducatelle R. Clostridium Perfringens in Poultry: An Emerging Threat for Animal and Public Health. *Avian Pathol* (2004) 33(6):537–49. doi: 10.1080/03079450400013162
2. Mcdevitt RM, Brooker JD, Acamovic T, Sparks N. Necrotic Enteritis; a Continuing Challenge for the Poultry Industry. *World's Poultry Sci J* (2006) 62(2):221–47. doi: 10.1079/WPS200593
3. Coccia M, Harrison OJ, Schiering C, Asquith MJ, Becher B, Powrie F, et al. IL-1beta Mediates Chronic Intestinal Inflammation by Promoting the Accumulation of IL-17A Secreting Innate Lymphoid Cells and CD4(+) Th17 Cells. *J Exp Med* (2012) 209(9):1595–609. doi: 10.1084/jem.20111453
4. Wang KC, Lee WL, Wang PH. Lactobacillus Supplementation and Group B Streptococcus Infection. *Taiwan J Obstet Gynecol* (2017) 56(1):121–2. doi: 10.1016/j.tjog.2016.12.010
5. Alex P, Zachos NC, Nguyen T, Gonzales L, Chen TE, Conklin LS, et al. Distinct Cytokine Patterns Identified From Multiplex Profiles of Murine DSS and TNBS-Induced Colitis. *Inflamm Bowel Dis* (2009) 15(3):341–52. doi: 10.1002/ibd.20753
6. Kim WH, Lillehoj HS, Min W. Indole Treatment Alleviates Intestinal Tissue Damage Induced by Chicken Coccidiosis Through Activation of the Aryl Hydrocarbon Receptor. *Front Immunol* (2019) 10:560:560. doi: 10.3389/fimmu.2019.00560
7. Ulluwishewa D, Anderson RC, McNabb WC, Moughan PJ, Wells JM, Roy NC. Regulation of Tight Junction Permeability by Intestinal Bacteria and Dietary Components. *J Nutr* (2011) 141(5):769–76. doi: 10.3945/jn.110.135657
8. Liu WC, Guo Y, Zhao ZH, Jha R, Balasubramanian B. Algae-Derived Polysaccharides Promote Growth Performance by Improving Antioxidant Capacity and Intestinal Barrier Function in Broiler Chickens. *Front Vet Sci* (2020) 7:601336:601336. doi: 10.3389/fvets.2020.601336
9. Ho Do M, Seo YS, Park HY. Polysaccharides: Bowel Health and Gut Microbiota. *Crit Rev Food Sci Nutr* (2021) 61(7):1212–24. doi: 10.1080/10408398.2020.1755949
10. Liu WC, Ou BH, Liang ZL, Zhang R, Zhao ZH. Algae-Derived Polysaccharides Supplementation Ameliorates Heat Stress-Induced Impairment of Bursa of Fabricius *via* Modulating NF-kappaB Signaling Pathway in Broilers. *Poult Sci* (2021) 100(8):101139. doi: 10.1016/j.psj.2021.101139
11. Wang X, Li Y, Shen J, Wang S, Yao J, Yang X. Effect of Astragalus Polysaccharide and its Sulfated Derivative on Growth Performance and Immune Condition of Lipopolysaccharide-Treated Broilers. *Int J Biol Macromol* (2015) 76:188–94. doi: 10.1016/j.ijbiomac.2015.02.040
12. Zhao HM, Wang Y, Huang XY, Huang MF, Xu R, Yue HY, et al. Astragalus Polysaccharide Attenuates Rat Experimental Colitis by Inducing Regulatory T Cells in Intestinal Peyer's Patches. *World J Gastroenterol* (2016) 22(11):3175–85. doi: 10.3748/wjg.v22.i11.3175
13. Geuking MB, Burkhard R. Microbial Modulation of Intestinal T Helper Cell Responses and Implications for Disease and Therapy. *Mucosal Immunol* (2020) 13(6):855–66. doi: 10.1038/s41385-020-00335-w
14. Lv H, Tang Y, Zhang H, Li S, Fan Z. Astragalus Polysaccharide Supplementation Improves Production Performance, Egg Quality, Serum Biochemical Index and Gut Microbiota in Chongren Hens. *Anim Sci J* (2021) 92(1):e13550. doi: 10.1111/asj.13550
15. Liu YS, Li S, Wang XF, Xing T, Li JL, Zhu XD, et al. Microbiota Populations and Short-Chain Fatty Acids Production in Cecum of Immunosuppressed Broilers Consuming Diets Containing Gamma-Irradiated Astragalus Polysaccharides. *Poult Sci* (2021) 100(1):273–82. doi: 10.1016/j.psj.2020.09.089
16. Qiao H, Zhang L, Shi H, Song Y, Bian C. Astragalus Affects Fecal Microbial Composition of Young Hens as Determined by 16S rRNA Sequencing. *AMB Express* (2018) 8(1):70. doi: 10.1186/s13568-018-0600-9
17. Wu Y, Shao Y, Song B, Zhen W, Wang Z, Guo Y, et al. Effects of Bacillus Coagulans Supplementation on the Growth Performance and Gut Health of Broiler Chickens With Clostridium Perfringens-Induced Necrotic Enteritis. *J Anim Sci Biotechnol* (2018) 9(1):9. doi: 10.1186/s40104-017-0220-2
18. Zhang S, Liao B, Li X, Li L, Ma L, Yan X. Effects of Yeast Cell Walls on Performance and Immune Responses of Cyclosporine A-Treated, Immunosuppressed Broiler Chickens. *Br J Nutr* (2012) 107(6):858–66. doi: 10.1017/S000711451100362X
19. Fair JM, Taylor-McCabe KJ, Shou Y, Marrone BL. Immunophenotyping of Chicken Peripheral Blood Lymphocyte Subpopulations: Individual Variability and Repeatability. *Vet Immunol Immunopathol* (2008) 125(3-4):268–73. doi: 10.1016/j.vetimm.2008.05.012

20. Jarosz L, Marek A, Gradzki Z, Kwiecien M, Kalinowski M. The Effect of Feed Supplementation With Zinc Chelate and Zinc Sulphate on Selected Humoral and Cell-Mediated Immune Parameters and Cytokine Concentration in Broiler Chickens. *Res Vet Sci* (2017) 112:59–65. doi: 10.1016/j.rvsc.2016.09.007
21. Vidanarachchi JK, Mikkelsen LL, Constantinoiu CC, Choct M, Iji PA. Natural Plant Extracts and Prebiotic Compounds as Alternatives to Antibiotics in Broiler Chicken Diets in a Necrotic Enteritis Challenge Model. *Anim Production Sci* (2013) 53(12):1247–59. doi: 10.1071/An12374
22. Wang W, Li Z, Lv Z, Zhang B, Lv H, Guo Y. Effects of Kluyveromyces Marxianus Supplementation on Immune Responses, Intestinal Structure and Microbiota in Broiler Chickens. *PloS One* (2017) 12(7):e0180884. doi: 10.1371/journal.pone.0180884
23. Magoc T, Salzberg SL. FLASH: Fast Length Adjustment of Short Reads to Improve Genome Assemblies. *Bioinformatics* (2011) 27(21):2957–63. doi: 10.1093/bioinformatics/btr507
24. Caporaso JG, Kuczynski J, Stombaugh J, Bittinger K, Knight R, Caparose JGKJ, et al. QIIME Allows Analysis of High-Throughput Community Sequencing Data. Nat Met 7: 335-336. *Nat Methods* (2010) 7(5):335–6. doi: 10.1038/nmeth.f.303
25. Edgar RC, Haas BJ, Clemente JC, Quince C, Knight R. UCHIME Improves Sensitivity and Speed of Chimera Detection. *Bioinformatics* (2011) 27 (16):2194–200. doi: 10.1093/bioinformatics/btr381
26. Edgar RC. UPARSE: Highly Accurate OTU Sequences From Microbial Amplicon Reads. *Nat Methods* (2013) 10(10):996–8. doi: 10.1038/nmeth.2604
27. DeSantis TZ, Hugenholtz P, Larsen N, Rojas M, Brodie EL, Keller K, et al. Greengenes, a Chimera-Checked 16S rRNA Gene Database and Workbench Compatible With ARB. *Appl Environ Microbiol* (2006) 72(7):5069–72. doi: 10.1128/AEM.03006-05
28. Langille MG, Zaneveld J, Caporaso JG, McDonald D, Knights D, Reyes JA, et al. Predictive Functional Profiling of Microbial Communities Using 16S rRNA Marker Gene Sequences. *Nat Biotechnol* (2013) 31(9):814–21. doi: 10.1038/nbt.2676
29. Minoru K, Susumu G, Yoko S, Miho F, Mao T. KEGG for Integration and Interpretation of Large-Scale Molecular Data Sets. *Nucleic Acids Res* (2012) 40 (D1):D109–14. doi: 10.1093/nar/gkr988
30. Geier MS, Mikkelsen LL, Torok VA, Allison GE, Olnood CG, Boulianne M, et al. Comparison of Alternatives to in-Feed Antimicrobials for the Prevention of Clinical Necrotic Enteritis. *J Appl Microbiol* (2010) 109(4):1329–38. doi: 10.1111/j.1365-2672.2010.04758.x
31. Song BC, Li HX, Wu YY, Zhen WR, Wang Z, Xia ZF, et al. Effect of Microencapsulated Sodium Butyrate Dietary Supplementation on Growth Performance and Intestinal Barrier Function of Broiler Chickens Infected With Necrotic Enteritis. *Anim Feed Sci Tech* (2017) 232:6–15. doi: 10.1016/j.anifeedsci.2017.07.009
32. Chen HL, Li DF, Chang BY, Gong LM, Dai JG, Yi GF. Effects of Chinese Herbal Polysaccharides on the Immunity and Growth Performance of Young Broilers. *Poult Sci* (2003) 82(3):364–70. doi: 10.1093/ps/82.3.364
33. Wang HF. Effects of Astragalus Membranaceus on Growth Performance, Carcass Characteristics, and Antioxidant Status of Broiler Chickens. *Acta Agriculturae Scandinavica* (2010) 60(3):151–8. doi: 10.1080/09064702.2010.511255
34. Yin FG, Liu YL, Yin YL, Kong XF, Huang RL, Li TJ, et al. Dietary Supplementation With Astragalus Polysaccharide Enhances Ileal Digestibilities and Serum Concentrations of Amino Acids in Early Weaned Piglets. *Amino Acids* (2009) 37(2):263–70. doi: 10.1007/s00726-008-0142-6
35. Yuan SL, Piao XS, Li DF, Kim SW, Lee HS, Guo PF. Effects of Dietary Astragalus Polysaccharide on Growth Performance and Immune Function in Weaned Pigs. *Animalence* (2006) 82(04):501–7. doi: 10.1079/ASC200653
36. Tan J, Liu S, Guo Y, Applegate TJ, Eicher SD. Dietary L-Arginine Supplementation Attenuates Lipopolysaccharide-Induced Inflammatory Response in Broiler Chickens. *Br J Nutr* (2014) 111(8):1394–404. doi: 10.1017/S0007114513003863
37. Hong YH, Song W, Lee SH, Lillehoj HS. Differential Gene Expression Profiles of Beta-Defensins in the Crop, Intestine, and Spleen Using a Necrotic Enteritis Model in 2 Commercial Broiler Chicken Lines. *Poult Sci* (2012) 91(5):1081–8. doi: 10.3382/ps.2011-01948
38. Liu L, Shen J, Zhao C, Wang X, Yao J, Gong Y, et al. Dietary Astragalus Polysaccharide Alleviated Immunological Stress in Broilers Exposed to Lipopolysaccharide. *Int J Biol Macromol* (2015) 72:624–32. doi: 10.1016/j.ijbiomac.2014.08.057
39. Hou YC, Wu JM, Wang MY, Wu MH, Chen KY, Yeh SL, et al. Modulatory Effects of Astragalus Polysaccharides on T-Cell Polarization in Mice With Polymicrobial Sepsis. *Mediators Inflamm* (2015) 2015:826319. doi: 10.1155/2015/826319
40. Wageha A, Claudia H, Michael H. Enteric Pathogens and Their Toxin-Induced Disruption of the Intestinal Barrier Through Alteration of Tight Junctions in Chickens. *Toxins* (2017) 9(2):60. doi: 10.3390/toxins9020060
41. Timbermont L, Haesebrouck F, Ducatelle R, Van Immerseel F. Necrotic Enteritis in Broilers: An Updated Review on the Pathogenesis. *Avian Pathol* (2011) 40(4):341–7. doi: 10.1080/03079457.2011.590967
42. Zhang L, Liu R, Song M, Hu Y, Pan B, Cai J, et al. Eimeria Tenella: Interleukin 17 Contributes to Host Immunopathology in the Gut During Experimental Infection. *Exp Parasitol* (2013) 133(2):121–30. doi: 10.1016/j.exppara.2012.11.009
43. Dong N, Li X, Xue C, Zhang L, Wang C, Xu X, et al. Astragalus Polysaccharides Alleviates LPS-Induced Inflammation *via* the NF-Kappab/MAPK Signaling Pathway. *J Cell Physiol* (2020) 235(7-8):5525–40. doi: 10.1002/jcp.29452
44. Mohd Shaufi MA, Sieo CC, Chong CW, Gan HM, Ho YW. Deciphering Chicken Gut Microbial Dynamics Based on High-Throughput 16S rRNA Metagenomics Analyses. *Gut Pathog* (2015) 7:4. doi: 10.1186/s13099-015-0051-7
45. Foster TJ. Potential for Vaccination Against Infections Caused by Staphylococcus Aureus. *Vaccine* (1991) 9(4):221–7. doi: 10.1016/0264-410x(91)90103-d
46. Witte W. Antibiotic Resistance in Gram-Positive Bacteria: Epidemiological Aspects. *J Antimicrob Chemother* (1999) 44 Suppl A:1–9. doi: 10.1093/jac/44.suppl_1.1
47. Munyaka PM, Rabbi MF, Khafipour E, Ghia JE. Acute Dextran Sulfate Sodium (DSS)-Induced Colitis Promotes Gut Microbial Dysbiosis in Mice. *J Basic Microbiol* (2016) 56(9):986–98. doi: 10.1002/jobm.201500726
48. Mangifesta M, Mancabelli L, Milani C, Gaiani F, de'Angelis N, de'Angelis GL, et al. Mucosal Microbiota of Intestinal Polyps Reveals Putative Biomarkers of Colorectal Cancer. *Sci Rep* (2018) 8(1):13974. doi: 10.1038/s41598-018-32413-2
49. Gerritsen J, Fuentes S, Grievink W, van Niftrik L, Tindall BJ, Timmerman HM, et al. Characterization of Romboutsia Ilealis Gen. Nov., Sp. Nov., Isolated From the Gastro-Intestinal Tract of a Rat, and Proposal for the Reclassification of Five Closely Related Members of the Genus Clostridium Into the Genera Romboutsia Gen. Nov., Intestinibacter Gen. Nov., Terrisporobacter Gen. Nov. And Asaccharospora Gen. Nov. *Int J Syst Evol Microbiol* (2014) 64(Pt 5):1600–16. doi: 10.1099/ijs.0.059543-0
50. Fleming SE, Fitch MD, DeVries S, Liu ML, Kight C. Nutrient Utilization by Cells Isolated From Rat Jejunum, Cecum and Colon. *J Nutr* (1991) 121 (6):869–78. doi: 10.1093/jn/121.6.869
51. Boyen F, Haesebrouck F, Vanparys A, Volf J, Mahu M, Van Immerseel F, et al. Coated Fatty Acids Alter Virulence Properties of Salmonella Typhimurium and Decrease Intestinal Colonization of Pigs. *Vet Microbiol* (2008) 132(3-4):319–27. doi: 10.1016/j.vetmic.2008.05.008
52. Arpaia N, Campbell C, Fan X, Dikiy S, van der Veeken J, deRoos P, et al. Metabolites Produced by Commensal Bacteria Promote Peripheral Regulatory T-Cell Generation. *Nature* (2013) 504(7480):451–5. doi: 10.1038/nature12726
53. Lima Cavendish R, de Souza Santos J, Belo Neto R, Oliveira Paixao A, Valeria Oliveira J, Divino de Araujo E, et al. Antinociceptive and Anti-Inflammatory Effects of Brazilian Red Propolis Extract and Formononetin in Rodents. *J Ethnopharmacol* (2015) 173:127–33. doi: 10.1016/j.jep.2015.07.022
54. Wu D, Wu K, Zhu Q, Xiao W, Shan Q, Yan Z, et al. Formononetin Administration Ameliorates Dextran Sulfate Sodium-Induced Acute Colitis by Inhibiting NLRP3 Inflammasome Signaling Pathway. *Mediators Inflamm* (2018) 2018:3048532. doi: 10.1155/2018/3048532
55. Hang S, Paik D, Yao L, Kim E, Trinath J, Lu J, et al. Author Correction: Bile Acid Metabolites Control TH17 and Treg Cell Differentiation. *Nature* (2020) 579(7798):E7. doi: 10.1038/s41586-020-2030-5
56. Jia W, Xie G, Jia W. Bile Acid-Microbiota Crosstalk in Gastrointestinal Inflammation and Carcinogenesis. *Nat Rev Gastroenterol Hepatol* (2018) 15 (2):111–28. doi: 10.1038/nrgastro.2017.119
57. Schuller-Levis GB, Park E. Taurine and its Chloramine: Modulators of Immunity. *Neurochem Res* (2004) 29(1):117–26. doi: 10.1023/b:nere.0000010440.37629.17
58. Marcinkiewicz J, Kontny E. Taurine and Inflammatory Diseases. *Amino Acids* (2014) 46(1):7–20. doi: 10.1007/s00726-012-1361-4

59. Song X, Sun X, Oh SF, Wu M, Zhang Y, Zheng W, et al. Microbial Bile Acid Metabolites Modulate Gut RORgamma(+) Regulatory T Cell Homeostasis. *Nature* (2020) 577(7790):410–5. doi: 10.1038/s41586-019-1865-0
60. Masilamani M, Wei J, Sampson HA. Regulation of the Immune Response by Soybean Isoflavones. *Immunol Res* (2012) 54(1-3):95–110. doi: 10.1007/s12026-012-8331-5
61. Di Cagno R, Mazzacane F, Rizzello CG, Vincentini O, Silano M, Giuliani G, et al. Synthesis of Isoflavone Aglycones and Equol in Soy Milks Fermented by Food-Related Lactic Acid Bacteria and Their Effect on Human Intestinal Caco-2 Cells. *J Agric Food Chem* (2010) 58(19):10338–46. doi: 10.1021/jf101513r
62. Murota K, Nakamura Y, Uehara M. Flavonoid Metabolism: The Interaction of Metabolites and Gut Microbiota. *Biosci Biotechnol Biochem* (2018) 82(4):600–10. doi: 10.1080/09168451.2018.1444467
63. Dumlu FA, Aydin T, Odabasoglu F, Berktas OA, Kutlu Z, Erol HS, et al. Anti-Inflammatory and Antioxidant Properties of Jervine, a Sterodial Alkaloid From Rhizomes of Veratrum Album. *Phytomedicine* (2019) 55:191–9. doi: 10.1016/j.phymed.2018.06.035
64. Conforti-Andreoni C, Spreafico R, Qian HL, Riteau N, Ryffel B, Ricciardi-Castagnoli P, et al. Uric Acid-Driven Th17 Differentiation Requires Inflammasome-Derived IL-1 and IL-18. *J Immunol* (2011) 187(11):5842–50. doi: 10.4049/jimmunol.1101408
65. Su KH, Cuthbertson C, Christophi C. Review of Experimental Animal Models of Acute Pancreatitis. *HPB (Oxford)* (2006) 8(4):264–86. doi: 10.1080/13651820500467358
66. Stojanović NM, Mitić KV, Randjelović P, Stevanović M, Stojiljković N, Ilić S, et al. Thymol Regulates the Functions of Immune Cells in the Rat Peritoneal Cavity After L-Arginine-Induced Pancreatitis. *Life Sci* (2021) 280:119704. doi: 10.1016/j.lfs.2021.119704

Conflict of Interest: Author HL is employed by Beijing Centre Biology Co., Ltd.

The remaining authors declare that the research was conducted in the absence of any commercial or financial relationships that could be construed as a potential conflict of interest.

frontiers in Nutrition

ORIGINAL RESEARCH
published: 11 March 2022
doi: 10.3389/fnut.2022.851541

Prevention of High-Fat Diet-Induced Hypercholesterolemia by *Lactobacillus reuteri* Fn041 Through Promoting Cholesterol and Bile Salt Excretion and Intestinal Mucosal Barrier Functions

Mengyao Lu[1†], *Jin Sun*[1†], *Yuning Zhao*[1], *Haowen Zhang*[1], *Xinyue Li*[1], *Jingbo Zhou*[1], *Hongyang Dang*[1], *Jidong Zhang*[2], *Wenjing Huang*[3], *Ce Qi*[1*] *and Duo Li*[1*]

[1] *Institute of Nutrition and Health, Qingdao University, Qingdao, China,* [2] *Department of Cardiology, The Affiliated Hospital of Medical College, Qingdao University, Qingdao, China,* [3] *Department of Paediatrics, The Affiliated Hospital of Medical College, Qingdao University, Qingdao, China*

OPEN ACCESS

Edited by:
Julio Villena, CONICET Centro de Referencia para Lactobacilos (CERELA), Argentina

Reviewed by:
María Fernanda Raya Tonetti, Consejo Nacional de Investigaciones Científicas y Técnicas (CONICET), Argentina
Roxana Beatriz Medina, CONICET Centro de Referencia para Lactobacilos (CERELA), Argentina

***Correspondence:**
Ce Qi
ceqi@qdu.edu.cn
Duo Li
duoli@qdu.edu.cn

[†] *These authors have contributed equally to this work*

Specialty section:
This article was submitted to Nutritional Immunology, a section of the journal Frontiers in Nutrition

Received: *10 January 2022*
Accepted: *17 February 2022*
Published: *11 March 2022*

Citation:
Lu M, Sun J, Zhao Y, Zhang H, Li X, Zhou J, Dang H, Zhang J, Huang W, Qi C and Li D (2022) Prevention of High-Fat Diet-Induced Hypercholesterolemia by Lactobacillus reuteri Fn041 Through Promoting Cholesterol and Bile Salt Excretion and Intestinal Mucosal Barrier Functions. Front. Nutr. 9:851541. doi: 10.3389/fnut.2022.851541

Objectives: *Lactobacillus reuteri* Fn041 (Fn041) is a probiotic isolated from immunoglobulin A coated microbiota in the human breast milk of Gannan in China with a low incidence of hypercholesterolemia. This study aims to explore the role and mechanism of Fn041 in preventing hypercholesterolemia caused by a high-fat diet in mice.

Methods: C57BL/6N mice were fed a low-fat diet or a high-fat diet and gavage with Fn041 and *Lactobacillus rhamnosus* GG (LGG) for 8 weeks.

Results: Both Fn041 and LGG prevented the occurrence of hypercholesterolemia, liver and testicular fat accumulation. In addition, a high-fat diet causes intestinal dysbiosis and mucosal barrier damage, which is associated with hypercholesterolemia. Fn041 prevented the high-fat diet-induced reduction in alpha diversity of intestinal microbiota and intestinal mucosal barrier damage. Fn041 treatment significantly increased fecal total cholesterol and total bile acids.

Conclusions: Fn041 prevented hypercholesterolemia by enhancing cholesterol excretion and mucosal barrier function.

Keywords: *Lactobacillus reuteri*, high-fat diet, gut microbiota, cholesterol, bile acid

INTRODUCTION

Chronic exposure to a high-fat diet can lead to an accumulation of cholesterol in the blood (1). An elevated plasma total cholesterol (TC) level is a recognized risk factor for coronary heart disease, atherosclerosis, and strokes (2). Successful management of cholesterol metabolism disorders can effectively prevent these diseases (3). There is growing evidence that gut microbiota dysbiosis strongly influences the development of cholesterol metabolism (4, 5). Statins are currently the most effective cholesterol-lowering drugs. However, their long-term use can have side effects such as hepatotoxicity and muscle toxicity (6). Therefore, there is a need to develop nutritional interventions with no side effects.

In the past decade, several researchers have confirmed that a 70 kg man contains about 3.8×10^{13} bacteria and interact with each other (7). Probiotics are defined by the World Health Organization as live microorganisms that provide health benefits to the host when given in sufficient amounts and are presently being evaluated for their efficacy in lowering TC and low-density lipoprotein cholesterol (LDL-C) levels in humans (8). Some probiotics, mainly *Lactobacillus* and *Bifidobacterium*, have potential cholesterol-lowering benefits in the gastrointestinal tracts of mammals (6, 9, 10). Early animal studies have shown that short-term prophylaxis and intervention with low doses of specific *Lactobacillus reuteri* can exert cholesterol-lowering effects (11). A recent meta-analysis compiled 15 foreign randomized controlled trials on lipid modulation using probiotics and showed that consuming *L. reuteri* significantly reduced total serum cholesterol and LDL-C levels (12). A population-based trial indicated that yogurt containing *L. reuteri* CRL 1098 reduces LDL-C and TC levels in patients with high cholesterol levels (13). Healthy hypercholesterolemic adults can reduce their cholesterol levels by taking capsules containing *L. reuteri* NCIMB 30242 (14). We previously isolated *L. reuteri* Fn041 from the breast milk samples of healthy mothers in the Gannan agricultural and pastoral areas of Gansu Province (15). The prevalence of hypercholesterolemia in the population of this region is lower than that in the highly industrialized areas of the East and South (16). The acid tolerance, bile salt tolerance, hydrophobicity, and mucus adhesion of Fn041 were higher than those of the typical probiotic *Lactobacillus rhamnosus* GG (LGG) (unpublished data). The former strain showed a high bile acid resistance, suggesting its potential role in the regulation of lipid metabolism. In our previous study, we found that Fn041 alleviates the effect of high-fat diet-induced dyslipidemia in mice (17); therefore, we further increased the fat supply ratio to observe whether Fn041 could prevent dyslipidemia and compared its results with those of the typical probiotic LGG to determine whether the cholesterol-lowering efficacies and mechanisms of the two strains were the same.

Based on previous studies, the following hypotheses have been proposed regarding the anti-cholesterol effects of probiotics: *Lactobacillus* degrades bile salts in the intestine; it also promotes the following: excretion of bile salt degradation products from the feces (18, 19), the production of short fatty acids (20), cholesterol assimilation (21), the coprecipitation of cholesterol with deconjugated bile and cholesterol conversion to coprostanol (22), cholesterol transport by intestinal epithelial cells for excretion (23), and cholesterol synthesis in the liver (24–26). Among these hypotheses, we are most concerned about the conversion of uncoupled bile acids into secondary bile acids by colonic microbes to control serum cholesterol levels (19).

This study aimed to explore whether Fn041 and LGG can prevent dyslipidemia and mucosal barrier damage caused by a high-fat diet. We also investigated the effects of strains Fn041 and LGG on intestinal microbiota and how they lower cholesterol levels *in vivo*.

MATERIALS AND METHODS

Diets and Animals

Sixty male C57BL/6N mice weighing 18–21 g (6 weeks old) were provided by Vital River Laboratory Animals Co., Ltd. (Beijing, China). All animal experimental procedures were performed in accordance with the Guidelines for Care and Use of Laboratory Animals of Qingdao University and approved by the Animal Ethics Committee of the Affiliated Hospital of Qingdao University (Approval No. QYFYWZLL25869). The mice were fed in the Experimental Animal Center of Qingdao University with a 12 h light/dark cycle, constant temperature ($22 \pm 1°C$), and constant humidity ($50 \pm 5\%$). All mice were given free access to water and a standard diet. After a week of acclimation, the mice were randomly divided into the following five groups ($n = 12$/group): LF, low-fat diet-fed mice; LF+Fn041, low-fat diet-fed mice treated with Fn041; HF (60% energy from fat), high-fat diet-fed mice; HF+Fn041, high-fat diet-fed mice treated with Fn041; HF+LGG, high-fat diet-fed mice treat with LGG. Fn041 and LGG were suspended in saline, and 1×10^9 colony-forming units (CFU) were administered daily via gavage. The same volume (100 μL) of saline was administered daily to low-fat and high-fat control mice. The probiotic treatment lasted for 8 weeks. The mice were weighed weekly; weight gain rate = (final week weight - starting weight)/starting weight. The compositions of the low-fat and high-fat diets are provided in the **Supplementary Table S1**.

Analyses of Biochemical Indicators

At the end of the animal experiment, the mice were anesthetized after 16 h of fasting and sacrificed via decortication. After the mouse was anesthetized, blood samples were collected using eyeball removal method. Blood samples were collected and isolated via centrifugation (Sigma3K15, Germany) at 1500 × *g* and 4°C for 10 min. TC, triglycerides (TG), LDL-C, and high-density lipoprotein cholesterol (HDL-C) levels in plasma, and catalase and malondialdehyde concentrations in liver tissue homogenates were measured using assay kits (Nanjing Jiancheng Bioengineering Institute, Nanjing, Jiangsu, China). Plasma levels of tumor necrosis factor α (TNF-α), interleukin 6 (IL-6), lipopolysaccharide (LPS), and lipopolysaccharide-binding protein (LBP) were quantified using enzyme-linked immunosorbent assay kits (Xiamen Huijia Biotechnology Co., Ltd, China). The enzyme-linked immunosorbent assay kits were also used to detect the contents of TC and total bile acid in feces (Xiamen Huijia Biotechnology Co., Ltd, China).

Histological Analysis of Fat and Liver Tissues

Fresh liver and testicular fat tissues were fixed with 4% paraformaldehyde and embedded in paraffin. Tissue sections of 5 μm thickness were prepared for hematoxylin and eosin and Oil Red O staining. Images were captured using a light microscope. The calculations for relevant indexes are as follows: Testicular fat index = testicular fat weight/body weight, perirenal fat index = perirenal fat weight/body weight, and liver index = liver fat weight/body weight.

Determination of Intestinal Permeability

The mice were subjected to fasting for 6 h and gavaged with 150 μL of 80 mg/mL 4.4 kDa fluorescein isothiocyanate-dextran (FD4; Sigma, St Louis, MO). Plasma was collected at 4 h post-gavage, diluted 1:5 (v/v) in phosphate-buffered saline, and transferred to a black opaque-bottom 96-well plate. Fluorescence was measured spectrophotometrically in 96-well plates (excitation, 485 nm; emission, 530 nm).

16S rRNA Gene Sequencing Analysis

Total genomic DNA was extracted from the ileum content using a QIAamp DNA Stool Mini Kit (Qiagen, Hilden, Germany). The DNA concentration was monitored using an Equalbit dsDNA HS Assay Kit. Then, two highly variable regions of prokaryotic 16S rDNA, including V3 and V4, were amplified using 20–30 ng DNA as a template using polymerase chain reaction (PCR) primers. The V3–V4 regions of the 16S rRNA gene were amplified via PCR using universal primers (forward: 5′- ACTCCTACGGGAGGCAGCA-3′ and reverse: 5′-GGACTACHVGGGTWTCTAAT-3′). Thermal cycling consisted of 94°C for 3 min, followed by 30 cycles at 94°C for 45 s, 56°C for 1 min, and 72°C for 1 min, with a final extension at 72°C for 10 min. Then, a linker with an index was added to the end of the PCR product of 16S rDNA via PCR for next-generation sequencing. Library concentrations were measured using zymography and quantified at 10 nM. PE250/FE300 double-end sequencing was performed using Illumina MiSeq (Illumina, San Diego, CA, USA) instruments, and sequence information was read using MiSeq Control Software. The sequences were joined and depleted of barcodes, and sequences < 200 bp and those with ambiguous base calls were removed. The final obtained sequences were used for operational taxonomic unit clustering, and sequence clustering was performed using VSEARCH (1.9.6; sequence similarity was set to 97%); Silva 132 was the 16S rRNA reference database used for the comparison. The raw data of 16S rRNA gene libraries generated during this study are publicly available at the Sequence Read Archive portal of NCBI under accession number PRJNA747157.

Real-Time Quantitative PCR

Total RNA was extracted from the liver and intestinal tissues and then reverse transcribed into cDNA. Real-time PCR was used to detect mRNA expressions using β-actin as an internal reference. Genes studied for liver included cholesterol-7α-hydroxylase (*Cyp7a1*) with a forward primer (5′ to 3′) of AGCAATGAAAGCAGCCTCTGA and a reverse sequence (5′ to 3′) of TGATGCTATCTAGTACTGGCAGGT, as well as liver X receptor alpha (*Lxr*) with a forward primer sequence (5′ to 3′) of TGGAGACGTCACGGAGGTACA and a reverse sequence (5′ to 3′) of CAGCTCATTCATGGCTCTGGA. Ileum *Slc10a2* was detected with a forward primer sequence (5′ to 3′) of TAGATGGCGACATGGACCTCA and a reverse sequence (5′ to 3′) of CCCGAGTCAACCCACATCTTG. The amplification conditions were as follows: 95°C for 30 s, 1 cycle; 95°C for 5 s, 60°C for 32 s, 40 cycles; 95°C, 15 s, 60°C, 60 s, and 95°C, 1 s, 1 cycle.

Feces and Ileum Content Collection

Feces were collected one day before the mice were sacrificed, and the mice were placed on a disposable tablecloth. After the animals excreted, the fecal samples were immediately transferred to Eppendorf tubes and placed in liquid nitrogen tanks for quick freezing. On the day of sacrificing, the ileum was isolated, and the ileum contents were extruded with forceps.

Statistical Analysis

The mean differences between the groups were analyzed using one-way analysis of variance followed by *post-hoc* Tukey's test or Kruskal–Wallis test. Data were statistically analyzed using SPSS software (version 23.0; SPSS Inc., Chicago, IL, USA) and expressed as mean ± standard error of the mean. The statistical significance was set at $p < 0.05$ or $p < 0.01$. For the gut microbiota taxon analysis, the Kruskal–Wallis rank test was performed, and *p*-values were adjusted for multiple comparisons using the false discovery rate. Based on the operational taxonomic unit analysis results, using random sampling, the sample sequences were flat. Shannon, Chao1 alpha diversity index via the R package, vegan (v2.5-6), and the differences in β-diversity were visualized via principal coordinates analysis plots and tested for inferences using a permutational multivariate analysis of variance (Adonis from the package vegan, with 999 permutations); ggplot was used to construct a heatmap. GraphPad Prism 8.0 was used for additional graphs.

RESULTS

L. reuteri Fn041 Alleviates High-Fat Diet-Induced Hyperlipidemia and Fat Accumulation

After 8 weeks of high-fat diet feeding, the body weight of mice increased significantly, and the body weight of mice was 17.6% higher in the HF group than in the LF group. At the end of the experiment, the HF+LGG and HF+Fn041 groups had significantly lower weight gains throughout the experiment compared to the HF group ($p < 0.05$ or $p < 0.01$; **Figures 1A,B**, respectively). TC and LDL-C levels were significantly higher in the HF group than in the LF group. Compared with the HF group, both the Fn041 and LGG treatments significantly reduced TC ($p < 0.05$, **Figure 1C**) and LDL-C ($p < 0.01$, **Figure 1E**) levels. Plasma TG and HDL-C levels in both the LF and HF groups were identical to those of their counterpart groups (**Figures 1D,F**). Testicular fat ($p < 0.01$, **Figure 1G**) and perirenal fat ($p < 0.05$, **Figure 1H**) were significantly higher in the HF group than in the LF group. Testicular fat significantly decreased following the Fn041 treatment ($p < 0.05$, **Figure 1G**). Liver weights in both the LF and HF groups remained the same as those of their counterparts (**Figure 1I**).

Effect of *L. reuteri* Fn041 on the Morphology of the Liver and Testicular Fat

Inflammatory cell infiltration and lipid vacuolation were evident in the hematoxylin and eosin-stained liver sections of high-fat diet-fed mice (**Figure 2A**). The lipid accumulation in the liver

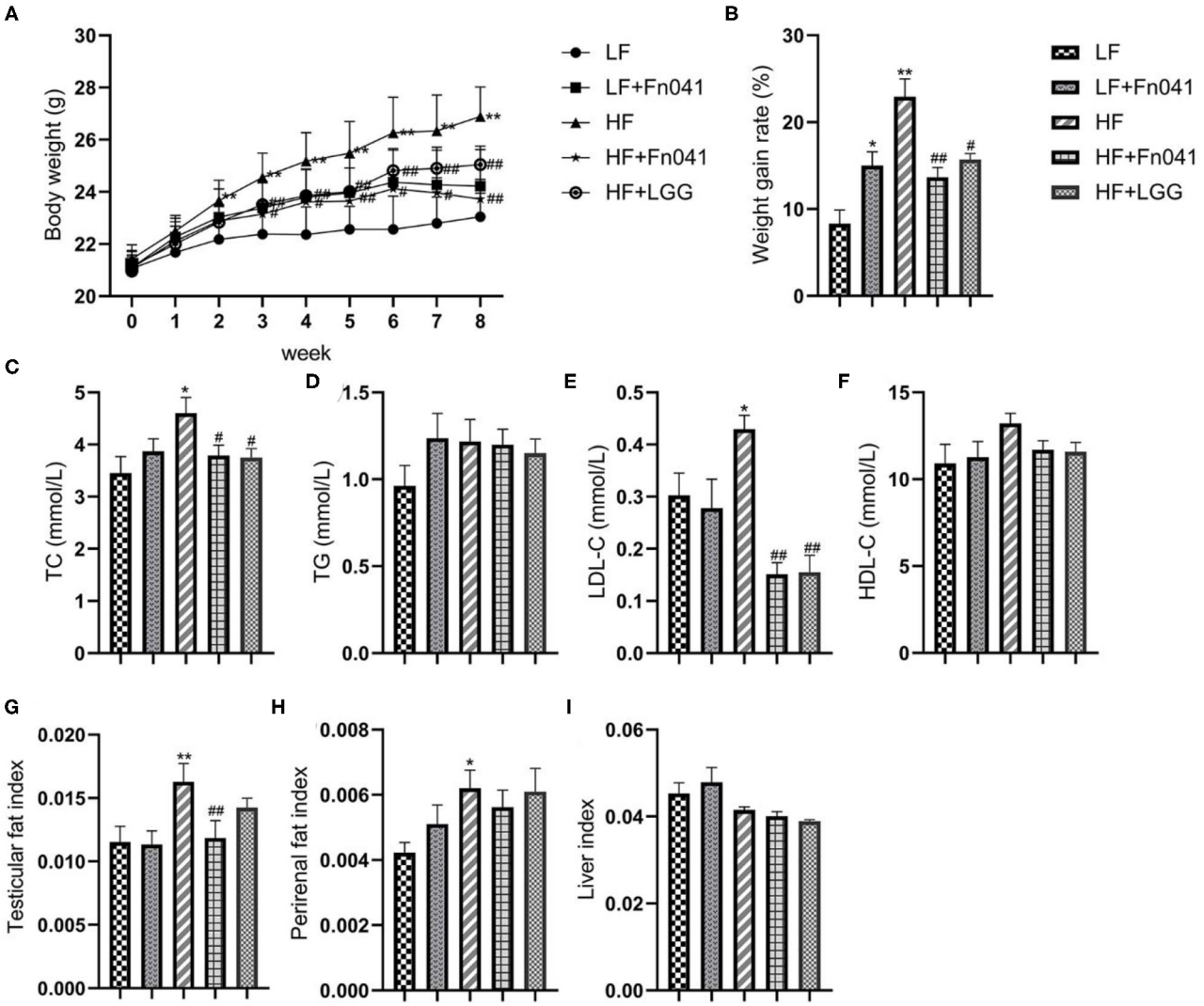

FIGURE 1 | Effect of *Lactobacillus reuteri* Fn041 on body weight, fat accumulation, and serum biochemical indexes in the high-fat diet mice. **(A)** Weight change; **(B)** The weight gain rate; **(C)** TC; **(D)** TG; **(E)** LDL-C; **(F)** HDL-C; **(G)** Testicular fat index; **(H)** Perirenal fat index; **(I)** Liver index. Data are presented as mean ± SEM (n = 12/group); $^{*}p < 0.05$, $^{**}p < 0.01$ as compared with the LF group; $^{\#}p < 0.05$, $^{\#\#}p < 0.01$ as compared with the HF group. LF, low-fat diet group; LF + Fn041, low-fat diet group treated with *L. reuteri* Fn041; HF, high-fat diet group; HF + Fn041, high-fat diet group treated with *L. reuteri* Fn041; HF + LGG, high-fat diet group treated with *Lactobacillus rhamnosus* GG. HDL-C, high-density lipoprotein cholesterol; LDL-C, low-density lipoprotein cholesterol; TC, total cholesterol; TG, triglyceride.

of the HF group was higher than that of the other groups in the Oil Red O strained section (**Figure 2B**), and the lipid droplet area percentage in the liver of the HF group was significantly higher than that of the LF group. By comparison, lipid accumulation and lipid droplet area percentage in the livers of HF+Fn041 and HF+LGG groups were significantly lower than those in the HF group ($p < 0.05$ or $p < 0.01$, **Figure 2E**). According to the hematoxylin and eosin-stained adipose tissue section, the high-fat diet led to a pronounced expansion of adipocyte size compared with the LF group (**Figure 2C**). The adipocyte size of mice in the HF group was significantly larger than that in the LF group but was significantly reduced following the Fn041 and LGG treatments ($p < 0.01$, **Figure 2D**).

Effects of *L. reuteri* Fn041 on Oxidative Stress in the Liver

Liver malondialdehyde levels significantly decreased in the HF+Fn041 group compared to the HF group ($p < 0.05$, **Figure 3A**). Catalase activity levels in the liver of Fn041-treated and LGG-treated mice were higher than that in the HF group ($p < 0.01$, **Figure 3B**).

Effects of *L. reuteri* Fn041 on Intestinal Permeability and Serum Endotoxin Levels

Fluorescence FD4 measurements showed that FD4 values were significantly lower in the HF+Fn041 and HF+LGG groups than

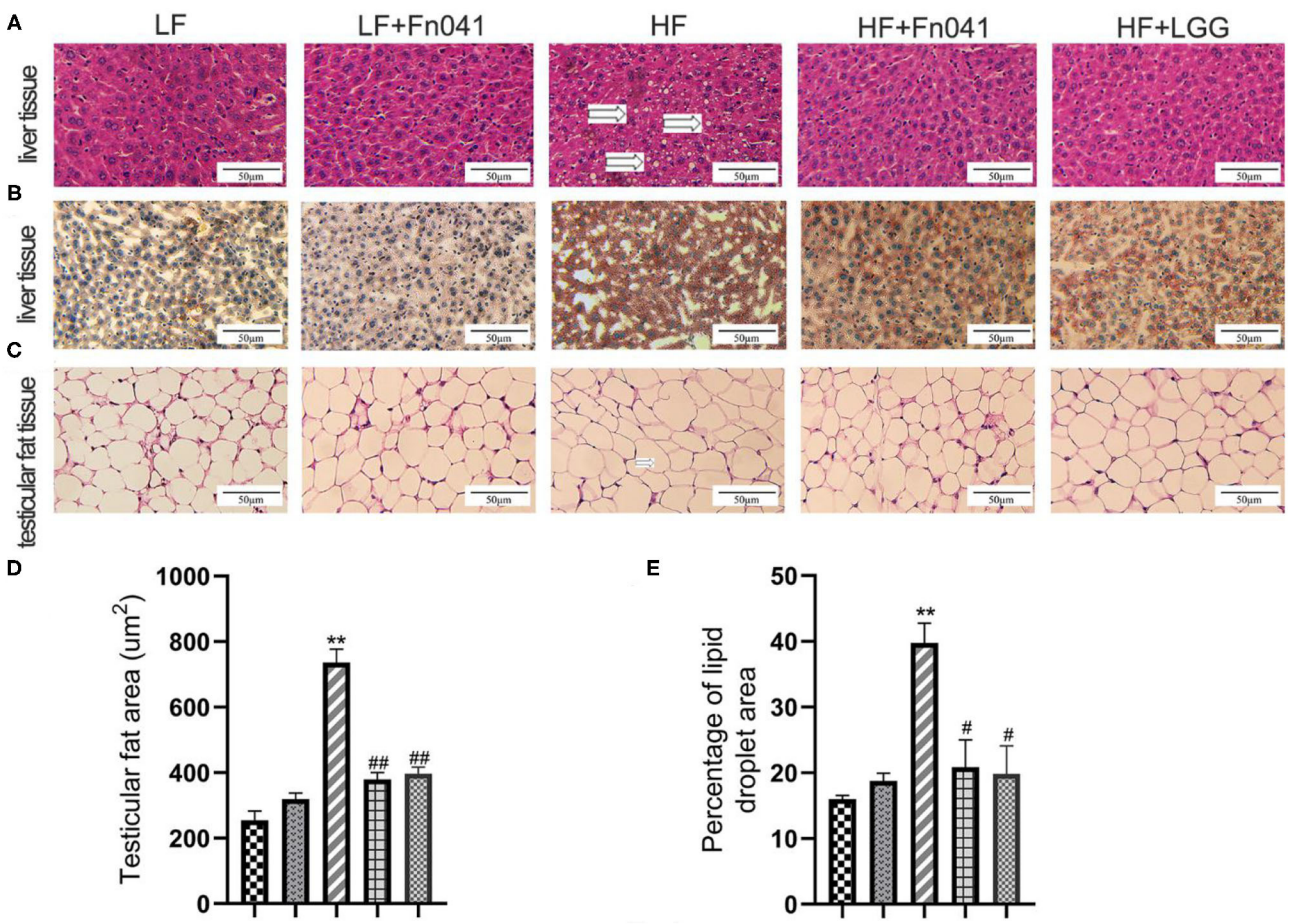

FIGURE 2 | Effect of *Lactobacillus reuteri* Fn041 on the morphology of the liver and testicular fat. **(A)** H&E staining of the liver; **(B)** Oil Red O staining of the liver; **(C)** H&E staining of the testicular fat; **(D)** Adipocyte size ($n = 5$/group); **(E)** Percentage of lipid droplet area ($n = 5$/group). $^{**}p < 0.01$ as compared with the LF group; $^{\#}p < 0.05$, $^{\#\#}p < 0.01$ as compared with the HF group. LF, low-fat diet group; LF + Fn041, low-fat diet group treated with *L. reuteri* Fn041; HF, high-fat diet group; HF + Fn041, high-fat diet group treated with *L. reuteri* Fn041; HF + LGG, high-fat diet group treated with *Lactobacillus rhamnosus* GG.

in the HF group ($p < 0.01$, **Figure 4A**). Plasma LPS and LPS-binding protein levels in the HF group were significantly higher than those in the LF group, whereas these levels were significantly lower in the HF+Fn041 and HF+LGG groups than in the HF group ($p < 0.01$, **Figures 4B,C**). We also examined the plasma levels of pro-inflammatory factors, including TNF-α and IL-6. In the HF group, plasma IL-6 and TNF-α levels were significantly higher than those in the LF group, and plasma IL-6 and TNF-α levels in the HF+Fn041 and HF+LGG groups were significantly lower than those in the HF group ($p < 0.01$, **Figures 4D,E**).

Effect of *L. reuteri* Fn041 on Ileum Microbiota

The microbial community richness indicated by the Chao1 estimators showed that the diversity of the HF group was significantly lower than that of the LF group, whereas the diversity levels of the HF+Fn041 and HF+LGG groups were significantly higher than those of the HF group ($p < 0.01$ or $p < 0.001$, **Figure 5A**). The community diversity estimated by the Shannon index was significantly increased in the HF+Fn041 and HF+LGG groups relative to the HF group ($p < 0.05$, $p < 0.01$, **Figure 5B**). According to the weighted UniFrac distances of PCo1 (22.35%), there was a significant difference in beta biodiversity between the HF group and HF+LGG ($p < 0.05$, **Figure 5C**). Combining the unweighted UniFrac distance of PCo1 (17.85%), both Fn041 and LGG induced significant changes in microbiota structure ($p < 0.001$, **Figure 5D**), which was confirmed by permutational multivariate analysis of variance (both permutational multivariate analysis of variance significances were $p < 0.01$, **Figures 5E,F**).

Effect of *L. reuteri* Fn041 on the Composition of the Ileum Microbiota

LDA Effect Size was used to analyze each group of signature genus (**Figure 6A**). Uncultured *Bacteroidales*_bacterium and *Bilophila* were enriched in the LF group mice, *Bifidobacterium* and *Ileibacterium* were dominant genera in the LF+Fn041 group mice, and *Lactobacillus*, *Enterorhabdus*, *Enterococcus*,

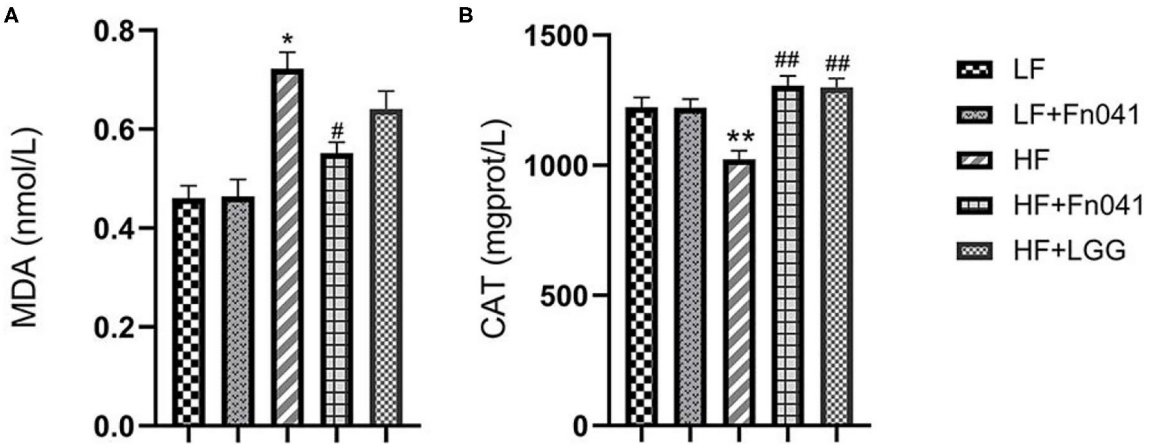

FIGURE 3 | Effects of *Lactobacillus reuteri* Fn041 on oxidative stress in the liver. **(A)** MDA level; **(B)** CAT activity; Data are presented as mean ± SEM ($n = 12$/group); $^{*}p < 0.05$, $^{**}p < 0.01$ as compared with the LF group; $^{\#}p < 0.05$, $^{\#\#}p < 0.01$ as compared with the HF group. LF, low-fat diet group; LF + Fn041, low-fat diet group treated with *L. reuteri* Fn041; HF, high-fat diet group; HF + Fn041, high-fat diet group treated with *L. reuteri* Fn041; HF + LGG, high-fat diet group treated with *Lactobacillus rhamnosus* GG. CAT, Catalase; MDA, Malondialdehyde.

Allobaculum, and *Candidatus_Stoquefichus* were enriched in the HF group mice. *Bacteroides*, *Lachnospiraceae*_NK4A136_group, and *Alloprevotella* were the dominant genera in the HF+Fn041 group mice; *Blautia* was enriched in the HF+LGG group ($p < 0.05$, **Figure 6A**). At the phylum level, the relative abundance of *Bacteroidetes* in the HF group was 21.92% lower than that in the LF group. By comparison, the relative level of *Firmicutes* in the HF group increased by 18.64% compared to that in the LF group ($p < 0.01$, **Figure 6B**). They recovered to similar levels as the LF group after Fn041 and LGG treatment, respectively (**Figure 6B**). A significant increase was observed in the ratio of *Firmicutes* to *Bacteroidetes* in the HF group compared to that in the LF group, which was significantly decreased by the Fn041 and LGG treatments ($p < 0.01$, **Figure 6C**). At the species level, *L. reuteri* and *Bifidobacterium*_Unclassified were significantly lower in the HF+Fn041 and HF+LGG groups than in the HF group ($p < 0.05$, $p < 0.01$, **Figures 6D,E**).

Effects of *L. reuteri* Fn041 on Feces Bile Acid and Cholesterol

We examined the contents of TC and total bile acids in the feces of mice at 8 weeks and found that the excretion of cholesterol and bile acids in the HF group was significantly higher than that in the LF group. Following the Fn041 and LGG treatments, the excretion rates of cholesterol and bile acids in the HF+Fn041 and HF+LGG groups were significantly higher than those in the HF group ($p<0.01$, **Figures 7A,B**). In the HF+Fn041 and HF+LGG groups, the liver *Cyp7a1* and *Lxr* mRNA expression levels were significantly higher than those in the HF group, and the ileal bile transport gene *Slc10a2* mRNA expression level was significantly lower than that in the HF group ($p < 0.01$, **Figures 7C–E**).

Association of the Different Genus With Biochemical Indicators and the Relationships of Different Bacteria With Endogenous Metabolites

As shown in **Figure 8**, *Erysipelatoclostridium* was negatively correlated with LDL-C ($r = -0.68$). Corynebacterium was negatively correlated with LPS ($r = -0.93$). *Allobaculum* was negatively correlated with LPS ($r = -0.69$), LDL-C ($r = -0.72$), and HDL-C ($r = -0.69$). *Dubosiella* was negatively correlated with HDL-C ($r = -0.66$) and TC ($r = -0.75$). *Faecalibaculum* was negatively correlated with LDL-C ($r = -0.59$), HDL-C ($r = -0.63$), and TC ($r = -0.67$). *Gordonibacter* ($r = -0.78$) was negatively correlated with malondialdehyde ($r = -0.74$). All these correlation coefficients were statistically significant ($p < 0.01$ or $p < 0.001$, **Figure 8**).

DISCUSSION

Our study demonstrated that Fn041 prevented high-fat diet-induced hypercholesterolemia, prevented intestinal barrier function damage, and improved intestinal microbiota disorders in mice. The cholesterol-lowering mechanism of action in this study was mainly related to the promotion of bile salt and cholesterol excretion as well as the regulation of intestinal microorganisms and an enhancement of intestinal barrier functions.

In the early 1970's, researchers discovered that a traditional African food fermented by *Lactobacillus* had a serum cholesterol-lowering effect (27). Previous studies have shown that some strains of *L. reuteri* exhibit hypocholesterolemic effects in different animal models. *Lactobacillus reuteri* GMNL-263 ameliorated hyperlipidemia and reduced serum TC and LDL-C levels in hamsters fed a high-fat diet (28). *Lactobacillus*

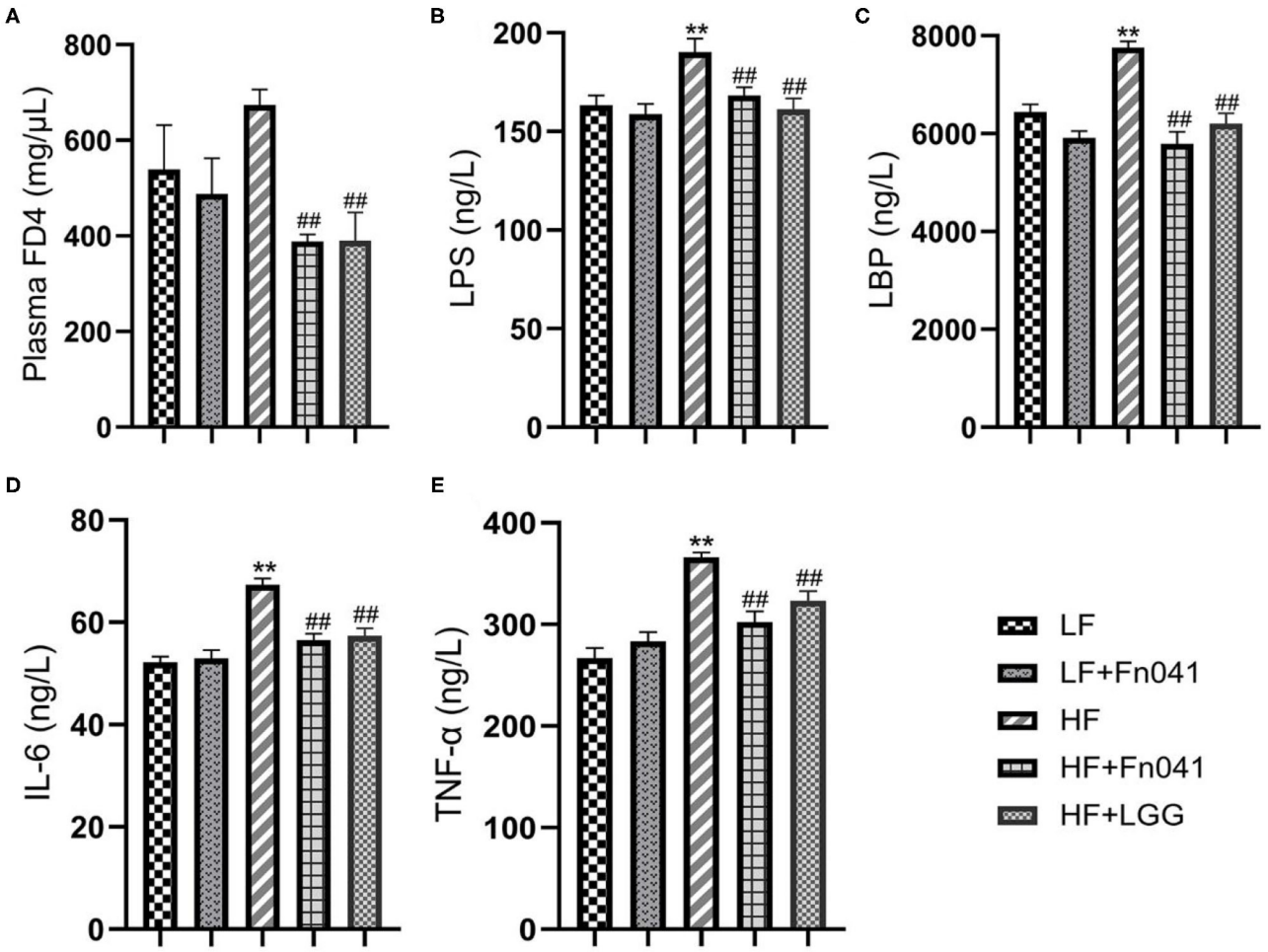

FIGURE 4 | Effects of *Lactobacillus reuteri* Fn041 on intestinal barrier dysfunction and chronic inflammation. **(A)** Plasma FITC-dextran 4000 (FD4) concentrations (λex = 485; λem = 530 nm) measured 4 h after gavage (n = 5/group); **(B)** plasma lipopolysaccharide (LPS); **(C)** plasma lipopolysaccharide-binding protein (LBP); **(D)** plasma IL-6; **(E)** plasma TNF-α. Data are presented as mean ± SEM (n = 12/group); **p < 0.01 as compared with the LF group; ##p < 0.01 as compared with the HF group. LF, low-fat diet group; LF + Fn041, low-fat diet group treated with *L. reuteri* Fn041; HF, high-fat diet group; HF + Fn041, high-fat diet group treated with *L. reuteri* Fn041; HF + LGG, high-fat diet group treated with *Lactobacillus rhamnosus* GG.

reuteri LR6 reduces serum TC, TG, and LDL-C levels in high-fat diet rats (29). We previously found that Fn041 alleviated hypercholesterolemia in C57BL/6 mice using an experimental intervention model in which 45% of the feed energy was provided by lard (12). In the current study, we have used a prophylactic animal model to demonstrate that Fn041 prevents hypercholesterolemia in C57BL/6 mice, in which 60% of the feed energy is provided by lard. This demonstrates that Fn041 can prevent and treat hypercholesterolemia. Unlike other strains, Fn041 is a breast milk-derived sIgA-coated bacterium that may target binding to the mucus layer in the intestine, thus acting at a closer distance to the intestinal epithelium (30, 31).

In the present study, Fn041 and LGG attenuated a high-fat diet-induced weight gain, demonstrating the efficacy of weight reduction. In general, weight gain is characterized by an increase in intracellular lipid content, adipocyte volume, and the number of adipocytes (32). In this study, Fn041 and LGG reduced high-fat diet-induced lipid accumulations in the adipose tissues of the epididymis and liver, which may at least partially explain their weight loss efficacy. This is consistent with the results of a previous intervention study that demonstrated that Fn041 exerts an inhibitory effect on high-fat diet-induced hepatic steatosis by downregulating *Fas* mRNA expression and upregulating *Srebp1c* mRNA expression (17, 33). LGG has also prevented liver steatosis and adipocyte enlargement caused by a high-fat diet (34). In addition, *L. reuteri* 8513 has attenuated high-fat diet-induced hepatic steatosis in rats (35). This is consistent with the results of the present study.

First, we also attempted to determine the mechanism of action through which Fn041 helps prevent hypercholesterolemia from several aspects. Some studies have shown that germ-free rats tend to accumulate more cholesterol than conventionally housed rats, and that bile acid and cholesterol absorption increase by

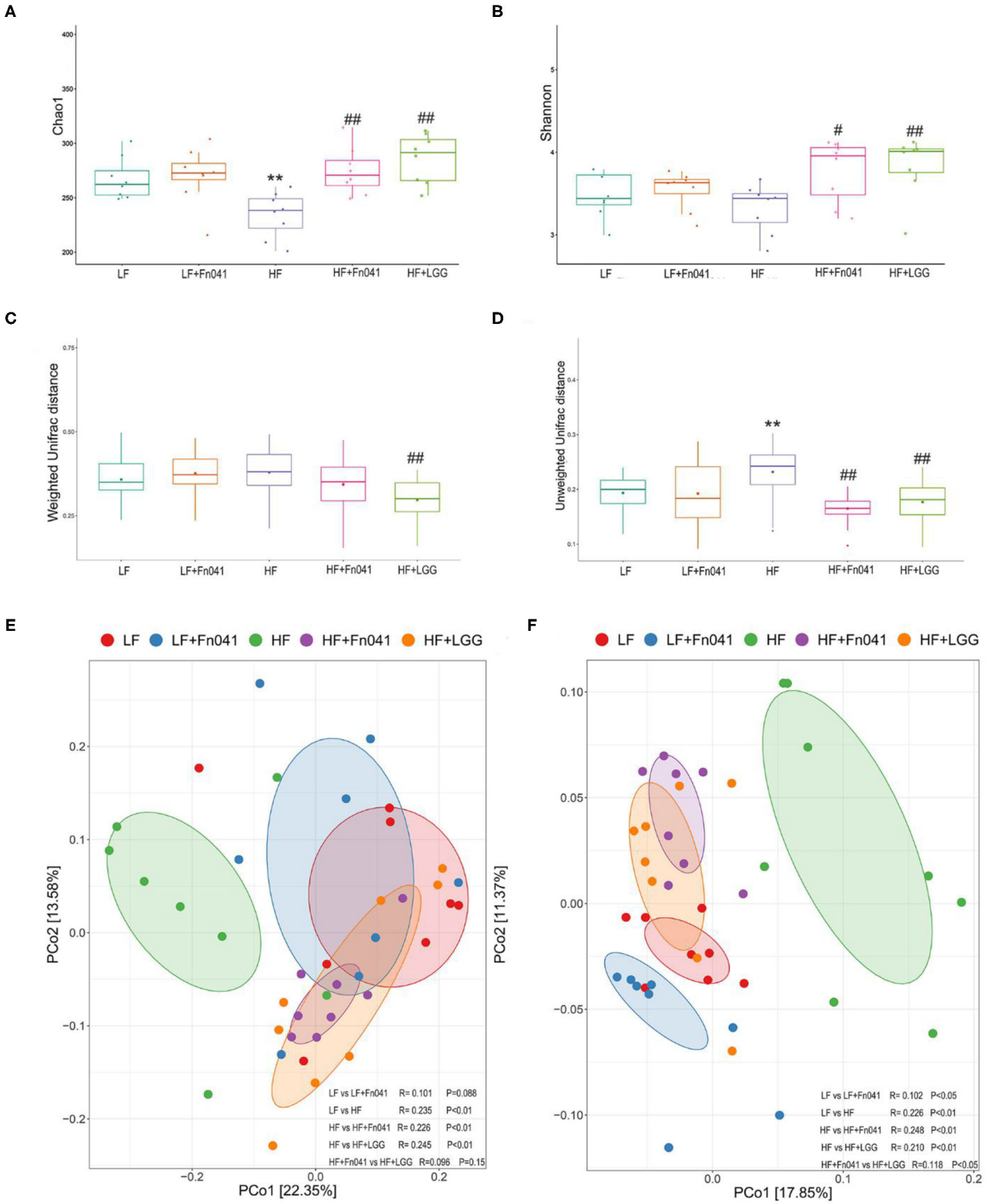

FIGURE 5 | Effect of *Lactobacillus reuteri* Fn041 on species diversity of microbiota in ileum contents. **(A)** Chao index; **(B)** Shannon index; **(C)** Weighted unifrac distance; **(D)** Unweighted unifrac distance; **(E)** Principal coordinate analysis (PCoA) based on weighted unifrac distance. **(F)** PCoA based on unweighted unifrac distance. $^{**}p < 0.01$ as compared with the LF group; $^{\#}p < 0.05$, $^{\#\#}p < 0.01$ as compared with the HF group. ($n = 8$/group). LF, low-fat diet group;

(Continued)

FIGURE 5 | LF + Fn041, low-fat diet group treated with *L. reuteri* Fn041; HF, high-fat diet group; HF + Fn041, high-fat diet group treated with *L. reuteri* Fn041; HF + LGG, high-fat diet group treated with *Lactobacillus rhamnosus* GG.

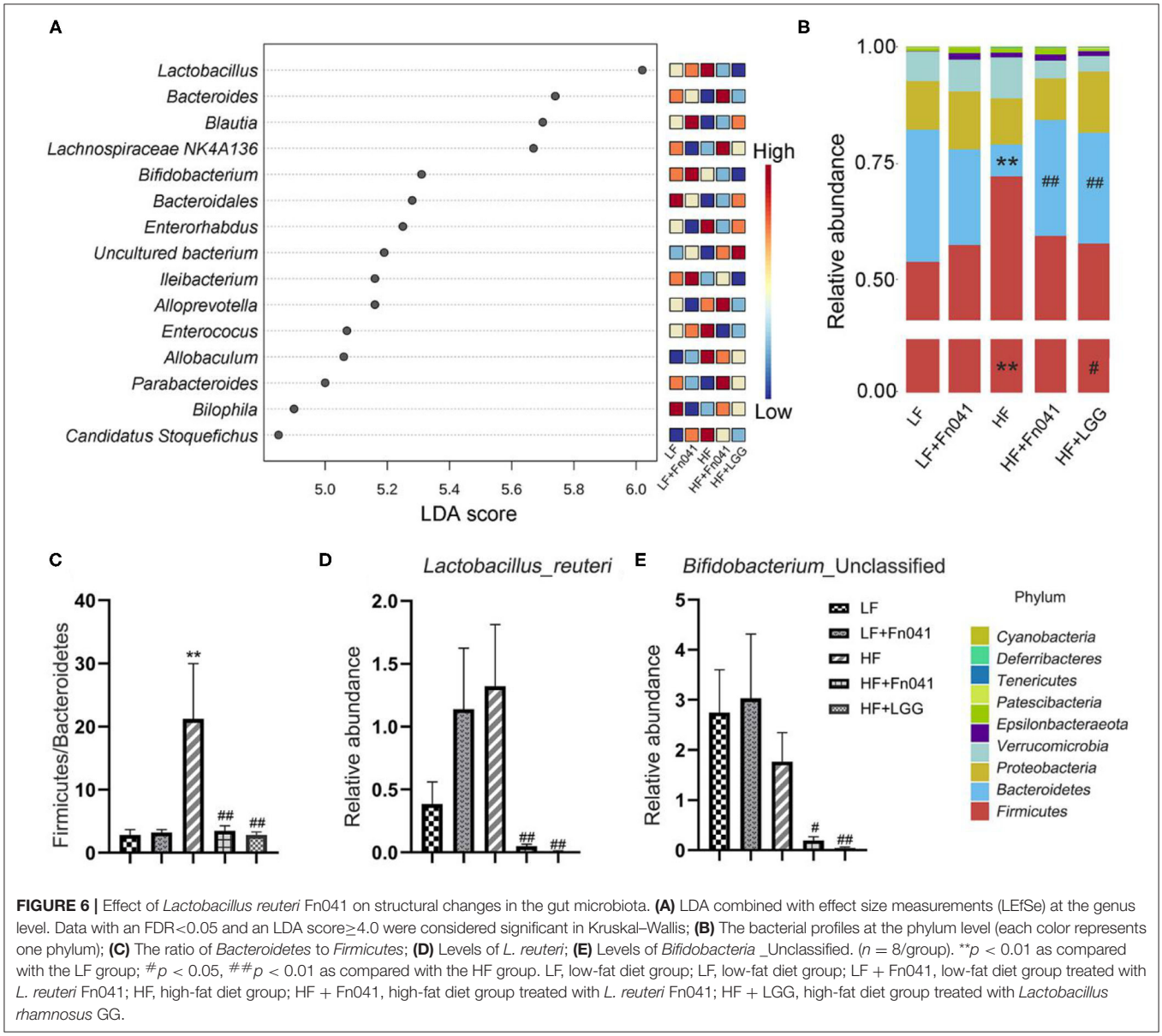

FIGURE 6 | Effect of *Lactobacillus reuteri* Fn041 on structural changes in the gut microbiota. **(A)** LDA combined with effect size measurements (LEfSe) at the genus level. Data with an FDR<0.05 and an LDA score≥4.0 were considered significant in Kruskal–Wallis; **(B)** The bacterial profiles at the phylum level (each color represents one phylum); **(C)** The ratio of *Bacteroidetes* to *Firmicutes*; **(D)** Levels of *L. reuteri*; **(E)** Levels of *Bifidobacteria* _Unclassified. ($n = 8$/group). $^{**}p < 0.01$ as compared with the LF group; $^{\#}p < 0.05$, $^{\#\#}p < 0.01$ as compared with the HF group. LF, low-fat diet group; LF, low-fat diet group; LF + Fn041, low-fat diet group treated with *L. reuteri* Fn041; HF, high-fat diet group; HF + Fn041, high-fat diet group treated with *L. reuteri* Fn041; HF + LGG, high-fat diet group treated with *Lactobacillus rhamnosus* GG.

300 and 25%, respectively, in the absence of gut microbiota (36). This is consistent with our experimental results. Fn041 and LGG can increase the abundance of intestinal microbiota, indicating that Fn041 can inhibit the absorption of cholesterol. The decrease in cholesterol concentration may be caused by several possible mechanisms, one of which is primarily the degradation of bile salts in the intestine by *Lactobacillus*, followed by the excretion of bile salts in the feces. In this case, the concentration of bile salts decreases, forcing the liver to continue to synthesize bile salts from intrahepatic cholesterol, thereby exerting a cholesterol-lowering effect in the body (18, 19, 37). In contrast, supplementation with *L. reuteri* NCIMB 30242 increased luminal bile salt hydrolase activity, which led to an increase in deconjugate bile acid excretion and a decrease in serum cholesterol levels (38). In another study, *L. reuteri* LR6 deconjugated bile salts, thereby exerting a hypocholesterolemic effect (29). Bile acids in feces are the main product of cholesterol metabolism; therefore, an increase in the excretion of fecal bile acids can reduce serum cholesterol levels (39). Fn041 increased TC and total bile acids in the feces. Activation of the liver CYP7A1I expression may promote the synthesis of bile acids and reduce cholesterol levels in the blood (40). The *Lxr* gene in the liver mainly synthesizes cholesterol in the blood into bile acids by regulating the bile acid synthesis rate enzyme *Cyp7a1*, thereby reducing the cholesterol level in the body (41). This is consistent with our experimental results. The Fn041 and LGG treatment

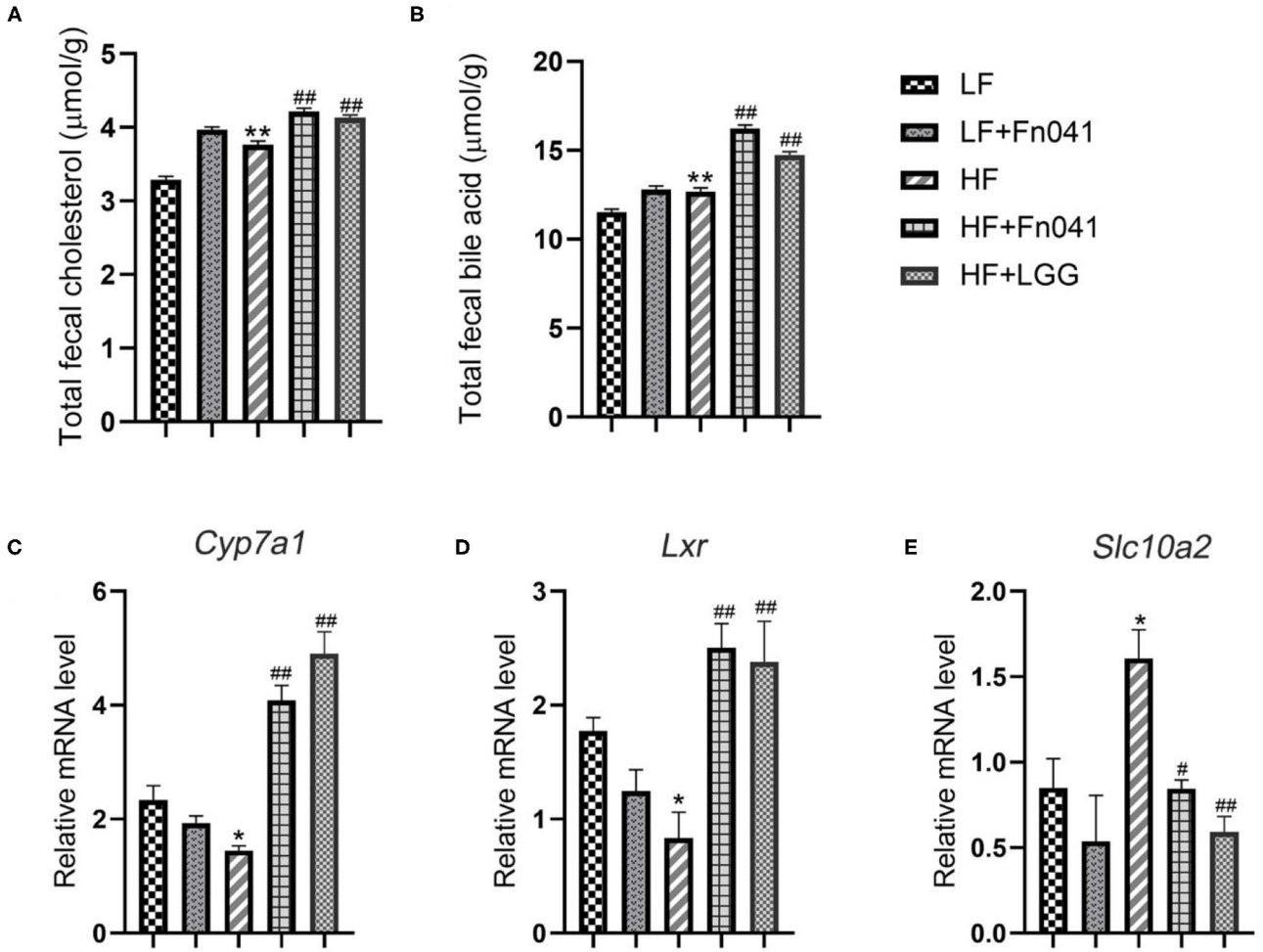

FIGURE 7 | Cholesterol and bile acids in the feces of mice. **(A)** Total cholesterol content in feces; **(B)** total bile acid content in feces; **(C)** liver expression of *Cyp7a1*; **(D)** liver expression of *Lxr*; **(E)** ileum expression of *Slc10a2*; $^{*}p < 0.05$, $^{**}p < 0.01$ as compared with the LF group; $^{\#}p < 0.05$, $^{\#\#}p < 0.01$ as compared with the HF group. ($n = 12$/group). LF, low-fat diet group; LF + R, low-fat diet group treated with *L. reuteri* Fn041; HF, high-fat diet group; HF + R, high-fat diet group treated with *L. reuteri* Fn041 and *Lactobacillus rhamnosus* GG.

groups upregulated the expression levels of *Lxr* and *Cyp7a1* in the liver and downregulated the expression levels of the ileal bile acid reabsorption transport gene *Slc10a2* (42). This shows that Fn041 and LGG mainly help inhibit bile acid absorption or promote bile acid excretion. In addition, some *L. reuteri* strains produce indole-3-aldehyde (43), indole-3-lactic acid (44), and other unknown aromatic hydrocarbon receptor ligands (45). Serum indole-3-aldehyde is substantially reduced in patients with atherosclerosis, suggesting that it is involved in negative cholesterol regulation (46). Therefore, Fn041 may release indole-3-aldehyde in the intestine and regulate cholesterol homeostasis.

Second, dysbiosis of the gut microbiota caused by a high-fat diet leads to increased intestinal permeability and impairment of intestinal epithelial barrier function (47). A high-fat diet leads to the proliferation of intestinal gram-negative bacteria or Proteobacteria and the release of excess LPS, which may induce intestinal barrier damage by decreasing the expression of tight junction proteins (48). Our previous study confirmed that Fn041 directly regulates the mRNA expression of several tight junction genes, such as Zo1, occludin, and claudin-6, to prevent barrier damage and endotoxemia caused by a high-fat diet (17). LPS is associated with an inflammatory response and is responsible for the pathogenesis of metabolic diseases, as the continuous subcutaneous low rate infusion of LPS induces most features of metabolic diseases (49, 50). For example, LPS injection induces hepatic oxidative stress and disorders of cholesterol metabolism in mice (51). Thus, there is a correlation between endotoxemia, impaired intestinal barrier functions, and host metabolic disorders. This is consistent with the results of our current experiments using plasma FD4 and LPS. We found that Fn041 and LGG alleviated mucosal barrier damage and reduced plasma LPS concentration; therefore, Fn041 prevented high-fat diet-induced barrier damage and endotoxemia (**Figure 4**).

Third, the gut microbiota and lipid metabolism are mutually regulated. Some studies have shown that a high-fat diet may cause a significant imbalance in the composition of the gut

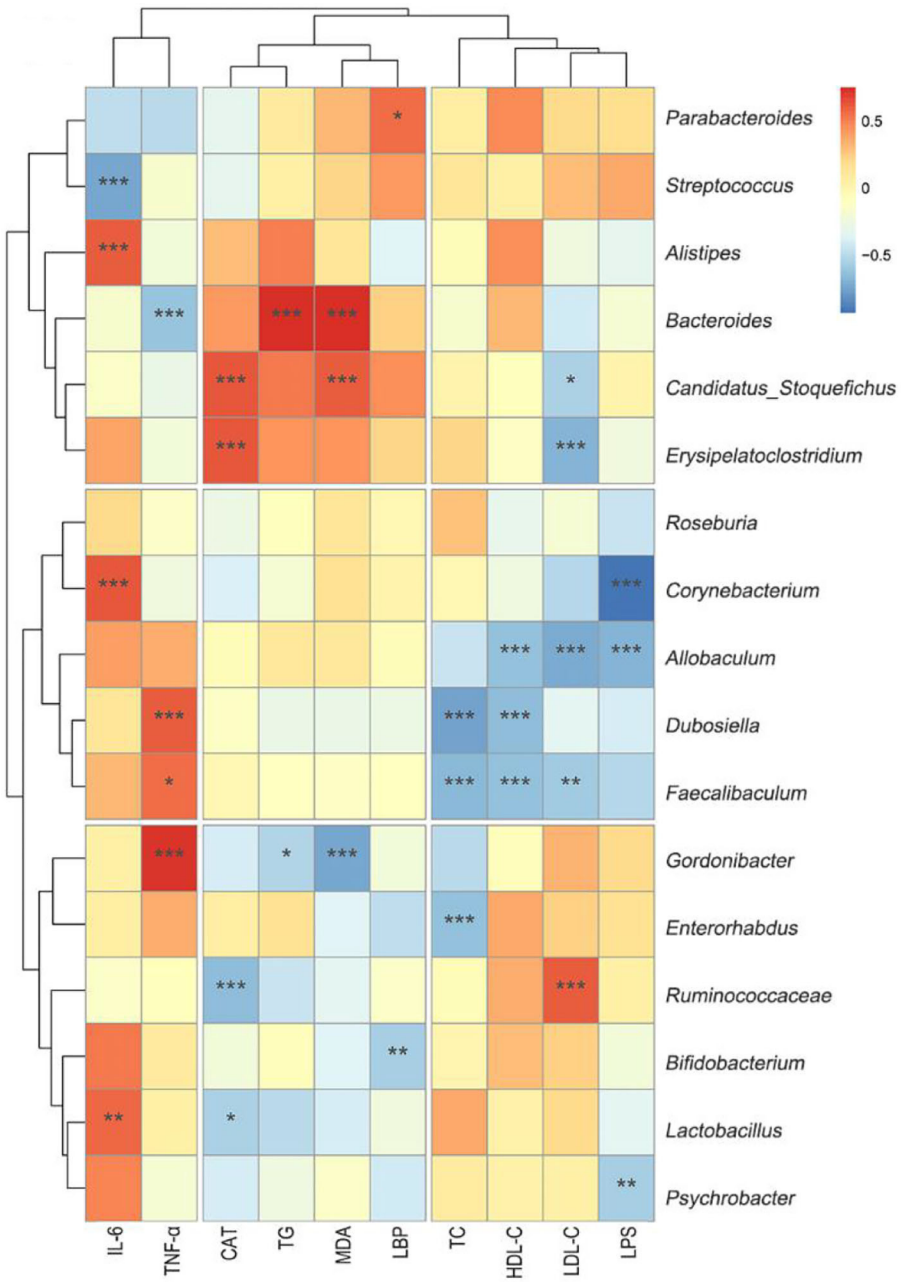

FIGURE 8 | Heat-map of the correlation analysis between different biochemical indicators and genus microbiota. Hierarchical clustering by average linkage of the significantly differentially affected genus as compared HF+Fn041 with the HF group. The differentially affected genus was identified with edgeR; the threshold was set to FDR < 0.05. The color bar indicates the correlation of the indicators (positive correlation, red; negative correlation, blue). $^{*}p < 0.05$; $^{**}p < 0.01$; $^{***}p < 0.001$ using Spearman correlation. ($n = 8$/group).

microbiota (52). Compared with a low-fat diet, a high-fat diet reduced the relative abundance of Bacteroides and significantly increased the abundance of *Firmicutes* (53, 54). Our results are in accordance with those of previous studies (**Figure 6**). We previously showed that Fn041 inhibited a reduction of the Chao 1 index, but had no significant effect on the Shannon index (17). In addition, LGG also inhibited the reduction of the Chao 1 index (34). However, in this study, the Fn041 strain increased the diversity of the gut microbiota and prevented the decrease of Chao 1 and Shannon index, which is in accordance with the results of β-diversity (**Figure 5**). This shows that Fn041 can alleviate the dysbiosis of gut microbiota caused by a high-fat diet. Studies have shown that a high-fat diet increases bile acid concentrations (55). *L. reuteri* and *Bifidobacteria*

demonstrate bile-salt hydrolase activity (34). The fewer the microbes associated with the activity rate of bile-salt hydrolase, the higher the concentration of ileal bound bile acids (56). After the LF group was treated with Fn041, the intestinal *L. reuteri* abundance levels increased significantly, whereas after the HF group was treated, the intestinal abundance levels of *L. reuteri* and *Bifidobacterium* were significantly reduced when the ileal bound bile acid concentration increased. On the one hand, Fn041 acts on the HF group, not by promoting bacterial colonization, but through inhibiting the reabsorption of bile acids in the ileum and promoting the excretion of cholesterol and bile acids (34). On the other hand, an increased intestinal bile concentration inhibits the proliferation of *Lactobacillus* and *Bifidobacterium* (57). Therefore, the levels of bile acids produced by the liver and excreted in the feces increase, and the concentration of cholesterol in the serum decreases. However, increased lumen bile acids may hinder the colonization of *L. reuteri*. *L reuteri* has reportedly been associated with increased body weight (58, 59), and in this study, *L. reuteri* Fn041 reduced intestinal abundance of *L. reuteri*, which may prevent excessive weight gain. Our experimental results showed that Fn041 increased the abundance of *Bacteroides* and *Alloprevotella*. These bacteria can produce short-chain fatty acids, thus lowering cholesterol levels in the body (60, 61). This result is consistent with our previous intervention experiments, where Fn041 increased the number of beneficial bacteria and reduced cholesterol levels in the body by inhibiting hepatic cholesterol synthesis through its metabolites of lactate, propionate, and butyrate (17).

CONCLUSIONS

In summary, our results suggest that Fn041 and LGG can significantly reduce plasma TC and LDL-C levels and prevent liver and testicular fat accumulation. Fn041 and LGG have protective effects on the dysregulation of the intestinal barrier and intestinal microbiota induced by a high-fat diet. In addition, the detection of mouse feces showed that Fn041 promoted the excretion of cholesterol and bile acids. Therefore, cholesterol reduction may be produced by promoting cholesterol excretion and enhancing the mucosal barrier. This study suggests that Fn041 may be a valid candidate for the regulatory function of cholesterol metabolism in foods. A deeper understanding of the molecular pathways by which Fn041 lowers cholesterol levels and changes cholesterol metabolism will potentially open new horizons for the development of related foods to prevent cholesterol metabolism disorders and related intestinal diseases. This would have important industrial implications.

DATA AVAILABILITY STATEMENT

The datasets presented in this study can be found in online repositories. The names of the repository/repositories and accession number(s) can be found in the article/**Supplementary Material**.

ETHICS STATEMENT

The animal study was reviewed and approved by the Guidelines for Care and Use of Laboratory Animals of Qingdao University.

AUTHOR CONTRIBUTIONS

ML and CQ participated in data collection, performed the analyses, and wrote the paper. JS designed the study, collected the data, and participated in data analysis. YZ, HZ, and XL performed animal experiments. JZho and WH participated in data analysis. JZha, HD, and JS performed microbiota data pre-processing. JS and DL participated in the study design and writing of the paper and was responsible for overall study coordination. All authors contributed to the article and approved the submitted version.

FUNDING

This research was supported by the Nutrition Science Research Foundation of BYHEALTH (No. ty202101004) and the Nutrition and Care of Maternal and Child Research Funding program (Grant #2020BINCMCF056).

ACKNOWLEDGMENTS

The authors gratefully acknowledge all team members for their contributions to this article.

SUPPLEMENTARY MATERIAL

The Supplementary Material for this article can be found online at: https://www.frontiersin.org/articles/10.3389/fnut.2022.851541/full#supplementary-material

REFERENCES

1. Huang H, Jiang X, Xiao Z, Yu L, Pham Q, Sun J, et al. Red Cabbage Microgreens Lower Circulating Low-Density Lipoprotein (LDL), Liver cholesterol, and Inflammatory Cytokines in Mice Fed a High-Fat Diet. *J Agric Food Chem.* (2016) 64:9161–71. doi: 10.1021/acs.jafc.6b03805
2. Robinson JG, Wang S, Smith BJ, Jacobson TA. Meta-analysis of the relationship between non-high-density lipoprotein cholesterol reduction and coronary heart disease risk. *J Am Coll Cardiol.* (2009) 53:316–22. doi: 10.1016/j.jacc.2008.10.024
3. Gao X, Tian Y, Randell E, Zhou H, Sun G. Unfavorable Associations Between Serum Trimethylamine N-Oxide and L-Carnitine Levels with Components of Metabolic Syndrome in the Newfoundland Population. *Front Endocrinol (Lausanne).* (2019) 10:168. doi: 10.3389/fendo.2019.00168
4. Araújo JR, Tomas J, Brenner C, Sansonetti PJ. Impact of high-fat diet on the intestinal microbiota and small intestinal physiology before and after the onset of obesity. *Biochimie.* (2017) 141:97–106. doi: 10.1016/j.biochi.2017.05.019

5. Ananthakrishnan AN, Luo C, Yajnik V, Khalili H, Garber JJ, Stevens BW, Cleland T, Xavier RJ. Gut Microbiome Function Predicts Response to Anti-integrin Biologic Therapy in Inflammatory Bowel Diseases. *Cell Host Microbe*. (2017) 21:603–610.e3. doi: 10.1016/j.chom.2017.04.010
6. Aminlari L, Shekarforoush SS, Hosseinzadeh S, Nazifi S, Sajedianfard J, Eskandari MH. Effect of Probiotics Bacillus coagulans and Lactobacillus plantarum on Lipid Profile and Feces Bacteria of Rats Fed Cholesterol-Enriched Diet. *Probiotics Antimicrob Proteins*. (2019) 11:1163–71. doi: 10.1007/s12602-018-9480-1
7. Ron S, Shai F, Ron M. Are we really vastly outnumbered? revisiting the ratio of bacterial to host cells in humans. *Cell*. (2016) 164:337–40. doi: 10.1016/j.cell.2016.01.013
8. Hasslöf P, Stecksén-Blicks C. Chapter 10: Probiotic Bacteria and Dental Caries. *Monogr Oral Sci*. (2020) 28:99–107. doi: 10.1159/000455377
9. Kim K, Jeong J, Kim D. Lactobacillus brevis OK56 ameliorates high-fat diet-induced obesity in mice by inhibiting NF- κ B activation and gut microbial LPS production. *J Funct Foods*. (2015) 13:183–91. doi: 10.1016/j.jff.2014.12.045
10. Bordoni A, Amaretti A, Leonardi A, Boschetti E, Danesi F, Matteuzzi D, et al. Cholesterol-lowering probiotics: in vitro selection and in vivo testing of bifidobacteria. *Appl Microbiol Biotechnol*. (2013) 97:8273–81. doi: 10.1007/s00253-013-5088-2
11. Taranto MP, Medici M, Perdigon G, Ruiz Holgado AP, Valdez GF. Effect of Lactobacillus reuteri on the prevention of hypercholesterolemia in mice. *J Dairy Sci*. (2000) 83:401–3. doi: 10.3168/jds.S0022-0302(00)74895-8
12. Wu Y, Zhang Q, Ren Y, Ruan Z. Effect of probiotic Lactobacillus on lipid profile: A systematic review and meta-analysis of randomized, controlled trials. *PLoS ONE*. (2017) 12:e0178868. doi: 10.1371/journal.pone.0178868
13. Malpeli A, Taranto MP, Cravero RC, Tavella M, Fasano V, Vicentin D, et al. Effect of Daily Consumption of Lactobacillus reuteri CRL 1098 on Cholesterol Reduction in Hypercholesterolemic Subjects. *Food Nutr Sci*. (2015)6:1583–90. doi: 10.4236/fns.2015.617163
14. Martoni CJ, Labbé A, Ganopolsky JG, Prakash S, Jones ML. Changes in bile acids, FGF-19and sterol absorption in response to bile salt hydrolase active L. reuteri NCIMB 30242. *Gut Microbes*. (2015) 6:57–65. doi: 10.1080/19490976.2015.1005474
15. Ding M, Qi C, Yang Z, Jiang S, Bi Y, Lai J, et al. Geographical location specific composition of cultured microbiota and Lactobacillus occurrence in human breast milk in China. *Food Funct*. (2019) 10:554–64. doi: 10.1039/C8FO02182A
16. Zhang M, Wang LM, Chen ZH, Zhao ZP, Li YC, Deng Q, et al. [Multilevel logistic regression analysis on hypercholesterolemia related risk factors among adults in China]. *Zhonghua Yu Fang Yi Xue Za Zhi*. (2018) 52:151–7. doi: 10.3760/cma.j.issn.0253-9624.2018.02.007
17. Li S, Qi C, Zhu H, Yu R, Xie C, Peng Y, et al. Lactobacillus reuteri improves gut barrier function and affects diurnal variation of the gut microbiota in mice fed a high-fat diet. *Food Funct*. (2019) 10:4705–15. doi: 10.1039/C9FO00417C
18. Jones ML, Tomaro-Duchesneau C, Martoni CJ, Prakash S. Cholesterol lowering with bile salt hydrolase-active probiotic bacteria, mechanism of action, clinical evidence, and future direction for heart health applications. *Expert Opin Biol Ther*. (2013) 13:631–42. doi: 10.1517/14712598.2013.758706
19. Kumar M, Nagpal R, Kumar R, Hemalatha R, Verma V, Kumar A, et al. Cholesterol-lowering probiotics as potential biotherapeutics for metabolic diseases. *Exp Diabetes Res*. (2012) 2012:902917. doi: 10.1155/2012/902917
20. Ishimwe N, Daliri EB, Lee BH, Fang F, Du G. The perspective on cholesterol-lowering mechanisms of probiotics. *Mol Nutr Food Res*. (2015) 59:94–105. doi: 10.1002/mnfr.201400548
21. Michael DR, Moss JWE, Calvente DL, Garaiova I, Plummer SF, Ramji DP. Lactobacillus plantarum CUL66 can impact cholesterol homeostasis in Caco-2 enterocytes. *Benef Microbes*. (2016) 7:443–51. doi: 10.3920/BM2015.0146
22. Horáčková Š, Plocková M, Demnerová K. Importance of microbial defence systems to bile salts and mechanisms of serum cholesterol reduction. *Biotechnol Adv*. (2018) 36:682–90. doi: 10.1016/j.biotechadv.2017.12.005
23. Ji X, Shi S, Liu B, Shan M, Tang D, Zhang W, et al. Bioactive compounds from herbal medicines to manage dyslipidemia. *Biomed Pharmacother*. (2019) 118:109338. doi: 10.1016/j.biopha.2019.109338
24. Huang Y, Zheng Y. The probiotic Lactobacillus acidophilus reduces cholesterol absorption through the down-regulation of Niemann-Pick C1-like 1 in Caco-2 cells. *Br J Nutr*. (2010) 103:473–8. doi: 10.1017/S0007114509991991
25. Gorenjak M, Gradišnik L, Trapečar M, Pistello M, Kozmus CP, Škorjanc D, et al. Improvement of lipid profile by probiotic/protective cultures: study in a non-carcinogenic small intestinal cell model. *New Microbiol*. (2014) 37:51–64.
26. Huang Y, Wu F, Wang X, Sui Y, Yang L, Wang J. Characterization of Lactobacillus plantarum Lp27 isolated from Tibetan kefir grains: a potential probiotic bacterium with cholesterol-lowering effects. *J Dairy Sci*. (2013) 96:2816–25. doi: 10.3168/jds.2012-6371
27. Mann G V. Studies of a surfactant and cholesteremia in the Maasai. *Am J Clin Nutr*. (1974) 27:464–9. doi: 10.1093/ajcn/27.5.464
28. Ting WJ, Kuo WW, Kuo CH, Yeh YL, Shen CY, Chen YH, et al. Supplementary heat-killed Lactobacillus reuteri GMNL-263 ameliorates hyperlipidaemic and cardiac apoptosis in high-fat diet-fed hamsters to maintain cardiovascular function. *Br J Nutr*. (2015) 114:706–12. doi: 10.1017/S0007114515002469
29. Singh TP, Malik RK, Katkamwar SG, Kaur G. Hypocholesterolemic effects of Lactobacillus reuteri LR6 in rats fed on high-cholesterol diet. *Int J Food Sci Nutr*. (2015) 66:71–5. doi: 10.3109/09637486.2014.953450
30. Donaldson GP, Ladinsky MS, Yu KB, Sanders JG, Yoo BB, Chou WC, et al. Gut microbiota utilize immunoglobulin A for mucosal colonization. *Science*. (2018) 360:795–800. doi: 10.1126/science.aaq0926
31. Qi C, Ding M, Li S, Zhou Q, Li D, Yu R, et al. Sex-dependent modulation of immune development in mice by secretory IgA-coated Lactobacillus reuteri isolated from breast milk. *J Dairy Sci*. (2021) 104:3863–75. doi: 10.3168/jds.2020-19437
32. de Ferranti S, Mozaffarian D. The perfect storm: obesity, adipocyte dysfunction, and metabolic consequences. *Clin Chem*. (2008) 54:945–55. doi: 10.1373/clinchem.2007.100156
33. Gao X, Jiang Y, Xu Q, Liu F, Pang X, Wang M, et al. 4-Hydroxyderricin Promotes Apoptosis and Cell Cycle Arrest through Regulating PI3K/AKT/mTOR Pathway in Hepatocellular Cells. *Foods (Basel, Switzerland)*. (2021) 10:2036. doi: 10.3390/foods10092036
34. Joung H, Chu J, Kim BK, Choi IS, Kim W, Park TS. Probiotics ameliorate chronic low-grade inflammation and fat accumulation with gut microbiota composition change in diet-induced obese mice models. *Appl Microbiol Biotechnol*. (2021) 105:1203–13. doi: 10.1007/s00253-020-11060-6
35. Lew LC, Hor YY, Jaafar MH, Lau ASY, Lee BK, Chuah LO, et al. Lactobacillus Strains Alleviated Hyperlipidemia and Liver Steatosis in Aging Rats via Activation of AMPK. *Int J Mol Sci*. (2020) 21:5872. doi: 10.3390/ijms21165872
36. Wostmann BS, Wiech NL, Kung E. Catabolism and elimination of cholesterol in germfree rats. *J Lipid Res*. (1966) 7:77–82. doi: 10.1016/S0022-2275(20)39588-2
37. Taranto MP, Sesma F, Valdez GF De, Referencia D, Cerela L, Tucum M De. Localization and primary characterization of bile salt hydrolase from Lactobacillus reuteri. *Biotechnol Lett*. (1999) 21:935–8. doi: 10.1023/A:1005652501404
38. Jones ML, Martoni CJ, Prakash S. Cholesterol lowering and inhibition of sterol absorption by Lactobacillus reuteri NCIMB 30242: a randomized controlled trial. *Eur J Clin Nutr*. (2012) 66:1234–41. doi: 10.1038/ejcn.2012.126
39. Huang WC, Chen YM, Kan NW, Ho CS, Wei L, Chan CH, et al. Hypolipidemic effects and safety of Lactobacillus reuteri 263 in a hamster model of hyperlipidemia. *Nutrients*. (2015) 7:3767–82. doi: 10.3390/nu7053767
40. Wahlström A, Sayin SI, Marschall HU, Bäckhed F. Intestinal Crosstalk between Bile Acids and Microbiota and Its Impact on Host Metabolism. *Cell Metab*. (2016) 24:41–50. doi: 10.1016/j.cmet.2016.05.005
41. Chiang JYL. Bile acid regulation of gene expression: roles of nuclear hormone receptors. *Endocr Rev*. (2002) 23:443–63. doi: 10.1210/er.2000-0035
42. Wang L, Zhou Y, Wang X, Zhang G, Guo B, Hou X, et al. Mechanism of Asbt (Slc10a2)-related bile acid malabsorption in diarrhea after pelvic radiation. *Int J Radiat Biol*. (2020) 96:510–9. doi: 10.1080/09553002.2020.1707324
43. Zelante T, Iannitti RG, Cunha C, De Luca A, Giovannini G, Pieraccini G, et al. Tryptophan catabolites from microbiota engage aryl hydrocarbon receptor and balance mucosal reactivity via interleukin-22. *Immunity*. (2013) 39:372–85. doi: 10.1016/j.immuni.2013.08.003
44. Cervantes-Barragan L, Chai JN, Tianero MD, Di Luccia B, Ahern PP, Merriman J, et al. Lactobacillus reuteri induces

gut intraepithelial CD4(+)CD8αα(+) T cells. *Science.* (2017) 357:806–10. doi: 10.1126/science.aah5825
45. Özçam M, Tocmo R, Oh JH, Afrazi A, Mezrich JD, Roos S, et al. Gut Symbionts Lactobacillus reuteri R2lc and 2010 Encode a Polyketide Synthase Cluster That Activates the Mammalian Aryl Hydrocarbon Receptor. *Appl Environ Microbiol.* (2019) 85:e01661–18. doi: 10.1128/AEM.01661-18
46. Cason CA, Dolan KT, Sharma G, Tao M, Kulkarni R, Helenowski IB, et al. Plasma microbiome-modulated indole- and phenyl-derived metabolites associate with advanced atherosclerosis and postoperative outcomes. *J Vasc Surg.* (2018) 68:1552–62.e7. doi: 10.1016/j.jvs.2017.09.029
47. Fuke N, Nagata N, Suganuma H, Ota T. Regulation of Gut Microbiota and Metabolic Endotoxemia with Dietary Factors. *Nutrients.* (2019) 11:2277. doi: 10.3390/nu11102277
48. Wu W, Wang S, Liu Q, Shan T, Wang Y. Metformin Protects against LPS-Induced Intestinal Barrier Dysfunction by Activating AMPK Pathway. *Mol Pharm.* (2018) 15:3272–84. doi: 10.1021/acs.molpharmaceut.8b00332
49. Cheng XR, Guan LJ, Muskat MN, Cao CC, Guan B. Effects of Ejiao peptide-iron chelates on intestinal inflammation and gut microbiota in iron deficiency anemic mice. *Food Funct.* (2021) 12:10887–902. doi: 10.1039/D1FO01802G
50. Cani PD, Bibiloni R, Knauf C, Waget A, Neyrinck AM, Delzenne NM, et al. Changes in gut microbiota control metabolic endotoxemia-induced inflammation in high-fat diet-induced obesity and diabetes in mice. *Diabetes.* (2008) 57:1470–81. doi: 10.2337/db07-1403
51. El Kamouni S, El Kebbaj R, Andreoletti P, El Ktaibi A, Rharrassi I, Essamadi A, et al. Protective Effect of Argan and Olive Oils against LPS-Induced Oxidative Stress and Inflammation in Mice Livers. *Int J Mol Sci.* (2017) 18:2181. doi: 10.3390/ijms18102181
52. Murphy EA, Velazquez KT, Herbert KM. Influence of high-fat diet on gut microbiota: a driving force for chronic disease risk. *Curr Opin Clin Nutr Metab Care.* (2015) 18:515–20. doi: 10.1097/MCO.0000000000000209
53. Hu H, Zhang S, Liu F, Zhang P, Muhammad Z, Pan S. Role of the Gut Microbiota and Their Metabolites in Modulating the Cholesterol-Lowering Effects of Citrus Pectin Oligosaccharides in C57BL/6 Mice. *J Agric Food Chem.* (2019) 67:11922–30. doi: 10.1021/acs.jafc.9b03731
54. Chen K, Chen H, Faas MM, de Haan BJ, Li J, Xiao P, et al. Specific inulin-type fructan fibers protect against autoimmune diabetes by modulating gut immunity, barrier function, and microbiota homeostasis. *Mol Nutr Food Res.* (2017) 61:1248–9. doi: 10.1002/mnfr.201601006
55. Wan Y, Yuan J, Li J, Li H, Zhang J, Tang J, et al. Unconjugated and secondary bile acid profiles in response to higher-fat, lower-carbohydrate diet and associated with related gut microbiota: a 6-month randomized controlled-feeding trial. *Clin Nutr.* (2020) 39:395–404. doi: 10.1016/j.clnu.2019.02.037
56. Huang F, Zheng X, Ma X, Jiang R, Zhou W, Zhou S, et al. Theabrownin from Pu-erh tea attenuates hypercholesterolemia via modulation of gut microbiota and bile acid metabolism. *Nat Commun.* (2019) 10:4971. doi: 10.1038/s41467-019-12896-x
57. Hou G, Peng W, Wei L, Li R, Yuan Y, Huang X, et al. Lactobacillus delbrueckii Interfere With Bile Acid Enterohepatic Circulation to Regulate Cholesterol Metabolism of Growing-Finishing Pigs via Its Bile Salt Hydrolase Activity. *Front Nutr.* (2020) 7:617676. doi: 10.3389/fnut.2020.617676
58. Million M, Maraninchi M, Henry M, Armougom F, Richet H, Carrieri P, et al. Obesity-associated gut microbiota is enriched in Lactobacillus reuteri and depleted in Bifidobacterium animalis and Methanobrevibacter smithii. *Int J Obes.* (2012) 36:817–25. doi: 10.1038/ijo.2011.153
59. Chan YK, Brar MS, Kirjavainen PV, Chen Y, Peng J, Li D, et al. High fat diet induced atherosclerosis is accompanied with low colonic bacterial diversity and altered abundances that correlates with plaque size, plasma A-FABP and cholesterol: a pilot study of high fat diet and its intervention with Lactobacillus rhamn. *BMC Microbiol.* (2016) 16:264. doi: 10.1186/s12866-016-0883-4
60. Zhou L, Xiao X, Zhang Q, Zheng J, Deng M. Maternal Genistein Intake Mitigates the Deleterious Effects of High-Fat Diet on Glucose and Lipid Metabolism and modulates Gut Microbiota in Adult Life of Male Mice. *Front Physiol.* (2019) 10:985. doi: 10.3389/fphys.2019.00985
61. Li TT, Liu YY, Wan XZ, Huang ZR, Liu B, Zhao C. Regulatory Efficacy of the Polyunsaturated Fatty Acids from Microalgae Spirulina platensis on Lipid Metabolism and Gut Microbiota in High-Fat Diet Rats. *Int J Mol Sci.* (2018) 19:3075. doi: 10.3390/ijms19103075

Conflict of Interest: The authors declare that the research was conducted in the absence of any commercial or financial relationships that could be construed as a potential conflict of interest.

Publisher's Note: All claims expressed in this article are solely those of the authors and do not necessarily represent those of their affiliated organizations, or those of the publisher, the editors and the reviewers. Any product that may be evaluated in this article, or claim that may be made by its manufacturer, is not guaranteed or endorsed by the publisher.

frontiers | Frontiers in Nutrition

ORIGINAL RESEARCH
published: 06 April 2022
doi: 10.3389/fnut.2022.856282

Bioactive Components From *Gracilaria rubra* With Growth Inhibition on HCT116 Colon Cancer Cells and Anti-inflammatory Capacity in RAW 264.7 Macrophages

Lingxiao Yi[1], Qi Wang[1], Haiyan Luo[1], Daqing Lei[2], Zhonghai Tang[3], Sijia Lei[2]* and Hang Xiao[1]**

[1] Department of Food Science, University of Massachusetts, Amherst, MA, United States, [2] School of Food and Drug, Shenzhen Polytechnic, Shenzhen, China, [3] College of Food Science and Technology, Hunan Agricultural University, Changsha, China

OPEN ACCESS

Edited by:
Ce Qi,
Qingdao University, China

Reviewed by:
Minhao Xie,
Nanjing University of Finance and Economics, China
Yujiao Sun,
Shaanxi University of Science and Technology, China

***Correspondence:**
Zhonghai Tang
tangzh@hunau.edu.cn
Sijia Lei
leisijia@szpt.edu.cn
Hang Xiao
hangxiao@foodsci.umass.edu

Specialty section:
This article was submitted to Nutritional Immunology, a section of the journal Frontiers in Nutrition

Received: *17 January 2022*
Accepted: *23 February 2022*
Published: *06 April 2022*

Citation:
Yi L, Wang Q, Luo H, Lei D, Tang Z, Lei S and Xiao H (2022) Bioactive Components From Gracilaria rubra With Growth Inhibition on HCT116 Colon Cancer Cells and Anti-inflammatory Capacity in RAW 264.7 Macrophages. Front. Nutr. 9:856282. doi: 10.3389/fnut.2022.856282

Gracilaria rubra is rich in bioactive compounds with various potential health benefits. This study aimed to elucidate the profile of both extractable bioactive components (EBCs) and non-extractable bioactive components (NEBCs) of *G. rubra* and determine their anti-colon cancer and anti-inflammatory activities. Both EBCs and NEBCs displayed strong suppressive effects on the viability of HCT116 cells, which causes cell cycle arrest, induces cellular apoptosis, and regulates the expression of cyclin-dependent kinases (CDKs) and tumor suppressor proteins. Additionally, EBCs and NEBCs from *G. rubra* displayed anti-inflammatory functions *via* inhibiting the production of nitric oxide (NO), reactive oxygen species (ROS), and proinflammatory cytokines in activated macrophages and regulating the expression levels of cyclooxygenase-2 (COX-2), inducible nitric oxide synthase (iNOS), NADPH-quinone oxidoreductase-1 (NQO-1), and heme oxygenase 1 (HO-1). These findings provide a rationale for animal and human studies designed to evaluate the chemopreventive and anti-inflammatory potential of these bioactive compounds from *G. rubra*.

Keywords: *Gracilaria rubra*, extractable components, non-extractable components, anti-colon cancer, anti-inflammation

INTRODUCTION

Colon cancer is the third most commonly diagnosed cancer in the United States (1). The etiology of colon cancer is associated with various factors that include genetics, diet, lifestyle, and the immune system. The relationship between inflammation and colon cancer has been established and supported by genetic, pharmacological, and epidemiological data (2). For instance, patients with inflammatory bowel diseases (IBDs) are at higher risk of developing colon cancer, compared with age-matched general populations (3). The current research focuses on developing alternative approaches using food components to prevent cancers and chronic inflammation. Bioactive components from plant-based food, especially whole grains, fruits, and vegetables, have been reported with protective effects against colon cancer and colonic inflammation in cell and animal studies (4–6).

Seaweeds have been served as natural bioactive substances and possess health benefits against inflammation, obesity, diabetes, cancer, and oxidative stress (7). Seaweed extracts exerted

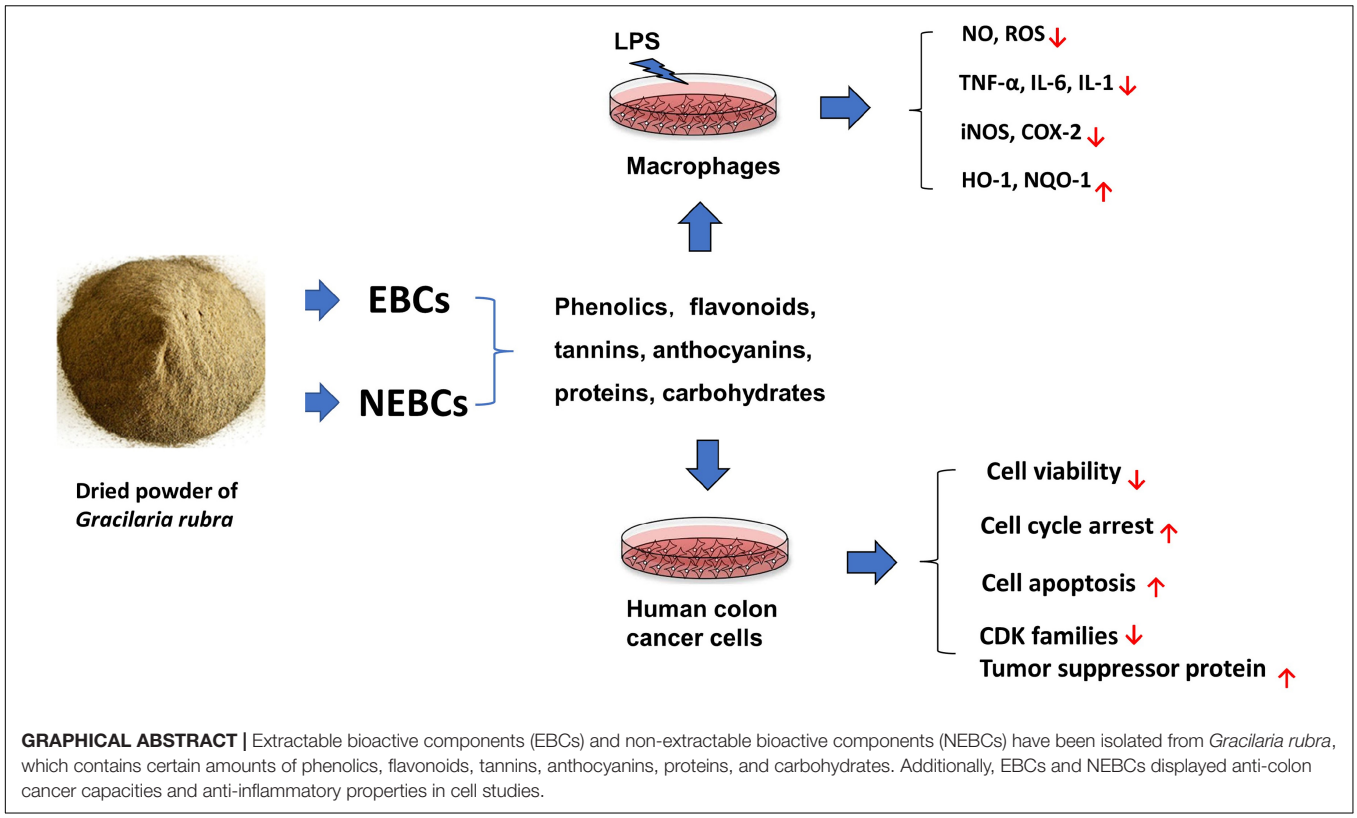

GRAPHICAL ABSTRACT | Extractable bioactive components (EBCs) and non-extractable bioactive components (NEBCs) have been isolated from *Gracilaria rubra*, which contains certain amounts of phenolics, flavonoids, tannins, anthocyanins, proteins, and carbohydrates. Additionally, EBCs and NEBCs displayed anti-colon cancer capacities and anti-inflammatory properties in cell studies.

suppressive effects on colon cancer and inflammatory agents in cell studies (8, 9). Moreover, anti-colon cancer and anti-inflammation abilities of seaweed extracts have been reported in rodent models (10, 11). The genus of *Gracilaria* is commonly found in the tropical regions that have been used in traditional Chinese medicine for obesity, cardiovascular disease, and chronic disease in the digestive system, respiratory system, urine system, and endocrine system (12). Various types of *Gracilaria* are rich in polyphenolic compounds and exert potent antioxidant capacity, which includes *G. changii* and *G. gracilis* (13, 14). Further studies found that bioactive components from the species of *Gracilaria* are reported with inhibitory effects on multiple types of cancer cells (15, 16). Recent studies reported that the sulfated polysaccharide from the *G. rubra* produced strong antioxidant and immunostimulating activities (17). However, the literature focused on the composition and biological activities for the components from *G. rubra* is rare, in comparison with other species of *Gracilaria*.

Multiple bioactive components have been quantified from *Gracilaria* with different biological properties against chronic disease (17, 18). Most of the bioactive components from *Gracilaria* are acquired by the extraction methods using organic solvents, which belong to the extractable bioactive components (EBCs). However, recent studies revealed that there were still some bioactive components that remained in the residues after extraction, such as non-extractable polyphenols, which are considered as non-extractable bioactive components (NEBCs) (19). These NEBCs may reach the colon intact and be released from the food matrix, producing small molecules which may possess health benefits (20). Until now, the literature concerning the bioactive components in *G. rubra* against inflammation and colon cancer is rare, particularly for the NEBCs from *Gracilaria*, which have been neglected. Thus, we aimed to elucidate the composition of EBCs and NEBCs from *G. rubra,* and also to investigate their potential anti-colon cancer and anti-inflammatory efficacy and mechanism in this study.

MATERIALS AND METHODS

Materials

Fresh *G. rubra* were harvested and collected from Sandu Gulf in Fujian province, China, in the summer of 2018. The seaweed sample was washed, freeze-dried, homogenized, and stored in the freezer before use. Apigenin, luteolin, epicatechin, gallocatechin (GC), epigallocatechin (EGC), epicatechin gallate (EGCG), rutin, hesperidin, morin, quecertin, caffeic acid, vanillic acid, and rosmarinic acid were acquired from Shyuanye (Shanghai, China).

Preparation of Bioactive Components

The dried powder of *G. rubra* was blended with 80% (v/v) chilled acetone aqueous. The blend was subjected to ultrasonic vibration

Abbreviations: EBCs, extractable bioactive components; NEBCs, non-extractable bioactive components; LPS, lipopolysaccharides; NO, nitrite oxide; ROS, reactive oxygen species; iNOS, inducible nitric oxide synthase; COX-2, cyclooxygenase-2; HO-1, heme oxygenase 1; NQO-1, NADPH-quinone oxidoreductase-1; TNF- α, tumor necrosis factors-α; IL, interleukin; PCs, phenolics contents; FCs, flavonoid contents; TCs, tannin contents; CCs, carbohydrate contents; RSCs, reduced sugar contents; ACs, anthocyanin contents; PRCs, protein contents; ORAC, oxygen radical absorbance capacity; CDK, cyclin-dependent kinase.

for half an hour and then spin at 3,000 g for 5 min. The same procedure was repeated three times to assess residues. After that, the supernatants were collected, concentrated, and used for the isolation of EBCs, and the rest residues were used for the isolation of NEBCs.

Preparation of Extractable Bioactive Components

The pooled supernatants were dissolved in ethanol, followed by the addition of hexane to isolate fat and chlorophyl II. After that, the ethanol layer was collected, concentrated, and assessed by the extraction of ethyl acetate three times. Finally, the upper layer was concentrated, dried, and stored in the freezer for further analysis.

Preparation of Non-extractable Bioactive Components

The residues were blended with sodium hydroxide (2M) at 37°C for 2 h under a nitrogen atmosphere to avoid the oxidation of phenolic compounds before the addition of concentrated hydrochloric acid adjusted pH to 2 to terminate the reaction. The blend was spinning at 4,000 g for 5 min before the aqueous supernatant was extracted three times with ethyl-acetate. Finally, the upper layer was collected, concentrated, dried, and stored in the freezer for further analysis.

Investigation of Total Phenolic Contents, Flavonoid Contents, Tannin Contents, Carbohydrate Contents, Reducing Sugar Contents, Anthocyanin Contents, Total Protein Contents, and Oxygen Radical Absorbance Capacity

Total phenolic contents (PCs) were assessed by Folin–Ciocalteu method with modifications, and gallic acid was used as standard (21). A volume of 20 μl of Folin–Ciocalteu reagent was mixed with 20 μl of distilled water and 20 μl of sample in a 96-well plate and stand at room temperature for 10 min, before adding 140 μl of 7% sodium carbonate solution to the plate. After incubation at room temperature for another 90 min, the absorbance was monitored at 760 nm using a spectrophotometer (BioTek Instrument, Inc., Winooski, VT, United States). PCs were calculated as μg of gallic acid equivalents per g dried powder (μg GAE/g dried powder).

Flavonoid contents (FCs) were determined using the aluminum trichloride method with modification, and catechin was used as standard (22). A volume of 20 μl of the sample was added to a 96-well plate with 10 μl of 5% sodium nitrite solution and 100 μl of distilled water, which was kept at room temperature for 6 min. Next, a volume of 20 μl of 10% aluminum chloride solution was added to the plate and reacted for 5 min, before adding 50 μl of 1 M NaOH and reacting for 2 min. The absorbance was monitored at 510 nm using a spectrophotometer (BioTek Instrument). FCs were calculated as μg of catechin equivalents per g dried powder (μg CE/g dried powder).

Tannin contents (TCs) were determined by the vanillin-sulfuric acid method with modification, and catechin was used as standard (23). The vanillin-H_2SO_4 solution was prepared with the same volume of 4% vanillin in methanol and 30% H_2SO_4 in methanol. A volume of 20 μl of the sample was mixed with 180 μl of vanillin-H_2SO_4 solution in a 96-well plate. The absorbance was calculated at 510 nm using a spectrophotometer (BioTek Instrument). FCs were presented as μg of catechin equivalents per g dried powder (μg CE/g dried powder).

Carbohydrate contents (CCs) were evaluated by phenol–sulfuric acid methods with modification, and glucose was used as standard (24). A volume of 50 μl of the sample was mixed with 30 μl of 5% phenol and 150 μl of concentrated sulfuric acid in a 96-well plate. After heating at 90°C for 5 min, the absorbance was monitored at 490 nm using a spectrophotometer (BioTek Instrument). CCs were calculated as μg of glucose equivalents per g dried powder (μg GE/g dried powder).

Reducing sugar contents (RSCs) were evaluated by the DNS method with minor modification, and glucose was used as standard (25). The dinitrosalicylic (DNS) solution was prepared with the 1:1:1:1 volumetric mixture of 1% 3,5-dinitrosalicylic acid, 40% Rochelle salt, 0.2% phenol, 0.5%, and potassium disulfide which was dissolved in 1.5% sodium hydroxide. A volume of 100 μl of the sample was added into 96-well plates with 100 μl of DNS solution. The plate was incubated at 90°C for 10 min before the absorbance was monitored at the wavelength of 540 nm. RSCs were presented as μg of glucose equivalents per g dried powder (μg GE/g dried powder).

Anthocyanin contents (ACs) were evaluated by the pH differential method with modification (26). A volume of 100 μl of the sample was added to the 96-well plate with two groups. A volume of 160 μl of potassium chloride buffer, pH 1.0, was added into one group, and the other with 160 μl sodium acetate buffer, pH 4.5. The absorbance was measured at 510 and 700 nm in buffers at pH 1.0 and 4.5, respectively. ACs have presented as μg cyanidin 3-glucoside equivalents per g sample.

Total protein contents (PRCs) were evaluated by the BCA method (27). The absorbance was monitored at 562 nm, and PRCs were presented as μg of protein per g dried powder (μg protein/g dried powder).

Oxygen radical absorbance capacity (ORAC) test was performed following the previously published method with modification, and Trolox was used as standard (28). A volume of 20 μl of the sample was mixed with 40 μl of 75 μM of fluorescencein solution in a 96-well plate and gently shaken at 37°C for 2 min, followed by adding 140 μl of 0.8 M of 2,2′-azobis(2-amidinopropane) dihydrochloride solution. The absorbance was measured at the excitation and emission wavelength at 485 and 528 nm, respectively. This process continued for 2 h, and the absorbance was recorded with an interval of 2 min. Results were calculated as μmol of Trolox equivalents per g dried powder (μmol TE/g dried powder).

HPLC/MS Analysis

Phenolic compounds were quantified by Ultimate 3000 RSLC HPLC coupled with Orbitrap Fusion Mass Spectrometer (Thermo Fisher Scientific, Waltham, MA, United States). Chromatography separation was carried out by the Zorbax SB-Aq C18 column (250 mm × 4.6 mm, 5 μm, Agilent Technologies, Santa Clara, CA, United States). Meanwhile, the mobile phase is made up of 5% methanol with 0.1% formic acid (solvent A) and 0.1% formic acid in 100% methanol (solvent B). The initial mobile phase was 10% B maintained for 4 min before linearly

increased to 80% within the next 11 min and maintained for 5 min. Then, the concentration of solvent B was linearly reduced to 10% within 10 min and maintained for 5 min. The flow rate was 600 μl/min, and the injection volume was 20 μl. Data were acquired in negative ESI mode using a spray voltage of 3,000 V, with sheath and aux gas set to 40 and 10, respectively, and also vaporizer and tube temperature set to 300 and 275°C. Data processing was accomplished using Xcalibur V4.1 (Thermo Fisher Scientific, Waltham, MA, United States).

Cell Viability Assay

Assay of cell viability was monitored as we reported previously (19). CCD-18Co (10,000 cells/well), HCT116 cells (2,500 cells/well), and RAW 264.7 (1,00,000 cells/well) were cultured in 96-well plate and incubated overnight, before posed to multiple concentrations of EBCs or NEBCs. CCD-18Co cells were assessed to MTT assay after 72 h of treatment. HCT116 cells were assessed to MTT assay after 24, 48, and 72 h of treatment, respectively. RAW 264.7 macrophages were carried out to MTT assay after 24 h of treatment.

Flow Cytometry Analysis

Flow cytometry analysis was carried out as we reported previously described with minor modifications (29). HCT116 cells (4×10^4 cells/ml) were cultured in 6-well plates and incubated overnight before posed to EBCs or NEBCs with 24 h for cell cycle analysis and 48 h for cell apoptosis analysis. Subsequently, media containing any floating cells were collected by trypsinization. Finally, cell pellets were washed by chilled PBS and subject flow cytometry as we reported previously (29).

Determination of Nitric Oxide and Reactive Oxygen Species Production

Griess reactions were carried out to evaluate NO production as previously reported (30). RAW264.7 cells (1×10^5 cells/well) were cultured into 96-well plates and incubated overnight before posed to multiple concentrations EBCs or NEBCs with 1 μg/ml lipopolysaccharides (LPS) for another 24 h. Next, culture media were assessed to Griess reaction.

Reactive oxygen species (ROS) production was measured according to the previous report with minor modifications (31). RAW264.7 cells were cultured in 96-well plates and incubated overnight before being processed by multiple concentrations of EBCs or NEBCs with 1 μg/ml LPS for 24 h. Then, the cells were assessed to a dichlorofluorescein-diacetate (DCFH-DA) assay.

Real-Time qRT-PCR Analysis

Real-time qRT-PCR analysis was carried out as we reported previously (30). The primer pairs were used for the cDNA amplification and are listed in **Supplementary Table 1**. Three independent parallel groups were carried out, and related messenger RNA (mRNA) expression was evaluated by the $2^{-\Delta\Delta Ct}$ method (32).

Immunoblotting Analysis

The whole-cell extract preparation was based on the previous report (30). The RIPA buffer containing protease inhibitor cocktail and phosphatase inhibitor (Boston BioProducts, Ashland, MA, United States) was used to lyse cells. The antibodies of iNOS, HO-1, NQO-1 COX-2, p53, and p21 were ordered from Santa Cruz Biotechnology (Dallas, TX, United States), and antibodies of CDK2, CDK4, and CDK6 were ordered from Cell Signaling Technology (Beverly, MA, United States). The antibody of β-actin was ordered from Sigma-Aldrich.

Statistical Analysis

Data were presented as mean ± standard derivation (SD) of more than three independent experiments. Analysis of variance (ANOVA) and Student's *t*-test were performed to compare the difference between two or more groups. *P*-Value < 0.05 was considered statistically significant.

RESULTS AND DISCUSSION

Composition of Extractable Bioactive Components and Non-extractable Bioactive Components

In this study, acidic acetone was used to isolate EBCs from *G. rubra,* and alkaline hydrolysis was performed to release NEBCs from the matrix of *G. rubra*. The yields of EBCs and NEBCs were 1,200 and 2,700 mg per 100 g dried powder, respectively. The total contents of PCs, FCs TCs, CCs, RSCs, PRCs, and ACs are shown in **Figure 1**. There were certain amounts of phenolics, flavonoids, tannins, carbohydrates, reducing sugar, and protein in the EBCs and NEBCs. In contrast, fewer amounts of anthocyanins and flavonoids were detected in EBCs and NEBCs. The amounts of PCs, FCs, TCs, CCs, RSCs, and PRCs in EBCs were lower than that in NEBCs. Few anthocyanins (less than 1 mg cyanidin 3-glucoside equivalents per g dry powder) were detected in EBCs and NEBCs. The ORAC was carried out to evaluate the antioxidant capacities of EBCs and NEBCs. The ORAC values of EBCs and NEBCs were 1,077.35 and 1,164.94 μmol TE/g (dried powder), respectively.

High-resolution MS was performed to analyze the polyphenol compounds, which are secondary plant metabolites with health benefits against different types of cancer, inflammation, cardiovascular disease, obesity, and diabetes (33). Rutin, morin, quercetin, caffeic acid, vanillic acid, EGCG, epicatechin, hesperidin dominated in EBCs, and few GC, ECG, apigenin, luteolin, and rosmarinic acid were identified (**Table 1**). The previous studies reported that rutin, morin, caffeic acid, ECG, EGCG, GC, hesperidin, eckol, phlorotannins were the major phenolic compounds identified in various types of seaweeds extracted by organic solvent (34). In NEBCs, the identified phenolic compounds contained rutin, epicatechin, morin, quercetin, and smaller amounts of EGCG, hesperidin, luteolin, rosmarinic acid, and apigenin (**Table 1**). Alkaloid hydrolysis was reported to release bioactive compounds such as polyphenols in the residues *via* breaking the ester and glycoside linkage (35). Herein, our results first clarified the chemical profiles of bioactive compounds in the non-extractable parts of the *Gracilaria*. NEBCs may be released by breaking down the covalent bonds, hydrogen

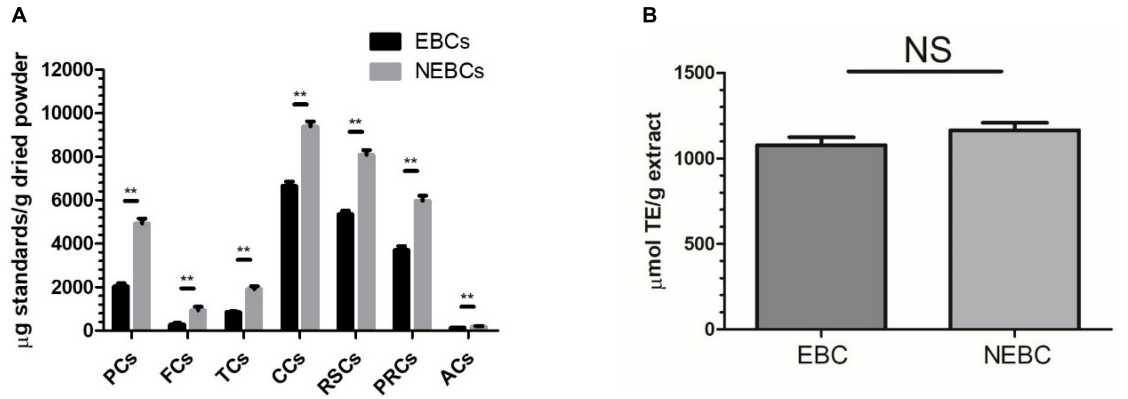

FIGURE 1 | (A) The total phenolics contents (PCs), flavonoids contents (FCs), tannin contents (TCs), carbohydrate contents (CCs), reducing sugar contents (RSCs), anthocyanin contents (ACs), total protein contents (PRCs) in the EBCs and NEBCs. **(B)** The ORAC value of the EBCs and NEBCs. Data were presented as mean ± SD (n = 3), ** indicates $P < 0.01$.

TABLE 1 | Phenolic compounds quantified in extractable bioactive components (EBCs) and non-extractable bioactive components (NEBCs) from *Gracilaria rubra*.

Compound	Retention time (min)	MS (m/z)	EBC (μ g/g extract)	NEBC (μ g/g extract)
Rutin	17.19	609.145 $[M-H]^-$	347.84 ± 42.12	267.74 ± 29.87
Morin	18.62	301.034 $[M-H]^-$	72.49 ± 8.54	17.74 ± 2.26
Epicatechin	13.78	289.071 $[M-H]^-$	295.21 ± 32.29	113.96 ± 14.07
Hesperidin	17.00	609.181 $[M-H]^-$	218.74 ± 27.22	78.86 ± 8.16
EGCG	14.74	457.077 $[M-H]^-$	128.78 ± 14.62	16.12 ± 1.88
Caffeic acid	15.39	179.034 $[M-H]^-$	100.39 ± 12.81	78.86 ± 8.16
Quecertin	19.05	301.034 $[M-H]^-$	19.14 ± 4.67	102.47 ± 12.28
Vanillic acid	15.57	167.034 $[M-H]^-$	38.45 ± 4.62	ND
GC	13.19	305.066 $[M-H]^-$	12.08 ± 2.52	ND
ECG	15.58	441.082 $[M-H]^-$	3.71 ± 0.53	ND
Rosmarinic acid	17.09	359.076 $[M-H]^-$	3.73 ± 0.58	0.65 ± 0.10
Luteolin	19.85	285.039 $[M-H]^-$	ND	0.57 ± 0.09
Apigenin	20.57	269.045 $[M-H]^-$	1.45 ± 0.24	0.96 ± 0.18

Results were presented as mean ± SD; ND, not detected.

bonds, and/or hydrophobic interaction linked to fiber, protein, and carbohydrate (36). The different composition between the EBCs and NEBCs could influence their biological properties. Next, we aimed to understand the protective effects of these novel *G. rubra* extracts against colon cancer and inflammation.

Extractable Bioactive Components and Non-extractable Bioactive Components Lowered the Viability of Colon Cancer Cells

MTT assay was carried out to monitor the suppressive properties of EBCs and NEBCs on the normal colon cells and colon cancer cells, respectively. As shown in **Figure 2**, EBCs and NEBCs did not display cytotoxicity effects on the growth of CCD18-Co cells up to 400 μg/ml for 72 h (**Figures 2A,C**). Moreover, EBCs and NEBCs slightly lowered the cell viability of HCT116 cells. Accurately, the half-maximal inhibitory concentration (IC_{50}) values of EBCs were 71.40, 53.50, and 43.90 μg/ml at 24, 48, and 72 h, respectively (**Figure 2B**), and the IC_{50} values of NEBCs were 283.7, 226.9, and 153.4 μg/ml at 24, 48, and 72 h, respectively (**Figure 2D**). Overview, our results illustrated that EBCs and NEBCs potently reduced the viability of colon cancer cells, whereas there were no cytotoxicity effects on the normal colon cells at higher concentrations. Furthermore, EBCs displayed stronger inhibitory effects on the growth of colon cancer cells, compared with the NEBCs. Thus, we selected EBCs, at 50 and 100 μg/ml, and NEBCs, at 200 and 300 μg/ml, according to the results of the MTT assay, for the further mechanistic test.

Extractable Bioactive Components and Non-extractable Bioactive Components Led Cell Cycle Arrest and Apoptosis in HCT116 Cells

Flow cytometry analysis was carried out to explore the molecular mechanism by which EBCs and NEBCs lowered the viability of colon cancer cells. Cell cycle analysis showed that both EBCs and NEBCs slightly elevated the cell percentage in the G0/G1 phase, which indicates a cell cycle arrest at G0/G1 phase (**Figures 3A,B**).

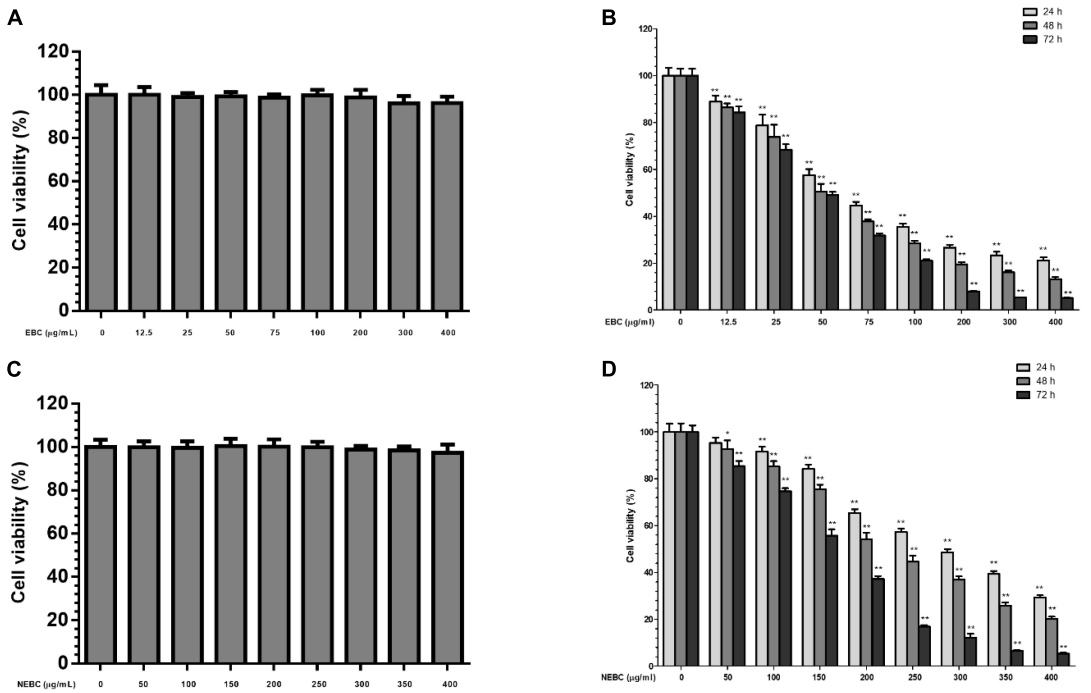

FIGURE 2 | Effects of EBCs **(A)** and NEBCs **(C)** on the growth of CCD18-Co cells for 72 h; Inhibitory effects of EBCs **(B)** and NEBCs **(D)** on the growth of HCT116 cells for 24, 48, and 72 h. * indicates $P < 0.05$ and ** indicates $P < 0.01$, when compared to the untreated control group.

EBCs at 50 and 100 μg/ml increased the cell percentage in the G0/G1 phase by 1.26- and 1.23-fold, respectively, whereas NEBCs at 200 and 300 μg/ml increased the cell percentage by 1.17- and 1.37-fold, respectively. Moreover, EBCs at 100 μg/ml increased the cell accumulation in the G2/M phase by 1.45-fold (**Figures 3A,B**).

Cell apoptosis analysis revealed that both EBCs and NEBCs significantly elevated the apoptotic cell populations. EBCs at 100 μg/ml potently induced late and early apoptotic cell populations by 16.53- and 16.87-fold, respectively. NEBCs at 300 μg/ml also markedly induced late and early apoptotic cell populations by 18.23- and 15.64-fold, respectively (**Figures 3C,D**). These results indicated that both EBCs and NEBCs lowered colon cancer cell growth *via* inducing cellular apoptosis and causing cell cycle arrest.

Extractable Bioactive Components and Non-extractable Bioactive Components Modified Cell Cycle and Apoptosis-Related Proteins

Tumor suppressor genes, such as p53 and p21, regulate cellular apoptosis and cell cycle (37). We found that both EBCs and NEBCs enhanced the expression of p53 and p21. EBCs at 100 μg/ml elevated the protein expression of p53 and p21 by 20 and 11%, respectively. Similarly, NEBCs at 300 μg/ml elevated the protein expression levels of p21 and p53 by 462 and 52%, respectively (**Figures 3E,F**). Moreover, cyclin-dependent kinase (CDK) involves regulating the cell cycle (37). We also found that both EBCs and NEBCs lowered the expression of the CDK family. Specifically, EBCs at 100 μg/ml suppressed the expression of CDK2, CDK4, and CDK6 by 22, 57, and 52%, respectively. NEBCs at 300 μg/ml suppressed the expression levels of CDK2, CDK4, and CDK6 by 31, 58, and 64%, respectively (**Figures 3E,F**). Overall, these results indicated that EBCs and NEBCs from *G. rubra* displayed anti-colon cancer properties by regulating the expression of multiple tumor suppresser genes and CDKs.

Inhibition of Extractable Bioactive Components and Non-extractable Bioactive Components on the Production of Nitric Oxide, Reactive Oxygen Species, and Proinflammatory Cytokines

In this study, macrophages activated by LPS were carried out to measure the anti-inflammation properties of EBCs and NEBCs. First, we monitored the cytotoxicity effects in macrophages up to 200 μg/ml for EBCs and up to 400 μg/ml for NEBCs, based on the MTT assay. We found that neither EBCs nor NEBCs showed cytotoxicity in the range aforementioned (**Figure 4A**). As shown in **Figure 4B**, LPS stimulation alone remarkably elevated the production of NO. However, EBCs and NEBCs reduced the LPS-induced NO production in a dose-dependent manner. More accurately, the IC_{50} values of EBCs and NEBCs were 44.81 and 107.05 μg/ml, respectively. The highest concentration of EBCs (200 μg/ml) and NEBCs (400 μg/ml) significantly reduced the NO production by 93.9 and 77.9%, respectively. LPS can

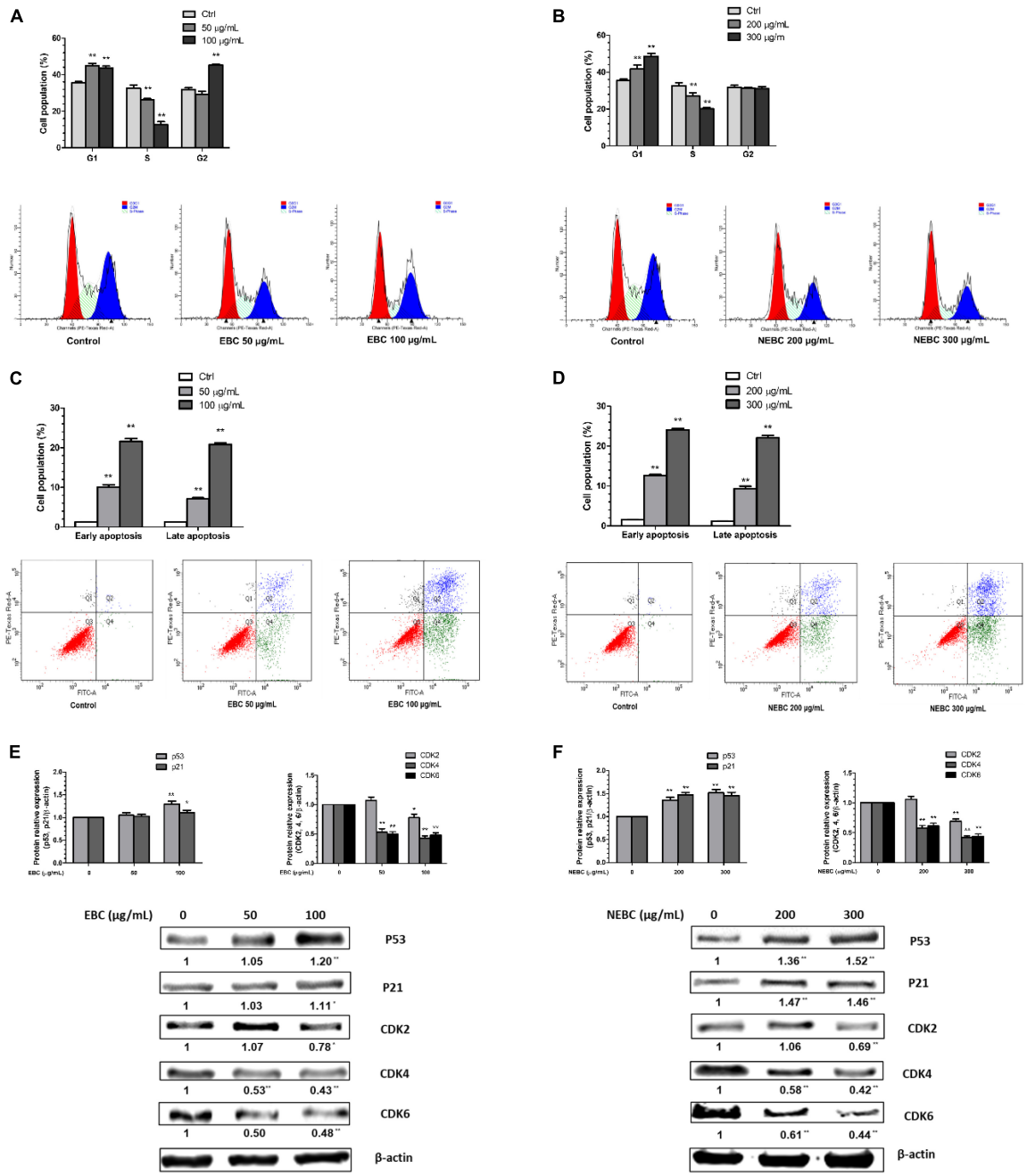

FIGURE 3 | Quantification of cell cycle after treatment of EBCs **(A)** and NEBCs **(B)** and the representative DNA histogram. Quantification of early and late apoptosis after treatment of EBCs **(C)** and NEBCs **(D)** and the representative Annexin V/PI co-staining dot plots. Effects of EBCs **(E)** and NEBCs **(F)** on the protein expression of tumor suppress genes and cyclin-dependent kinase in HCT 116 cells, as well as their representative image. * indicates $P < 0.05$ and ** indicates $P < 0.01$, when compared to the untreated control group.

induce cell oxidative damage *via* promoting ROS generation (31). As shown in **Figure 4C**, LPS stimulation alone greatly enhanced the production of ROS, whereas EBC and NEBC treatments lowered the ROS production in a dose-dependent manner. Specifically, the IC_{50} values of EBCs were 58.33 μg/ml, which is lower than the NEBCs at 148.52 μg/ml. EBCs at 200 μg/ml and NEBCs at 400 μg/ml significantly reduced the ROS production by 78.0 and 75.0%, respectively. These results indicated that EBCs and NEBCs exerted anti-inflammatory capacities *via* reducing the production of NO and ROS in activated macrophages. Moreover, EBCs displayed stronger anti-inflammatory capacities than NEBCs.

Furthermore, LPS stimulation significantly raised mRNA expression of tumor necrosis factor alpha (TNF-α), Interleukin (IL)-6, and IL-1β by 10. 72-, 60. 56-, and 53.04-fold compared with the control group, respectively.

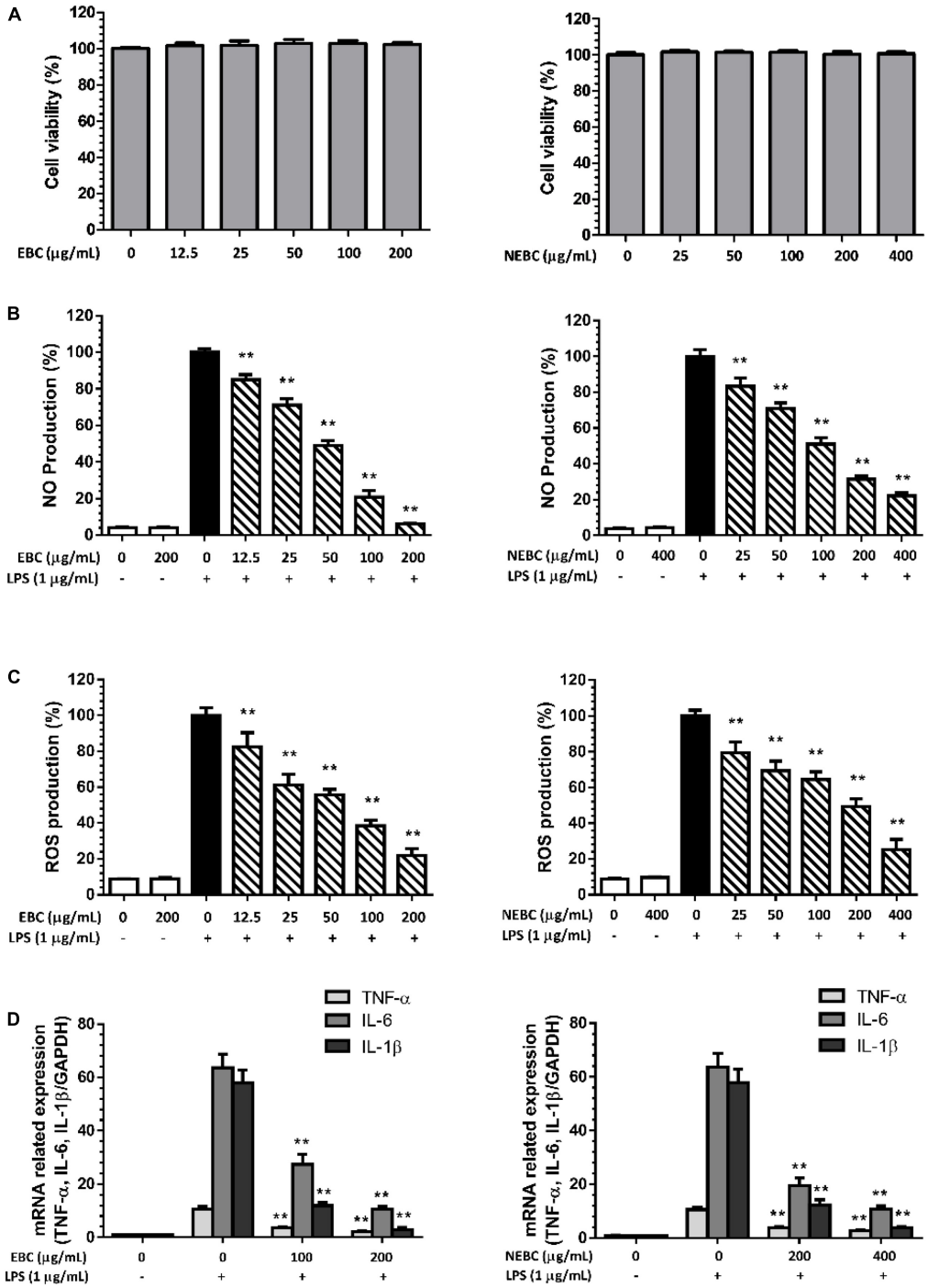

FIGURE 4 | Cytotoxicity of EBCs and NEBCs in macrophages **(A)**. Suppressive effects of EBCs and NEBCs on NO **(B)** and ROS **(C)** production in activated macrophages. Inhibitory effects of EBCs and NEBCs in messenger RNA (mRNA) expression level of tumor necrosis factor alpha (TNF-α), Interleukin (IL)-6 and IL-1β in activated macrophages **(D)**. ** indicates $P < 0.01$ in comparison with the LPS group.

EBCs and NEBCs reduced the raised expression of these cytokines in a dose-dependent manner (**Figure 4D**). EBCs at 200 μg/ml and NEBCs at 400 μg/ml greatly lowered mRNA expression of TNF-α by 79 and 73%, respectively. Similar patterns were obtained in the mRNA expression of IL-6 and IL-1β. Collectively, our results illustrated that EBCs and NEBCs exerted an anti-inflammatory role *via* attenuating the production of NO and ROS and downregulating expression levels of proinflammatory cytokines in activated macrophages.

Regulation of Inflammation-Related Signaling Proteins by Extractable Bioactive Components and Non-extractable Bioactive Components in Macrophages

Activated macrophages induce the overproduction of proinflammatory enzymes, namely, cyclooxygenase-2 (COX-2) and inducible nitric oxide synthase (iNOS) (38, 39). Compared with the control group, LPS stimulation significantly raised the expression of mRNA levels of iNOS by 13.26-fold. EBCs at 200 μg/ml significantly reduced the mRNA levels of iNOS by 72% and NEBCs at 400 μg/ml diminished iNOS expression levels by 67%, compared with the LPS group (**Figure 5A**). Additionally, LPS stimulation alone greatly elevated the protein levels of iNOS by 57.0-fold. EBCs at 200 μg/ml and NEBCs at

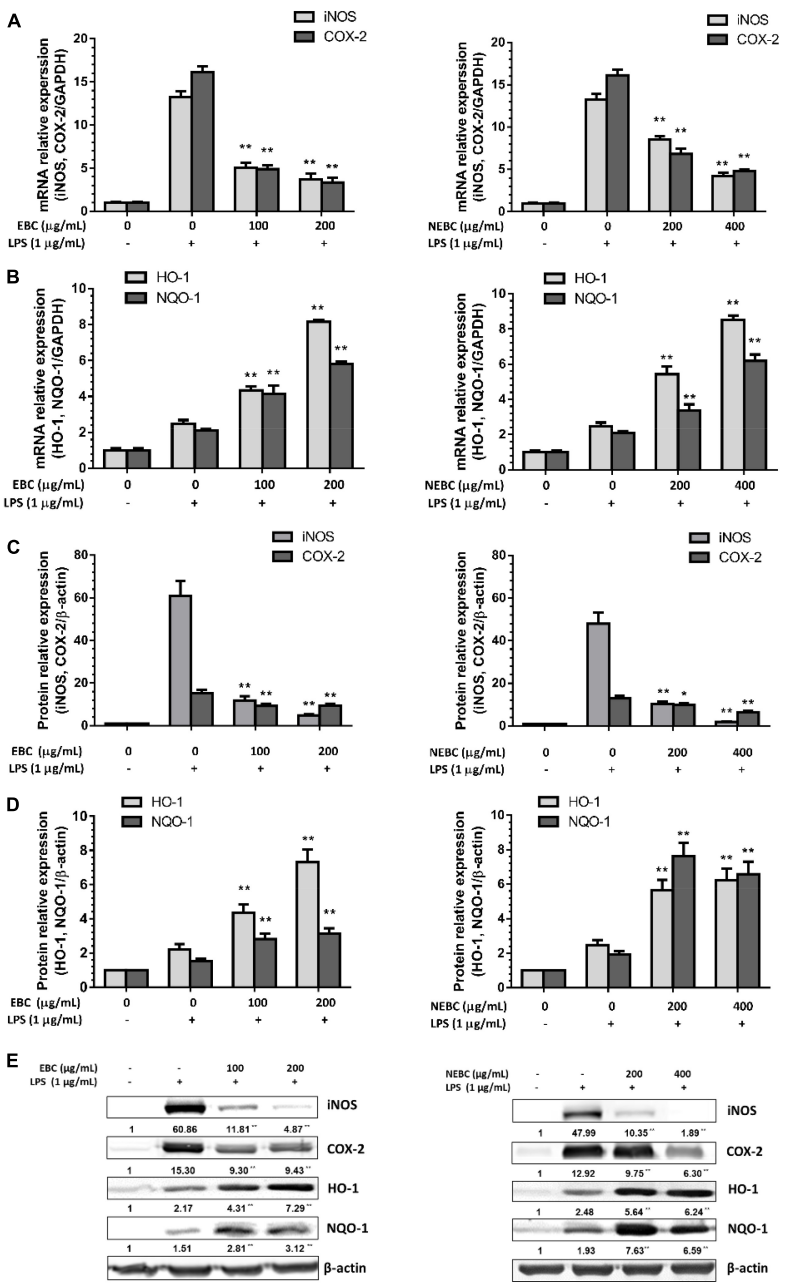

FIGURE 5 | Suppressive effects of EBCs and NEBCs on mRNA **(A)** expression and protein **(C)** expression levels of iNOS and COX-2 in activated macrophages. Effects of EBCs and NEBCs on mRNA **(B)** and protein **(D)** expression levels of HO-1 and NQO-1 in activated macrophages. Representative image of immunoblotting for the effects of EBCs and NEBCs on protein expression levels of iNOS, COX-2, HO-1 and NQO-1 in activated macrophages **(E)**. * indicates ($P < 0.05$) and ** indicates ($P < 0.01$), when compared to the LPS group.

400 μg/ml markedly lowered the protein levels of iNOS by 91 and 96%, compared with the LPS group (**Figures 5C,E**). Similar results were found in the analysis of mRNA and protein levels of COX-2 (**Figures 5A,C,E**). Our results suggested that EBCs and NEBCs attenuated the production of NO-induced by LPS *via* downregulating the iNOS and COX-2 signaling pathways.

Anti-oxidative enzymes, especially for HO-1 and NQO-1, are linked to anti-inflammatory functions (40). We found that EBCs at 200 μg/ml elevated the mRNA levels of HO-1 by 3.29-fold and NEBCs at 400 μg/ml elevated the mRNA levels of HO-1 by 2.35-fold, respectively, compared with LPS groups. Additionally, EBCs and NEBCs also enhanced mRNA expression levels NQO-1 (**Figure 5B**). The protein levels of HO-1 and NQO-1 were consistent with mRNA expression levels. EBCs at 200 μg/ml raised protein levels of HO-1 and NQO-1 by 2.18- and 1.89-fold, respectively, compared with the LPS group. NEBCs at 400 μg/ml increased the levels of HO-1 and NQO-1 by 3.66- and 5.79-fold, respectively (**Figures 5D,E**). Our results indicated that the upregulation of anti-oxidative enzymes HO-1 and NQO-1 by EBCs and NEBCs from *G. rubra* might repair the damage caused by oxidative stress in inflammatory diseases.

CONCLUSION

Our studies offered an incisive understanding of the composition and biological properties of different bioactive components present in *G. rubra*. These results, for the first time, evaluated the biological function of bioactive components in *G. rubra* against colon cancer and inflammation agent, especially for the NEBCs that are always ignored in the current research concerning the seaweed bioactive components. These components in NEBCs normally reach the colon intact, where they are released from the food matrix due to the fermentation by gut microbiota. EBCs and NEBCs from *G. rubra* contained varying amounts of phenolics, flavonoids, tannins, carbohydrates, and proteins and showed potent antioxidant capacities. Our research demonstrated that both EBCs and NEBCs from *G. rubra* exert potent biological activities against colon cancer and inflammation. Accurately, EBCs displayed robust inhibitory effects suppressing the growth of colon cancer cells and strong anti-inflammatory capacities in activated macrophages. Further studies indicated that EBCs and NEBCs suppressed the growth of HCT116 colon cancer cells *via* causing cellular apoptosis and cell cycle arrest. Also, EBCs and NEBCs displayed their anti-inflammatory function *via* downregulating the expression levels of NO, ROS, proinflammatory cytokines, and enzymes and upregulating the expression levels of antioxidant enzymes.

DATA AVAILABILITY STATEMENT

The original contributions presented in the study are included in the article/**Supplementary Materials**, further inquiries can be directed to the corresponding author/s.

AUTHOR CONTRIBUTIONS

LY: methodology, experiment performance, data collection, analysis, and writing—original draft preparation. QW: data collection and analysis. HL: sample preparation. DL: manuscript revision. ZT: supervision. SL: conceptualization and supervision. HX: conceptualization, supervision, writing reviewing, and editing. All authors contributed to the article and approved the submitted version.

FUNDING

This study was partially supported by the Shenzhen Strategic Emerging Industry Development Special Fund Project (Shenzhen Municipal Economic and Trade Information Commission, #20180130150742764 to SL), United States Department of Agriculture (MAS00450 and MAS00492, and NIFA grant #2019-67017-29249 and 2020-67017-30835 to HX), Hunan Science and Technology Plan Program (2019RS1055 to ZT), and Major Research plan of Changsha (kq1801016 to ZT).

SUPPLEMENTARY MATERIAL

The Supplementary Material for this article can be found online at: https://www.frontiersin.org/articles/10.3389/fnut.2022.856282/full#supplementary-material

REFERENCES

1. Pamudurthy V, Lodhia N, Konda VJA. Advances in endoscopy for colorectal polyp detection and classification. *Bayl Univ Med Cent Proc.* (2020) 33:28–35. doi: 10.1080/08998280.2019.1686327
2. Terzic J, Grivennikov S, Karin E, Karin M. Inflammation and colon cancer. *Gastroenterology.* (2010) 138:2101–14e5. doi: 10.1053/j.gastro.2010.01.058
3. Derikx LA, Smits LJ, van Vliet S, Dekker E, Aalfs CM, van Kouwen MC, et al. Colorectal cancer risk in patients with lynch syndrome and inflammatory bowel disease. *Clin Gastroenterol Hepatol.* (2017) 15: 454–8 e1. doi: 10.1016/j.cgh.2016.08.005
4. Wu X, Song M, Cai X, Neto C, Tata A, Han Y, et al. Chemopreventive effects of whole cranberry (*Vaccinium macrocarpon*) on colitis-associated colon tumorigenesis. *Mol Nutr Food Res.* (2018) 62:1800942. doi: 10.1002/mnfr.201800942
5. Bradbury KE, Appleby PN, Key TJ. Fruit, vegetable, and fiber intake in relation to cancer risk: findings from the European prospective investigation into cancer and nutrition (EPIC). *Am J Clin Nutr.* (2014) 100 (Suppl. 1):394s–8s. doi: 10.3945/ajcn.113.071357
6. Reddivari L, Charepalli V, Radhakrishnan S, Vadde R, Elias RJ, Lambert JD, et al. Grape compounds suppress colon cancer stem cells in vitro and in a rodent model of colon carcinogenesis. *BMC Complement Altern Med.* (2016) 16:278. doi: 10.1186/s12906-016-1254-2
7. Pangestuti R, Kim S-K. Biological activities and health benefit effects of natural pigments derived from marine algae. *J Funct Foods.* (2011) 3:255–66. doi: 10.1016/j.jff.2011.07.001
8. Namvar F, Mohamad R, Baharara J, Zafar-Balanejad S, Fargahi F, Rahman HS. Antioxidant, antiproliferative, and antiangiogenesis effects of polyphenol-rich seaweed (*Sargassum muticum*). *Biomed Res Intern.* (2013) 2013:604787. doi: 10.1155/2013/604787

9. Ryu B, Choi I-W, Qian Z-J, Heo S-J, Kang D-H, Oh C, et al. Anti-inflammatory effect of polyphenol-rich extract from the red alga *Callophyllis* japonica in lipopolysaccharide-induced RAW 264.7 macrophages. *Algae.* (2014) 29:343–53. doi: 10.4490/algae.2014.29.4.343
10. Bahtiar A, Anggraeni D. Influence of the extract of brown seaweed (*Turbinaria decurrens* Bory) on the histology of Colon on AOM-DSS mouse model. *Online J Biol Sci.* (2017) 17:382–6. doi: 10.3844/ojbsci.2017.382.386
11. Mahmoud AM, Abdella EM, El-Derby AM, Abdella EM. Protective effects of *Turbinaria ornata* and *Padina pavonia* against azoxymethane-induced colon carcinogenesis through modulation of PPAR gamma, NF-kappaB and oxidative stress. *Phytother Res.* (2015) 29:737–48. doi: 10.1002/ptr.5310
12. Gurgel C, Fredericq S. Systematics of the gracilariaceae (Gracilariales, Rhodophyta): a critical assessment based on rbcL sequence analyses. *J Phycol.* (2004) 40:138–59. doi: 10.1111/j.0022-3646.2003.02-129.x
13. Chan PT, Matanjun P, Yasir SM, Tan TS. Antioxidant activities and polyphenolics of various solvent extracts of red seaweed, *Gracilaria changii*. *J Appl Phycol.* (2014) 27:2377–86. doi: 10.1007/s10811-014-0493-1
14. Heffernan N, Smyth TJ, Soler-Villa A, Fitzgerald RJ, Brunton NP. Phenolic content and antioxidant activity of fractions obtained from selected Irish macroalgae species (*Laminaria digitata*, *Fucus serratus*, *Gracilaria gracilis* and *Codium fragile*). *J Appl Phycol.* (2014) 27:519–30. doi: 10.1007/s10811-014-0291-9
15. Sakthivel R, Muniasamy S, Archunan G, Devi KP. *Gracilaria edulis* exhibit antiproliferative activity against human lung adenocarcinoma cell line A549 without causing adverse toxic effect in vitro and in vivo. *Food Funct.* (2016) 7:1155–65. doi: 10.1039/c5fo01094b
16. Dwi Kurniasari K, Arsianti A, Astika Nugrahayning Aziza Y, Kirana Dyahningrum Mandasari B, Masita R, Ruhama Zulfa F, et al. Phytochemical analysis and anticancer activity of seaweed *Gracilaria verrucosa* against colorectal HCT-116 cells. *Orient J Chem.* (2018) 34:1257–62. doi: 10.13005/ojc/340308
17. Di T, Chen G, Sun Y, Ou S, Zeng X, Ye H. Antioxidant and immunostimulating activities in vitro of sulfated polysaccharides isolated from *Gracilaria rubra*. *J Funct Foods.* (2017) 28:64–75. doi: 10.1016/j.jff.2016.11.005
18. Martínez Sánchez S, Domínguez-Perles R, Montoro-García S, Gabaldón JA, Guy A, Durand T, et al. Bioavailable phytoprostanes and phytofurans from *Gracilaria longissima* have anti-inflammatory effects in endothelial cells. *Food Funct.* (2020) 11:5166–78. doi: 10.1039/D0FO00976H
19. Han Y, Huang M, Li L, Cai X, Gao Z, Li F, et al. Non-extractable polyphenols from cranberries: potential anti-inflammation and anti-colon-cancer agents. *Food Funct.* (2019) 10:7714–23. doi: 10.1039/C9FO01536A
20. González-Sarrías A, Espín JC, Tomás-Barberán FA. Non-extractable polyphenols produce gut microbiota metabolites that persist in circulation and show anti-inflammatory and free radical-scavenging effects. *Trends Food Sci Technol.* (2017) 69:281–8. doi: 10.1016/j.tifs.2017.07.010
21. Dewanto V, Wu X, Adom KK, Liu RH. Thermal processing enhances the nutritional value of tomatoes by increasing total antioxidant activity. *J Agric Food Chem.* (2002) 50:3010–4. doi: 10.1021/jf0115589
22. Kim D-O, Jeong SW, Lee CY. Antioxidant capacity of phenolic phytochemicals from various cultivars of plums. *Food Chem.* (2003) 81:321–6. doi: 10.1016/S0308-8146(02)00423-5
23. Jackson FS, Barry TN, Lascano C, Palmer B. The extractable and bound condensed tannin content of leaves from tropical tree, shrub and forage legumes. *J Sci Food Agric.* (1996) 71:103–10. doi: 10.1002/(sici)1097-0010(199605)71:13.0.co;2-8
24. Masuko T, Minami A, Iwasaki N, Majima T, Nishimura S-I, Lee YC. Carbohydrate analysis by a phenol–sulfuric acid method in microplate format. *Analyt Biochem.* (2005) 339:69–72. doi: 10.1016/j.ab.2004.12.001
25. Negrulescu A, Patrulea V, Stef - Mincea M, Ionascu C, Vlad-Oros B, Ostafe V. Adapting the reducing sugars method with dinitrosalicylic acid to microtiter plates and microwave heating. *J Braz Chem Soc* (2012) 23:2176–82. doi: 10.1590/S0103-50532013005000003
26. Brito A, Areche C, Sepulveda B, Kennelly EJ, Simirgiotis MJ. Anthocyanin characterization, total phenolic quantification and antioxidant features of some Chilean edible berry extracts. *Molecules.* (2014) 19:10936–55. doi: 10.3390/molecules190810936
27. Bainor A, Chang L, McQuade TJ, Webb B, Gestwicki JE. Bicinchoninic acid (BCA) assay in low volume. *Analyt Biochem.* (2011) 410:310–2. doi: 10.1016/j.ab.2010.11.015
28. Huang D, Ou B, Hampsch-Woodill M, Flanagan JA, Prior RL. High-throughput assay of oxygen radical absorbance capacity (ORAC) using a multichannel liquid handling system coupled with a microplate fluorescence reader in 96-well format. *J Agric Food Chem.* (2002) 50:4437–44. doi: 10.1021/jf0201529
29. Wu X, Li Z, Sun Y, Li F, Gao Z, Zheng J, et al. Identification of Xanthomicrol as a major metabolite of 5-demethyltangeretin in mouse gastrointestinal tract and its inhibitory effects on colon cancer cells. *Front Nutr.* (2020) 7:103. doi: 10.3389/fnut.2020.00103
30. Wu X, Song M, Rakariyatham K, Zheng J, Guo S, Tang Z, et al. Anti-inflammatory effects of 4'-demethylnobiletin, a major metabolite of nobiletin. *J Funct Foods.* (2015) 19(Pt A):278–87. doi: 10.1016/j.jff.2015.09.035
31. Shen L, Zhou T, Wang J, Sang X, Lan L, Luo L, et al. Daphnetin reduces endotoxin lethality in mice and decreases LPS-induced inflammation in Raw264.7 cells via suppressing JAK/STATs activation and ROS production. *Inflamm Res.* (2017) 66:579–89. doi: 10.1007/s00011-017-1039-1
32. Livak KJ, Schmittgen TD. Analysis of relative gene expression data using real-time quantitative PCR and the 2(-Delta Delta C(T)) Method. *Methods (San Diego, Calif).* (2001) 25:402–8. Epub 2002/02/16. PubMed doi: 10.1006/meth.2001.1262
33. Grosso G. Effects of polyphenol-rich foods on human Health. *Nutrients.* (2018) 10:1089. doi: 10.3390/nu10081089
34. Machu L, Misurcova L, Ambrozova JV, Orsavova J, Mlcek J, Sochor J, et al. Phenolic content and antioxidant capacity in algal food products. *Molecules.* (2015) 20:1118–33. doi: 10.3390/molecules20011118
35. Arranz S, Silvan JM, Saura-Calixto F. Nonextractable polyphenols, usually ignored, are the major part of dietary polyphenols: a study on the Spanish diet. *Mol Nutr Food Res.* (2010) 54:1646–58. doi: 10.1002/mnfr.200900580
36. Wu T, Phuong NNM, Van Camp J, Smagghe G, Le TT, Raes K. CHAPTER 4 Analysis of non-extractable polyphenols (NEPP). In: Saura-Calixto F, Pérez-Jiménez J editors. *Non-Extractable Polyphenols and Carotenoids: Importance in Human Nutrition and Health*. London: The Royal Society of Chemistry (2018). p. 46–67. doi: 10.1039/9781788013208-00046
37. Johnson DG, Walker CL. Cyclins and cell cycle checkpoints. *Annu Rev Pharmacol Toxicol.* (1999) 39:295–312. doi: 10.1146/annurev.pharmtox.39.1.295
38. Seibert K, Masferrer J, Zhang Y, Gregory S, Olson G, Hauser S, et al. Mediation of inflammation by cyclooxygenase-2. *Agents Actions Suppl.* (1995) 46:41–50. doi: 10.1007/978-3-0348-7276-8_5
39. Wong JM, Billiar TR. Regulation and function of inducible nitric oxide synthase during sepsis and acute inflammation. In: Ignarro L, Murad F editors. *Advances in Pharmacology*. (Vol. 34), Cambridge, MA: Academic Press (1995). p. 155–70. doi: 10.1016/s1054-3589(08)61084-4
40. Yeligar SM, Machida K, Kalra VK. Ethanol-induced HO-1 and NQO1 are differentially regulated by HIF-1α and Nrf2 to attenuate inflammatory cytokine expression. *J Biol Chem.* (2010) 285:35359–73. doi: 10.1074/jbc.M110.138636

Conflict of Interest: The authors declare that the research was conducted in the absence of any commercial or financial relationships that could be construed as a potential conflict of interest.

frontiers | Frontiers in Nutrition

ORIGINAL RESEARCH
published: 13 May 2022
doi: 10.3389/fnut.2022.856273

Inhibitory Effects of Polyphenols-Rich Components From Three Edible Seaweeds on Inflammation and Colon Cancer *in vitro*

Lingxiao Yi[1], *Qi Wang*[1], *Haiyan Luo*[1], *Daqing Lei*[2], *Zhonghai Tang*[3]*, *Sijia Lei*[2]* and *Hang Xiao*[1]*

[1] Department of Food Science, University of Massachusetts, Amherst, MA, United States, [2] School of Food and Drug, Shenzhen Polytechnic, Shenzhen, China, [3] College of Food Science and Technology, Hunan Agricultural University, Changsha, China

OPEN ACCESS

Edited by:
Ce Qi,
Qingdao University, China

Reviewed by:
Franklin Chamorro,
University of Vigo, Spain
Haohao Wu,
Ocean University of China, China
Gaoxing Ma,
Nanjing University of Finance and Economics, China

***Correspondence:**
Zhonghai Tang
tangzh@hunau.edu.cn
Sijia Lei
leisijia@szpt.edu.cn
Hang Xiao
hangxiao@foodsci.umass.edu

Specialty section:
This article was submitted to Nutritional Immunology, a section of the journal Frontiers in Nutrition

Received: *17 January 2022*
Accepted: *01 April 2022*
Published: *13 May 2022*

Citation:
Yi L, Wang Q, Luo H, Lei D, Tang Z, Lei S and Xiao H (2022) Inhibitory Effects of Polyphenols-Rich Components From Three Edible Seaweeds on Inflammation and Colon Cancer in vitro. Front. Nutr. 9:856273. doi: 10.3389/fnut.2022.856273

Polyphenols from edible seaweeds display various health benefits which have not been adequately studied. This study aimed to characterize the composition of extractable polyphenol-rich components (EPCs) and non-extractable polyphenol-rich components (NEPCs) from three edible seaweeds (i.e., *Laminaria japonica, Ulva lactuca*, and *Porphyra tenera*) and evaluate their anti-inflammatory capacities in activated macrophages and anticancer properties in colon cancer cells. Both EPCs and NEPCs from three edible seaweeds against lipopolysaccharides (LPS) stimulated nitric oxide in activated macrophages. Immunoblotting and qRT-PCR indicated that EPCs and NEPCs regulated the expression levels of proinflammatory enzymes, proinflammatory cytokines, and antioxidant enzymes in macrophages. Furthermore, EPCs and NEPCs lowered the viability of colon cancer cells, while normal colon cells were not affected. Additionally, EPCs and NEPCs induced cellular apoptosis and led to G0/G1 cell cycle arrest in HCT116 cells. Overall, these results provide a rationale for future animal and human studies designed to examine the anti-inflammatory and chemopreventive capacities of polyphenols-rich components from *L. japonica*, *U. lactuca*, and *P. tenera*.

Keywords: edible seaweeds, *Laminaria japonica*, *Ulva lactuca*, *Porphyra tenera*, polyphenols, anti-inflammation, anti-colon cancer

INTRODUCTION

Polyphenols are secondary metabolites from plants which may offer health benefits against chronic diseases, such as oxidative stress, inflammation, and cancer (1). Polyphenols can be divided into two categories during the process of extraction, namely, extractable polyphenols that can be acquired by aqueous organic solvent and non-extractable polyphenols that remained in the residues and were largely ignored in most prior studies (2). Non-extractable polyphenols include low molecular weight polyphenols (phenolic acids and flavonoids) cross-linking with dietary fiber and proteins, and macromolecules polyphenols (condensed tannins and proanthocyanidins) (3). These phenolic compounds interact with the food matrix *via* hydrogen bonding, covalent bonding, and hydrophobic interactions (4). Moreover, non-extractable polyphenols with lower bioavailability in

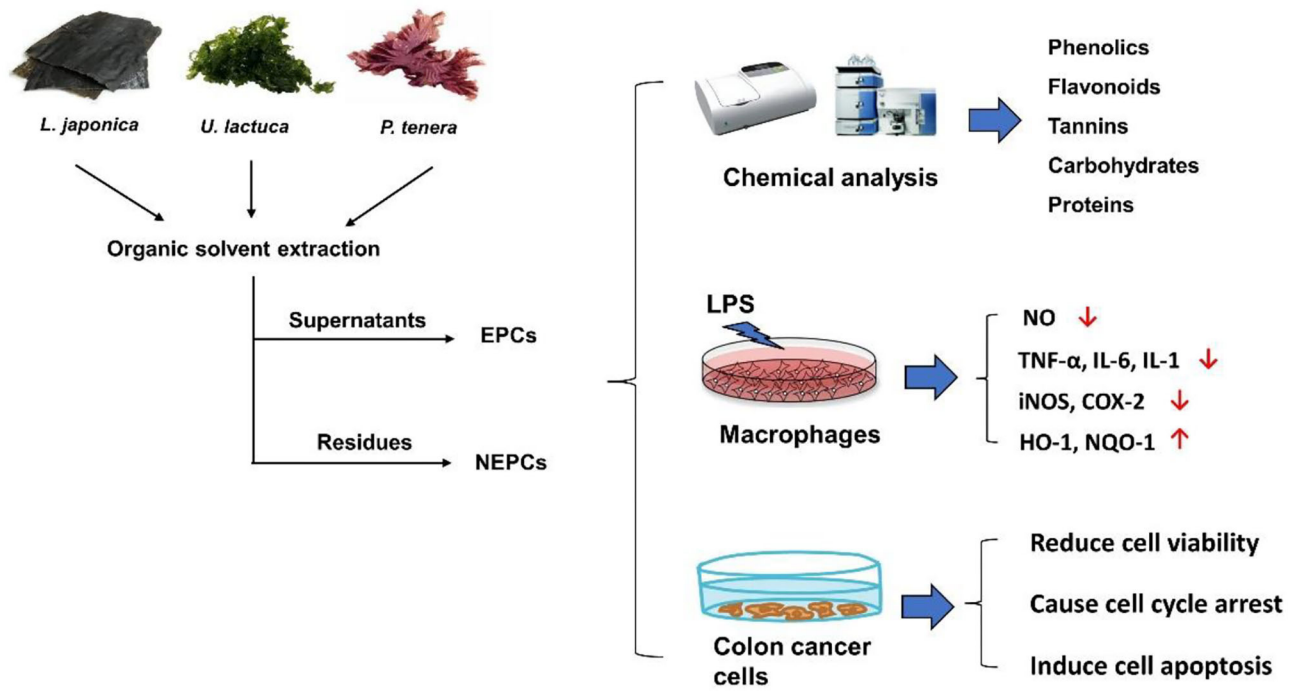

GRAPHICAL ABSTRACT | Extractable polyphenols-rich components (EPCs) and non-extractable polyphenols-rich components (NEPCs) have been isolated from three edible seaweeds. EPCs and NEPCs from three edible seaweeds contain certain amounts of phenolics, flavonoids, and tannins, and few amounts of carbohydrates and proteins. Further studies evaluated the efficacy and mechanism behind the anti-inflammatory capacities in activated macrophages and anticancer properties in colon cancer cells.

the stomach and small intestine reach the colon intact. Non-extractable polyphenols may release from the food matrix in the colon by the action of gut microbiota and then become bioactive and bioavailable (5). Additionally, non-extractable polyphenols compounds isolated from fruits, such as cranberry, strawberry, and apple, and vegetables have been reported with antioxidative, anti-inflammatory, and anti-cancer properties (6–9).

Inflammatory agent is an essential response to harmful stimuli caused by stress, infection, and injury and is characterized by symptoms such as heat, swelling, redness, and pain (10). Chronic inflammation has a strong association with chronic diseases, including cancer and heart disease (11). Macrophages stimulated by lipopolysaccharides (LPS) or interferon-gamma excessively secrete proinflammatory cytokines, including interleukin (IL)-1, IL-6, and tumor necrosis factor-α (TNF-α), which in turn induce the expression of proinflammatory enzymes, namely, cyclooxygenase-2 (COX-2) and inducible nitric oxide synthase (iNOS) (12). Studies have indicated that overexpression of these proinflammatory cytokines and enzymes is associated with tumor formation in the brain, breast, lung, colorectal, and prostate (13, 14). Natural bioactive compounds from terrestrial plants have been reported to offer beneficial effects against chronic disease. The application of seaweeds, the largest and most complex algae, as foodstuffs for human health traced back to several 100 years ago in Asian countries, due to the richness of bioactive compounds such as polysaccharides, polyphenols, minerals, fatty acids, bioactive peptides, and proteins (15). Phenolic compounds from seaweeds have been shown to be against inflammation and cancer in cell culture and animal studies (16–18).

To date, multiple phenolic compounds have been isolated and quantified from edible seaweeds and have been reported with various biological properties (16, 19, 20). These phenolic compounds belong to extractable polyphenols, where the potential health benefits of non-extractable polyphenols from these popular edible seaweeds remain unclear. However, polyphenol compounds from edible seaweeds, particularly for those with protective effects on inflammation and colon cancer, have not been adequately investigated. Brown seaweed *Laminaria japonica*, red seaweed *Porphyra tenra*, and green seaweed *Ulva lactuca* are three popular edible seaweeds, which are widely distributed in Asian countries and used as a drug in Traditional Chinese Medicine (21–23). Thus, this study aims to characterize the compositions of extractable polyphenol-rich components (EPCs) and non-extractable polyphenol-rich components (NEPCs) from *L. japonica, P. tenera*, and *U. lactuca* and to investigate

Abbreviations: EPCs, extractable polyphenols-rich components; NEPCs, non-extractable polyphenols-rich components; LPS, lipopolysaccharides; NO, nitrite oxide; iNOS, inducible nitric oxide synthase; COX-2, cyclooxygenase-2; HO-1, heme oxygenase 1; NQO-1, NADPH-quinone oxidoreductase-1; TNF- α, tumor necrosis factors-α; IL, interleukin; PCs, phenolics contents; FCs, flavonoids content; TCs, tannins contents; CCs, carbohydrates contents; PRCs, proteins contents; ORAC, oxygen radical absorbance capacity.

their anti-colon cancer and anti-inflammatory efficacy and mechanisms.

MATERIALS AND METHODS

Materials

Dried powders of *L. japonica* and *U. lactuca* were obtained from Wonderful LLC (Fuzhou, Fujian, China), and dried powder of *P. tenera* was purchased from PlantGift LLC (Haozhou, Anhui, China), in January 2020. The seaweed powders were stored at −20°C before use. 3-Hydrobenzoic acid, 4-hydrobenzoic acid, ferulic acid, iso-ferulic acid, sinapic acid, phloroglucinol, syringic acid, coumaric acid, rutin, hesperidin, luteolin, rosmamaric acid, apigenin, caffeic acid, gallic acid, chlorogenic acid, vanillic acid, myricetin, morin, quecertin, acacetin, kaempferol, catechin, epicatechin, gallo-catechin, epigallocatechin gallate, epigallocatechin, and epicatechin-gallate were ordered from Shyuanye (Shanghai, China). 3-(4, 5-dimethylthiazol-2-yl) 2, 5-diphenyltetrazolium bromide (MTT), 2,2'-Azobis (2-amidinopropane) dihydrochloride, potassium persulfate, propidium iodine (PI), and lipopolysaccharides (LPS) from *E. coli* O55:B5 were purchased from Sigma-Aldrich (Natick, MA, USA). Annexing V/PI double staining was obtained from Bio Vision (Mountain View, CA, USA). 1,1-Diphenyl-2-picrylhydrazyl (DPPH) free radical and 2.2′-azinobis (3-ethylbenzothiazoline-6-sulfonic acid ammonium salt) (ABTS) were purchased from TCI America (Portland, OR, USA). The antibodies of iNOS, COX-2, and HO-1 were ordered from Santa Cruz (Dallas, TX, USA), and the antibody of β-actin as the loading control was purchased from Sigma-Aldrich (Natick, MA, USA).

Preparation of Polyphenols-Rich Components

The extraction of polyphenols-rich components was conducted based on our previous report with some modifications (7). Briefly, a mass of 25 g of the dried powders of edible seaweeds was blended with 500 ml of chilled 70% (v/v) acetone aqueous solution (1% acetic acid). The blend was subjected to ultrasound vibration for half hour, before spinning at 3,000 g for 10 min. The residues were subjected to the same procedure two times. After that, the supernatant was pooled, concentrated, and subjected to the extraction of EPCs, and the residues were collected for the extractions of NEPCs.

For the preparations of EPCs, the resulting supernatants were dissolved in the same volume of methanol. The highly lipophilic molecules were removed by the extraction of hexane. After that, the methanol layers were pooled and concentrated, followed by the extraction of ethyl acetate three times. Finally, the upper layer was pooled, dried, and stored at −20°C for further analysis.

For the preparations of NEPCs, the residues were blended with sodium hydroxide (2M) at 37°C for 2 h, where the containers were purged with nitrogen. Then, concentrated hydrochloric acid was added to terminate the reaction, before spinning at 4,000 g for 10 min. Subsequently, the supernatant was processed for the extraction of ethyl acetate. Finally, the upper phase was pooled, dried, and stored at −20°C for further analysis.

Evaluation of Total Phenolics Contents, Flavonoids Contents, Tannins Contents, Carbohydrates Contents, and Proteins Content

Phenolics contents were measured by the Folin–Ciocalteu method according to a previous study (24). A volume of 20 μl of samples or gallic acid solutions (0 to 200 μg/ml) was added into a 96-well plate with 20 μL distilled water and 20 μl of Folin-Ciocalteu reagent. The plate was kept at room temperature for 10 min, before adding 140 μl of 7% sodium carbonate. Finally, the plate was kept at room temperature for another 90 min, followed by measuring absorbance at 760 nm using a spectrophotometer (BioTek Instrument, Inc. Winooski, VT, USA), and the results were presented as mg of gallic acid equivalents per hundred g seaweed powder (mg GAE/100 g seaweed powder).

Flavonoids contents were measured by the aluminum trichloride method according to a previous study (25). A volume of 20 μl of samples or catechin solutions (0 to 200 μg/ml) was added into a 96-well plate with 10 μl of 5% sodium nitrite and 100 μl of distilled water. First, the plate was kept at room temperature for 6 min before adding 20 μl of aluminum chloride. Then, the plate was incubated at room temperature for another 5 min before adding 50 μl of sodium hydroxide (1M). Finally, the absorbance was monitored at 510 nm using a spectrophotometer (BioTek Instrument, Inc. Winooski, VT, USA), and the results were presented as mg of catechin equivalents per hundred g seaweed powder (mg CE/100 g seaweed powder).

Tannins contents were measured by the vanillin-sulfuric acid method according to a previous study (26). A volume of 20 μl samples or catechin solutions (0 to 200 μg/ml) was added into a 96-well plate mixed with 90 μl of 30% concentrated sulfuric acid and 90 μl of 4% vanillin in methanol and was kept at room temperature for 5 min. Finally, the absorbance was read at 510 nm using a spectrophotometer (BioTek Instrument, Inc. Winooski, VT, USA), and the results were presented as mg of catechin equivalents per hundred g seaweed powder (mg CE/100 g seaweed powder).

Carbohydrates contents were assessed by the phenol-sulfuric acid method according to a previous study (27). A volume of 50 μl of samples or glucose solutions (0 to 200 μg/ml) was added into a 96-well plate, followed by adding 30 μl of 5% phenol and 150 μl of concentrated sulfuric acid rapidly. Finally, the plate was heated at 90°C for 5 min, followed by measuring the absorbance at 490 nm using a spectrophotometer (BioTek Instrument, Inc. Winooski, VT, USA), and the results were presented as mg of glucose equivalents per hundred g seaweed powder (mg GE/100 g seaweed powder).

Proteins contents were evaluated by the BCA method with minor modifications (28). Results were presented as mg of protein per hundred g seaweed powder (mg protein/100 g seaweed powder).

Evaluation of Antioxidant Properties of EPCs and NEPCs

Oxygen radical absorbance capacity (ORAC) was assessed following a previous study with minor modifications (29). A

volume of 20 μl samples or Trolox solutions (0 to 200 μM) was added into a 96-well plate with 40 μl of of fluorescencein solution (75 μM). The plate was gently shaken and stored at 37°C for 2 min, before adding 140 μl of 0.8 M 2,2'-Azobis (2-amidinopropane) dihydrochloride solution. Finally, the plate was subjected to a microplate fluorescence reader (BioTek Instrument, Inc., Winooski, VT, USA), excitation was measured at 485 nm, and emission was measured at 528 nm. This process continued for 2 h, and the absorbance was recorded at an interval of 2 min. Results were presented as μmol of Trolox equivalents per g extract (μmol TE/g extract).

The DPPH·scavenging capacity was determined following a previous study with minor modifications (30). A volume of 20 μl of samples or Trolox solutions was added into a 96-well plate mixed with 180 μl of 50 μM DPPH·ethanol solution. Finally, the plate was kept at room temperature for half-hour, followed by measuring absorbance at 517 nm by a spectrophotometer (BioTek Instrument, Inc. Winooski, VT, USA), and the results were presented as Trolox equivalent antioxidant capacity.

The ABTS + scavenging capacity was determined following a previous study with minor modifications (30). First, the ABTS working solution was prepared by the ratio of 7 mM ABTS solution to 2.45 mM potassium persulfate solution, which is 1:5. Subsequently, a volume of 10 μl of samples or Trolox solution was added into a 96-well plate with 200 μl of ABTS working solution. Finally, the plate was stored at room temperature, avoiding light for 7 min, followed by measuring absorbance at 734 nm using a spectrophotometer (BioTek Instrument, Inc. Winooski, VT, USA), and the results were presented as Trolox equivalent antioxidant capacity.

Identification of Phenolic Compounds

High-resolution LC/MS was performed by an Ultimate 3000 UHPLC system coupled with an Orbitrap Fusion mass spectrometer (Thermo Scientific, Waltham, MA, USA) in the mass spectrometry core facility at the University of Massachusetts Amherst. Chromatography separation was carried out by the reverse-phase Kinetex XB-C18 column (100 mm × 4.6 mm, 2.6 μm, Phenomenex, Torrance, CA, USA). Meanwhile, the mobile phase is made up of 5% acetonitrile with 0.1% formic acid (solvent A) and 0.1% formic acid in 100% acetonitrile (solvent B). The initial mobile phase composition was 15% solvent B and linearly elevated to 100% solvent B within 3 min and maintained for 10 min. Then, the concentration of solvent B was linearly decreased to 15% with 0.01 min and maintained for 1.99 min. The flow rate was 400 μl/min, and the injection volume was 5 μl. Data were acquired in positive ESI mode using a spray voltage of 3,250 V, with sheath and aux gas set to 50 and 15, respectively, and vaporizer and tube temperature both set to 300°C. Data processing was accomplished using Xcalibur V4.2 (Thermo Scientific, Waltham, MA, USA).

Cytotoxicity and Nitrite Oxide Assay of RAW 264.7 Cells

The cytotoxicity of EPCs and NEPCs on macrophages was tested according to the MTT assay, and the Griess test was carried out to investigate nitrite concentration as described earlier (31). RAW 264.7 cells (5×10^5 cells/ml) were cultured into a 96-well plate (200 μl/well) and incubated for 24 h, before being treated with or without LPS (1 μg/ml) and coupled with an aliquot of EPCs or NEPCs at multiple concentrations for another 24 h. The cells and the culture media were subjected to MTT assay and Griess reaction, respectively.

Cell Viability of Normal Colon Cells and Colon Cancer Cells

The cell viability was performed as reported in a previous study (32). CCD-18Co cells (50,000 cells/ml) and HCT116 cells (12,500 cells/ml) were cultured into a 96-well plate (200 μl/well) and incubated at 37°C overnight, before being posed to multiple concentrations of EPCs and NEPCs for another 48 h or 72 h. Finally, the cells were assessed by MTT assay.

Flow Cytometer Analysis

Flow cytometer analysis was performed following previous studies (32, 33). HCT116 cells (4×10^4 cells/ml) were cultured in 6-well plates and incubated overnight, before being posed to EPCs or NEPCs for 24 h for cell cycle analysis and for 48 h for cell apoptosis analysis. Then, media containing any floating cells were collected by trypsinization. Finally, cell pellets were washed by chilled PBS and subjected to flow cytometer analysis.

qRT-PCR Analysis

Total RNA from macrophages was isolated by TRIzol reagent. The real-time qRT-PCR assay was carried out as reported in a previous study (31). The primer sequences used for cDNA amplification were listed in **Supplementary Table S1**. Three independent parallel groups were used, and related mRNA expression was determined using the $2^{-\Delta\Delta Ct}$ method (34).

Immunoblotting

The whole-cell protein extraction was based on a previous study (31). Briefly, macrophages were cultured in plates and incubated for 24 h, before being posed to multiple concentrations of EPCs or NEPCs with or without LPS for another 24 h. Then, the cell lysate was collected and assessed for immunoblotting following previous studies.

Statistical Analysis

Data were presented as mean ± standard deviation (SD) of more than three independent parallel experiments. Statistical comparison among groups was performed using the one-way ANOVA followed by the student's *t*-test. A $p < 0.05$ was considered statistically significant.

RESULTS AND DISCUSSION

Chemical Profiles of EPCs and NEPCs in *L. japonica*, *U. lactuca*, and *P. tenera*

Seaweed polyphenols have been reported to offer health benefits against oxidative stress, inflammation, and cancer (16, 18, 35). However, most studies into polyphenols focused only on the EPCs. NEPCs, the fraction of polyphenols remaining in the residue after extraction, were largely neglected by prior studies

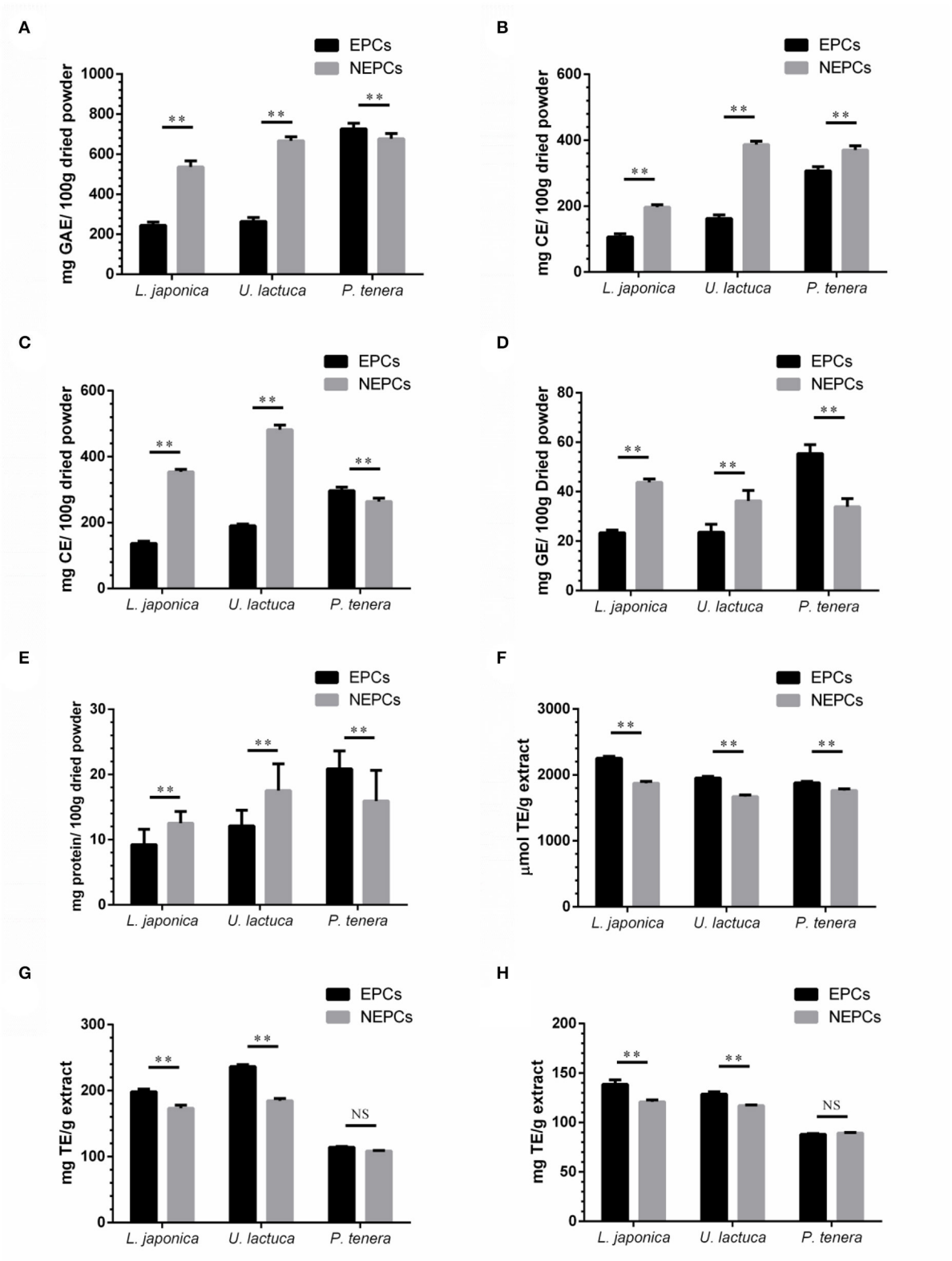

FIGURE 1 | Total phenolic contents (PCs) **(A)**, flavonoid contents (FCs) **(B)**, tannin contents (TCs) **(C)**, carbohydrate content (CCs) **(D)**, and protein contents (PRCs) **(E)** in EPCs and NEPCs from three edible seaweeds. The levels of ORAC **(F)**, DPPH **(G)**, and ABTS **(H)** of the EPCs and NEPCs from three edible seaweeds. Data were presented as mean ± SD ($n = 6$). NS indicate no statistical difference, $^{**}p < 0.01$ indicate a statistical difference.

TABLE 1 | Selected phenolic compounds identified in the EPCs and NEPCs in *L. japonica*, *U. lactuca*, and *P. tenera*.

Compounds	Retention time	MS(m/z)	*L. japonica*		*U. lactuca*		*P. tenera*	
			EPCS (μg/g extract)	NEPCs (μg/g extract)	EPCS (μg/g extract)	NEPCs (μg/g extract)	EPCS (μg/g extract)	NEPCs (μg/g extract)
3-hydrobenzoic acid	3.96	139.039 $^+$	770.80 ± 48.92	26.66 ± 2.23	235.27 ± 14.25	23.02 ± 2.24	566.86 ± 50.25	133.70 ± 12.23
4-hydrobenzoic acid	3.15	139.039 $^+$	550.59 ± 33.52	ND	781.87 ± 59.82	ND	ND	ND
Phloroglucinol	2.91	127.039 $^+$	163.63 ± 15.21	ND	ND	211.60 ± 13.21	814.38 ± 78.82	433.62 ± 41.29
Sinapic acid	4.20	225.076 $^+$	530.84 ± 49.89	23.31 ± 2.04	506.95 ± 37.89	3.72 ± 0.92	742.58 ± 67.89	98.11 ± 8.02
Ferulic acid	4.25	195.065 $^+$	1175.76 ± 88.13	127.35 ± 2.65	16.32 ± 1.25	36.15 ± 2.52	211.24 ± 18.32	1020.73 ± 92.56
Iso ferulic acid	4.28	195.065 $^+$	ND	17.03 ± 1.52	ND	25.52 ± 1.78	89.69 ± 81.55	1256.29 ± 118.51
Syringic acid	4.33	199.060 $^+$	ND	ND	ND	ND	2726.17 ± 182.76	ND
Coumaric acid	3.70	165.055 $^+$	392.77 ± 4.44	ND	997.78 ± 93.42	ND	1436.86 ± 124.32	17.84 ± 1.84
Rosmarinic acid	4.20	361.092 $^+$	1446.66 ± 99.23	244.04 ± 19.21	ND	147.04 ± 12.23	815.44 ± 76.62	1027.65 ± 102.23
Chlorogenic acid	3.47	355.102 $^+$	1529.15 ± 111.13	ND	753.70 ± 61.53	191.01 ± 18.11	1928.50 ± 161.25	191.01 ± 18.11
Caffeic acid	3.16	181.050 $^+$	628.49 ± 41.22	ND	947.91 ± 81.24	189.36 ± 16.88	1323.60 ± 121.22	193.16 ± 17.89
Vanilic acid	3.15	169.050 $^+$	547.75 ± 51.23	8.82 ± 0.87	847.43 ± 31.63	ND	1325.73 ± 71.63	8.82 ± 0.87
Gallic acid	10.98	171.023 $^+$	2491.88 ± 216.21	ND	ND	ND	ND	ND
Luteolin	4.52	287.055 $^+$	2.39 ± 0.34	221.53 ± 16.54	411.52 ± 39.85	949.12 ± 86.54	408.16 ± 40.12	1074.05 ± 96.54
Rutin	3.88	611.161 $^+$	ND	ND	4033.13 ± 378.18	ND	3752.20 ± 368.28	ND
Hesperidin	4.00	611.197 $^+$	ND	ND	3120.40 ± 202.13	72.46 ± 6.85	2250.90 ± 202.13	104.55 ± 9.85
Myricetin	4.30	319.045 $^+$	897.06 ± 68.89	9.82 ± 0.75	724.98 ± 58.89	1.23 ± 0.07	422.91 ± 28.81	2.82 ± 1.75
Apigenin	4.77	271.060 $^+$	100.20 ± 9.13	15.65 ± 1.98	85.12 ± 6.78	33.31 ± 2.98	362.73 ± 26.78	92.51 ± 6.98
Morin	4.44	303.050 $^+$	44.30 ± 3.55	5.02 ± 0.51	405.14 ± 3.55	3.42 ± 2.12	1353.32 ± 123.52	1.99 ± 0.12
Quecertin	4.56	303.050 $^+$	937.03 ± 92.23	16.99 ± 1.96	1842.13 ± 89.23	5.99 ± 0.96	481.89 ± 29.35	8.99 ± 0.96
Acacetin	5.43	285.076 $^+$	ND	909.85 ± 92.97	ND	110.51 ± 9.24	4.91 ± 0.32	201.82 ± 19.24
Kaempferol	4.52	287.056 $^+$	3915.07 ± 256.11	213.06 ± 2.55	477.52 ± 36.11	929.76 ± 8.55	ND	988.04 ± 78.34
Catechin	3.70	291.086 $^+$	913.19 ± 82.23	1.12 ± 0.03	1926.78 ± 119.23	1.52 ± 0.43	2528.84 ± 231.23	6.22 ± 0.43
Epicatechin	3.86	291.086 $^+$	1263.01 ± 102.13	1.78 ± 0.76	737.84 ± 72.13	2.58 ± 0.76	1342.42 ± 132.13	12.58 ± 2.76
Gallocatechin	2.97	307.081 $^+$	854.06 ± 71.23	1.03 ± 0.16	1348.26 ± 71.23	ND	892.31 ± 16.35	ND
Epigallocatechin gallate	3.91	459.092 $^+$	1525.35 ± 109.12	132.26 ± 11.91	3357.55 ± 209.12	1195.54 ± 101.91	28475.45 ± 254.11	ND
Epigallocatehin	3.15	307.081 $^+$	1111.54 ± 96.15	ND	2016.63 ± 154.15	ND	2830.86 ± 211.81	8.18 ± 0.75
Epicatechin gallate	4.06	443.097 $^+$	ND	28.26 ± 1.95	397.85 ± 29.12	100.01 ± 12.95	2144.65 ± 121.53	136.59 ± 12.95

Results were expressed as mean ± SD. ND means not detected.

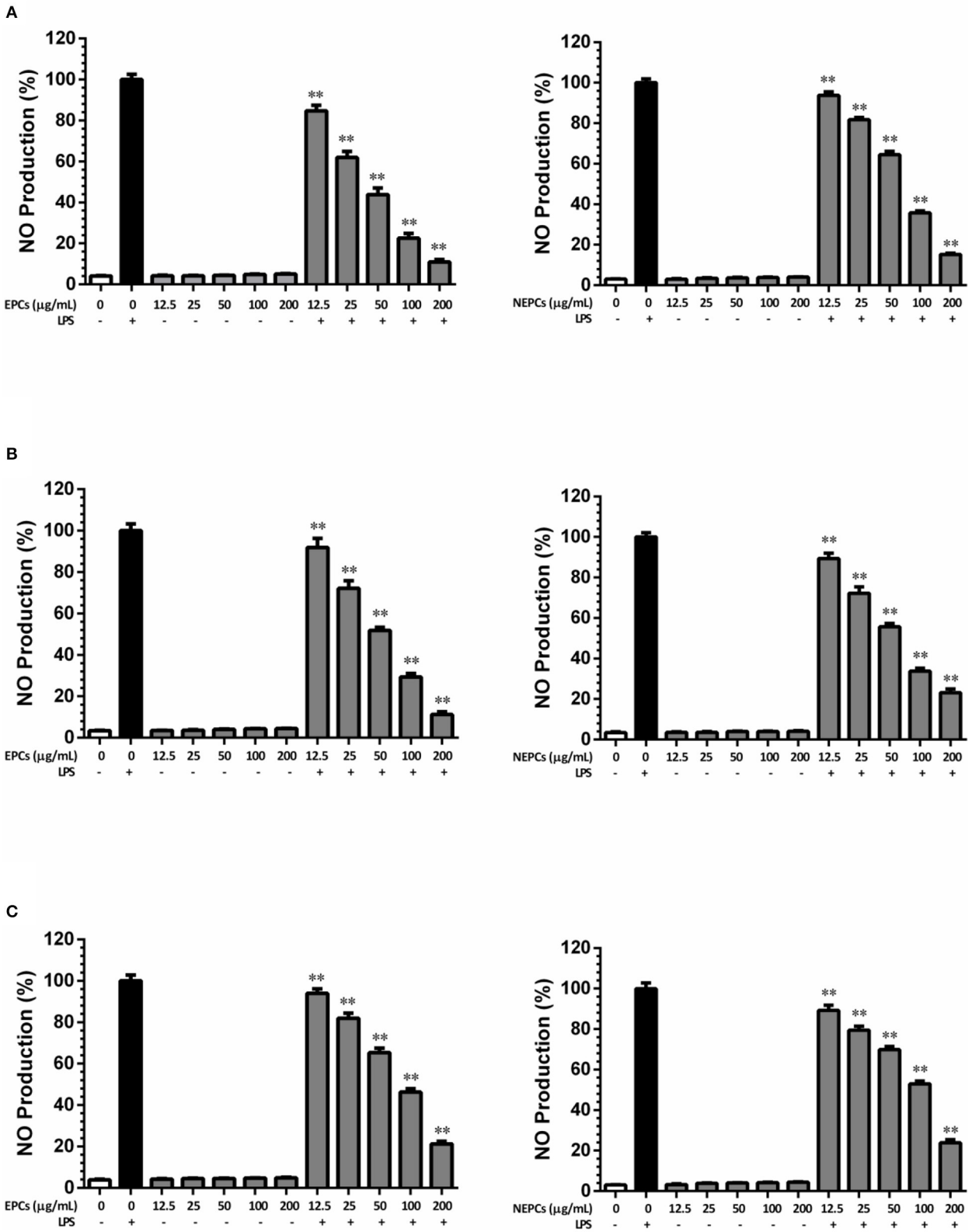

FIGURE 2 | Inhibitory effects of EPCs and NEPCs from *L. japonica* **(A)**, *U. lactuca* **(B)**, *P. tenera* **(C)** on NO production in activated macrophages. Results were expressed as mean ± SD ($n = 6$). *$p < 0.05$ and **$p < 0.01$ indicates statistically differences from LPS-treated group.

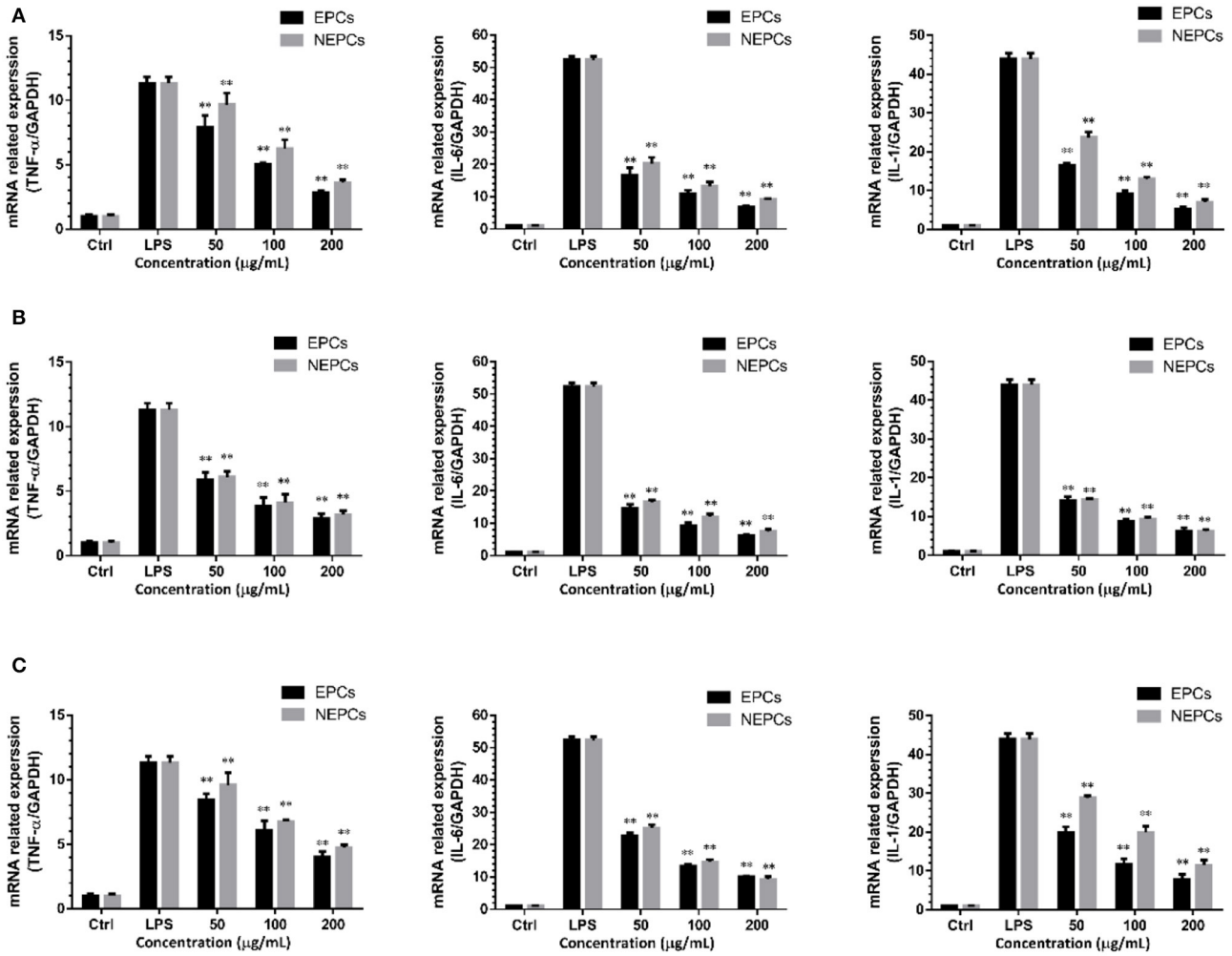

FIGURE 3 | Suppressive effects of EPCs and NEPCs from *L. japonica* **(A)**, *U. lactuca* **(B)**, *P. tenera* **(C)** on mRNA expression of TNF-α, IL-6, IL-1 in activated macrophages. Results were expressed as mean ± SD ($n = 6$). *$p < 0.05$ and **$p < 0.01$ indicate statistically differences from LPS-treated group.

(2). In this study, we sought to elucidate the compositions of EPCs and NEPCs in three edible seaweeds, namely, *L. japonica*, *U. lactuca*, and *P. tenera*, and evaluate their potential protective effects on inflammation and colon cancer in this study.

The yield of EPCs from *L. japonica*, *U. lactuca*, and *P. tenera* was 9.85, 17.26, and 13.27 mg/g dried powder, respectively. The yield of NEPCs from *L. japonica*, *U. lactuca,* and *P. tenera* was 15.24, 17.75, and 19.45 mg/g dried powder, respectively. The total PCs, FCs, TCs, CCs, and PRCs in EPCs and NEPCs from the three edible seaweeds are shown in **Figure 1**. Interestingly, the PCs, FCs, and TCs in NEPCs from *L. japonica* were all higher than those in its EPCs. Similar patterns were observed in *U. lactuca*. Moreover, the PCs and TCs in EPCs were higher than those in its NEPCs in *P. tenera*. The FCs in NEPCs were also higher than those in EPCs in *P. tenera* (**Figure 1**). Small amounts of CCs and PRCs (< 60 mg/100 g dried powder) were identified in EPCs and NEPCs. The relative abundance of PCs in NEPCs and EPCs was comparable with other plant-based foods, such as apples, bananas, carrots, broccoli, and lettuce (36). Also, both EPCs and NEPCs from *L. japonica* and *U. lactuca* contain more tannins than flavonoids.

The selected phenolic compounds in this study were identified and quantified by UHPLC/MS. Briefly, the abundance of phenolic compounds in the EPCs was higher than those in the NEPCs in the three edible seaweeds. But the amounts of phenolic compounds in *L. japonica*, *U. lactuca*, and *P. tenera* were different (**Table 1**). Hydrobenzoic acid, coumaric acid, chlorogenic acid, vanillic acid, caffeic acid, sinapic acid, quercetin, myricetin, catechin, epicatechin, and epigallocatechin gallate were the major constituents in the EPCs. In contrast, isoferulic acid, rosmarinic acid, luteolin, acacetin, and kaempferol were the major constituents in the NEPCs. Overall, this study offered an incisive understanding of the chemical profiles and biological effects of different bioactive components in *L. japonica*, *U. lactuca*, and *P. tenera*. More importantly, for the first time, we characterized the chemical profiles of their NEPCs.

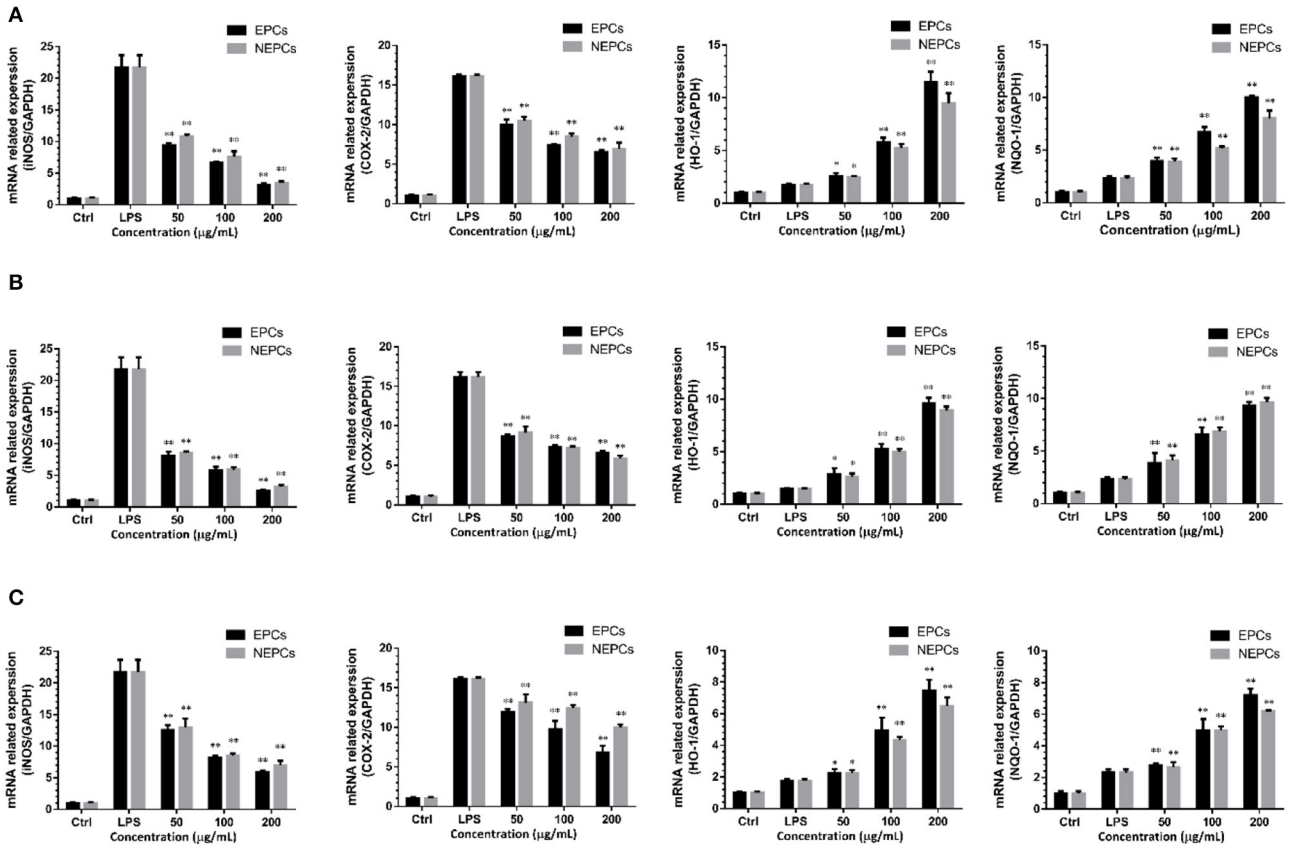

FIGURE 4 | Effects of EPCs and NEPCs from *L. japonica* **(A)**, *U. lactuca* **(B)**, *P. tenera* **(C)** on mRNA expression of iNOS, COX-2, HO-1 and NQO-1 in activated macrophages. Results were expressed as mean ± SD ($n = 3$), $^{*}p < 0.05$ and $^{**}p < 0.01$ indicate statistically differences from LPS-treated group.

Antioxidant Capacities of the EPCs and NEPCs in *L. japonica*, *U. lactuca*, and *P. tenera*

The abundance of phenolics, flavonoids, and tannins in EPCs and NEPCs of these seaweeds may have contributed to the antioxidant capacities. The ORAC values were ranging from 1,870 to 2,280 μmol TE/g in EPCs and from 1,750 to 1,880 μmol TE/g in NEPCs. Furthermore, the ORAC values of both EPCs and NEPCs from *L. japonica* were higher than the *U. lactuca* and *P. tenera* (**Figure 1F**). The DPPH values were ranging from 110 to 240 mg TE/g in EPCs and from 100 to 190 mg TE/g in NEPCs (**Figure 1G**). The ABTS values were ranging from 85 to 140 mg TE/g in EPCs and from 87 to 122 mg TE/g in NEPCs (**Figure 1H**). The antioxidant activity of EPCs from *L. japonica* and *U. lactuca* was all significantly higher than the NEPCs measured by the DPPH method and the ABTS method. There was no difference between the activity of EPCs and NEPCs from *P. tenera*. Overall, EPCs and NEPCs from *L. japonica* and *U. lactuca* exhibited stronger antioxidant activities than those from *P. tenera*.

EPCs and NEPCs Reduced the NO Production in Activated Macrophages

Epidemiological data have revealed that a higher intake of polyphenols might reduce the risk of inflammation (37). Then, we sought to understand the protective effects of EPCs and NEPCs from the three edible seaweeds against inflammation in LPS-treated macrophages. First, their cytotoxicity on RAW264.7 macrophages was monitored by MTT assay at multiple concentrations. Both EPCs and NEPCs from the three edible seaweeds did not display any cytotoxicity up to 200 μg/ml (**Supplementary Figure S1**). Subsequently, these nontoxic ranges were used to evaluate their anti-inflammatory effects on activated macrophages.

Nitrite oxide (NO) is a signaling molecule, and overproduction of NO during the inflammation process can induce proinflammatory cytokines in macrophages (38). In this study, LPS alone significantly stimulated NO production, when compared with the control group. Without LPS stimulation, EPCs or NEPCs from the three edible seaweeds did not trigger the overproduction of NO, while they significantly decreased the overproduction of NO stimulated by LPS in a dose-dependent manner. More specifically, the IC_{50} values of EPCs from *L. japonica*, *U. lactuca*, and *P. tenera* were 39.98, 52.43, and 82.43 μg/ml, respectively (**Figures 2A–C**). The IC_{50} values of NEPCs from *L. japonica*, *U. lactuca*, and *P. tenera* were 69.59, 60.83, and 93.54 μg/ml, respectively (**Figures 2A–C**). Overall, EPCs had stronger inhibitory effects on NO production in activated

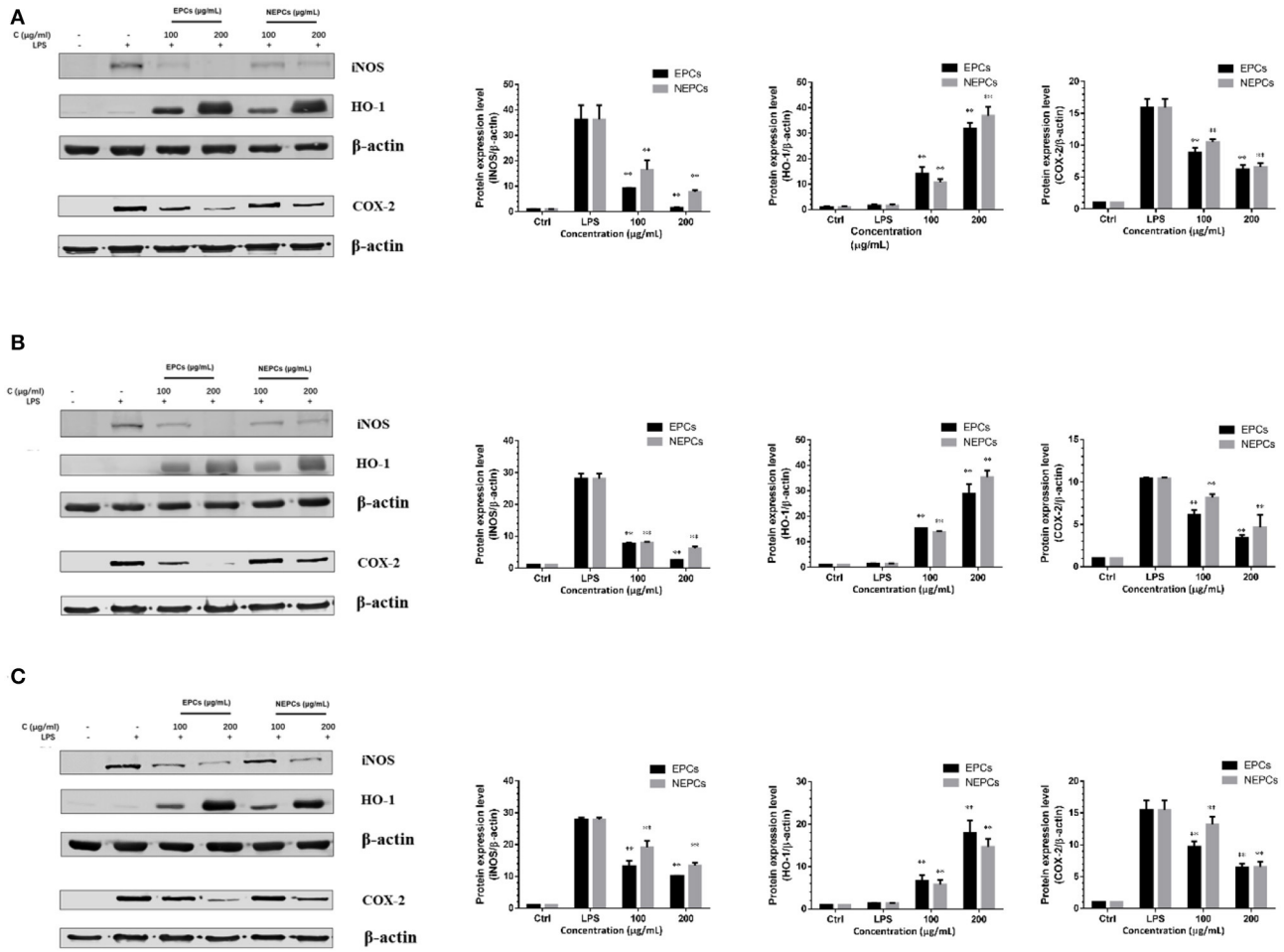

FIGURE 5 | Effects of EPCs and NEPCs from *L. japonica* **(A)**, *U. lactuca* **(B)**, *P. tenera* **(C)** on protein expression of iNOS, COX-2 and HO-1 in activated macrophages. Results were expressed as mean ± SD ($n = 3$), $^{*}p < 0.05$ and $^{**}p < 0.01$ indicate statistically differences from LPS-treated group.

macrophages than NEPCs. Also, *L. japonica* and *U. lactuca* showed a stronger suppression for the production of NO than *P. tenera*.

EPCs and NEPCs Lowered the Gene Expression of Proinflammatory Cytokines

The LPS stimulation also activates the macrophages to generate proinflammatory cytokines (39). The mRNA expression levels of IL-1, IL-6, and TNF-α were all slightly raised in response to LPS treatment, and these elevated cytokines were diminished by the treatment of EPCs or NEPCs (**Figure 3**). EPCs from *L. japonica*, *U. lactuca*, and *P. tene*ra, at 200 μg/ml, suppressed the mRNA expression levels of TNF-α by 74.86, 74.69, and 64.69%, respectively. NEPCs from *L. japonica*, *U. lactuca*, and *P. tenera*, at 200 μg/ml, reduced the mRNA expression levels of TNF-α by 68.14, 71.85, and 57.96%, respectively (**Figures 3A–C**). Moreover, similar patterns were observed in the mRNA expression levels of IL-6 and IL-1 (**Figure 3**). Our results indicated that both EPCs and NEPCs exerted anti-inflammatory effects *via* suppressing the overproduction of the aforementioned cytokines.

EPCs and NEPCs Suppressed INOS and COX-2 Expression in Activated Macrophages

Proinflammatory enzymes, especially for the COX-2 and iNOS, play a vital role in inflammatory response (40). The expressions of iNOS and COX-2 were greatly elevated in response to LPS stimulation. EPCs and NEPCs from the *three* edible seaweeds lowered their expression (**Figures 4**, **5**). Specifically, EPCs from *L. japonica*, *U. lactuca*, and *P. tenera*, at 200 μg/ml, suppressed the mRNA expression levels of iNOS by 85.89, 88.47, and 72.99%, respectively. NEPCs from *L. japonica*, *U. lactuca,* and *P. tenera*, at 200 μg/ml, inhibited the mRNA expression levels of iNOS by 83.96, 85.11, and 67.92%, respectively (**Figures 4A–C**). Furthermore, the effects of EPCs and NEPCs from the three edible seaweeds on the protein expression of iNOS were similar to the mRNA expression levels. EPCs and NEPCs from the three edible seaweeds, at 200 μg/ml, reduced the protein expression of iNOS ranging from 52.27 to 95.74% (**Figures 5A–C**). Similar patterns were acquired in the expression of COX-2 (**Figures 4**,

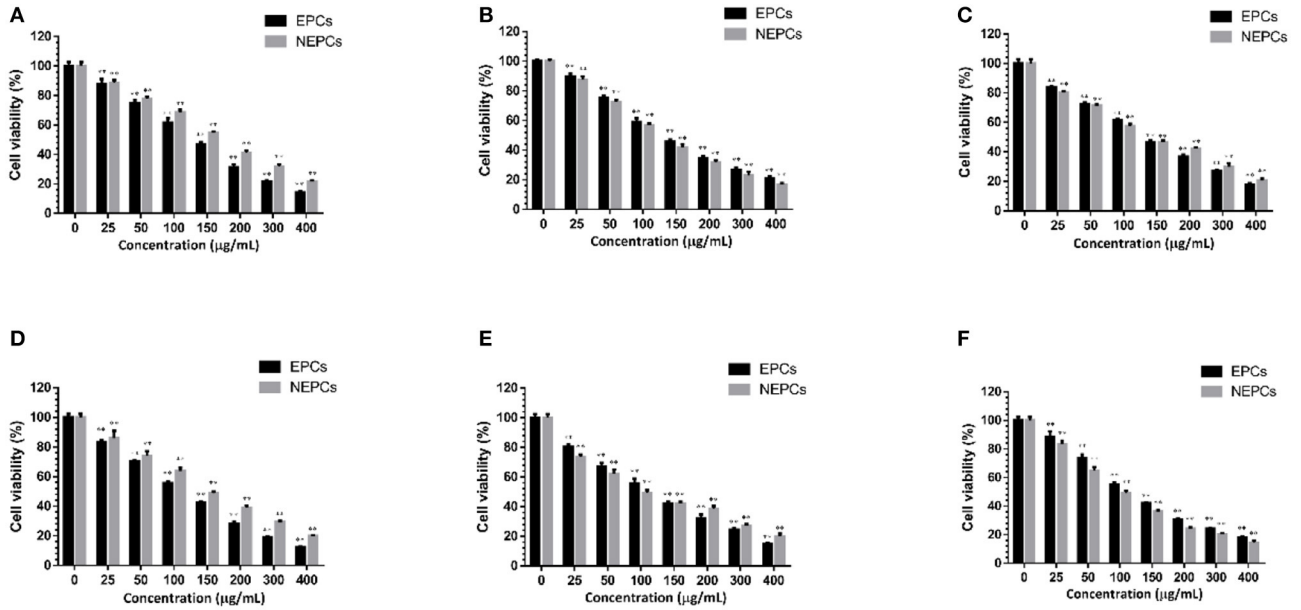

FIGURE 6 | Suppressive effects of the EPCs and NEPCs from *L. japonica* **(A)**, *P. tenera* **(B)** and *U. lactuca* **(C)** on HCT116 cells for 48 hours; Suppressive effects of the EPCs and NEPCs from *L. japonica* **(D)**, *P. tenera* **(E)** and *U. lactuca* **(F)** on HCT116 cells for 72 hours. Results were presented as mean ± SD ($n = 6$). $^{**}p < 0.01$ indicate statistically differences from untreated group.

5). These findings suggested that EPCs and NEPCs lowered the production of NO by downregulating iNOS and COX-2 signaling pathways.

EPCs and NEPCs Elevated the Expression Levels of Antioxidant Enzymes in Activated Macrophages

Elevated expressions of HO-1 and NQO-1, two antioxidant enzymes, have been reported to reduce the overproduction of inflammatory enzymes and proinflammatory cytokines (41). As shown in **Figure 4**, EPCs and NEPCs from *L. japonica*, *U. lactuca*, and *P. tenera* significantly elevated the mRNA expression level of HO-1 and NQO-1, when compared with the LPS group. Specifically, EPCs from *L. japonica*, *U. lactuca*, and *P. tenera*, at 200 μg/ml, potently elevated the mRNA expression of HO-1 by 6.59-, 5.50-, and 5.59-fold, respectively. NEPCs from *L. japonica*, *U. lactuca,* and *P. tenera* enhanced the HO-1 mRNA expression by 5.45-, 5.02-, and 4.43-fold, respectively (**Figures 4A–C**). Similar patterns were obtained in the mRNA expression of NQO-1 (**Figures 4A–C**). In addition to the mRNA expression, EPCs and NEPCs from the three edible seaweeds also greatly upregulated the HO-1 protein expression, and their results were consistent with the qRT-PCR results (**Figures 5A–C**).

EPCs and NEPCs Suppressed the Viability of Colon Cancer Cells

A large number of phytochemicals with anti-inflammatory and antioxidant capacities also display protective effects on colon cancer (42). We found that EPCs and NEPCs from the three edible seaweeds did not cause any suppressive effects on the CCD18-Co cells up to 400 μg/ml for 72 h (**Supplementary Figure S2**). Thus, these concentrations were used to evaluate the anti-colon cancer effects in HCT116 cells. Furthermore, we found that EPCs and NEPCs from three edible seaweeds greatly lowered the cell viability of HCT116 cells in a time- and dose-dependent manner. Specifically, the IC_{50} values of EPCs from *L. japonica*, *U. lactuca*, and *P. tenera* after 48 h treatment were 124.2, 129.5, and 127.2 μg/ml, respectively. The IC_{50} values of NEPCs from *L. japonica*, *U. lactuca*, and *P. tenera* after 48 h treatment were 160.4, 130.5, and 127.5 μg/ml, respectively (**Figures 6A–C**). Moreover, the IC_{50} values of EPCs from *L. japonica*, *U. lactuca*, and *P. tenera* after 72 h treatment were 105.2, 115.6, and 104.9 μg/ml, respectively. In addition, the IC_{50} values of NEPCs from *L. japonica*, *U. lactuca*, and *P. tenera* after 72 h treatment were 139.3, 95.7, and 94.9 μg/ml, respectively (**Figures 6D–F**). Our results indicated that EPCs and NEPCs potently suppressed the viability of colon cancer cells, while normal colon cells were not affected at much higher concentrations.

EPCs and NEPCs Led Cell Cycle Arrest and Apoptosis

Cell proliferation and apoptosis are two important therapeutic targets for cancer (43). In this study, we selected EPCs and NEPCs at the dose of 150 μg/ml for flow cytometry analysis. EPCs and NEPCs from *L. japonica* and *U. lactuca* noticeably elevated the cell accumulation in the G0/G1 phase. EPCs and NEPCs from *L. japonica* elevated the populations of HCT116 cells in the G0/G1 phase by 1.93- and 1.68-fold, respectively (**Figure 7A**,

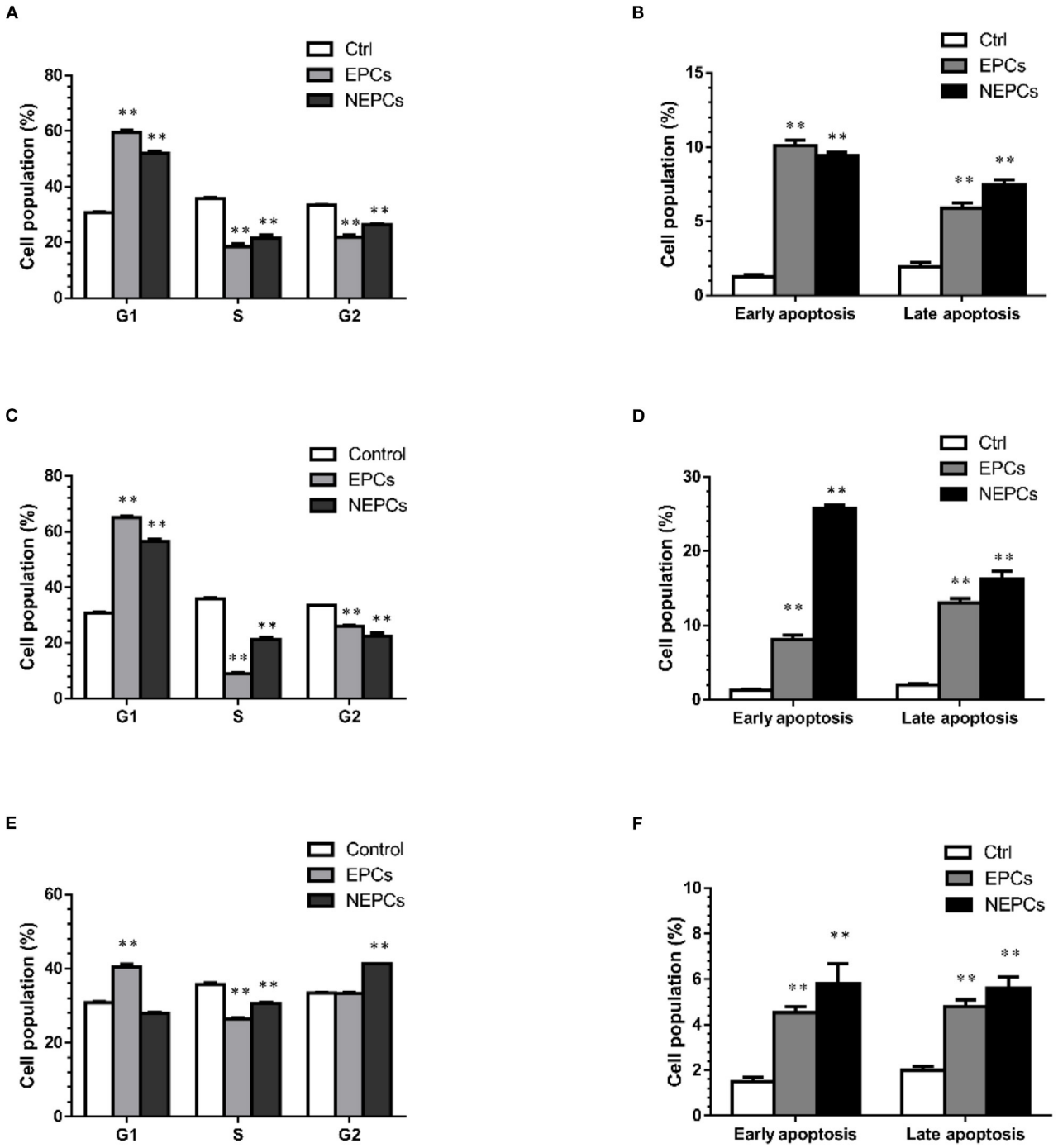

FIGURE 7 | Quantification of cell cycle distribution posed to EPCs and NEPCs from *L. japonica* **(A)**, *U. lactuca* **(C)** and *P. tenera* **(E)**. Quantification of early and late apoptosis posed to EPCs and NEPCs from *L. japonica* **(B)**, *U. lactuca* **(D)**, *P. tenera* **(F)**. Results were presented as mean ± SD ($n = 3$). $^{**}p < 0.01$ indicate statistically differences from untreated group.

Supplementary Figure S3). Similar patterns were acquired in the analysis of the effects of EPCs and NEPCs from *U. lactuca* on the cell cycle distribution (**Figure 7C**, **Supplementary Figure S3**). Moreover, EPCs from *P. tenera* enhanced the populations of HCT116 cells in the G0/G1 phase by 31.14%, and NEPCs from *P. tenera* elevated the populations of HCT116 cells in the G2/S phase by 23.50% (**Figure 7E**, **Supplementary Figure S3**). For cell apoptosis analysis, EPCs and NEPCs greatly enhanced the

apoptotic cell population. Specifically, EPCs from *L. japonica* raised cell population in the early and late apoptosis by 7.76- and 7.25-fold, respectively. NEPCs from *L. japonica*, increased cell population in the early and late apoptosis by 3.01- and 3.80-fold, respectively (**Figure 7B**, **Supplementary Figure S4**). Finally, the patterns of EPCs and NEPCs from *U. lactuca* and *P. tenera* were consistent with those of EPCs and NEPCs from *L. japonica* (**Figures 7D,F**, **Supplementary Figure S4**). These findings indicated that EPCs and NEPCs from the three edible seaweeds inhibited the growth of human colon cancer cells *via* the activation of cell cycle arrest and cellular apoptosis.

CONCLUSION

These results, for the first time, elucidated the composition of polyphenols-rich components from the three edible seaweeds, *L. japonica*, *P. tenera,* and *U. lactuca*, and we further investigated their efficacy and mechanisms against inflammation and colon cancer in cell studies. We found that EPCs and NEPCs exerted potent inhibitory effects in activated macrophages *via* suppressing proinflammatory cytokines and enzymes and activating antioxidant enzymes. At the same time, they lowered the proliferation of HCT116 cells by inducing cell cycle arrest and cell apoptosis. The novel extracts of edible seaweeds may offer a safe, inexpensive, and efficacious dietary strategy to prevent colon cancer in humans, especially in individuals with chronic inflammation. Further work will comprehensively evaluate the anti-inflammatory capacities and anticancer properties of polyphenols-rich components from edible seaweeds in animal and human studies.

DATA AVAILABILITY STATEMENT

The original contributions presented in the study are included in the article/**Supplementary Materials**, further inquiries can be directed to the corresponding authors.

AUTHOR CONTRIBUTIONS

LY: methodology, experiment performance, and writing—original draft preparation. HX: writing—reviewing and editing. SL and HX: conceptualization. SL, HX, and ZT: supervision. DL: manuscript revision. HL: sample preparation. QW and LY: data collection and analysis. All authors contributed to the article and approved the submitted verison.

FUNDING

This work was partially supported by the Shenzhen Strategic Emerging Industry Development Special Fund Project (Shenzhen Municipal Economic and Trade Information Commission, #20180130150742764 to SL), United States Department of Agriculture (MAS00450, MAS00492, NIFA grant #2019-67017-29249 and 2020-67017-30835 to HX), and Hunan Science and Technology Plan Program and Major Research Plan of Changsha (2019RS1055 and kq1801016 to ZT).

SUPPLEMENTARY MATERIAL

The Supplementary Material for this article can be found online at: https://www.frontiersin.org/articles/10.3389/fnut.2022.856273/full#supplementary-material

REFERENCES

1. Pandey KB, Rizvi SI. Plant Polyphenols as dietary antioxidants in human health and disease. *Oxid Med Cell Longev.* (2009) 2:270–8. doi: 10.4161/oxim.2.5.9498
2. Saura-Calixto F, Serrano J, Goñi I. Intake and bioaccessibility of total polyphenols in a whole diet. *Food Chem.* (2007) 101:492–501. doi: 10.1016/j.foodchem.2006.02.006
3. Domínguez-Rodríguez G, Marina ML, Plaza M. Strategies for the extraction and analysis of non-extractable polyphenols from plants. *J Chromatogr A.* (2017) 1514:1–15. doi: 10.1016/j.chroma.2017.07.066
4. Perez-Jimenez J, Diaz-Rubio ME, Saura-Calixto F. Non-extractable polyphenols, a major dietary antioxidant: occurrence, metabolic fate and health effects. *Nutr Res Rev.* (2013) 26:118–29. doi: 10.1017/S0954422413000097
5. González-Sarrías A, Espín JC, Tomás-Barberán FA. Non-extractable polyphenols produce gut microbiota metabolites that persist in circulation and show anti-inflammatory and free radical-scavenging effects. *Trends Food Sci Technol.* (2017) 69:281–8. doi: 10.1016/j.tifs.2017.07.010
6. Tow WW, Premier R, Jing H, Ajlouni S. Antioxidant and antiproliferation effects of extractable and nonextractable polyphenols isolated from apple waste using different extraction methods. *J Food Sci.* (2011) 76:T163–T72. doi: 10.1111/j.1750-3841.2011.02314.x
7. Han Y, Huang M, Li L, Cai X, Gao Z, Li F, et al. Non-extractable polyphenols from cranberries: potential anti-inflammation and anti-colon-cancer agents. *Food Funct.* (2019) 10:7714–23. doi: 10.1039/C9FO01536A
8. Cheng A, Han C, Fang X, Sun J, Chen X, Wan F. Extractable and non-extractable polyphenols from blueberries modulate LPS-induced expression of iNOS and COX-2 in RAW2647 macrophages via the NF-κB signalling pathway. *J Sci Food Agric.* (2016) 96:3393–400. doi: 10.1002/jsfa.7519
9. Huang M, Han Y, Li L, Rakariyatham K, Wu X, Gao Z, et al. Protective effects of non-extractable phenolics from strawberry against inflammation and colon cancer *in vitro*. *Food Chem.* (2022) 374:131759. doi: 10.1016/j.foodchem.2021.131759
10. Cheung RC, Ng TB, Wong JH, Chen Y, Chan WY. Marine natural products with anti-inflammatory activity. *Appl Microbiol Biotechnol.* (2016) 100:1645–66. doi: 10.1007/s00253-015-7244-3
11. Donath MY, Dalmas É, Sauter NS, Böni-Schnetzler M. Inflammation in obesity and diabetes: islet dysfunction and therapeutic opportunity. *Cell Metab.* (2013) 17:860–72. doi: 10.1016/j.cmet.2013.05.001
12. Dinarello CA. Proinflammatory cytokines. *Chest.* (2000) 118:503–8. doi: 10.1378/chest.118.2.503
13. Lechner M, Lirk P, Rieder J. Inducible nitric oxide synthase (iNOS) in tumor biology: the two sides of the same coin. *Semin Cancer Biol.* (2005) 15:277–89. doi: 10.1016/j.semcancer.2005.04.004
14. Gately S, Li WW. Multiple roles of COX-2 in tumor angiogenesis: a target for antiangiogenic therapy. *Semin Oncol.* (2004) 31(2 Suppl 7):2–11. doi: 10.1053/j.seminoncol.2004.03.040
15. Pal A, Kamthania MC, Kumar A. Bioactive compounds and properties of seaweeds—a review. *OALib Journal.* (2014) 1:1–17. doi: 10.4236/oalib.1100752

16. Kazlowska K, Hsu T, Hou CC, Yang WC, Tsai GJ. Anti-inflammatory properties of phenolic compounds and crude extract from Porphyra dentata. *J Ethnopharmacol.* (2010) 128:123–30. doi: 10.1016/j.jep.2009.12.037
17. Kim J-H, Kim SA, Edwards MS, Lee I-A. Anti-inflammatory Effects of Polyphenol Extracts from Ulva linza (Ulvophyceae, Chlorophyta). *Toxicol Environ Health Sci.* (2018) 10:212–9. doi: 10.1007/s13530-018-0366-0
18. Namvar F, Mohamed S, Fard SG, Behravan J, Mustapha NM, Alitheen NBM, et al. Polyphenol-rich seaweed (*Eucheuma cottonii*) extract suppresses breast tumour *via* hormone modulation and apoptosis induction. *Food Chem.* (2012) 130:376–82. doi: 10.1016/j.foodchem.2011.07.054
19. Ryu B, Choi I-W, Qian Z-J, Heo S-J, Kang D-H, Oh C, et al. Anti-inflammatory effect of polyphenol-rich extract from the red alga *Callophyllis japonica* in lipopolysaccharide-induced RAW 2647 macrophages. *Algae.* (2014) 29:343–53. doi: 10.4490/algae.2014.29.4.343
20. Chen L, Liu R, He X, Pei S, Li D. Effects of brown seaweed polyphenols, a class of phlorotannins, on metabolic disorders via regulation of fat function. *Food Funct.* (2021) 12:2378–88. doi: 10.1039/D0FO02886J
21. Li N, Zhang Q, Song J. Toxicological evaluation of fucoidan extracted from *Laminaria japonica* in Wistar rats. *Food Chem Toxicol.* (2005) 43:421–6. doi: 10.1016/j.fct.2004.12.001
22. Venkatraman KL, Mehta A. Health benefits and pharmacological effects of porphyra species. *Plant Foods Hum Nutr.* (2019) 74:10–7. doi: 10.1007/s11130-018-0707-9
23. Abd-Ellatef G-EF, Ahmed OM, Abdel-Reheim ES, Abdel-Hamid A-HZ. Ulva lactuca polysaccharides prevent Wistar rat breast carcinogenesis through the augmentation of apoptosis, enhancement of antioxidant defense system, and suppression of inflammation. *Breast Cancer.* (2017) 9:67–83. doi: 10.2147/BCTT.S125165
24. Dewanto V, Wu X, Adom KK, Liu RH. Thermal processing enhances the nutritional value of tomatoes by increasing total antioxidant activity. *J Agric Food Chem.* (2002) 50:3010–4. doi: 10.1021/jf0115589
25. Kim D-O, Jeong SW, Lee CY. Antioxidant capacity of phenolic phytochemicals from various cultivars of plums. *Food Chem.* (2003) 81:321–6. doi: 10.1016/S0308-8146(02)00423-5
26. Jackson FS, Barry TN, Lascano C, Palmer B. The extractable and bound condensed tannin content of leaves from tropical tree, shrub and forage legumes. *J Sci Food Agric.* (1996) 71:103–10.
27. Masuko T, Minami A, Iwasaki N, Majima T, Nishimura S-I, Lee YC. Carbohydrate analysis by a phenol–sulfuric acid method in microplate format. *Anal Biochem.* (2005) 339:69–72. doi: 10.1016/j.ab.2004.12.001
28. Bainor A, Chang L, McQuade TJ, Webb B, Gestwicki JE. Bicinchoninic acid (BCA) assay in low volume. *Anal Biochem.* (2011) 410:310–2. doi: 10.1016/j.ab.2010.11.015
29. Huang D, Ou B, Hampsch-Woodill M, Flanagan JA, Prior RL. High-throughput assay of oxygen radical absorbance capacity (ORAC) using a multichannel liquid handling system coupled with a microplate fluorescence reader in 96-well format. *J Agric Food Chem.* (2002) 50:4437–44. doi: 10.1021/jf0201529
30. Xiao F, Xu T, Lu B, Liu R. Guidelines for antioxidant assays for food components. *Food Frontiers.* (2020) 1:60–9. doi: 10.1002/fft2.10
31. Wu X, Song M, Rakariyatham K, Zheng J, Guo S, Tang Z, et al. Anti-inflammatory effects of 4'-demethylnobiletin, a major metabolite of nobiletin. *J Funct Foods.* (2015) 19:278–87. doi: 10.1016/j.jff.2015.09.035
32. Qiu P, Dong P, Guan H, Li S, Ho CT, Pan MH, et al. Inhibitory effects of 5-hydroxy polymethoxyflavones on colon cancer cells. *Mol Nutr Food Res.* (2010) 54 Suppl 2:S244–52. doi: 10.1002/mnfr.200900605
33. Wu X, Li Z, Sun Y, Li F, Gao Z, Zheng J, et al. Identification of xanthomicrol as a major metabolite of 5-demethyltangeretin in mouse gastrointestinal tract and its inhibitory effects on colon cancer cells. *Front nutr.* (2020) 7:103. doi: 10.3389/fnut.2020.00103
34. Livak KJ, Schmittgen TD. Analysis of relative gene expression data using real-time quantitative PCR and the 2(-Delta Delta C(T)) Method. *Methods.* (2001) 25:402–8. doi: 10.1006/meth.2001.1262
35. Machu L, Misurcova L, Ambrozova JV, Orsavova J, Mlcek J, Sochor J, et al. Phenolic content and antioxidant capacity in algal food products. *Molecules.* (2015) 20:1118–33. doi: 10.3390/molecules20011118
36. Pérez-Jiménez J, Saura-Calixto F. Macromolecular antioxidants or non-extractable polyphenols in fruit and vegetables: Intake in four European countries. *Food Res Int.* (2015) 74:315–23. doi: 10.1016/j.foodres.2015.05.007
37. Ambriz-Pérez DL, Leyva-López N, Gutierrez-Grijalva EP, Heredia JB. Phenolic compounds: Natural alternative in inflammation treatment. A review. *Cogent Food Agric.* (2016) 2:1131412. doi: 10.1080/23311932.2015.1131412
38. Moncada S, Palmer RM, Higgs EA. Nitric oxide: physiology, pathophysiology, and pharmacology. *Pharmacol Rev.* (1991) 43:109–42.
39. Zhang JM, An J. Cytokines, inflammation, and pain. *Int Anesthesiol Clin.* (2007) 45:27–37. doi: 10.1097/AIA.0b013e318034194e
40. Murakami A, Ohigashi H. Targeting NOX, INOS and COX-2 in inflammatory cells: chemoprevention using food phytochemicals. *Int J Cancer.* (2007) 121:2357–63. doi: 10.1002/ijc.23161
41. Rushworth SA, MacEwan DJ, O'Connell MA. Lipopolysaccharide-induced expression of NAD(P)H:quinone oxidoreductase 1 and heme oxygenase-1 protects against excessive inflammatory responses in human monocytes. *J Immunol.* (2008) 181:6730–7. doi: 10.4049/jimmunol.181.10.6730
42. Kaur V, Kumar M, Kumar A, Kaur K, Dhillon VS, Kaur S. Pharmacotherapeutic potential of phytochemicals: implications in cancer chemoprevention and future perspectives. *Biomed Pharmacother.* (2018) 97:564–86. doi: 10.1016/j.biopha.2017.10.124
43. Evan GI, Vousden KH. Proliferation, cell cycle and apoptosis in cancer. *Nature.* (2001) 411:342–8. doi: 10.1038/35077213

Conflict of Interest: The authors declare that the research was conducted in the absence of any commercial or financial relationships that could be construed as a potential conflict of interest.

Publisher's Note: All claims expressed in this article are solely those of the authors and do not necessarily represent those of their affiliated organizations, or those of the publisher, the editors and the reviewers. Any product that may be evaluated in this article, or claim that may be made by its manufacturer, is not guaranteed or endorsed by the publisher.

frontiers | Frontiers in Nutrition

ORIGINAL RESEARCH
published: 18 May 2022
doi: 10.3389/fnut.2022.903218

Physicochemical Characterization and Antioxidant and Hypolipidaemic Activities of a Polysaccharide From the Fruit of *Kadsura coccinea* (Lem.) A. C. Smith

Hairong Long[1,2†], Xianghua Xia[1,3†], Suqi Liao[1], Tao Wu[2], Lijun Wang[1], Qianping Chen[1], Shugen Wei[1], Xiaoyu Gu[1] and Zhenjun Zhu[4]**

[1] Guangxi Botanical Garden of Medicinal Plants, No. 189, Nanning, China, [2] Key Laboratory of Food Nutrition and Safety, Ministry of Education, Tianjin Key Laboratory of Food Nutrition and Safety, Tianjin University of Science and Technology, Tianjin, China, [3] Institute of High Energy Physics, Chinese Academy of Sciences, Beijing, China, [4] Department of Food Science and Engineering, College of Science and Engineering, Jinan University, Guangzhou, China

OPEN ACCESS

Edited by:
Yanhui Han,
University of Massachusetts Amherst, United States

Reviewed by:
Zhichang Qiu,
Shandong Agricultural University, China
Daoyuan Ren,
Shaanxi Normal University, China

***Correspondence:**
Xiaoyu Gu
13597342807@163.com
Zhenjun Zhu
zzj1904@jnu.edu.cn

[†] These authors have contributed equally to this work

Specialty section:
This article was submitted to Nutritional Immunology, a section of the journal Frontiers in Nutrition

Received: 24 March 2022
Accepted: 28 April 2022
Published: 18 May 2022

Citation:
Long H, Xia X, Liao S, Wu T, Wang L, Chen Q, Wei S, Gu X and Zhu Z (2022) Physicochemical Characterization and Antioxidant and Hypolipidaemic Activities of a Polysaccharide From the Fruit of Kadsura coccinea (Lem.) A. C. Smith. Front. Nutr. 9:903218. doi: 10.3389/fnut.2022.903218

Kadsura coccinea fruit, a novel fruit resource, has attracted wide interest, but the physicochemical characteristics and biological activities of its polysaccharides remain unclear. This study investigated the physicochemical properties of a polysaccharide extracted from *K. coccinea* fruit polysaccharide (KCFP) and evaluated its antioxidant and hypolipidaemic activities *in vitro* and *in vivo*. KCFP is an amorphous, thermally stable pectin heteropolysaccharide with an average molecular weight of 204.6 kDa that is mainly composed of mannose, rhamnose, glucose, galactose, xylose, arabinose, galacturonic acid (molar percentage >70%) and glucuronic acid. 2,2-Diphenyl-1-picrylhydrazyl (DPPH) and 2,2′-azino-bis(3-ethylbenzothiazoline-6-sulfonic acid) (ABTS) free radical scavenging assays and an iron reducing antioxidant power assay showed that KCFP has strong antioxidant capacity, while the bile acid binding assay showed that KCFP has hypolipidaemic potential *in vitro*. The antioxidant and hypolipidaemic activities of KCFP were further evaluated in high-fat diet-induced hyperlipidaemic mice. KCFP significantly increased the activities of superoxide dismutase, glutathione peroxidase and catalase, decreased the malondialdehyde content, significantly reduced the total cholesterol (TC), triglyceride (TG) and low-density lipoprotein cholesterol (LDL-C) levels, and increased the amount of high-density lipoprotein cholesterol (HDL-C). These findings suggest that KCFP could be used as a functional food to remedy oxidative damage and hyperlipidaemia.

Keywords: structural characterization, antioxidant activity, *Kadsura coccinea* fruit, polysaccharide, hypolipidaemic activity

INTRODUCTION

Hyperlipidaemia is caused by abnormal lipid metabolism or transport, which leads to increases in lipid levels in plasma and multiple tissues, is a major factor contributing to fatty liver disease, hyperlipidaemia and diabetes (1). Dyslipidaemia is an important factor influencing cardiovascular disease that has become a global health problem (2). In clinical practice, synthetic

compounds used to treat hyperlipidaemia, including statins and fibrates, cause many side effects (3). Therefore, research and development on natural medicines for the prevention and treatment of hyperlipidaemia and its complications are urgently needed.

Polysaccharides are important natural macromolecules with unique physicochemical properties and biological properties, such as immunoregulatory, antitumour, antioxidant, hypoglycaemic, antiglycation, and anti-fatigue activities. In recent years, plant-derived polysaccharides have received extensive attention from researchers (4).

Kadsura coccinea (Lem.) A. C. Smith is a vine that is mainly distributed in southern and southwestern China, Vietnam and Myanmar. The roots and stems of *K. coccinea* are traditional medicines that are commonly and widely used among the Zhuang and Yao populations in China. The peculiar, aggregate fruits of *K. coccinea* consist of 30 to 70 separate carpels. Once ripe, the fruits are red or dark purple and typically 6 to 10 cm in diameter. As nonmedicinal parts of the plant, *K. coccinea* fruits have not been well developed or utilized and are even discarded. Our previous studies showed that *K. coccinea* fruits contain a variety of nutrients, including important polysaccharides (5). To date, there have been no published reports on the physicochemical properties and biological activities of a specific *K. coccinea* fruit polysaccharide (KCFP).

Hence, the purpose of this study was to elucidate the physicochemical properties of water-extracted KCFP and investigate its antioxidant and hypolipidaemic activities *in vitro* and *in vivo*. This research will provide a reference for the scientific utilization of *K. coccinea* plant resources.

MATERIALS AND METHODS

Materials and Chemicals

Kadsura coccinea fruit was collected from a research farm in Guangxi, China. Monosaccharide standards and dextrans with different molecular weights were purchased from the National Institute for Food and Drug Control (Beijing, China). 2,2-Diphenyl-1-picrylhydrazyl (DPPH), 2,2′-azino-bis(3-ethylbenzothiazoline-6-sulfonic acid) diammonium salt (ABTS), cholic acid (CA), deoxycholic acid (DCA), taurocholic acid (TCA) and glycocholic acid (GCA) were purchased from Macklin (Shanghai, China). 1-Phenyl-3-methyl-5-pyrazolone (PMP), pancreatin and cholestyramine resin were purchased from Sigma–Aldrich (St. Louis, MO, United States). High-fat chow and regular chow were purchased from Beijing Keaoxieli Feedstuff Co., Ltd. (Beijing, China). Assay kits for total cholesterol (TC), triglyceride (TG), low-density lipoprotein cholesterol (LDL-C), high-density lipoprotein cholesterol (HDL-C), glutathione peroxidase (GSH-Px), malondialdehyde (MDA), total superoxide dismutase (SOD) and catalase (CAT) were obtained from the Nanjing Jiancheng Bioengineering Institute (Nanjing, Jiangsu, China). All other reagents used in the present study were of analytical grade.

Extraction and Purification of *Kadsura coccinea* Fruit Polysaccharide

The fruits were dried at 50°C with hot air, crushed into a powder, and passed through a 40-mesh sieve. One hundred grams of dried fruit powder was degreased and decolorized with 95% ethanol. The filtered residue was dissolved in distilled water (1 L) and stirred at 95 °C under reflux for 4 h. The reaction mixture was centrifuged (8000 *g*, 15 min) twice, and the combined supernatants were concentrated to 200 mL with a rotary evaporator. The solution was precipitated with a final concentration of 80% ethanol, and the precipitate was washed sequentially with absolute ethanol, acetone, and anhydrous ether and then dissolved in water to remove free protein using the Sevag method. The sample was then dialyzed (Mw cut-off 3500 Da) and lyophilized to obtain KCFP (4.2 g). The obtained KCFP was analyzed using high-performance liquid chromatography with an evaporative light scattering detector (HPLC-ELSD; Agilent 380ELSD, United States) in combination with a TSKgel-G5000 PW_{XL} gel chromatography column to confirm homogeneity.

Analysis of the Physical and Chemical Properties of *Kadsura coccinea* Fruit Polysaccharide

Analysis of the Chemical Composition

The total carbohydrate content of KCFP was measured according to the phenol−sulfuric acid method. The total protein content was measured according to the Bradford method. The uronic acid content was determined using the sulfuric acid-carbazole method, using galacturonic acid (GalA) as the standard. The sulfate content was determined with ion chromatography (DIONEX ICS-90, United States). The contents of C, H, and N were detected with a CHN628 elemental analyser (LECO, United States), and the S content was determined with a Multi EA4000 elemental analyser (Jena, Germany).

Determination of the Average Molecular Weight

The average molecular weight of KCFP was estimated using gel permeation chromatography (GPC) (Waters-Alliance, United States) with a TSK G5000 PW_{XL} column, an e2695 separation module, and a 2414 refractive index detector. The sample injection volume was 50 μL (2 mg/mL), distilled water (pH 7.0) was used as the mobile phase, the flow rate was 0.6 mL/min, and the column temperature was 60°C. The molecular weight was estimated by referring to a calibration curve prepared from a standard dextran series (Mw values of 4.32, 12.6, 73.8, 126, 289, and 496 kDa).

Analysis of the Monosaccharide Composition

The monosaccharide composition was measured using HPLC (Agilent 1260, United States) with PMP precolumn derivatization as described in a previous study (6).

Thermogravimetry and X-Ray Diffraction Analysis

The thermal properties of KCFP were determined by thermogravimetry and derivative thermogravimetry, and

thermal analysis curves were obtained by simultaneous thermal analysis with an STA449F5 instrument (NETZSCH, Germany). KCFP (5 mg) was transferred to an alumina crucible for thermogravimetry analysis under a nitrogen atmosphere at a heating rate of 10 °C/min in the range of 30–800°C.

X-ray diffraction (XRD) patterns were obtained on a D/max-2500 diffractometer (Rigaku, Japan). The diffractometer had a scanning angle of 5–90° and a scanning rate of 5°/min.

Morphological Observations

The lyophilized polysaccharide powder was affixed to the sample stage using double-sided conductive tape, and images were captured at different magnifications using a Phenom Pro scanning electron microscope (SEM, Phenom-World, Netherlands). The KCFP sample was completely dissolved in pure water at a concentration of 5 μg/mL, and 5 μL of the solution was dropped on a freshly cleaved mica surface to acquire atomic force microscopy (AFM) images. After air drying, the morphology was observed using a Dimension Edge AFM (Bruker, Germany).

Fourier Transform Infrared Spectral Analysis

Kadsura coccinea fruit polysaccharide was mixed with dry KBr (1:50) and pressed into transparent films. The films were scanned using a Tensor II fourier transform infrared (FTIR) spectrometer (Bruker, Germany) from 4000 to 400 cm^{-1}.

Nuclear Magnetic Resonance Analysis

^{1}H and ^{13}C nuclear magnetic resonance (NMR) spectra of KCFP were acquired using a 600 MHz NMR spectrometer (Varian, United States). Briefly, after drying the KCFP at 50 °C to constant weight, approximately 15 mg of sample was dissolved in 0.6 mL of 99.98% D_2O, and the ^{1}H NMR spectrum was collected using the PRESAT water signal suppression method described by the manufacturer. In addition, approximately 30 mg of KCFP was dissolved in 0.6 mL of 99.98% D_2O for ^{13}C NMR spectroscopy. Each sample was scanned 1024 times for ^{1}H NMR analysis and 70000 times for ^{13}C NMR analysis.

Rheological Properties

The rheological properties of a 5 mg/mL KCFP aqueous solution were determined at 25 ± 0.1°C with a HAAKE MARS40 rheometer (Thermo, Germany) equipped with a P35 parallel plate (35 mm in diameter, gap of 0.5 mm). For each measurement, 1 mL of sample solution was carefully loaded onto the Peltier plate of the rheometer. The flow curve was obtained at 25 °C with shear rates ranging from 0.1 to 1000 s^{-1}. A frequency sweep from 0.1 to 10 Hz was conducted at 25°C at a constant stress within the region of linear viscoelasticity.

Antioxidant and Hypolipidaemic Activities of *Kadsura coccinea* Fruit Polysaccharide *in vitro*

2,2-Diphenyl-1-Picrylhydrazyl Radical Scavenging Activity

The ability of KCFP to scavenge DPPH free radicals was analyzed as previously described (7). Briefly, 0.1 mL aliquots of sample solutions at different concentrations (0.05, 0.1, 0.25, 0.5, and 1.0 mg/mL) were transferred to a 96-well plate. Then, 0.1 mL of DPPH in ethanol (0.1 mmol/L) was added to each well of the plate, and the mixtures were stirred well. The plate was incubated at room temperature for 30 min in the dark. Trolox served as the positive control. The absorbance was measured using an Infinite 200 PRO microplate reader (Tecan, Switzerland) at 517 nm. The DPPH radical scavenging activity was calculated using the following formula:

$$\text{Scavenging rate (\%)} = \left(1-\frac{A_2-A_1}{A_0}\right) \times 100 \quad (1)$$

where, A_1 is the absorbance of the sample solution after reaction with solvent (distilled water); A_2 is the absorbance of the sample solution after reaction with DPPH; and A_0 is the absorbance of the solution containing solvent (distilled water) and DPPH.

ABTS Radical Scavenging Assay

The ABTS radical scavenging activity of KCFP was assessed using a reported procedure (8) with some modifications. ABTS (7.4 mmol/L) was mixed with an equal volume of a 2.6 mmol/L $K_2S_2O_8$ solution to obtain an $ABTS^{+}$ stock solution. The stock solution was stored in the dark for 12–16 h and then diluted with deionized water to obtain a working solution; the absorbance of the working solution at 734 nm was adjusted to 0.70. Then, 0.05 mL of various concentrations of KCFP solution (0.05, 0.1, 0.25, 0.5, and 1.0 mg/mL) were added to 0.2 mL of the $ABTS^{+}$ working solution. After reacting for 6 min at 25°C, the absorbance was measured at 734 nm. Trolox was used as the positive control. The ABTS radical scavenging activity was calculated with the following equation:

$$\text{Scavenging rate (\%)} = \left(1-\frac{A_2-A_1}{A_0}\right) \times 100 \quad (2)$$

where, A_1 is the absorbance of the sample solution after reaction with solvent (distilled water); A_2 is the absorbance of the sample solution after reaction with the $ABTS^{+}$ working solution; and A_0 is the absorbance of the solution containing solvent (distilled water) and the $ABTS^{+}$ working solution.

Ferric Reducing Antioxidant Power

The ferric reducing antioxidant power (FRAP) test was conducted based on published methods (9, 10). A standard curve was prepared using different concentrations (10–500 μmol/L) of $FeSO_4{\cdot}7H_2O$. The antioxidant capacity, based on the ability of the sample to reduce ferric ions, was calculated from the linear calibration curve and is reported as the concentration of sample having a ferric reducing ability equivalent to that of 1 μmol/L $FeSO_4{\cdot}7H_2O$.

Bile Acid Binding Capacity

The *in vitro* bile acid binding capacity of KCFP was investigated according to our previously reported method (4). Under simulated gastrointestinal digestion conditions, the ability of KCFP to bind CA, DCA, GCA and TCA was evaluated. The bile acid binding ability of KCFP is expressed in μmol of bile acid per 100 mg of dry matter (DM).

Antioxidant and Hypolipidaemic Activities of *Kadsura coccinea* Fruit Polysaccharide in High-Fat Diet-Induced Hyperlipidaemic Mice

Animal Experimental Design

The *in vivo* antioxidant and hypolipidaemic activities of KCFP were further evaluated in high-fat diet-induced hyperlipidaemic mice. All experimental procedures were performed in accordance with the "Guidelines for the Care and Use of Laboratory Animals: Eighth Edition." Eighteen male C57BL/6N mice aged 5–6 weeks were purchased from Beijing Vital River Laboratory Animal Technology Co., Ltd. After 1 week of adaptive feeding, the mice were divided into two groups: 6 mice in the normal control group (NC) were fed a basal diet, and 12 mice in the high-fat diet group were fed a high-fat diet. After 8 weeks of feeding, the mice in the high-fat diet group were randomly divided into two groups (n = 6), named the model control (MC) group and the KCFP group. Both the MC group and the KCFP group continued to be fed a high-fat diet, and the KCFP group was administered a daily dose of 300 mg KCFP/kg body weight. After 8 weeks of feeding, serum and liver samples from the experimental mice were collected for analysis.

Histopathological Examination of Liver Tissues

Liver tissues were cut into 5 μm thick sections and stained with haematoxylin and eosin (H&E). The stained samples were assessed for histopathological changes using a BX43 light microscope (Olympus, Tokyo, Japan).

Biochemical Measurements of the Serum and Liver Samples

The relevant antioxidant parameters (SOD, GSH-Px, CAT and MDA) and hypolipidaemic parameters (TC, TG, LDL-C and HDL-C) were measured using assay kits (Nanjing Jiancheng Bioengineering Institute, Nanjing, China).

Data Processing

The experimental data were processed using SPSS software and are presented as the means ± standard deviation. Data were further analyzed using one-way analysis of variance (ANOVA) and Tukey's multiple comparison tests. Differences were determined to be significant at $p < 0.05$.

RESULTS AND DISCUSSION

Analysis of the Physical and Chemical Properties

Analysis of the Chemical Composition of *Kadsura coccinea* Fruit Polysaccharide

Kadsura coccinea fruit polysaccharide was composed of 60.42 ± 1.76% carbohydrates, 2.30 ± 0.26% proteins and 0.48 ± 0.08% sulfate. The elemental N and S contents were analyzed and were found to be consistent with the protein and sulfate contents, respectively. As shown in **Figure 1A**, the average molecular weight of KCFP was approximately 204.6 kDa. The monosaccharide composition analysis showed that KCFP was a heteropolysaccharide consisting of mainly mannose, rhamnose, glucose, galactose, xylose, arabinose, GalA and glucuronic acid at a molar ratio of 1.00:3.56:1.03:2.01:7.81:10.11:3.67:72.10 (**Figure 1B**). The molar percentage of GalA exceeded 70%, which is consistent with the uronic acid content test results (79.80 ± 1.98%). The polysaccharides of *Schisandra* fruits of the same genus were previously reported to be mainly composed of GalA and xylose (11). These results suggested that KCFP is an acidic heteropolysaccharide composed of homogalacturonic acid.

Thermal and X-Ray Diffraction Analyses of *Kadsura coccinea* Fruit Polysaccharide

The thermogravimetry curves showed that KCFP underwent two major mass loss processes (**Figure 1C**). The first mass loss occurred at 60–190°C and was attributed to the loss of both free water and bound water absorbed in KCFP. The second mass loss occurred at 210–400°C, which was the mass loss caused by KCFP decomposition. When the temperature increased above 600 °C, the mass loss was gradual, and the mass of the remaining residue at 800 °C was 28.6%. Under a nitrogen atmosphere, this material is mainly carbon residue (12).

The derivative thermogravimetry curve (**Figure 1C**) showed two peaks in the range of 210–400°C. The peak with the highest intensity was observed at 232.3°C, indicating that the mass loss rate of KCFP was greatest at this temperature (4). In addition, the derivative thermogravimetry peak at 283.0°C may be due to the fact that KCFP consists of two main structural units. As the temperature increased, one of the polysaccharide units decomposed first at 231°C, while the other polysaccharide unit decomposed at 283°C (13). The thermal analysis results indicated that KCFP should not be subjected to temperatures greater than 210°C; otherwise, it will decompose.

X-Ray Diffraction is often used to determine the crystalline or amorphous properties of polymers. The pattern of KCFP had a broad diffraction peak at approximately $2\theta = 22°$ and a shoulder peak at $2\theta = 13°$ (**Figure 1D**), indicating an amorphous nature. The XRD pattern showed no sharp peaks, which indicated that KCFP does not contain crystalline impurities (14).

Observations of *Kadsura coccinea* Fruit Polysaccharide Morphology Using Scanning Electron Microscope and Atomic Force Microscopy

Scanning electron microscope micrographs of KCFP at different magnifications are shown in **Figures 2A–C**. At a magnification of 500×, KCFP generally displayed a sheet-like structure with some filament-like, rod-like and pebble-like features (**Figure 2A**). At a magnification of 2000×, the edges of the various shapes and structures were rounded (**Figure 2B**). When the magnification increased to 10000× (**Figure 2C**), dense and small convex features were clearly visible on the KCFP surface. KCFP has a rough surface and filamentous structure, which is probably related to the presence of various hydroxyl and carboxyl groups in the polysaccharide (15).

Atomic force microscopy is a powerful tool for observing the morphology of polysaccharides at the nanometre scale (16, 17). As shown in **Figures 2D,E**, KCFP was evenly distributed

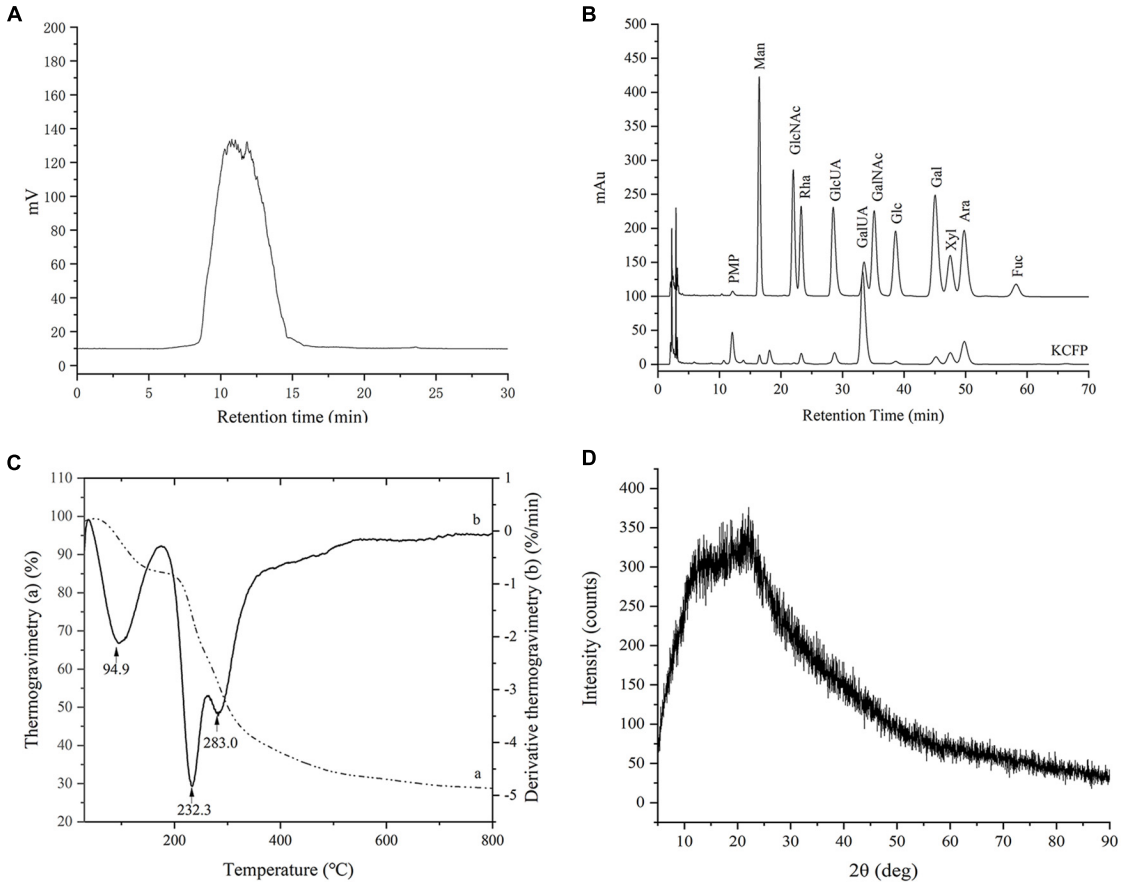

FIGURE 1 | GPC analysis **(A)**, monosaccharide composition **(B)**, thermogravimetry analysis **(C)**, and XRD analysis **(D)** of KCFP. PMP, 1-phenyl-3-methyl-5-pyrazolone; Man, mannose; GlcNAc, N-acetyl-glucosamine; Rha, rhamnose; GlcUA, glucuronic acid; GalUA, galacturonic acid; GalNAc, N-acetyl-galactosamine; Glc, glucose; Gal, galactose; Xyl, xylose; Ara, arabinose; Fuc, fucose; GPC, gel permeation chromatography; XRD, X-ray diffraction; KCFP, *Kadsura coccinea* fruit polysaccharide.

in the field of view, which allowed for easy observation of its morphology and structure. KCFP is composed of a main chain and multiple side chains, and these side chains exhibited clear irregular flexible extensions and a high degree of branching. The side chains are also cross-linked in places. These cross-links form a longer molecular chain, which increases the chain length and forms an irregular network structure that is similar to the simulated structure of pectin (18, 19). The 3D image in **Figure 2F** shows the roughness of KCFP, which is consistent with the results from the SEM observations.

Fourier Transform Infrared and Nuclear Magnetic Resonance Spectroscopy

The structural characteristics of KCFP were further analyzed using FTIR and NMR spectroscopy (**Figure 3**). The strong peaks observed in the FTIR spectrum at 3401 cm^{-1} and 2934 cm^{-1} might be attributed to the stretching vibrations of O-H and C-H, respectively. In addition, the strong peak at 1020–1150 cm^{-1} was due to the stretching vibrations of the C-O-H and C-O-C moieties contained in rings (4). These peaks are the characteristic absorptions of carbohydrates, indicating that KCFP is a carbohydrate. The sharp peaks at 1743 cm^{-1} and 1651 cm^{-1} were assigned to the C = O stretching vibrations of methylesterified carboxyl groups and free carboxyl groups, respectively, which are characteristic peaks of pectic polysaccharides (20–22). Moreover, absorption bands at 1147, 1103, 1078, 1049, 1020, and 970 cm^{-1} were also observed in the previously reported pectin spectrum (23). Together, these findings suggest that KCFP is a pectin-like polysaccharide. In addition, the peak at 917 cm^{-1} suggested the presence of a glucopyranosyl moiety with a nonsymmetric ring (24), and the peaks at 830 cm^{-1} and 890 cm^{-1} suggested the presence of both α- and β-linkages (25, 26).

In the ^{1}H NMR spectrum of KCFP, we observed signals for 8 anomeric protons at 5.80, 5.26/5.22, 5.19/5.16, 5.10, 5.04, 4.97, 4.60, and 4.47 ppm, implying the presence of 8 types of monosaccharide residues, which is consistent with our analysis of the monosaccharide composition. In addition, both α-type and β-type glycoside residues have been found in KCFP (27). The peaks at 3.82, 1.97–2.25 and 1.23/1.30 in the ^{1}H NMR spectrum indicate the presence of methoxy groups, O-acetyl substituents and the C-6 methyl protons of rhamnose, respectively (28–30). Similar to

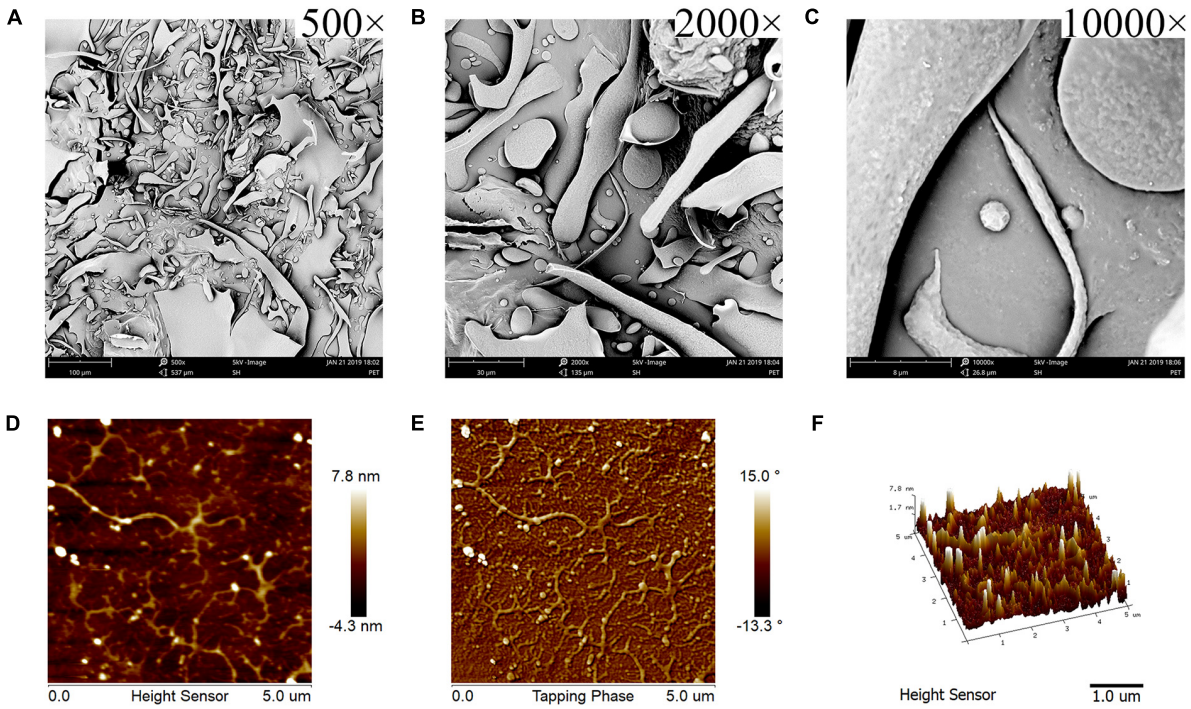

FIGURE 2 | SEM and AFM images of KCFP **(A–C)** SEM images captured at 500×, 2000×, and 10,000× magnification, respectively. **(D–F)** AFM 2D, phase and 3D images, respectively. SEM, scanning electron microscopy; AFM, atomic force microscopy; KCFP, *Kadsura coccinea* fruit polysaccharide.

the ^{1}H NMR spectrum, certain structural characteristics of KCFP were also observed in the ^{13}C NMR spectrum. For example, the signals with chemical shifts of 19.41 and 90–110 ppm were attributed to the methyl carbons of rhamnose and anomeric carbons, respectively (29, 31). The signal at 55.79 ppm was assigned to the O-methyl group, and the peak at 173.6 ppm was ascribed to the carboxy carbon (32). Moreover, some new structural characteristics were identified in KCFP from analysis of the ^{13}C NMR spectrum. For example, the signal at ∼103.31 ppm was assigned to C-1 of GalA (29). In addition, the signal at 110.42 ppm was derived from C-1 of arabinose, indicating that arabinose is the main neutral sugar in KCFP (33). Taken together, these results show that KCFP is a typical pectin polysaccharide.

Rheological Properties of *Kadsura coccinea* Fruit Polysaccharide

The relationship between the storage modulus (G′) and loss modulus (G″) of a 5 mg/mL KCFP solution over the oscillation frequency range of 0.1 to 10 Hz is shown in **Figure 4A**. In the oscillation frequency range of 0.1–7.66 Hz, G′ > G,″ indicating that the solution exhibited weak gel properties. When the oscillation frequency was greater than 7.66 Hz (G′ < G″), the solution displayed fluid properties. The plots in **Figure 4B** show the relationship between the viscosity and the shear rate of the 5 mg/mL KCFP solution. At shear rates of 0.01–1000 s^{-1}, the viscosity of the KCFP solution decreased with increasing shear rate, showing characteristics of shear thinning, which is typical of pseudoplastic fluids. When the shear rate was greater than 100 s^{-1}, the characteristics of the solution approached those of a Newtonian fluid.

Antioxidant and Hypolipidaemic Activity *in vitro*

2,2-Diphenyl-1-Picrylhydrazyl Radical Scavenging Activity

Different concentrations of KCFP were used to scavenge DPPH free radicals, and the results are shown in **Figure 5A**. In this experiment, Trolox served as the positive control. At KCFP concentrations ranging from 0.05 to 1.0 mg/mL, the KCFP concentration and DPPH free radical scavenging activity were positively correlated; that is, as the KCFP concentration increased, the scavenging rate increased. Trolox at a concentration of 0.05 mg/mL had a scavenging rate of 91.6%, while the DPPH free radical scavenging rate of KCFP at this same concentration was very low at only 26.7%.

The concentration of KCFP required to obtain 50% of the maximum effect (IC_{50} value) determined from the DPPH free radical scavenging experiments was 0.150 mg/mL, which was calculated with GraphPad Prism 8.0 software (United States). This result is much lower than those of other pectin polysaccharides, such as the pectin extracted from jackfruit peel (IC_{50} = 1.1 mg/mL) (34), the pectic polysaccharide in apple pomace (IC_{50} = 4.69 mg/mL), commercial apple pectin (IC_{50} = 6.50 mg/mL) (35) and the pectin polysaccharide extracted from Guara fruits (IC_{50} = 10.8 mg/mL) (36). These data show that the DPPH free radical scavenging ability of KCFP is superior to

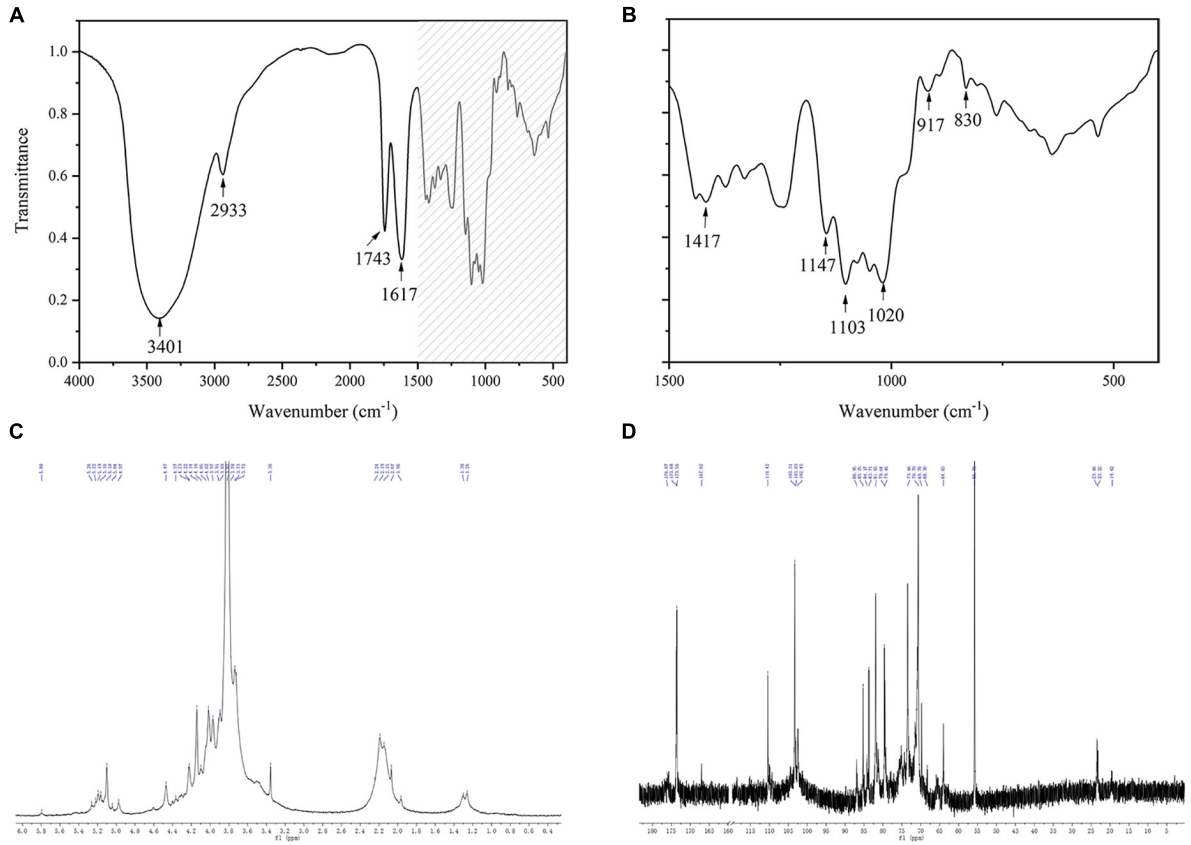

FIGURE 3 | FTIR and 1D NMR spectra of KCFP **(A,B)** Infrared spectra. **(C,D)** ^{1}H NMR and ^{13}C NMR spectra, respectively. FTIR, Fourier transform infrared; NMR, nuclear magnetic resonance; KCFP, *Kadsura coccinea* fruit polysaccharide.

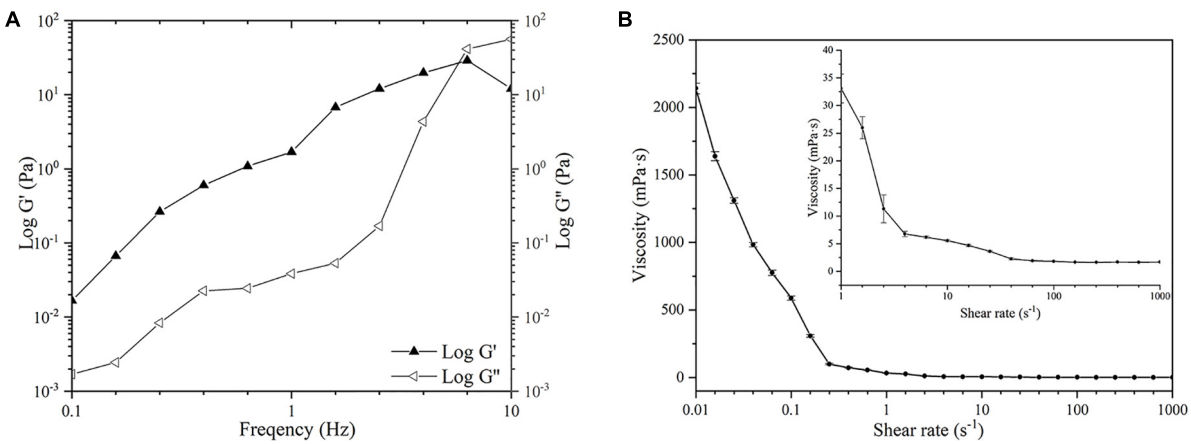

FIGURE 4 | Rheological properties of KCFP **(A)** Frequency sweep **(B)** Flow curve. KCFP, *Kadsura coccinea* fruit polysaccharide.

those of pectin polysaccharides from other sources; thus, KCFP presents potential antioxidant application value.

ABTS Free Radical Scavenging Ability

The ABTS radical scavenging abilities of KCFP and Trolox at concentrations ranging from 0.05 to 1.0 mg/mL are shown in **Figure 5B**. As shown in **Figure 5B**, the ABTS free radical scavenging abilities of both KCFP and Trolox increased with their increasing concentration. At concentrations ranging from 0.05 to 0.25 mg/mL, the ABTS free radical scavenging ability of KCFP was significantly greater than that of Trolox. When the sample concentration reached 0.5 mg/mL, the scavenging rates

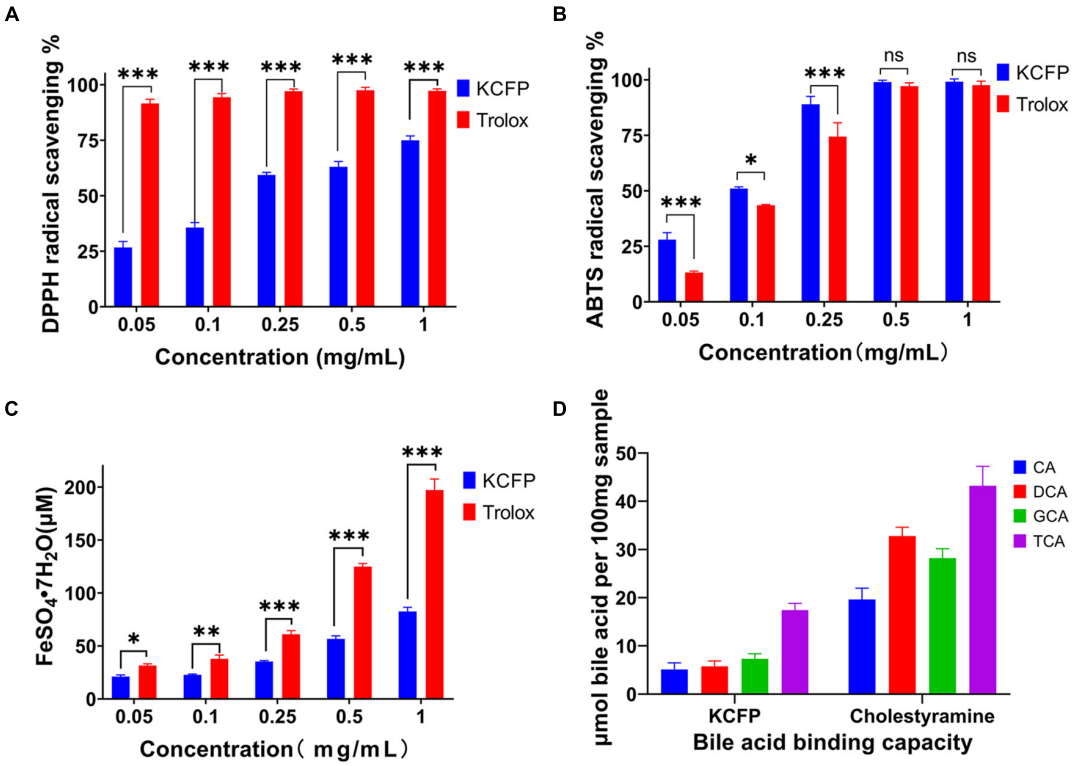

FIGURE 5 | Antioxidant activity and bile acid binding capacity of KCFP (n=3; ns: not significant, $^{*}p < 0.05$, $^{**}p < 0.01$, and $^{***}p < 0.001$). **(A)** DPPH free radical scavenging ability. **(B)** ABTS free radical scavenging ability. **(C)** Total antioxidant capacity. **(D)** Bile acid binding capacity. DPPH, 2,2-Diphenyl-1-picrylhydrazyl; ABTS, 2,2′-azino-bis(3-ethylbenzothiazoline-6-sulfonic acid) diammonium salt; CA, cholic acid; DCA, deoxycholic acid; GCA, glycocholic acid; TCA, taurocholic acid; KCFP, *Kadsura coccinea* fruit polysaccharide.

of both compounds were close to 100%. The IC_{50} value of KCFP in the ABTS free radical scavenging experimental system was 0.121 mg/mL, showing strong free radical scavenging ability.

Ferric Reducing Antioxidant Power

A FRAP assay was used to estimate the ability of the tested samples to withstand the transformation of Fe^{3+} to Fe^{2+} in the presence of tripyridyltriazine (TPTZ). At concentrations ranging from 10 to 500 μM, the concentration of $FeSO_4{\cdot}7H_2O$ showed a linear relationship with the absorbance of the sample. This linear equation was C = 420.0A–13.101, and the correlation coefficient (R^2) was 0.9989. The antioxidant capacities of the KCFP samples were calculated from this equation and are reported as the concentration of $FeSO_4{\cdot}7H_2O$ standard solution (μM $FeSO_4{\cdot}7H_2O$) (**Figure 5C**). The FRAP experiment showed that the total antioxidant capacities of different concentrations of KCFP and Trolox were different and increased with increasing concentration. Notably, when KCFP and Trolox were analyzed at the same concentration, the antioxidant capacity of KCFP was inferior to that of the positive control Trolox. This trend is similar to the trend reported by Liu et al. (10).

Bile Acid Binding Capacity

Cholic acid, DCA, GCA and TCA are the main bile acids synthesized in the human body. Many studies have shown that polysaccharides and soluble dietary fiber lower blood lipid levels, especially serum TC and LDL-C levels (37). **Figure 5D** shows the bile acid binding capacity of KCFP with cholestyramine (CT) serving as a positive control. On an equal DM basis, the bile acid binding capacity of CT was significantly higher than that of KCFP. Under the same experimental conditions, the abilities of KCFP to bind CA, DCA, GCA and TCA were 32.78, 20.59, 41.31, and 44.15% those of CT, respectively. CT, a lipid-lowering drug, interacts with bile acids to facilitate intestinal excretion, which in turn stimulates the conversion of cholesterol into bile acids in the liver, reducing TC and LDL-C levels. The mechanism by which polysaccharides lower blood lipid levels may be similar to that of CT (38).

The biological activity of polysaccharides is closely related to their structural characteristics, including monosaccharide composition, molecular weight, glycosidic linkages and polysaccharide conformation (10). Uronic acid content is generally considered an important indicator of the antioxidant capacity of polysaccharides; namely, polysaccharides containing high contents of uronic acid usually exhibit robust antioxidant activities (10, 39, 40). The mechanism by which pectin polysaccharides scavenge free radicals is that the hydrogen atom of the hydroxyl group of GalA reacts with the electron of the free radical through electron transfer. A stronger interaction between the hydrogen atoms and electrons results

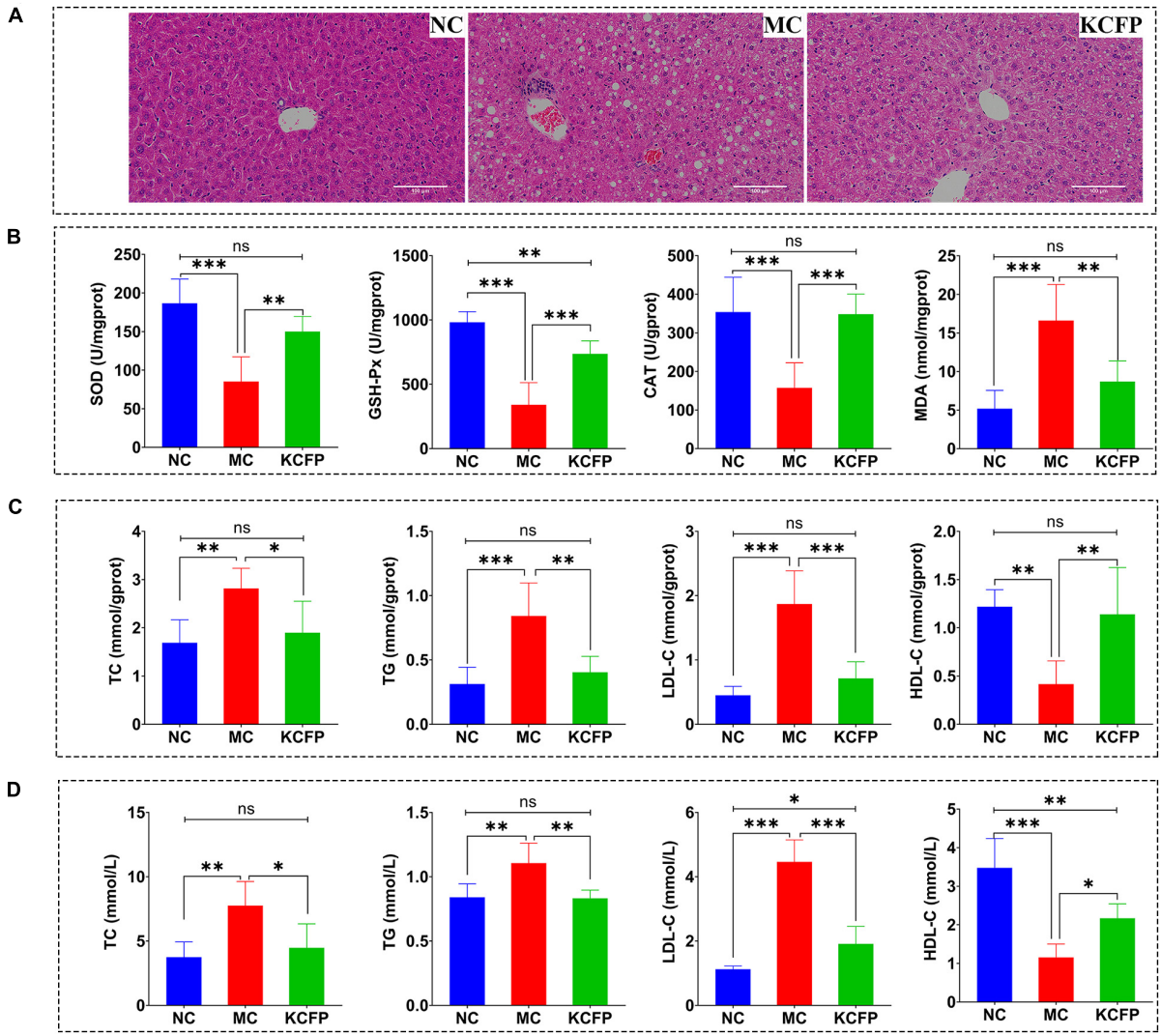

FIGURE 6 | Effects of KCFP on high-fat diet-induced hyperlipidaemia in C57BL/6N mice ($n = 6$; ns: not significant, *: $p < 0.05$, **: $p < 0.01$, and ***: $p < 0.001$). **(A)** H&E-stained sections of liver tissue (200×). **(B)** Hepatic antioxidant enzyme activity. **(C)** Liver lipid levels. **(D)** Serum lipid levels. NC, normal control; MC, model control; KCFP, *Kadsura coccinea* fruit polysaccharide; TC, total cholesterol; TG, triglyceride; LDL-C, low-density lipoprotein cholesterol; HDL-C, high-density lipoprotein cholesterol; GSH-Px, glutathione peroxidase; SOD, superoxide dismutase; CAT, catalase; MDA, malondialdehyde.

in increased antioxidant activity of the pectin polysaccharides (41). Therefore, the great antioxidant activity of KCFP has a close relationship with its high GalA content (79.8%). A bile acid binding experiment was conducted to evaluate the potential hypolipidaemic activity of KCFP. The bile acid binding capacity of polysaccharides is related to their molecular weight, characteristic groups, rheological properties, solution conformation and other factors (4, 38). The results of this study showed that KCFP has the ability to bind bile acids. Although KCFP could not bind bile acids as well as the positive control (CT resin), KCFP still shows certain potential hypolipidaemic effects.

Hyperlipidaemia is one of the main risks of cardiovascular disease (42). Research has shown that polysaccharides generally exert both antioxidant and hypolipidaemic effects (43, 44). Recent studies have suggested that hyperlipidaemia occurs due to oxidative stress and that the hypolipidaemic activity of polysaccharides is attributable to their antioxidant capacity (45). KCFP was shown here to have better antioxidant activity than most polysaccharides in addition to its good ability to bind bile acids *in vitro*. Therefore, the *in vivo* antioxidant and hypolipidaemic effects of KCFP are worthy of further study.

Antioxidant and Hypolipidaemic Activities of *Kadsura coccinea* Fruit Polysaccharide in High-Fat Diet-Induced Hyperlipidaemic Mice

A high-fat diet causes oxidative damage in the body (46), increases serum and liver levels of TC, TG, and LDL-C, and reduces HDL-C contents, which may lead to cardiovascular

disease (47, 48). Thus, the antioxidant and hypolipidaemic activities of KCFP were investigated by analyzing liver tissue sections, liver antioxidant enzymes, and liver and serum lipid levels.

Histopathological examination of the mouse liver tissue showed that KCFP intervention significantly reduced the symptoms of liver injury, fat accumulation and inflammation induced by a high-fat diet, as shown in **Figure 6A**. The effect of KCFP on the hepatic antioxidant enzyme activity in high-fat diet-fed mice is shown in **Figure 6B**. Compared with the NC group, the activities of SOD, CAT and GSH-Px were significantly decreased in the liver tissue from the mice in the MC group ($p < 0.001$). After KCFP intervention, the activities of SOD, CAT and GSH-Px were significantly increased compared with those in the MC group ($p < 0.01$). In addition, the MDA level in the MC group was significantly higher than that in the NC group ($p < 0.001$). Although KCFP intervention decreased the MDA concentration, a significant difference was not observed between the KCFP and NC groups ($p > 0.05$).

The effects of KCFP on liver and serum lipid levels are shown in **Figures 6C,D**. In this study, the levels of TC, TGs and LDL-C in the mice in the MC group were significantly higher than those in the NC group ($p < 0.01$), while the HDL-C level was significantly lower than that in the NC group ($p < 0.01$). After 8 weeks of KCFP intervention, the serum and liver levels of TC, TG and LDL-C in the mice in the KCFP group decreased significantly compared with those in the MC group ($p < 0.05$), and the level of HDL-C increased significantly ($p < 0.05$). The serum TC and TG levels in the mice in the KCFP group were restored to those in the NC group; similarly, the TC, TG, LDL-C and HDL-C levels in the livers of the KCFP group of mice also returned to those of the NC group ($p > 0.05$). These results fully indicate that KCFP possesses significant hypolipidaemic activity *in vivo*, which is consistent with previous reports on the hypolipidaemic activity of pectin polysaccharides (41, 44, 49).

Previous studies have shown that polysaccharides can correct the disorder of free radical metabolism, maintain the dynamic balance of oxidative and antioxidant systems, reduce the toxic side effects of free radicals, and decrease the damage to the body caused by lipid peroxidation (50). Therefore, the hypolipidaemic effects of KCFP may be achieved by regulating antioxidant enzyme activity.

CONCLUSION

Our results suggested that KCFP exhibited the characteristics of a pectin-like polysaccharide. In addition, KCFP showed strong antioxidant and hypolipidaemic activities both *in vitro* and *in vivo*, which may be related to its high uronic acid content and highly branched structure. Our study extends the understanding of the physicochemical characteristics and antioxidant and hypolipidaemic activities of KCFP, but its exact structure and mechanism of action should be investigated in further studies.

DATA AVAILABILITY STATEMENT

The original contributions presented in the study are included in the article/supplementary material, further inquiries can be directed to the corresponding authors.

ETHICS STATEMENT

The animal study was reviewed and approved by Committee on the Ethics of Animal Experiments of Guangxi Botanical Garden of Medicinal Plants.

AUTHOR CONTRIBUTIONS

HL and XX: conceptualization. HL: methodology, writing—original draft preparation, and visualization. QC and SW: software. XX, SL, and LW: validation. ZZ: formal analysis. HL, XX, SL, and LW: investigation. XX: resources and supervision. XG: data curation. XG and ZZ: writing—review and editing. SL: project administration. HL, TW, and ZZ: funding acquisition. All authors have read and agreed to the published version of the manuscript.

FUNDING

This research was supported by grants from Guangxi Natural Science Foundation (Grant No. 2021GXNSFAA075034), the Guangxi Key Technologies R&D Program (Grant Nos. AB17292023 and AB20159014), the Project Program of Key Laboratory of Food Nutrition and Safety, Ministry of Education and Tianjin Key Laboratory of Food Nutrition and Safety, China (Grant No. JYB201902), and the Guangxi Botanical Garden of Medicinal Plants Research and Innovation Team Building Project (Grant No. GYCH2019008).

REFERENCES

1. Dong Y, Qi Y, Liu M, Song X, Zhang C, Jiao X, et al. Antioxidant, anti-hyperlipidemia and hepatic protection of enzyme-assisted *Morehella esculenta* polysaccharide. *Int J Biol Macromol.* (2018) 120:1490–9. doi: 10.1016/j.ijbiomac.2018.09.134
2. Bian Y, Li X, Li X, Ju J, Liang H, Hu X, et al. Daming capsule, a hypolipidaemic drug, lowers blood lipids by activating the ampk signalling pathway. *Biomed Pharmacother.* (2019) 117:109176. doi: 10.1016/j.biopha.2019.109176
3. Okopień B, Bułdak A, Bołdys A. Benefits and risks of the treatment with fibrates—-a comprehensive summary. *Expert Rev Clin Pharmacol.* (2018) 11:1099–112. doi: 10.1080/17512433.2018.1537780
4. Long H, Gu X, Zhou N, Zhu Z, Wang C, Liu X, et al. Physicochemical characterization and bile acid-binding capacity of water-extract polysaccharides fractionated by stepwise ethanol precipitation from *Caulerpa lentillifera*. *Int J Biol Macromol.* (2020) 150:654–61. doi: 10.1016/j.ijbiomac.2020.02.121

5. Wang L, Liao S, Long H, Xia X, Chen Q, Liang J, et al. Analysis and evaluation of nutritional components of *Kadsura coccinea* fruit peel and pulp (in chinese). *Food Ferment Industr.* (2021) 47:124–31. doi: 10.13995/j.cnki.11-1802/ts.025882
6. Long H, Gu X, Zhu Z, Wang C, Xia X, Zhou N, et al. Effects of bottom sediment on the accumulation of nutrients in the edible green seaweed *Caulerpa lentillifera* (sea grapes). *J Appl Phycol.* (2020) 32:705–16. doi: 10.1007/s10811-019-01949-9
7. Chen Y, Xie M, Nie S, Li C, Wang Y. Purification, composition analysis and antioxidant activity of a polysaccharide from the fruiting bodies of *Ganoderma atrum*. *Food Chem.* (2008) 107:231–41. doi: 10.1016/j.foodchem.2007.08.021
8. Li L, Thakur K, Liao B, Zhang J, Wei Z. Antioxidant and antimicrobial potential of polysaccharides sequentially extracted from *Polygonatum cyrtonema* Hua. *Int J Biol Macromol.* (2018) 114:317–23. doi: 10.1016/j.ijbiomac.2018.03.121
9. Benzie IFF, Strain JJ. The ferric reducing ability of plasma (FRAP) as a measure of "antioxidant power": the FRAP assay. *Anal Biochem.* (1996) 239:70–6. doi: 10.1006/abio.1996.0292
10. Liu X, Liu H, Yan Y, Fan L, Yang J, Wang X, et al. Structural characterization and antioxidant activity of polysaccharides extracted from jujube using subcritical water. *LWT.* (2020) 117:108645. doi: 10.1016/j.lwt.2019.108645
11. Wang H, Jiang H, Wang S, Li X, Yao D, Dong J, et al. Extraction, purification and preliminary characterization of polysaccharides from *Kadsura marmorata* fruits. *Carbohydr Polym.* (2013) 92:1901–7. doi: 10.1016/j.carbpol.2012.11.060
12. Vazquez A, Foresti ML, Cerrutti P, Galvagno M. Bacterial cellulose from simple and low cost production media by *Gluconacetobacter xylinus*. *J Polym Environ.* (2013) 21:545–54. doi: 10.1007/s10924-012-0541-3
13. Yang H, Wang D, Deng J, Yang J, Shi C, Zhou F, et al. Activity and structural characteristics of peach gum exudates. *Int J Polym Sci.* (2018) 2018:1–5. doi: 10.1155/2018/4593735
14. Kouadri I, Layachi A, Makhlouf A, Satha H. Optimization of extraction process and characterization of water-soluble polysaccharide (Galactomannan) from algerian biomass; *Citrullus colocynthis* seeds. *Int J Polym Anal Chem.* (2018) 23:362–75. doi: 10.1080/1023666X.2018.1455343
15. Ji X, Cheng Y, Tian J, Zhang S, Jing Y, Shi M. Structural characterization of polysaccharide from jujube (*Ziziphus jujuba* Mill.) Fruit. *Chem Biol Technol Agric.* (2021) 8:54. doi: 10.1186/s40538-021-00255-2
16. Liu W, Wang H, Yu J, Liu Y, Lu W, Chai Y, et al. Structure, chain conformation, and immunomodulatory activity of the polysaccharide purified from *Bacillus* Calmette Guerin formulation. *Carbohyd Polym.* (2016) 150:149–58. doi: 10.1016/j.carbpol.2016.05.011
17. Wang J, Nie S. Application of atomic force microscopy in microscopic analysis of polysaccharide. *Trends Food Sci Tech.* (2019) 87:35–46. doi: 10.1016/j.tifs.2018.02.005
18. Wu HC, Bulgakov VP, Jinn TL. Pectin methylesterases: cell wall remodeling proteins are required for plant response to heat stress. *Front Plant Sci.* (2018) 9:1612. doi: 10.3389/fpls.2018.01612
19. Cohen E, Merzendorfer H. *Extracellular sugar-based biopolymers matrices*. (Vol. 12). Cham: Springer (2019). p. 487.
20. Jiang Y, Xu Y, Li F, Li D, Huang Q. Pectin extracted from persimmon peel: a physicochemical characterization and emulsifying properties evaluation. *Food Hydrocoll.* (2020) 101:105561. doi: 10.1016/j.foodhyd.2019.105561
21. Yang X, Nisar T, Hou Y, Gou X, Sun L, Guo Y. Pomegranate peel pectin can be used as an effective emulsifier. *Food Hydrocoll.* (2018) 85:30–8. doi: 10.1016/j.foodhyd.2018.06.042
22. Matharu AS, Houghton JA, Lucas-Torres C, Moreno A. Acid-free microwave-assisted hydrothermal extraction of pectin and porous cellulose from mango peel waste – towards a zero waste mango biorefinery. *Green Chem.* (2016) 18:5280–7. doi: 10.1039/C6GC01178K
23. Kačuráková M, Capek P, Sasinková V, Wellner N, Ebringerová A. FT-IR study of plant cell wall model compounds: pectic polysaccharides and hemicelluloses. *Carbohyd Polym* (2000) 43:195–203. doi: 10.1016/S0144-8617(00)00151-X
24. Wang P, Huang Q, Chen C, You L, Liu RH, Luo Z, et al. The chemical structure and biological activities of a novel polysaccharide obtained from *Fructus mori* and its zinc derivative. *J Funct Foods.* (2019) 54:64–73. doi: 10.1016/j.jff.2019.01.008
25. Wang N, Zhang Y, Wang X, Huang X, Fei Y, Yu Y, et al. Antioxidant property of water-soluble polysaccharides from poria cocos Wolf using different extraction methods. *Int J Biol Macromol.* (2016) 83:103–10. doi: 10.1016/j.ijbiomac.2015.11.032
26. Chylińska M, Szymańska-Chargot M, Zdunek A. FT-IR and FT-Raman characterization of non-cellulosic polysaccharides fractions isolated from plant cell wall. *Carbohyd Polym.* (2016) 154:48–54. doi: 10.1016/j.carbpol.2016.07.121
27. Su Y, Li L. Structural characterization and antioxidant activity of polysaccharide from four auriculariales. *Carbohyd Polym.* (2020) 229:115407. doi: 10.1016/j.carbpol.2019.115407
28. Gao X, Qu H, Shan S, Song C, Baranenko D, Li Y, et al. A novel polysaccharide isolated from *Ulva pertusa*: structure and physicochemical property. *Carbohyd Polym.* (2020) 233:115849. doi: 10.1016/j.carbpol.2020.115849
29. Shakhmatov EG, Toukach PV, Makarova EN. Structural studies of the pectic polysaccharide from fruits of *Punica granatum*. *Carbohyd Polym.* (2020) 235:115978. doi: 10.1016/j.carbpol.2020.115978
30. Guo Q, Du J, Jiang Y, Goff HD, Cui SW. Pectic polysaccharides from hawthorn: physicochemical and partial structural characterization. *Food Hydrocoll.* (2019) 90:146–53. doi: 10.1016/j.foodhyd.2018.10.011
31. Zhao J, Zhang F, Liu X, St. Ange K, Zhang A, Li Q, et al. Isolation of a lectin binding rhamnogalacturonan-I containing pectic polysaccharide from pumpkin. *Carbohyd Polym.* (2017) 163:330–6. doi: 10.1016/j.carbpol.2017.01.067
32. Cheng HN. NMR analysis of compositional heterogeneity in polysaccharides. *Pure Appl Chem.* (2017) 89:877–83. doi: 10.1515/pac-2016-1020
33. Zou S, Zhang X, Yao W, Niu Y, Gao X. Structure characterization and hypoglycemic activity of a polysaccharide isolated from the fruit of *Lycium barbarum* L. *Carbohyd Polym.* (2010) 80:1161–7. doi: 10.1016/j.carbpol.2010.01.038
34. Xu S, Liu J, Huang X, Du L, Shi F, Dong R, et al. Ultrasonic-microwave assisted extraction, characterization and biological activity of pectin from jackfruit peel. *LWT.* (2018) 90:577–82. doi: 10.1016/j.lwt.2018.01.007
35. Wang X, Lü X. Characterization of pectic polysaccharides extracted from apple pomace by hot-compressed water. *Carbohyd Polym.* (2014) 102:174–84. doi: 10.1016/j.carbpol.2013.11.012
36. Hua D, Zhang D, Huang B, Yi P, Yan C. Structural characterization and DPPH radical scavenging activity of a polysaccharide from Guara fruits. *Carbohyd Polym.* (2014) 103:143–7. doi: 10.1016/j.carbpol.2013.12.009
37. Gunness P, Gidley MJ. Mechanisms underlying the cholesterol-lowering properties of soluble dietary fibre polysaccharides. *Food Funct.* (2010) 1:149. doi: 10.1039/c0fo00080a
38. Gao J, Lin L, Sun B, Zhao M. A comparison study on polysaccharides extracted from *Laminaria japonica* using different methods: structural characterization and bile acid-binding capacity. *Food Funct.* (2017) 8:3043–52. doi: 10.1039/C7FO00218A
39. Zhu R, Zhang X, Wang Y, Zhang L, Zhao J, Chen G, et al. Characterization of polysaccharide fractions from fruit of *Actinidia arguta* and assessment of their antioxidant and antiglycated activities. *Carbohyd Polym.* (2019) 210:73–84. doi: 10.1016/j.carbpol.2019.01.037
40. Wang CC, Chang SC, Inbaraj BS, Chen BH. Isolation of carotenoids, flavonoids and polysaccharides from Lycium barbarum L. and evaluation of antioxidant activity. *Food Chem.* (2010) 120:184–92. doi: 10.1016/j.foodchem.2009.10.005
41. Zeng H, Miao S, Zhang Y, Lin S, Jian Y, Tian Y, et al. Isolation, preliminary structural characterization and hypolipidemic effect of polysaccharide fractions from *Fortunella margarita* (Lour.) Swingle. *Food Hydrocoll.* (2016) 52:126–36. doi: 10.1016/j.foodhyd.2015.05.028
42. Nelson RH. Hyperlipidemia as a risk factor for cardiovascular disease. *Prim Care Clin Off Pract.* (2013) 40:195–211. doi: 10.1016/j.pop.2012.11.003
43. Xu Y, Zhang X, Yan X, Zhang J, Wang L, Xue H, et al. Characterization, hypolipidemic and antioxidant activities of degraded polysaccharides from *Ganoderma lucidum*. *Int J Biol Macromol.* (2019) 135:706–16. doi: 10.1016/j.ijbiomac.2019.05.166
44. Rjeibi I, Feriani A, Hentati F, Hfaiedh N, Michaud P, Pierre G. Structural characterization of water-soluble polysaccharides from *Nitraria retusa* fruits and their antioxidant and hypolipidemic activities. *Int J Biol Macromol.* (2019) 129:422–32. doi: 10.1016/j.ijbiomac.2019.02.049

45. Tang Z, Gao H, Wang S, Wen S, Qin S. Hypolipidemic and antioxidant properties of a polysaccharide fraction from *Enteromorpha prolifera*. *Int J Biol Macromol.* (2013) 58:186–9. doi: 10.1016/j.ijbiomac.2013.03.048
46. Zhu Z, Lin Z, Jiang H, Jiang Y, Zhao M, Liu X. Hypolipidemic effect of Youcha in hyperlipidemia rats induced by high-fat diet. *Food Funct.* (2017) 8:1680–7. doi: 10.1039/C7FO00089H
47. Zhang Y, Wang Z, Jin G, Yang X, Zhou H. Regulating dyslipidemia effect of polysaccharides from *Pleurotus ostreatus* on fat-emulsion-induced hyperlipidemia rats. *Int J Biol Macromol.* (2017) 101:107–16. doi: 10.1016/j.ijbiomac.2017.03.084
48. Zhu Z, Zhu B, Sun Y, Ai C, Wang L, Wen C, et al. Sulfated polysaccharide from sea cucumber and its depolymerized derivative prevent obesity in association with modification of gut microbiota in high-fat diet-fed mice. *Mol Nutr Food Res.* (2018) 62:1800446. doi: 10.1002/mnfr.201800446
49. Ru Y, Chen X, Wang J, Guo L, Lin Z, Peng X, et al. Polysaccharides from *Tetrastigma hemsleyanum* Diels et Gilg: extraction optimization, structural characterizations, antioxidant and antihyperlipidemic activities in hyperlipidemic mice. *Int J Biol Macromol.* (2019) 125:1033–41. doi: 10.1016/j.ijbiomac.2018.11.236
50. Feng L, Yu C, Ying K, Hua J, Dai X. Hypolipidemic and antioxidant effects of total flavonoids of *Perilla frutescens* leaves in hyperlipidemia rats induced by high-fat diet. *Food Res Int.* (2011) 44:404–9. doi: 10.1016/j.foodres.2010.09.035

Conflict of Interest: The authors declare that the research was conducted in the absence of any commercial or financial relationships that could be construed as a potential conflict of interest.

Publisher's Note: All claims expressed in this article are solely those of the authors and do not necessarily represent those of their affiliated organizations, or those of the publisher, the editors and the reviewers. Any product that may be evaluated in this article, or claim that may be made by its manufacturer, is not guaranteed or endorsed by the publisher.

frontiers | Frontiers in Nutrition

ORIGINAL RESEARCH
published: 24 May 2022
doi: 10.3389/fnut.2022.894307

Carnosol Maintains Intestinal Barrier Function and Mucosal Immune Homeostasis in DSS-Induced Colitis

Xiang Xu[1†], Gao Zhang[1†], Kun Peng[1], Yanping Gao[1], Jinxia Wang[1], Caiping Gao[2], Chong He[1] and Fang Lu[1*]*

[1] *Clinical Immunology Translational Medicine Key Laboratory of Sichuan Province, Sichuan Provincial People's Hospital, University of Electronic Science and Technology of China, Chengdu, China,* [2] *Department of Gastroenterology, Sichuan Provincial People's Hospital, University of Electronic Science and Technology of China, Chengdu, China*

Ulcerative colitis (UC) is a chronic inflammatory disease, characterized by recurrent flares of mucosal inflammation, which is limited in the colon and rectum. Compromised epithelial barrier functions have been indicated in the initiation of UC. Carnosol (CA), a natural active ortho-diphenol diterpene compound, is one of the active ingredients in plants such as rosemary and sage. The anti-inflammatory and anti-oxidative effects of CA have been reported in several animal models, but its effect on mucosal inflammation remains elusive. We established a mouse experimental colitis model characterized by epithelial barrier destruction using dextran sulfate sodium (DSS). CA was intraperitoneally administrated. Flow cytometry was performed to determine phenotypes of intraepithelial lymphocytes and lamina propria cells. qRT-PCR was used for gene expression. ER stress in the colon was determined by immunofluorescence staining and qRT-PCR. Thapsigargin was used to induce ER stress in HCT-116 cells *in vitro*. We found CA significantly alleviated DSS-induced colitis in mice marked by relieved clinical symptoms and colonic pathological damage. Inflammatory cell infiltration and cytokine expression in the colon were suppressed by CA during colitis. Furthermore, CA restored epithelial barrier functions and intestinal intraepithelial lymphocyte (IEL) homeostasis in mice with DSS insults. Mechanistically, we induced endoplasmic reticulum (ER) stress in HCT-116 cells (an intestinal epithelial cell line) with thapsigargin, and CA reversed this effect. In addition, we collected inflamed mucosal biopsies from 23 patients with UC, and cultured overnight with or without CA, showing CA significantly reduced expression of ER stress signaling molecule and pro-inflammatory agents. Our data demonstrate that CA acts as an effective drug for experimental colitis and maintains proper epithelial barrier functions via suppressing epithelial ER stress, providing new evidence that CA might be a promising therapeutic candidate for UC.

Keywords: ulcerative colitis, experimental colitis, carnosol, intestinal epithelial cells, endoplasmic reticulum stress

OPEN ACCESS

Edited by:
Fang Li,
Columbia University Irving Medical Center, United States

Reviewed by:
Danyvid Olivares-Villagómez, Vanderbilt University Medical Center, United States
Hu Zhang, Sichuan University, China

****Correspondence:***
Fang Lu
lufangfang@126.com
Chong He
herrickhoo@163.com

† These authors have contributed equally to this work

Specialty section:
This article was submitted to Nutritional Immunology, a section of the journal Frontiers in Nutrition

Received: *11 March 2022*
Accepted: *26 April 2022*
Published: *24 May 2022*

Citation:
Xu X, Zhang G, Peng K, Gao Y, Wang J, Gao C, He C and Lu F (2022) Carnosol Maintains Intestinal Barrier Function and Mucosal Immune Homeostasis in DSS-Induced Colitis. Front. Nutr. 9:894307. doi: 10.3389/fnut.2022.894307

INTRODUCTION

Inflammatory bowel disease (IBD) has been recognized as a chronic inflammatory disease of the digestive tract. Over the past decades, studies show that the incidence and prevalence of UC have increased worldwide, leading to a substantial healthcare burden (1, 2). Ulcerative colitis (UC) is one of two clinical types of IBD and characterized by a typical natural course with recurrent flares of

mucosal inflammation, which is limited in the colon and rectum. Although multiple factors have been implicated in the pathogenesis of the disease, such as immune responses, mucosal barrier, antimicrobial defense, and gut microbiota (3), the exact molecular mechanisms underlying the induction and development of UC remain largely unknown.

Carnosol (CA), a natural active ortho-diphenol diterpene compound, is one of the active ingredients in plants such as rosemary and sage (4). It is reported that CA has many biological activities such as anti-tumor, anti-inflammation and anti-oxidation (4, 5). For example, CA can inhibit tumor cell proliferation in diseases such as breast cancer (6), colon cancer (7), and prostate cancer (8). In addition, CA has been identified as a potent antioxidant and implicated in the treatment of various disease. For instance, CA inhibits AKT/mTOR, MAPK, NF-κB and other signaling pathways, and significantly down-regulated the expression of oxidative stress effector molecules such as COX-1/2, NO and iNOS (5). In diabetic microangiopathy, CA alleviates vascular endothelial cell damage by reducing the production of reactive oxygen species and maintaining tight junctions between endothelial cells (9). Lee et al. reported that CA effectively inhibited endotoxin-induced nitric oxide production and down-regulated the expression levels of pro-inflammatory cytokines in the peripheral blood of mice with odorous dermatitis, including TNF-α and IL-1β (10) As for their effect on regulating autoimmune disease, a recent study on experimental autoimmune encephalomyelitis (EAE), a mouse model of autoimmune disease of the central nervous system, demonstrated the anti-inflammatory effect of CA. Mice treated with CA were less susceptible to EAE induction, characterized by significantly lower inflammatory lesions and decreased inflammatory cell infiltration (11). However, how CA regulates intestinal inflammation and whether it plays a role in maintaining epithelial barrier functions remain unclear.

In the current study, we found that CA exerted a potent anti-inflammatory function in dextran sulfate sodium (DSS)-induced mouse colitis. Mice administrated with CA showed remarkably alleviated colonic inflammation after DSS insults, marked with less disrupted IEC barrier function and reduced inflammatory cell infiltration. Additionally, we found that CA down-regulated epithelial endoplasmic reticulum (ER) stress in colitis. Our data thereby demonstrate a potential role of CA in the treatment of IBD and the potential mechanism whereby CA maintains intestinal homeostasis.

MATERIALS AND METHODS

Patients and Samples

This study was conducted in accordance with the Declaration of Helsinki and approved by the Institutional Review Board for Clinical Research of Sichuan Provincial People's Hospital (No.201685). Participants enrolled in the current study were well-informed and signed an informed consent before participation. Patients with UC (n = 23) were all recruited from the Department of Gastroenterology, Sichuan Provincial People's Hospital (Chengdu, China). Mucosa biopsy tissues were collected during endoscopic examinations, immediately kept in RPMI-1640 medium supplemented with 10% fetal bovine serum (FBS) (FBS-RPMI 1640) and then sent to our laboratory for tissue culture. To examine the *ex vivo* effect of CA on human mucosal inflammation, we performed tissue culture as reported previously (12). Briefly, mucosa tissues (2–3 pieces from each patient) were incubated overnight in FBS-RPMI 1640 with CA (10 μM) at 37°C and 5% CO_2. As controls, mucosa tissues from the same patients were incubated overnight in FBS-RPMI 1640 in the absence of CA. After overnight incubation, tissues were collected for mRNA analysis.

Induction of Colitis and Treatment

All procedures were approved by the Animal Care and Use Committee at Sichuan Provincial People's Hospital and performed in accordance with National Institutes of Health guidelines for animal care and use. Male C57BL/6 mice (purchased from the Shanghai Model Organisms, Shanghai, China) were used at their age of 10–12 weeks. All mice were raised in our facility in a specific pathogens-free environment. DSS-induced colitis was established as reported previously (13). Briefly, mice were fed *ad lib* with 2.5% (w/v) DSS solution (36,000–50,000 Da, MP Biomedicals, LLC; Solon, OH, USA) for 7 days, followed by a 3-day recover period with drinking water. To evaluate the severity of colitis, the weight, disease activity index (DAI), stool consistency, and the presence of blood in stools were daily monitored during the modeling period as reported previously (14). The DAI was calculated as follows: normal stools = 0, soft stools = 1, soft stools and slight bleeding = 2, loose stools and slight bleeding = 3, watery diarrhea or loose stools and gross bleeding = 4. Mice with *ad lib* drinking water served as naïve controls (NC). For CA treatment, DSS-exposed mice were intraperitoneally administrated with CA (50 mg/kg/day, dissolved in DMSO) or DMSO (the same volume as CA solution) from day 0 to day 10. On day 10, all mice were sacrificed by cervical dislocation, and colon samples were collected for further analysis.

Intestinal Intraepithelial Lymphocyte (IEL) and Lamina Propria Leukocyte (LPL) Isolation

After sacrificing the mice, the whole gastrointestinal tract was immediately removed and mesenteric fat were carefully dissected. The colon was opened longitudinally and rinsed by phosphate buffered saline (PBS) to remove luminal content, which were then cut into 5–10 mm pieces. The pieces were incubated in 30 ml EDTA solution (5 mM EDTA, 10% FBS in Ca^{2+}/Mg^{2+} free PBS) with continuous brisk stirring for 30 min at 37°C. The supernatants were filtered rapidly by a 70 μm cell strainer to remove cellular debris, which were centrifuged at 1,500 rpm at 4°C for 8 min to collect intestinal epithelial cells (IEC) and IEL. The residual tissues were collected for LPL isolation as reported previously (12). To purify IEL from IEC, cell pellets were resuspended in 4 ml of 40% percoll solution and layered onto 2 ml of 80% percoll solution, followed by gradient separation (centrifuge at 2,000 rpm at room temperature for 20 min). IEL

were collected at the 40/80% interface, which were washed three times in FBS-RPMI 1640 for subsequent analysis. To obtain LPL, the residual tissues from the EDTA step were minced into smaller fragments (∼0.5 mm) and incubated in 10 ml digestion solution, which contained type IV collagenase (1 mg/ml, Sigma Aldrich, Burlington, MA, USA) and FBS-RPMI 1640, in a shaking incubator at 37°C for 30 min. After incubation, the supernatants were passed through a 70 μM cell filter. Percoll gradient (40%/80%) separation of LPL was performed as mentioned above.

Intestinal Permeability Assay

Intestinal barrier function was measured as previously described (15). Briefly, mice were deprived of food and water for 6–8 h, and then gavaged with FD-4 (FITC conjugated Dextran, FITC-Dextran, Sigma-Aldrich) at the dose of 0.5 mg/kg body weight. After 4 h, blood samples were collected by cardiac puncture and the fluorescence intensity in sera was measured (excitation, 485 nm; emission, 530 nm). The FD-4 concentration is determined by the standard curve produced by the dilution of FD-4 series. Quantitative colorimetric Limulus amebocyte Lysate (LAL) QCL-1000 assay kit (LONZA) was used to detect serum LPS concentrations according to the manufacturer's protocol.

Flow Cytometry

Flow cytometry was performed as described previously (12, 13, 16). Briefly, 10^6 cells were counted and collected in a FACS tube (5 ml) for each flow cytometric test. For surface staining, cells were incubated in dark with 20 μL Staining Buffer (BD Bioscience, San Diego, CA, USA) containing a viability dye (LIVE/DEAD™ Fixable Near-IR Dead Cell Stain Kit, Invitrogen, Thermo Fisher Scientific, USA) and indicated fluorochrome-conjugated antibodies for 30 min at 4°C. For intracellular cytokine staining, cells were pre-stimulated with a Cell Activation Cocktail (with Brefeldin A) (BioLegend, San Diego, CA, USA) for 5 h. After harvesting, cells were used for surface staining as mentioned above. Subsequently, the cells were fixed and permeabilized using a Cyto-Fast™ Fix/Perm Buffer Set (BioLegend), and fluorochrome-conjugated anti-mouse cytokine antibodies were added to stain the intracellular cytokines. A BD FACSCanto II was used to acquire the flow cytometric data, which were then analyzed with FlowJo version 10 for Windows (Tree Star, Ashland, OR, USA).

Immunofluorescence

As reported previously (17), immunofluorescence assay was performed on 6 μm-thick frozen sections of colon tissue. Slides were baked for 30 min at 37°C. Next, the colonic sections were washed 3 times for 5 min by PBS. Cryosections (6 μm) were blocked in 5% BSA, 0.5% Triton × 100 in PBS for 2 h at room temperature. The sections were then incubated overnight at 4°C with indicated primary antibodies. When the incubation was completed, the slides were washed three times for 6 min using PBS. Secondary antibodies were added and incubated with colonic sections at room temperature for 2 h. The slides were sealed with neutral resin, and then photographed for analysis.

Hematoxylin and Eosin (H&E) and Periodic Acid-Schiff (PAS) Staining

Dissected colon tissues were fixed with 4% paraformaldehyde (PFA) for 48 h, and then dehydrated using an automatic tissue processor and embedded in paraffin blocks. Paraffin blocks were cut into sections (4 μm) with a microtome (Leica), which were placed on slides for staining. After dewaxing, the sections were stained according to the instructions of hematoxylin and eosin (H-E) staining kit (Servicebio, Wuhan, China). The colonic goblet cells were labeled by alcian blue pas (AB-PAS) staining. After dewaxing and hydration, the slides were incubated in AB for 20 min, and then were washed with water, followed by incubation in 1% periodic acid for 10 min. After the appellate step, the slides were incubated in Schiff's reagent for 10 min. The slides were finally re-stained with hematoxylin for 30 s, washed and dehydrated, and then fixed with Pertex. The stained sections were evaluated and observed under optical microscope (Leica).

Quantitative Real-Time PCR (qRT-PCR)

As discribed previously (12, 18), total RNA was extracted from indicated samples using TRIzol reagent (TransGen Biotech, China) according to the manufacturer's instructions. The Reverse Transcription Reaction System (TransGen Biotech) was used to Reverse transcribe was performed with 1μg of total RNA. For qRT-PCR analysis, the SYBR Green Kit (TaKaRa, Dalian, China) was applied to amplified cDNA according to the manufacturer's protocol. qRT-PCR detection was performed on a CFX96 Real-time RT-PCR system (Bio-Rad). Relative gene expression was normalized to endogenous GAPDH.

Statistical Analysis

Statistical analyses were carried out with GraphPad Prism version 8.4 for Windows (GraphPad Software, San Diego, CA, USA). Unpaired Student's *t*-test (two-tailed) was applied for comparison between two groups were analyzed, and one-way analysis of variance (ANOVA) followed by Tukey's multiple comparisons test was applied to analyze differences among three or more groups. Statistical significance was set at $^*P < 0.05$.

RESULTS

CA Alleviates DSS-Induced Colitis

To examine whether administration of CA could alleviate intestinal mucosal inflammation, colitis was induced in mice by oral treatment of DSS, and CA was injected intraperitoneally from on day 0 to day 10. The clinical signs of colitis were monitored daily, including body weight, stool consistency and rectal bleeding. CA significantly alleviated the weight loss (**Figure 1A**) induced by DSS administration and reduced the disease activity index (**Figure 1B**), diarrhea (**Figure 1C**) and fecal blood scores (**Figure 1D**) during the progression of colitis, suggesting a protective role of CA in experimental colitis. On day 10, mice were sacrificed and CA attenuated the colonic shortening (**Figure 1E**), splenomegaly (**Figure 1F**), and mesenteric lymphadenopathy (**Figure 1G**) induced by DSS, compared with DSS-exposed mice without CA. To further explore the role of CA in mucosal inflammation and damage,

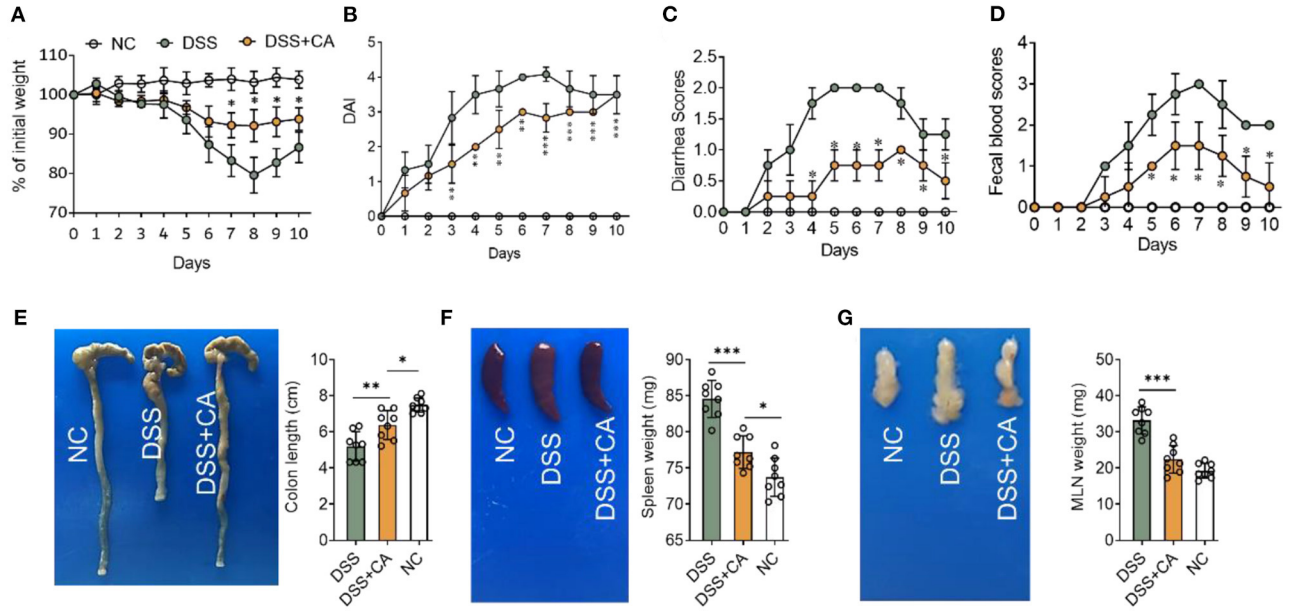

FIGURE 1 | Carnosol (CA) alleviates the clinical signs in mice with DSS-induced colitis. Experimental colitis was induced by DSS (exposure to DSS for 7 days, followed by 3 days of recovery). Mice were fed with DSS (2.5%, w/v) in their drinking water with or without daily intraperitoneally with CA, while naïve control (NC) mice received regular drinking water. **(A)** Body weight changes following DSS induction of colitis. Data were recorded as a percentage of the initial body weight. **(B)** The DAI scores were recorded every day. The DAI scores were calculated according to weight loss, diarrhea and rectal bleeding. **(C)** Diarrhea was scored as follows: normal stool = 0, soft = 1, and watery = 2. **(D)** Rectal bleeding scores were determined as follows: no bleeding in stool = 0, blood traces in stool visible = 1, gross rectal bleeding = 3. Data are expressed as mean ± SD. **(A–D)** DSS group: $n = 8$, DSS+CA group: $n = 8$, NC group: $n = 8$. **(E)** Representative colon photos (left) and quantification of colon length (cm) of 3 groups (right). Colon length comparisons were shown in histogram. Representative gross morphology of spleens (**F**, left) and lymph nodes (**G**, left). Quantitative analysis of the weight (mg) of spleens (**F**, right) and lymph nodes (**G**, right). One-way analysis of variance (ANOVA) followed by Tukey's multiple comparisons test, $^{*}p < 0.05$, $^{**}p < 0.01$, and $^{***}p < 0.001$.

H-E staining and evaluation were performed on colonic sections in different groups. Immune infiltrate, flattening of the glands, disruption to the epithelial lining, destruction of mucosal epithelium, and goblet cell loss (**Figure 2A**) were observed in colon tissues from DSS mice. CA treatment significantly relived mucosal damage in DSS mice. No significant mucosal damage was observed in NC mice. As shown in **Figures 2B,C**, DSS mice exhibited a markedly higher pathology score (19), characterized by increased epithelial disruption, follicle aggregation, enhanced erosion, increased crypt loss and increased infiltration of immune cells compared to CA-treated DSS mice. In addition, CA treatment could ameliorate symptoms of on-going DSS-induced colitis (**Supplementary Figure 1**).

CA Modulates Mucosal Immune Cell Infiltration and Inflammatory Responses

Since DSS-induced colitis was characterized by the of immune cell infiltration (especially innate immune cells) and proinflammatory cytokine accumulation (20), we next sought to investigate whether CA could suppress DSS-induced mucosal inflammatory responses in mice. To this end, we first looked at the number of innate cells in the lamina propria using our previously established flow cytometric gating strategy (**Figure 3A**) (21). Compared with CA-treated DSS mice, flow cytometric staining for CD45 and CD11b showed a significant increase in $CD45^{+}$ $CD11b^{+}$ cells (total myeloid cells) in the lamina propria of DSS mice (**Figure 3B**). We employed CD11c and Ly6G to identify dendritic cells (DC) and neutrophils from total myeloid cells. CA significantly decreased the number of total DC (**Figure 3C**) and their subsets (**Figures 3D,E**), which has been reported to be associated with intestinal inflammation (22). Neutrophil infiltration is a hallmark of human UC and mouse DSS-induced colitis (23). We found $Ly6G^{+}$ neutrophil accumulation was evidently lower in CA-treated DSS mice than DSS counterparts (**Figure 3F**). In addition, we checked the monocyte/macrophage population ($CD11b^{+}$ $CD11c^{-}$ $Ly6G^{-}$), and found that CA significantly alleviated monocyte/macrophage infiltration in the lamina propria of DSS mice (**Figure 3G**). Moreover, we analyzed the phenotype of monocytes/macrophages by using additional markers (Ly6C and MHC II) (24, 25) and found that the number of pro-inflammatory monocytes/macrophages ($Ly6C^{+}$ $MHCII^{-}$) was significantly decreased (**Figure 3H**) but the anti-inflammatory subset ($Ly6C^{-}$) was up-regulated (**Figure 3I**) in CA DSS mice than DSS mice. Given overexpression of pro-inflammatory cytokines was a hallmark of experimental colitis, we then analyzed the effect of CA on colonic mucosal cytokine expression in colitis. As illustrated in **Figures 3J–M**, colonic TNF-α, IL-1β, IL-6, and IFN-γ expression was significantly increased by DSS, which was suppressed by CA treatment. Collectively, CA could inhibit mucosal

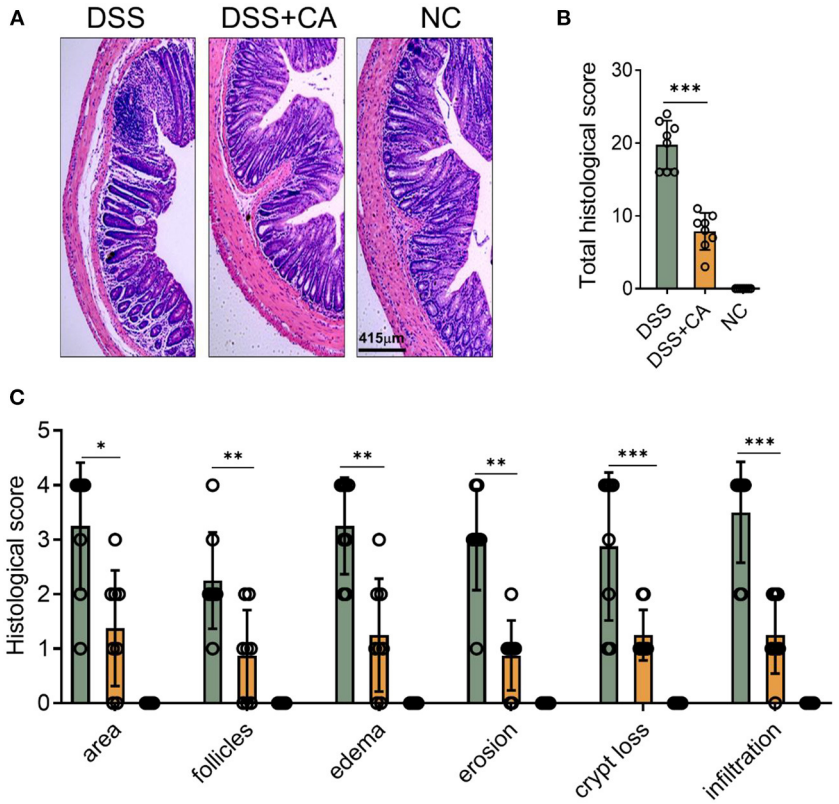

FIGURE 2 | CA alleviates pathological alterations in DSS-induced colitis. Colitis was induced as described in **Figure 1** and colon samples were collected on day 10. **(A)** Histological analysis of colonic sections. Representative images of H-E-stained colonic sections of each group. **(B)** Total histological scores were the sum of all sub-scores shown in **(C)**. **(C)** Colonic sections were scored on a scale of 0–4 based on the percentage of colon involvement by inflammation, percentage of crypt loss, presence of lymphoid follicles, edema, erosions, and density of infiltrating inflammatory cells. Data are presented as mean ± SD. Representative data of three independent experiments are shown. One-way analysis of variance (ANOVA) followed by Tukey's multiple comparisons test, $^{*}p < 0.05$, $^{**}p < 0.01$, and $^{***}p < 0.001$.

immune cell infiltration and inflammatory responses during DSS-induced colitis.

CA Restores Epithelial Barrier Functions During Colitis

We next explored whether CA affect intestinal barrier functions during colitis. Firstly, we found that DSS insults led to a breakdown of epithelial barrier, identified by an increase in serum levels of FD-4 (**Figure 4A**) and LPS (**Figure 4B**). We performed immunofluorescent staining for E-cadherin, which is an essential component of epithelial tight junctions. We found severe loss of E-cadherin in DSS mice, and CA potently restored E-cadherin expression during colitis (**Figure 4C**), suggesting that CA could protect epithelial tight junctions from breakdown induced by DSS. This observation was also evidenced by mRNA analysis of ZO-1, claudin-1, and occludin expression (**Figure 4D**). In addition, since goblet cells contribute majorly to the epithelial barrier homeostasis and goblet impairment is a critical hallmark of UC (26), we explored the role of CA on goblet cells during colitis. As shown in **Figure 4E**, CA remarkably reversed DSS-induced decreases of mucus-producing goblet cells in the colon, which further confirmed by qRT-PCR analysis (**Figure 4F**). Taken together, CA is found to be protective for epithelial barrier function during colitis.

CA Restores IEL Homeostasis During DSS-Induced Colitis

Intestinal epithelial lymphocytes (IEL) are essential components of the epithelial barrier, which can rapidly respond to pathogen antigens and play a major role to maintain intestinal barrier functions. Dysregulation of IEL subpopulations contributes to mucosal inflammation. To determine the role of CA on IEL during DSS colitis, we isolated IEL from the colon and performed flow cytometry to evaluate IEL subpopulations (**Figure 5A** shows the gating strategy) (27). CA-treated DSS mice showed significantly higher number of TCR$\gamma\delta^{+}$ (**Figure 5B**), TCR$\gamma\delta^{+}$ CD8$\alpha\alpha^{+}$ (**Figure 5E**), TCRβ^{+} CD8$\alpha\beta^{+}$ (**Figure 5F**), and TCR$\gamma\delta^{-}$ TCRβ^{-} CD8$\alpha\alpha^{+}$ (**Figure 5G**) IEL in comparison with their DSS counterparts. Although CA-treated DSS mice showed higher number of total TCRβ^{+} IEL and lower number of TCRβ^{+} CD4^{+} IEL than DSS mice, the differences didn't reach a statistical significance (**Figures 5C,D**). These data suggest that CA can restore IEL homeostasis in mice with DSS-induced colitis.

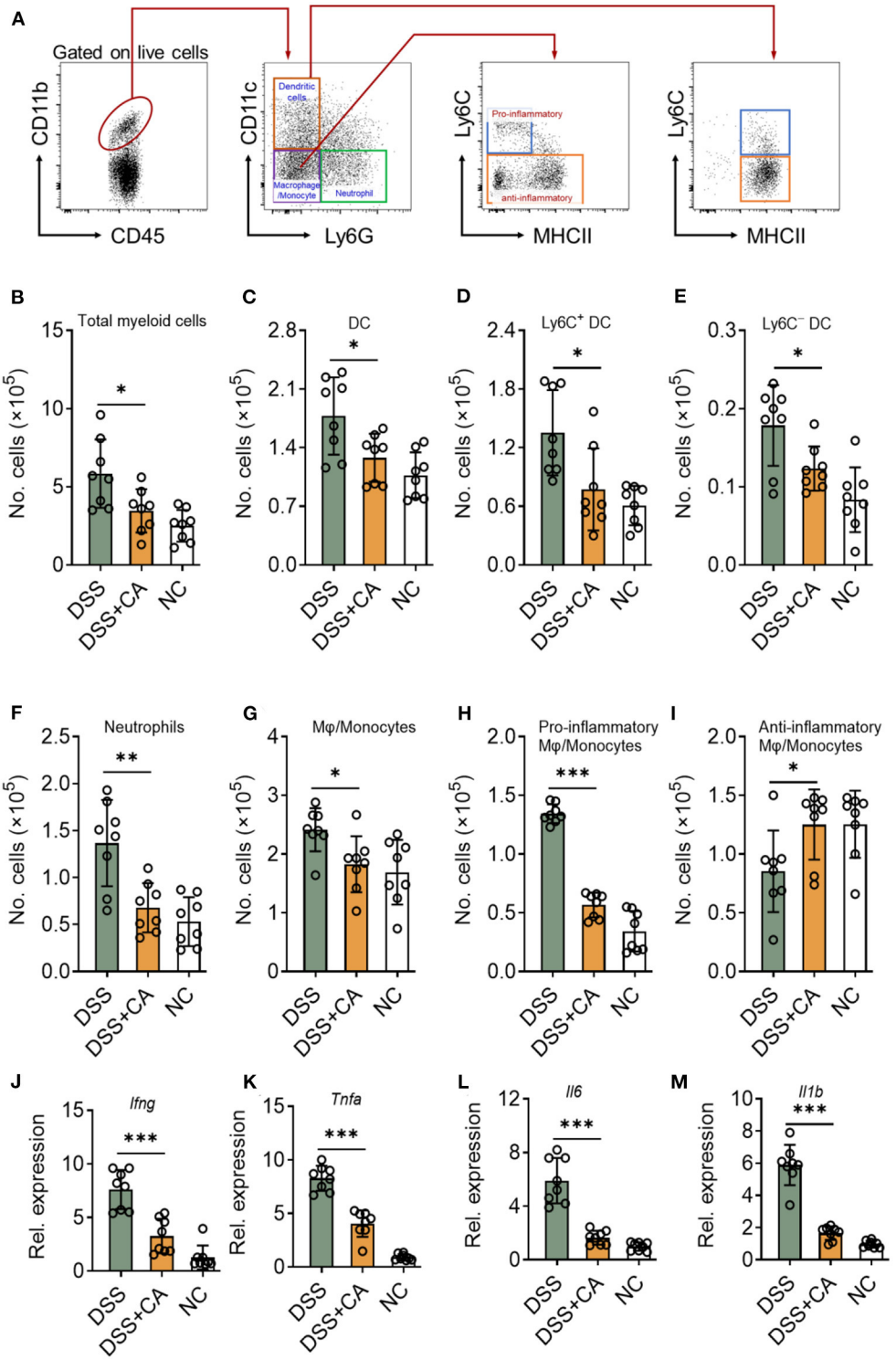

FIGURE 3 | CA suppresses colonic inflammatory responses in DSS-treated mice. Colitis was induced as described in **Figure 1** and colon lamina propria leukocyte (LPL) were isolated on day 10. **(A)** Gating strategy for lamina propria myeloid cells. Different cell populations were identified as follows: total myeloid cells ($CD45^+$ $CD11b^+$), dendritic cells (DC, $CD45^+$ $CD11b^+$ $Ly6G^-$ $CD11c^+$), neutrophils ($CD45^+$ $CD11b^+$ $Ly6G^+$), monocytes/macrophages ($CD45^+$ $CD11b^+$ $CD11c^-$ $Ly6G^-$), $Ly6C^+$ DC ($CD45^+$ $CD11b^+$ $Ly6G^-$ $CD11c^+$ $Ly6C^+$), $Ly6C^-$ DC ($CD45^+$ $CD11b^+$ $Ly6G^-$ $CD11c^+$ $Ly6C^-$), total myeloid cells ($CD45^+$ $CD11b^+$), pro-inflammatory monocytes/macrophages ($CD45^+$ $CD11b^+$ $CD11c^-$ $Ly6G^-$ $Ly6C^+$ MHC II^-), and anti-inflammatory monocytes/macrophages ($CD45^+$ $CD11b^+$ $CD11c^-$ $Ly6G^-$ $Ly6C^-$). Quantification of different cell populations are shown in **(B–I)**. **(J–M)** The expression levels of indicated inflammatory agents in colons were determined by qRT-PCR. Dates are presented as mean ± SD. Representative data of three independent experiments are shown. One-way analysis of variance (ANOVA) followed by Tukey's multiple comparisons test, $^*p < 0.05$, $^{**}p < 0.01$, and $^{***}p < 0.001$.

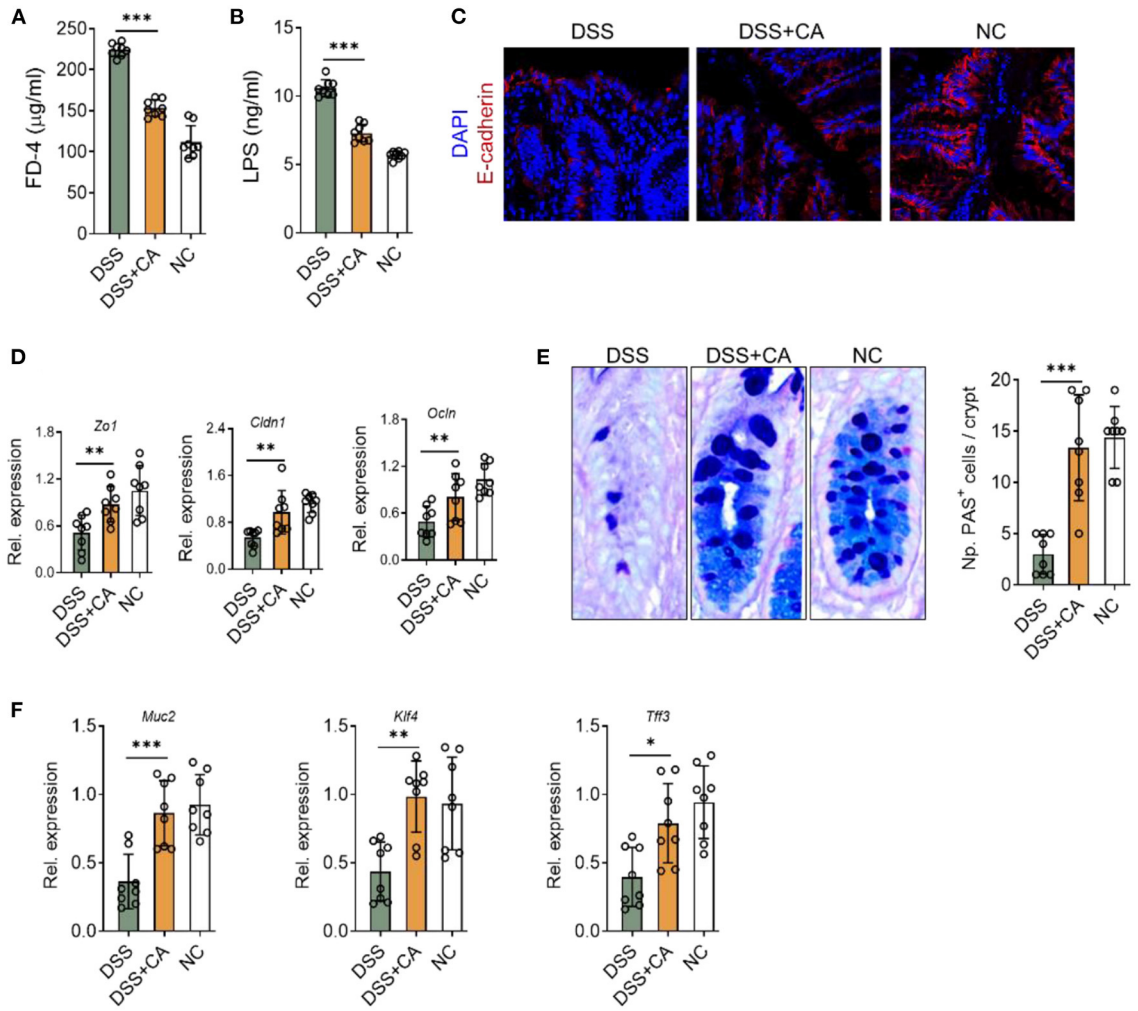

FIGURE 4 | CA restores epithelial barrier functions in intestinal inflammation. Colitis was induced as described in **Figure 1**. **(A**,**B)** Intestinal permeability in all three groups was assessed on day 10. **(A)** Serum FD-4 levels were measured 4 h after oral gavage of FD-4. **(B)** Levels of serum lipopolysaccharides (LPS) were measured. **(C)** Colonic sections were stained for E-cadherin and DAPI. Representative immunofluorescence images are shown. **(D)** Expression levels of colonic ZO-1, claudin-1, and occludin in all three groups by qRT-PCR. **(E)** Colonic goblet cells were identified by PAS staining. Representative images are shown (left) and the number of goblet cells was quantified. **(F)** The expression of colonic MUC2, KLF4, and TFF3 were detected by qRT-PCR. Data are presented as mean ± SD. Representative data of three independent experiments are shown. One-way analysis of variance (ANOVA) followed by Tukey's multiple comparisons test, $^{*}p < 0.05$, $^{**}p < 0.01$, and $^{***}p < 0.001$.

CA Suppresses ER Stress in IEC During DSS-Induced Colitis

Given growing evidence have suggested that inflammation-induced ER stress responses could compromise epithelial barrier functions and deteriorate intestinal inflammation IBD (28). Therefore, we asked whether the anti-colitic and barrier-protective effects of CA were associated with a decrease of molecular features of ER stress responses in the colonic mucosa. Expectedly, we found that CA greatly reduced epithelial expression of Bip (**Figure 6A**), a feature marker of ER stress, which was strongly induced in colitis. qRT-PCR was performed to analyze molecular features of ER stress responses and showed that CA inhibited IEC expression of Bip, CHOP, and XBP1s, which were all induced by DSS (**Figure 6B**). Additionally, we aimed to determine whether CA indeed regulated ER stress signaling. To this end, HCT-116 cells were cultured *in vitro* with an ER-stress inducer (thapsigargin), which induced ER stress, indicated by increased expression of Bip, CHOP, and XBP1s. Thapsigargin-induced ER stress was significantly suppressed by CA (**Figure 6C**). Taken together, our data suggest that CA maintains intestinal barrier functions, probably via inhibiting ER stress.

CA Reduces Inflammatory Responses and ER Stress in Mucosal Tissues of UC Patients

Based on the data found in mouse model, we next investigated whether CA regulated mucosal inflammatory responses and ER

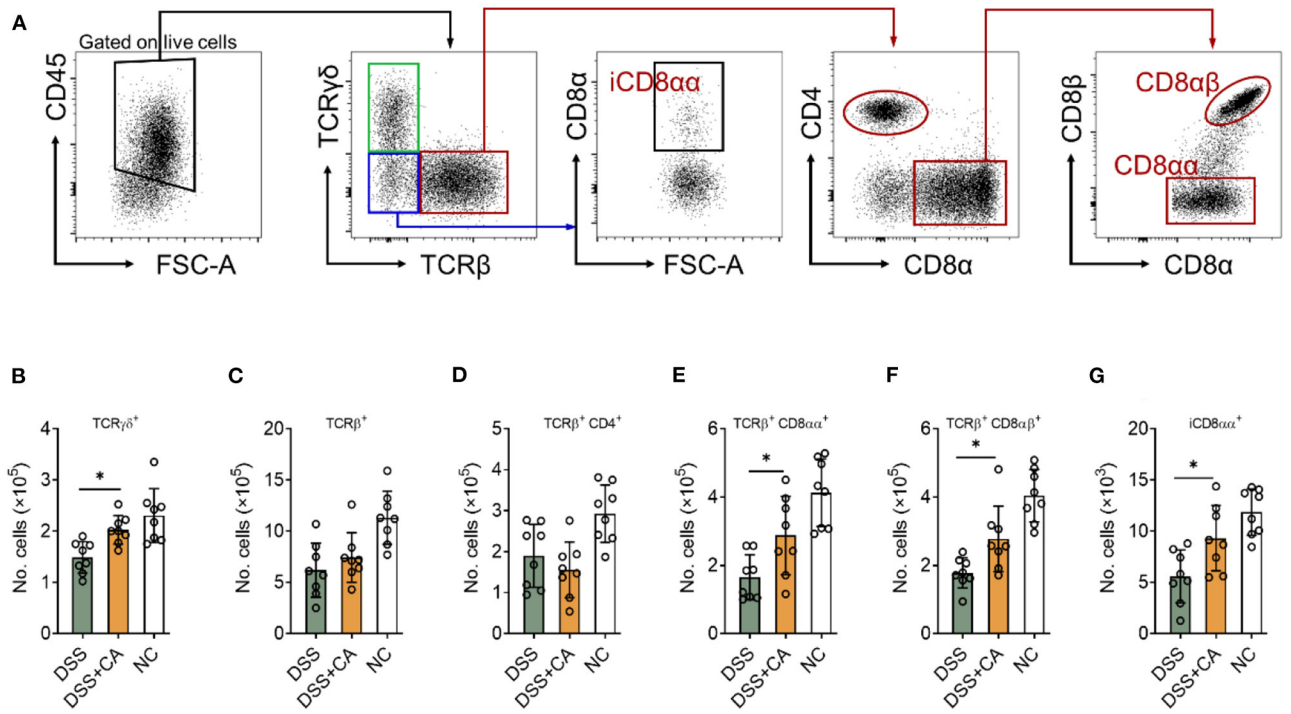

FIGURE 5 | CA restores intestinal intraepithelial lymphocyte (IEL) homeostasis during DSS-induced colitis. Colitis was induced as described in **Figure 1** and IEL were isolated on day 10. Flow cytometry was performed to determine IEL subpopulations. **(A)** Gating strategy. **(B–G)** Quantification of **(B)** TCRγδ$^+$, **(C)** TCRβ$^+$, **(D)** TCRβ$^+$ CD4$^+$, **(E)** TCRβ$^+$ CD8αα$^+$, **(F)** TCRβ$^+$ CD8αβ$^+$, and **(G)** iCD8αα$^+$ subpopulations are shown. Data are presented as mean ± SD. Representative data of three independent experiments are shown. One-way analysis of variance (ANOVA) followed by Tukey's multiple comparisons test, $^*p < 0.05$.

stress in human UC. To this end, we collected inflamed mucosal biopsies from 23 patients with UC, and cultured overnight with CA. Tissues cultured in medium alone served as controls. After overnight incubation, tissues were harvested and qRT-PCR was performed to analyze cytokine and ER stress signaling molecule expression. Incubation with CA resulted in significantly reduced expression of ER stress signaling molecule (**Figures 7A–D**) and pro-inflammatory agents (**Figures 7E–H**). Collectively, our data demonstrated that CA exerts a crucial anti-inflammatory function in human UC and mouse colitis.

DISCUSSION

Although the role of adaptive immunity in UC has been noted, epithelial barrier is the first defense line against luminal pathogens through forming a physical barrier, so that they exert essential function in maintaining intestinal homeostasis (29). It is reported that impaired IEC barrier function may be one of the important causes of IBD (30). In recent years, many studies have focused on the value of natural metabolites to prevent and cure diseases. Advances in biological techniques has enhanced the understanding of the characteristics and properties of natural plant products, as well as their therapeutic potential. However, the composition of natural metabolites is complex and pharmacologically active moieties need further exploration. Therefore, an in-depth understanding of the nature of biologically active compounds as well as their pharmacological function can further enhance their utility in diseases, such as IBD. In the current study, we established a mouse experimental colitis, which mimicks human UC. In this model, we investigated the effect of CA on intestinal inflammation and epithelial barrier functions. We found that: (1) CA significantly alleviates mucosal injuries caused by DSS; (2) lumina propria immune cell infiltration was efficiently reduced by CA in DSS mice; (3) CA maintained epithelial barrier functions during colitis; (4) CA suppresses ER stress in IEC; (5) The immunoregulatory effects of CA were also observed on human UC mucosa samples. Our findings provide new evidences that CA might be a promising candidate as a therapeutic cure for IBD.

Intestinal epithelial cells (IEC) are the first line protecting the host from luminal antigens and includes several cell types, such as enterocytes, Paneth cells, and goblet cells (31). Enterocytes, also called intestinal absorptive cells, constitutes a barrier through cell-cell adhesion, which allows a very limited passage of material in both directions. Furthermore, mucus produced by goblet cells together with antimicrobial agents secreted by Paneth cells forms another physical barrier against intestinal antigens. Growing evidences have demonstrated that IEC play a crucial role in maintaining intestinal homeostasis, and compromised barrier function has been indicated in the initiation of intestinal mucosal inflammation. Beyond

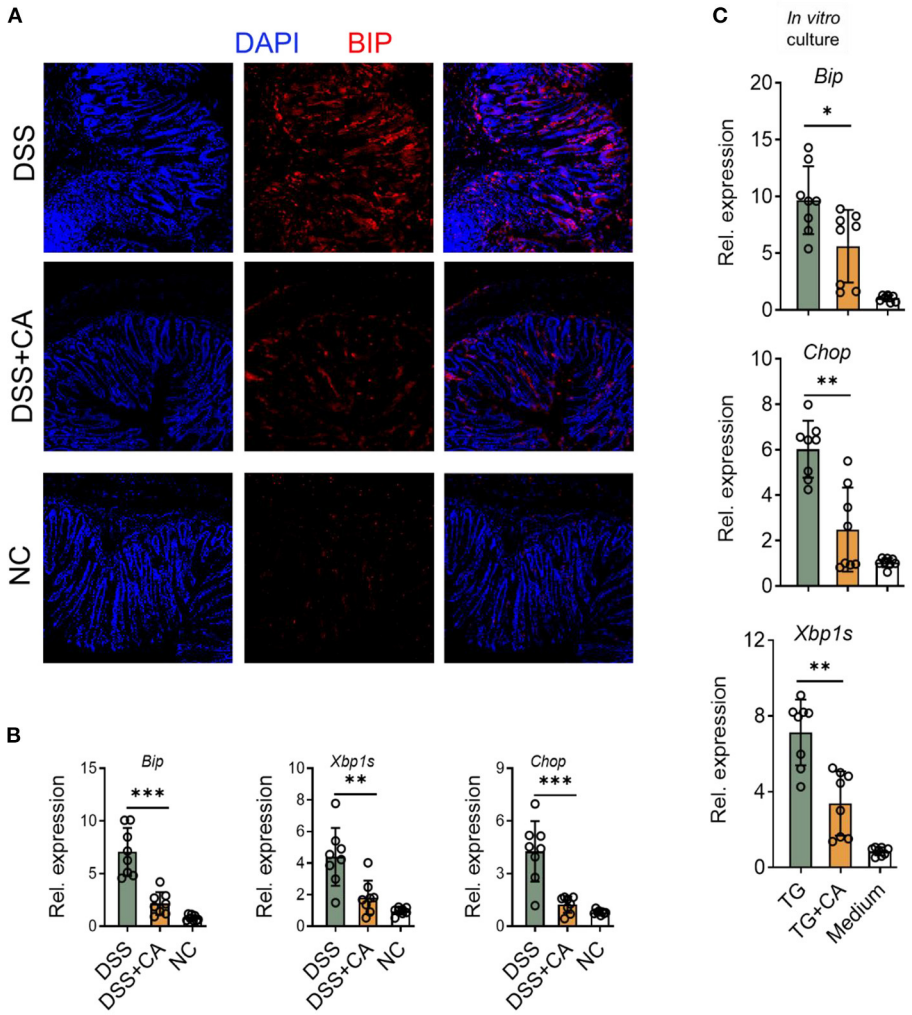

FIGURE 6 | CA suppresses ER stress in IEC. Colitis was induced as described in **Figure 1** and colon samples were collected on day 10. **(A)** Colonic sections were stained for BIP and DAPI. Representative immunofluorescence images are shown. **(B)** The expression levels of BIP, XBP1s, and CHOP were determined by qRT-PCR. **(C)** HCT-116 cells (an intestinal epithelial cell line) were incubated overnight with Thapsigargin (TG, 100 nM) in the presence or absence of CA (10 μM). The expression levels of BIP, CHOP, and XBP1s were determined by qRT-PCR. Data are presented as mean ± SD. Representative data of three independent experiments are shown. One-way analysis of variance (ANOVA) followed by Tukey's multiple comparisons test, $^{*}p < 0.05$, $^{**}p < 0.01$, and $^{***}p < 0.001$.

that, disruption of intestinal epithelial barrier is also able to cause systemic immune activation. The interactions between microbiota and the host occur at the surface of IEC, which contribute to a variety of diseases at a broad range of extra-intestinal sites, including primary sclerosing cholangitis, multiple sclerosis, and type 1 diabetes (29, 32). Therefore, a full-functional IEC barrier is essential for maintaining mucosal immune homeostasis of the host and comprehensively understanding the regulation of their properties is benefit of developing new strategies to prevent and treat IBD. Here, we demonstrate CA protects epithelial barrier functions by several means, including maintaining tight junction integrity, reversing inflammatory-induced decrease of goblet cells, and restoring IEL homeostasis, suggesting a critical role of CA in mucosal homeostasis.

IEL represent one of the largest immunological populations in the body, which reside within the IEC monolayer and cooperate with IEC to maintain the barrier functions (33). The basis of TCR expression, IEL can be classified into two major subpopulations: IEL expressing TCR and TCR-negative IEL. The former subpopulation can be further divided into TCRαβ^{+} CD4^{+}, TCRαβ^{+} CD8αα^{+}, TCRαβ^{+} CD8αβ^{+}, and TCRγδ^{+} cells. The TCR-negative subpopulation includes innate lymphoid cells (ILC) and T cells containing intracellular CD3γ-chains (iCD3^{+}). A subset of iCD3^{+} T cells expresses CD8αα, which is named as iCD8α^{+} (34). Due to their anatomical location, IEL play a critical role as sentinels surveilling luminal microbial and food antigens, providing protection against potential pathogen invasion (35). To exert their immunological functions, IEL need to maintain their homeostasis. However, since IEL

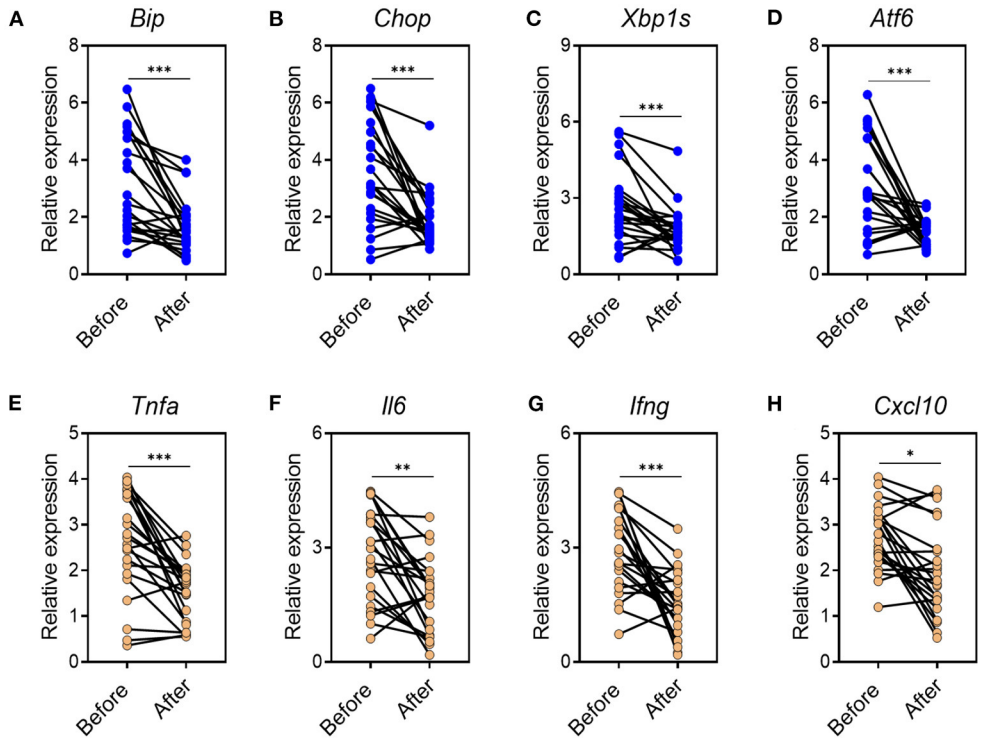

FIGURE 7 | CA reduces inflammatory responses and ER stress in mucosal tissues of UC patients. Inflamed mucosal tissues were obtained from patients with UC ($n = 23$) as indicated and incubated overnight with or without CA (10 μ M). qRT-PCR was performed for gene expression. **(A–D)** ER stress signaling gene expression (**A**, BIP; **B**, CHOP; **C**, XBP1s; **D**, ATF6) and **(E–H)** inflammatory agent expression (**E**, TNF-a; **F**, IL-6; **G**, IFN-g; **H**, CXCL10) are shown. Data are presented as mean ± SD. Unpaired Student's *t* test (two-tailed), $^{*}p < 0.05$, $^{**}p < 0.01$, and $^{***}p < 0.001$.

population are heterogenic, requirements for their homeostasis largely depend on the particular type of IEL. It has been demonstrated that TCRγδ^{+} cells are responsible for pathogen surveillance, tissue repair, and barrier protection (36). iCD8α cells can protect against necrotizing enterocolitis by fighting against *Citrobacter rodentium* (37). TCRαβ^{+} CD8αα^{+} IEL can ameliorate experimental colitis, showing an immunoregulatory and protective role in mucosal homeostasis (38). Our results in this study reveal that CA is critical for the homeostasis of several IEL subpopulations (TCRγδ^{+}, TCRαβ^{+} CD8αα^{+}, TCRαβ^{+} CD8αβ^{+}, and iCD8αα^{+}). These findings suggest that CA treatment ensures proper homeostasis of most types of IEL, thus maintaining intestinal epithelial barrier functions.

The importance of IEC in intestinal homeostasis has been evidenced by numerous animal studies and genome-wide association studies, in which a number of genes were identified to be tightly associated with IEC functions. Cellular stress signaling such as ER stress has been linked to the proliferation, differentiation, apoptosis, and normal functions of different subsets of IEC in the gut (39). Multiple molecular mechanisms have been reported regarding how IEC ER stress induces mucosal inflammation (28), including (1) ER stress causes epithelial cell death, which directly destructs the barrier; (2) ER stress impairs goblet cell and Paneth cell functions, resulting in compromised antimicrobial peptide and mucin secretion; (3) ER stress triggers inflammatory signaling in IEC. Additionally, patients with UC exhibit up-regulated ER stress in IEC located in inflammatory mucosa (40). Considering the importance of ER homeostasis in IEC, it has been suggested that epithelial ER stress might be a promising therapeutic target for UC. For example, glutamine, as an energy source for colonocytes, was found to be a potent ER stress suppressor. Glutamine treatment significantly ameliorated experimental colitis in rats (41). Salubrinal, a recently identified inhibitor of eIF2α dephosphorylation, is capable to protect against ER stress in various model systems. Salubrinal has been shown to relief colonic inflammation in mice with deficiency in IL-10 and NADPH oxidase 1 or DSS-induced colitis (42, 43). Here, we demonstrate that CA is able to suppress colitis-induced ER stress in IEC, revealing potential mechanisms whereby CA maintains epithelial barrier functions and protects against DSS-induced colitis in mice.

In summary, we here revealed that CA, a natural active ortho-diphenol diterpene compound, acted as an effective drug for experimental colitis, which maintains proper epithelial barrier functions, probably via suppressing IEC ER stress. Our findings provide new evidence that CA might be a promising candidate as a therapeutic cure for IBD.

DATA AVAILABILITY STATEMENT

The original contributions presented in the study are included in the article/**Supplementary Material**,

further inquiries can be directed to the corresponding author/s.

ETHICS STATEMENT

The studies involving human participants were reviewed and approved by the Institutional Review Board for Clinical Research of Sichuan Provincial People's Hospital. The patients/participants provided their written informed consent to participate in this study. The animal study was reviewed and approved by the Animal Care and Use Committee at Sichuan Provincial People's Hospital.

AUTHOR CONTRIBUTIONS

FL and CH conceptualized and designed the study plan and edited the manuscript. XX, GZ, KP, and YG conducted the experiments. CG diagnosed the patients and collected the clinical samples. FL, CH, XX, and GZ analyzed the data and prepared the original draft. All authors discussed and revised the manuscript and agreed to the published version of the manuscript.

FUNDING

This work was financially supported by grants from the National Natural Science Foundation of China (82070985) and Foundation of Sichuan Science and Technology Department (2021JDJQ0044).

SUPPLEMENTARY MATERIAL

The Supplementary Material for this article can be found online at: https://www.frontiersin.org/articles/10.3389/fnut.2022.894307/full#supplementary-material

REFERENCES

1. Kaplan GG. The global burden of IBD: from 2015 to 2025. *Nat Rev Gastroenterol Hepatol.* (2015) 12:720–7. doi: 10.1038/nrgastro.2015.150
2. Beard JA, Franco DL, Click BH. The burden of cost in inflammatory bowel disease: a medical economic perspective and the future of value-based care. *Curr Gastroenterol Rep.* (2020) 22:6. doi: 10.1007/s11894-020-0744-z
3. Sun M, He C, Cong Y, Liu Z. Regulatory immune cells in regulation of intestinal inflammatory response to microbiota. *Mucosal Immunol.* (2015) 8:969–78. doi: 10.1038/mi.2015.49
4. Loussouarn M, Krieger-Liszkay A, Svilar L, Bily A, Birtic S, Havaux M. Carnosic acid and carnosol, two major antioxidants of rosemary, act through different mechanisms. *Plant Physiol.* (2017) 175:1381–94. doi: 10.1104/pp.17.01183
5. Kashyap D, Kumar G, Sharma A, Sak K, Tuli HS, Mukherjee TK. Mechanistic insight into carnosol-mediated pharmacological effects: recent trends and advancements. *Life Sci.* (2017) 169:27–36. doi: 10.1016/j.lfs.2016.11.013
6. Alsamri H, El Hasasna H, Al Dhaheri Y, Eid AH, Attoub S, Iratni R. Carnosol, a natural polyphenol, inhibits migration, metastasis, and tumor growth of breast cancer via a ROS-dependent proteasome degradation of STAT3. *Front Oncol.* (2019) 9:743. doi: 10.3389/fonc.2019.00743
7. Valdes A, Garcia-Canas V, Artemenko KA, Simo C, Bergquist J, Cifuentes A. Nano-liquid chromatography-orbitrap MS-based quantitative proteomics reveals differences between the mechanisms of action of carnosic acid and carnosol in colon cancer cells. *Mol Cell Proteomics.* (2017) 16:8–22. doi: 10.1074/mcp.M116.061481
8. Johnson JJ. Carnosol: a promising anti-cancer and anti-inflammatory agent. *Cancer Lett.* (2011) 305:1–7. doi: 10.1016/j.canlet.2011.02.005
9. Li X, Zhang Q, Hou N, Li J, Liu M, Peng S, et al. Carnosol as a Nrf2 activator improves endothelial barrier function through antioxidative mechanisms. *Int J Mol Sci.* (2019) 20:880. doi: 10.3390/ijms20040880
10. Lee DY, Hwang CJ, Choi JY, Park MH, Song MJ, Oh KW, et al. Inhibitory effect of carnosol on phthalic anhydride-induced atopic dermatitis via inhibition of STAT3. *Biomol Ther.* (2017) 25:535–44. doi: 10.4062/biomolther.2017.006
11. Li X, Zhao L, Han JJ, Zhang F, Liu S, Zhu L, et al. Carnosol modulates Th17 cell differentiation and microglial switch in experimental autoimmune encephalomyelitis. *Front Immunol.* (2018) 9:1807. doi: 10.3389/fimmu.2018.01807
12. He C, Shi Y, Wu R, Sun M, Fang L, Wu W, et al. miR-301a promotes intestinal mucosal inflammation through induction of IL-17A and TNF-alpha in IBD. *Gut.* (2016) 65:1938–50. doi: 10.1136/gutjnl-2015-309389
13. He C, Yu T, Shi Y, Ma C, Yang W, Fang L, et al. MicroRNA 301A promotes intestinal inflammation and colitis-associated cancer development by inhibiting BTG1. *Gastroenterology.* (2017) 152:1434–48 e15. doi: 10.1053/j.gastro.2017.01.049
14. Xiao J, Wang J, Chen Y, Zhou Z, Gao C, Guo Z. Sauchinone ameliorates intestinal inflammation and promotes Th17 cell production of IL-10 via Blimp-1. *Biochem Biophys Res Commun.* (2020) 522:435–41. doi: 10.1016/j.bbrc.2019.11.122
15. Xiu W, Chen Q, Wang Z, Wang J, Zhou Z. Microbiota-derived short chain fatty acid promotion of Amphiregulin expression by dendritic cells is regulated by GPR43 and Blimp-1. *Biochem Biophys Res Commun.* (2020) 533:282–8. doi: 10.1016/j.bbrc.2020.09.027
16. Sun M, He C, Chen L, Yang W, Wu W, Chen F, et al. RORgammat represses IL-10 production in Th17 cells to maintain their pathogenicity in inducing intestinal inflammation. *J Immunol.* (2019) 202:79–92. doi: 10.4049/jimmunol.1701697
17. Peng K, Xiao J, Wang J, Song Y, Wu L, Xiu W, et al. MAdCAM-1 mediates retinal neuron degeneration in experimental colitis through recruiting gut-homing CD4(+) T cells. *Mucosal Immunol.* (2021) 14:152–63. doi: 10.1038/s41385-020-0282-x
18. Shi Y, He C, Ma C, Yu T, Cong Y, Cai W, et al. Smad nuclear interacting protein 1 (SNIP1) inhibits intestinal inflammation through regulation of epithelial barrier function. *Mucosal Immunol.* (2018) 11:835–45. doi: 10.1038/mi.2017.95
19. Klepsch V, Gerner RR, Klepsch S, Olson WJ, Tilg H, Moschen AR, et al. Nuclear orphan receptor NR2F6 as a safeguard against experimental murine colitis. *Gut.* (2018) 67:1434–44. doi: 10.1136/gutjnl-2016-313466
20. Eichele DD, Kharbanda KK. Dextran sodium sulfate colitis murine model: an indispensable tool for advancing our understanding of inflammatory bowel diseases pathogenesis. *World J Gastroenterol.* (2017) 23:6016–29. doi: 10.3748/wjg.v23.i33.6016
21. Xu X, Dong Q, Zhong Q, Xiu W, Chen Q, Wang J, et al. The flavonoid kurarinone regulates macrophage functions via aryl hydrocarbon receptor and alleviates intestinal inflammation in irritable bowel syndrome. *J Inflamm Res.* (2021) 14:4347–59. doi: 10.2147/JIR.S329091
22. Zigmond E, Varol C, Farache J, Elmaliah E, Satpathy AT, Friedlander G, et al. Ly6C hi monocytes in the inflamed colon give rise to proinflammatory effector cells and migratory antigen-presenting cells. *Immunity.* (2012) 37:1076–90. doi: 10.1016/j.immuni.2012.08.026
23. Zhou GX, Liu ZJ. Potential roles of neutrophils in regulating intestinal mucosal inflammation of inflammatory bowel disease. *J Dig Dis.* (2017) 18:495–503. doi: 10.1111/1751-2980.12540
24. Biswas A, Shouval DS, Griffith A, Goettel JA, Field M, Kang YH, et al. WASP-mediated regulation of anti-inflammatory macrophages is IL-10

dependent and is critical for intestinal homeostasis. *Nat Commun.* (2018) 9:1779. doi: 10.1038/s41467-018-03670-6
25. Tamoutounour S, Henri S, Lelouard H, de Bovis B, de Haar C, van der Woude CJ, et al. CD64 distinguishes macrophages from dendritic cells in the gut and reveals the Th1-inducing role of mesenteric lymph node macrophages during colitis. *Eur J Immunol.* (2012) 42:3150–66. doi: 10.1002/eji.201242847
26. Knoop KA, Newberry RD. Goblet cells: multifaceted players in immunity at mucosal surfaces. *Mucosal Immunol.* (2018) 11:1551–7. doi: 10.1038/s41385-018-0039-y
27. Nazmi A, Greer MJ, Hoek KL, Piazuelo MB, Weitkamp JH, Olivares-Villagomez D. Osteopontin and iCD8alpha cells promote intestinal intraepithelial lymphocyte homeostasis. *J Immunol.* (2020) 204:1968–81. doi: 10.4049/jimmunol.1901168
28. Cao SS. Epithelial ER stress in Crohn's disease and ulcerative colitis. *Inflamm Bowel Dis.* (2016) 22:984–93. doi: 10.1097/MIB.0000000000000660
29. Maloy KJ, Powrie F. Intestinal homeostasis and its breakdown in inflammatory bowel disease. *Nature.* (2011) 474:298–306. doi: 10.1038/nature10208
30. Xavier RJ, Podolsky DK. Unravelling the pathogenesis of inflammatory bowel disease. *Nature.* (2007) 448:427–34. doi: 10.1038/nature06005
31. Peterson LW, Artis D. Intestinal epithelial cells: regulators of barrier function and immune homeostasis. *Nat Rev Immunol.* (2014) 14:141–53. doi: 10.1038/nri3608
32. Artis D. Epithelial-cell recognition of commensal bacteria and maintenance of immune homeostasis in the gut. *Nat Rev Immunol.* (2008) 8:411–20. doi: 10.1038/nri2316
33. Cheroutre H, Lambolez F, Mucida D. The light and dark sides of intestinal intraepithelial lymphocytes. *Nat Rev Immunol.* (2011) 11:445–56. doi: 10.1038/nri3007
34. Van Kaer L, Olivares-Villagomez D. Development, homeostasis, and functions of intestinal intraepithelial lymphocytes. *J Immunol.* (2018) 200:2235–44. doi: 10.4049/jimmunol.1701704
35. Olivares-Villagomez D, Van Kaer L. Intestinal intraepithelial lymphocytes: sentinels of the mucosal barrier. *Trends Immunol.* (2018) 39:264–75. doi: 10.1016/j.it.2017.11.003
36. Ismail AS, Severson KM, Vaishnava S, Behrendt CL, Yu X, Benjamin JL, et al. Gammadelta intraepithelial lymphocytes are essential mediators of host-microbial homeostasis at the intestinal mucosal surface. *Proc Natl Acad Sci USA.* (2011) 108:8743–8. doi: 10.1073/pnas.1019574108
37. Van Kaer L, Algood HMS, Singh K, Parekh VV, Greer MJ, Piazuelo MB, et al. CD8alphaalpha(+) innate-type lymphocytes in the intestinal epithelium mediate mucosal immunity. *Immunity.* (2014) 41:451–64. doi: 10.1016/j.immuni.2014.08.010
38. Poussier P, Ning T, Banerjee D, Julius M. A unique subset of self-specific intraintestinal T cells maintains gut integrity. *J Exp Med.* (2002) 195:1491–7. doi: 10.1084/jem.20011793
39. Cao SS. Endoplasmic reticulum stress and unfolded protein response in inflammatory bowel disease. *Inflamm Bowel Dis.* (2015) 21:636–44. doi: 10.1097/MIB.0000000000000238
40. Heazlewood CK, Cook MC, Eri R, Price GR, Tauro SB, Taupin D, et al. Aberrant mucin assembly in mice causes endoplasmic reticulum stress and spontaneous inflammation resembling ulcerative colitis. *PLoS Med.* (2008) 5:e54. doi: 10.1371/journal.pmed.0050054
41. Crespo I, San-Miguel B, Prause C, Marroni N, Cuevas MJ, Gonzalez-Gallego J, et al. Glutamine treatment attenuates endoplasmic reticulum stress and apoptosis in TNBS-induced colitis. *PLoS ONE.* (2012) 7:e50407. doi: 10.1371/journal.pone.0050407
42. Okazaki T, Nishio A, Takeo M, Sakaguchi Y, Fukui T, Uchida K, et al. Inhibition of the dephosphorylation of eukaryotic initiation factor 2alpha ameliorates murine experimental colitis. *Digestion.* (2014) 90:167–78. doi: 10.1159/000366414
43. Treton X, Pedruzzi E, Guichard C, Ladeiro Y, Sedghi S, Vallee M, et al. Combined NADPH oxidase 1 and interleukin 10 deficiency induces chronic endoplasmic reticulum stress and causes ulcerative colitis-like disease in mice. *PLoS ONE.* (2014) 9:e101669. doi: 10.1371/journal.pone.0101669

Conflict of Interest: The authors declare that the research was conducted in the absence of any commercial or financial relationships that could be construed as a potential conflict of interest.

Publisher's Note: All claims expressed in this article are solely those of the authors and do not necessarily represent those of their affiliated organizations, or those of the publisher, the editors and the reviewers. Any product that may be evaluated in this article, or claim that may be made by its manufacturer, is not guaranteed or endorsed by the publisher.

frontiers | Frontiers in Nutrition

TYPE Original Research
PUBLISHED 27 July 2022
DOI 10.3389/fnut.2022.871325

OPEN ACCESS

EDITED BY
Xin Zhao,
McGill University, Canada

REVIEWED BY
Kefeng Zhai,
Suzhou University, China
Marcus O. Muench,
Vitalant Research Institute,
United States

*CORRESPONDENCE
Chin-Fah Wang
cfwang@niu.edu.tw

†These authors have contributed equally to this work

SPECIALTY SECTION
This article was submitted to Nutritional Immunology, a section of the journal Frontiers in Nutrition

RECEIVED 08 February 2022
ACCEPTED 04 July 2022
PUBLISHED 27 July 2022

CITATION
Wong W-T, Wu C-H, Li L-H, Hung D-Y, Chiu H-W, Hsu H-T, Ho C-L, Chernikov OV, Cheng S-M, Yang S-P, Chung C-H, Hua K-F and Wang C-F (2022) The leaves of the seasoning plant *Litsea cubeba* inhibit the NLRP3 inflammasome and ameliorate dextran sulfate sodium-induced colitis in mice. *Front. Nutr.* 9:871325. doi: 10.3389/fnut.2022.871325

The leaves of the seasoning plant *Litsea cubeba* inhibit the NLRP3 inflammasome and ameliorate dextran sulfate sodium-induced colitis in mice

Wei-Ting Wong[1†], Chun-Hsien Wu[2†], Lan-Hui Li[3,4], De-Yu Hung[1], Hsiao-Wen Chiu[1], Hsien-Ta Hsu[5,6], Chen-Lung Ho[7], Oleg V. Chernikov[8], Shu-Meng Cheng[2], Shih-Ping Yang[2], Chih-Hsin Chung[9], Kuo-Feng Hua[1,4,10] and Chin-Fah Wang[11*]

[1]Department of Biotechnology and Animal Science, National Ilan University, Ilan, Taiwan, [2]Division of Cardiology, Department of Internal Medicine, National Defense Medical Center, Tri-Service General Hospital, Taipei, Taiwan, [3]Department of Laboratory Medicine, Linsen, Chinese Medicine and Kunming Branch, Taipei City Hospital, Taipei, Taiwan, [4]Department of Pathology, National Defense Medical Center, Tri-Service General Hospital, Taipei, Taiwan, [5]Division of Neurosurgery, Taipei Tzu Chi Hospital, Buddhist Tzu Chi Medical Foundation, New Taipei City, Taiwan, [6]School of Medicine, Buddhist Tzu Chi University, Hualien, Taiwan, [7]Division of Wood Cellulose, Taiwan Forestry Research Institute, Taipei, Taiwan, [8]G.B. Elyakov Pacific Institute of Bioorganic Chemistry FEB RAS, Vladivostok, Russia, [9]Department of Forestry and Natural Resources, National Ilan University, Ilan, Taiwan, [10]Department of Medical Research, China Medical University Hospital, China Medical University, Taichung, Taiwan, [11]Center for General Education, National Ilan University, Ilan, Taiwan

The intracellular sensor NACHT, LRR, and PYD domain-containing protein 3 (NLRP3) inflammasome controls caspase-1 activity and the maturation and release of the cytokines interleukin (IL)−1β and IL−18. The NLRP3 inflammasome has attracted the attention of the pharmaceutical industry because it promotes the pathogenesis of many diseases, making it a promising target for drug development. *Litsea cubeba* (Lour.) is a plant traditionally used as a seasoning in Taiwan and in other Asian countries. In this study, we investigated the inhibitory activity of the leaves of *L. cubeba* against the NLRP3 inflammasome. We found that the ethanol extract of *L. cubeba* leaves (MLE) inhibited the NLRP3 inflammasome in macrophages by reducing caspase−1 activation and IL−1β secretion. MLE reduced pyroptosis in macrophages and inhibited the release of NLRP3 and apoptosis-associated speck-like protein containing a CARD (ASC). In a mechanistic study, MLE reduced mitochondrial reactive oxygen species (ROS) production and preserved mitochondrial integrity, which led to reduced mitochondrial DNA release into the cytosol. MLE did not reduce the expression levels of NLRP3, IL−1β precursor or TNF-α in lipopolysaccharide (LPS)-activated macrophages. These results indicated that MLE inhibited the NLRP3 inflammasome by suppressing the activation signals of the NLRP3 inflammasome but not by reducing the priming signal

induced by LPS. In addition, oral administration of MLE (20–80 mg/kg) ameliorated dextran sulfate sodium (DSS)–induced colitis in a mouse model. Notably, mice that received MLE (1 and 2 g/kg) daily for 7 days did not exhibit visible side effects. Gas chromatography-mass spectrometry (GC-MS) analysis found that α-Terpinyl acetate (27.2%) and 1,8–Cineole (17.7%) were the major compounds in MLE. These results indicated that *L. cubeba* leaves have the potential to be a nutraceutical for preventing and improving NLRP3 inflammasome-related diseases.

KEYWORDS

NLRP3 inflammasome, *Litsea cubeba*, macrophages, dextran sulfate sodium-induced colitis, cytokines

Introduction

The intracellular sensor NACHT, LRR, and PYD domain-containing protein 3 (NLRP3) inflammasome is a multiprotein complex composed of NLRP3, apoptosis-associated speck-like protein containing a caspase recruitment domain (ASC), and cysteine protease caspase−1 that controls caspase-1 activity and the maturation and release of the cytokines interleukin (IL)−1β and IL-18 (1). The NLRP3 inflammasome responds to medically relevant danger signals, including foreign molecules derived from pathogens and endogenous molecules associated with tissue damage or metabolic imbalances (2). Full activation of the NLRP3 inflammasome requires both a priming signal from pathogen-associated molecular patterns and an activation signal from a second stimulus, e.g., damage-associated molecular patterns, the former controlling the expression of NLRP3 and IL-1β precursor and the latter controlling caspase-1 activation (3). Aberrant activation of the NLRP3 inflammasome can be detected in many diseases. Pharmaceutical or genetic inhibition of NLRP3 prevents or improves these diseases. Aberrant activation of the NLRP3 inflammasome promotes the pathogenesis of inflammatory diseases, including chronic kidney disease, type II diabetes, atherosclerosis, neurodegenerative diseases, inflammatory bowel disease, gout, rheumatoid arthritis, cancers, and some infectious diseases (2).

The importance of the NLRP3 inflammasome has attracted the interest of researchers and biotech companies, and the field of NLRP3 inflammasome research is booming. Increasing evidence shows that the NLRP3 inflammasome is a promising therapeutic target in many diseases (4). Inhibition of the NLRP3 inflammasome did not dampen the broader immune responses needed to fight infection because the host defense ability can be covered by other inflammasomes, offering practical, effective, and safe therapy. The development of NLRP3 inhibitors has become an important topic in the pharmaceutical industry and scientific community (5). Although no NLRP3-targeting drugs have yet hit the market, various pharmaceutical companies are taking a wide range of strategies to tackle the NLRP3 inflammasome.

Litsea cubeba (Lour.) belongs to the family Lauraceae and genus Litsea. *L. cubeba* is a deciduous shrub with perennial rootstock, mostly distributed in the low-elevation mountain slopes of the central and eastern regions in Taiwan. The whole plant has a pungent spicy ginger scent. The indigenous Taiwanese call *L. cubeba* "Makauy." Makauy is a traditional seasoning and medicinal plant used by indigenous people in Taiwan. The fruit is the most widely used part of *L. cubeba* and has a variety of biological activities. *L. cubeba* fruit essential oil inhibited the growth of drug-resistant *Staphylococcus aureus* and *Acinetobacter baumannii* (6, 7). *L. cubeba* fruit essential oil also inhibited the expression levels of tumor necrosis factor-α (TNF-α) and IL-12 in bacterial endotoxin (lipopolysaccharide, LPS)-stimulated bone marrow-derived dendritic cells and reduced contact hypersensitivity responses in mice (8). A new diterpene, cubelin, isolated from a methanol extract of *L. cubeba* fruits induced apoptosis in HeLa cells (9). *L. cubeba* fruit chloroform extracts showed insecticidal activities against Sitophilus zeamais Motschulsky (10). In our previous studies, we demonstrated that citral, a major compound in the *L. cubeba* fruit essential oil, improved focal segmental glomerulosclerosis (11) and lupus nephritis (12) in mice by reducing renal inflammation.

In recent years, the unique flavor of *L. cubeba* fruits has attracted public attention. However, insufficient production of *L. cubeba* fruits leads to price increases and restricts industrial development. Leaves are a sustainable and renewable resource; however, the leaves are currently the unused part of *L. cubeba*. In this study, we tested the inhibition potential of the ethanolic

extract of *L. cubeba* leaves against the NLRP3 inflammasome in macrophages and in a mouse model of dextran sulfate sodium (DSS)-induced colitis.

Materials and methods

Reagents

Escherichia coli LPS and protease inhibitor cocktail were purchased from Sigma-Aldrich (St. Louis, MO). The NLRP3 activator ATP, nigericin and monosodium urate (MSU) were purchased from InvivoGen (San Diego, CA). Antibodies against IL-1β were purchased from R&D Systems (Minneapolis, MN). Antibodies against NLRP3 and caspase-1 were purchased from Adipogen Life Science (San Diego, CA). Antibodies against ASC, pro-IL-1β and actin were purchased from Santa Cruz Biotechnology (Santa Cruz, CA). ELISA kits, MitoSOX, MitoTracker Deep Red and MitoTracker Green were purchased from Thermo Fisher Scientific (Waltham, MA). The CytoScan LDH Cytotoxicity Assay kit was purchased from G-Bioscience (St. Louis, MO). DSS (MW: 36,000–50,000) was purchased from MP Biomedicals (LLC, France). RIPA lysis buffer, polyvinylidenedifloride membrane and RapidStep ECL Reagent were purchased from EMD Millipore (Darmstadt, Germany).

Preparation of the ethanol extract of *Litsea cubeba* leaves

The *L. cubeba* leaves were collected from Lunpi, Datong Township, Yilan County 267002, Taiwan. The leaves were rinsed thoroughly and air-dried. Air-dried leaves (1,000 g) were extracted with 10 L of 95% methanol for 3 days at room temperature, which was repeated five times. The extract was filtered and concentrated to give an ethanolic extract of 200 g, named the Makauy leaf ethanol extract (MLE).

MEL analysis by gas chromatography-mass spectrometry

The analytical gas chromatography (GC)-flame ionization detector (FID) and GC-mass spectrometry (MS) were used to analyze the major components of MLE as described previously with slight modifications (13). In the GC-FID analysis, briefly, a Hewlett-Packard 6,890 gas chromatograph with a DB-5 capillary columns (5% Phenyl/95% methylpolysiloxane, 30 m × 0.25 mm × 0.25 μm film thickness) was used. The MLE components were quantitatively determined by the FID. The oven heat program was 50°C for 2 min, then increase to 250°C at 5°C per min. The temperatures of injector and detector were heated to 270 and 250°C, respectively. The split ratio was 1:10 and hydrogen was used as carrier gas with a flow rate of 1 ml/min. One μl MLE sample [MLE/ethyl acetate 1:100 (v/v)] was injected in split mode. The linear retention indices of compounds were calculated with reference to a homologous series of C_8-C_{30} *n*-alkanes (14). Relative proportions of compounds were calculated based on GC-FID peak areas measured on the DB-5 capillary column without use of correction factor. In the GC-MS analysis, briefly, a Hewlett-Packard 6,890/5,973 GG-MS system with a DB-5 capillary columns (the same parameters used in the GC-FID analysis) was used. Helium was used as carrier gas with a flow rate of 1 ml/min. The MS conditions were ionization voltage 70 eV, full scan mode: scan time: 0.3 s, and mass range was m/z 30–500. Compounds identification were based on calculated linear retention indices comparison with previous reports (14–16) or with the standard pure compounds and by comparison of their MS with those obtained in the NIST library "NIST 17" and "WILEY 11," and in some components by co-injection with standard pure compounds.

Cell culture

Mouse macrophage J774A.1 cells were purchased from the American Type Culture Collection (Rockville, MD). Cells were cultured in RPMI-1640 medium with 10% heat-inactivated fetal bovine serum at 37°C in a 5% CO_2 incubator.

Inhibition of the NLRP3 inflammasome by makauy leaf ethanol extract

Cells were primed with 1 μg/ml LPS for 4 h followed by incubation with 12.5, 25, or 50 μg/ml MLE or vehicle (0.1% DMSO) for 0.5 h. MLE was dissolved in DMSO to make stock solution and 0.1% volume of MLE stock was added to the cultures to make the working concentration. Cells were then incubated with 5 mM ATP for 0.5 h, 10 μM nigericin for 0.5 h, or 100 μg/ml MSU for 24 h. The levels of IL-1β in the supernatants were measured by ELISA as described previously with slight modifications (17). Briefly, prepared a mixture containing 50 μl of supernatants and 50 μl of biotinylated antibody. The mixture was added to a IL-1β antibodies pre-coated well and incubated for 2 h. After washes with washing buffer [phosphate-buffered saline (PBS) with 0.1% Tween 20], 100 μl of diluted HRP-conjugated streptavidin concentrate was added to each well and incubated for 0.5 h. After wash, 100 μl of a premixed tetramethylbenzidine substrate solution was added to each well and incubated for 0.5 h in the dark. The reaction was stopped by adding 100 μl of 2 M H_2SO_4 to each well,

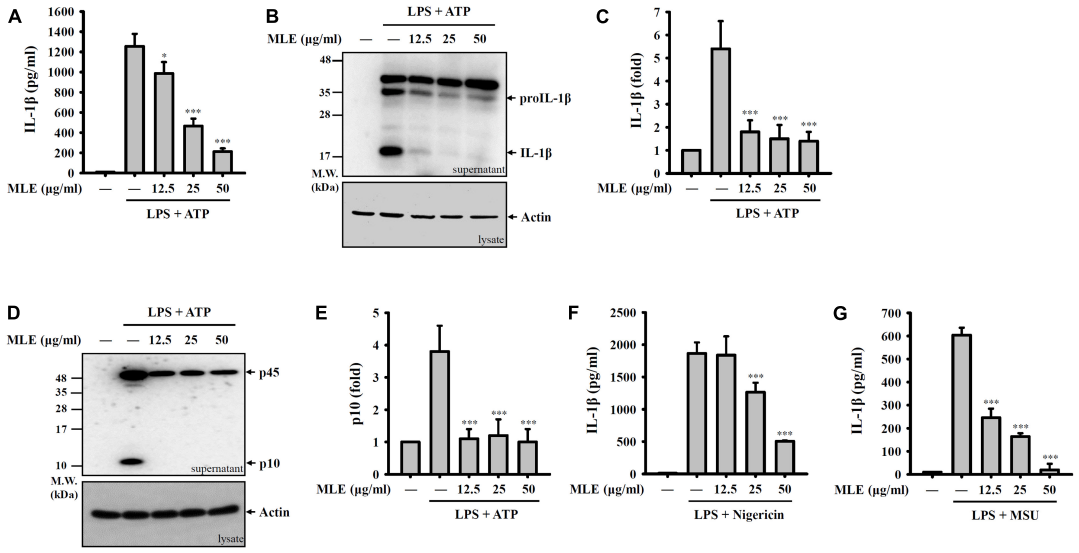

FIGURE 1
MLE inhibits the NLRP3 inflammasome. **(A–E)** LPS-primed J774A.1 macrophages were incubated with MEL for 0.5 h before ATP stimulation for an additional 0.5 h. The levels of IL-1β in the supernatants were analyzed by ELISA **(A)** and western blot **(B)**. **(C)** The column diagram represents the fold change of IL-1β in **(B)** compared with the control group analyzed by ImageJ. **(D)** The levels of pro-caspase-1 (p45) and active caspase-1 (p10) in the supernatants were analyzed by western blot. **(E)** The column diagram represents the fold change of p10 in **(D)** compared with the control group analyzed by ImageJ. **(F,G)** LPS-primed J774A.1 macrophages were incubated with MEL for 0.5 h before nigericin stimulation for an additional 0.5 h **(F)** or MSU stimulation for an additional 24 h **(G)**. The levels of IL-1β in the supernatants were analyzed by ELISA. The western blot images are representative of three different experiments. The data are expressed as the mean ± SD of three separate experiments. $*p < 0.05$ and $***p < 0.001$ compared to NLRP3 inflammasome-activated cells.

and the absorbance was read in an ELISA reader at 450 nm. The levels of pro-IL-1β/IL-1β and pro-caspase-1 (p45)/active caspase-1 (p10) in the supernatants were measured by western blotting as described previously with slight modifications (18). Briefly, protease inhibitor cocktail contained RIPA lysis buffer was used to lyse the cells. 30 μg protein of each samples were separated by SDS-polyacrylamide gel electrophoresis and then transferred to a polyvinylidenedifloride membrane. The membranes were blocked with blocking buffer (5% non-fat milk in PBS with 0.1% Tween 20) at room temperature for 2 h, and then were incubated with primary and HRP-conjugated secondary antibody in blocking buffer at room temperature for 1 and 0.5 h, respectively. After washes with washing buffer (PBS with 0.1% Tween 20), the membrane was developed using a RapidStep ECL Reagent. The signals were acquired using the GE Healthcare Life Sciences Amersham Imager 600 image system (Chicago, IL).

Cytotoxic effect of makauy leaf ethanol extract

Cells were incubated with 12.5, 25, 50, 100, or 200 μg/ml MLE or 0.1% DMSO (vehicle) for 24 h. The cell numbers were calculated by the Trypan Blue exclusion test. For the LDH release assay, cells were incubated with 12.5, 25, 50, 100, or 200 μg/ml MLE, lysis buffer (maximum LDH release), or 0.1% DMSO (spontaneous LDH release) for 24 h. The LDH levels in the supernatants were measured by a CytoScan LDH Cytotoxicity Assay kit. The LDH release% was calculated as 100 X (sample OD − spontaneous OD)/(maximum OD − spontaneous OD).

Inhibition of pyroptosis by makauy leaf ethanol extract

Cells were primed with 1 μg/ml LPS for 4 h followed by incubation with 12.5, 25, or 50 μg/ml MLE or vehicle (0.1% DMSO) for 0.5 h. Cells were then incubated with 5 mM ATP for 0.5 h. The levels of LDH in the supernatants were measured by the LDH release assay. The levels of NLRP3 and ASC in the supernatants were measured by western blotting.

Inhibition of lipopolysaccharide-mediated responses by makauy leaf ethanol extract

Cells were incubated with 12.5, 25, or 50 μg/ml MLE or vehicle (0.1% DMSO) for 0.5 h, followed by incubation

with 1 μg/ml LPS for 6 h. The levels of TNF-α and IL-6 in the supernatants were measured by ELISA. The levels of NLRP3 and proIL-1β in the cell lysates were measured by western blotting.

Reduction of mitochondrial damage by makauy leaf ethanol extract

Cells were primed with 1 μg/ml LPS for 4 h, followed by incubation with 50 μg/ml MLE or vehicle (0.1% DMSO) for 0.5 h. Cells were then incubated with 5 mM ATP for 0.5 h. For the mitochondrial ROS production assay, cells were stained with 5 μM MitoSOX for 15 min. For the mitochondrial membrane integrity assay, cells were stained with 25 nM MitoTracker Deep Red and 25 nM MitoTracker Green for 15 min. The fluorescent signals of MitoSOX and MitoTracker were acquired by flow cytometry. For the mitochondrial DNA release assay, the levels of mitochondrial DNA in the cytosol were measured by detection of cytochrome c oxidase I DNA in the cytosol using quantitative PCR. The protocol and primer sequences are shown in our previous study (19).

Mouse model of dextran sulfate sodium-induced colitis

Six-week-old male C57BL/6JNal mice were purchased from The National Laboratory Animal Center (Taipei, Taiwan). The mice were housed in a room controlled for temperature (23 ± 3°C) and relative humidity (40–60%). Mice were acclimated in the animal facility for a week before the experiments. Animal experiments were performed with the approval of the Institutional Animal Care and Use Committee of the National Ilan University (approval number: No. 102-40). The mice were randomized into 7 groups: Group I, vehicle + H_2O, received normal drinking water with oral administration of vehicle daily, n = 5; Group II, vehicle + DSS, received 3% (wt/vol) DSS in drinking water with oral administration of vehicle daily, n = 5; Group III, DSS + 20 mg/kg MLE, received 3% DSS in drinking water with oral administration of 20 mg/kg MLE daily, n = 5; Group IV, DSS + 40 mg/kg MLE, received 3% DSS in drinking water with oral administration of 40 mg/kg MLE daily, n = 5; Group V, DSS + 80 mg/kg MLE, received 3% DSS in drinking water with oral administration of 80 mg/kg MLE daily, n = 5; Group VI, 80 mg/kg 5-ASA + DSS, received 3% DSS in drinking water with oral administration of 80 mg/kg 5-ASA daily, n = 5; and Group VII, 80 mg/kg MLE + H_2O, received normal drinking water with oral administration of 80 mg/kg MLE daily, n = 5. For DSS treatment, mice were treated with 3% DSS in drinking water *ad libitum* for 7 days, followed by normal water for 1 day. MLE or 5-ASA was administered intragastrically daily during DSS treatment. The body weight of each mouse was recorded daily. On Day 8 following induction with DSS, mice were sacrificed for the collection of colonic tissue and spleen.

Analysis of the levels of IL-1β and IL-6 in colons

The total colon protein from mice in each group was extracted by homogenization with lysis buffer and centrifuged at 13,000 rpm at 4°C for 20 min. The supernatants were taken, and the protein concentration was determined by the BCA protein assay before IL-1β and IL-6 ELISA analysis.

Safety evaluation of mice exposed to makauy leaf ethanol extract

Six-week-old male C57BL/6JNal mice were intragastrically administered 1 or 2 g/kg MLE or vehicle daily for 7 days. The mice were sacrificed for organ collection on Day 21 post-administration. The body weight of each mouse was recorded daily before sacrifice.

H&E analysis

The histological analysis was performed as described previously with slight modifications (20). Part of the colon was fixed in 10% buffered formalin and embedded in paraffin. Sections were stained with H&E according to standard protocols conducted by Energenesis Biomedical Co., Ltd. (Taipei, Taiwan).

Statistical analysis

Two-tailed t-tests and ANOVA with Dunnett's multiple comparisons test were used for statistical analysis for two groups and three or more groups, respectively. Error bars represent the standard deviation of three separate experiments. *, **, and *** represent $p < 0.05$, $p < 0.01$, and $p < 0.001$, respectively.

Results

Makauy leaf ethanol extract inhibits the NLRP3 inflammasome

To investigate whether MLE inhibits the activation of the NLRP3 inflammasome, macrophages were primed with LPS for

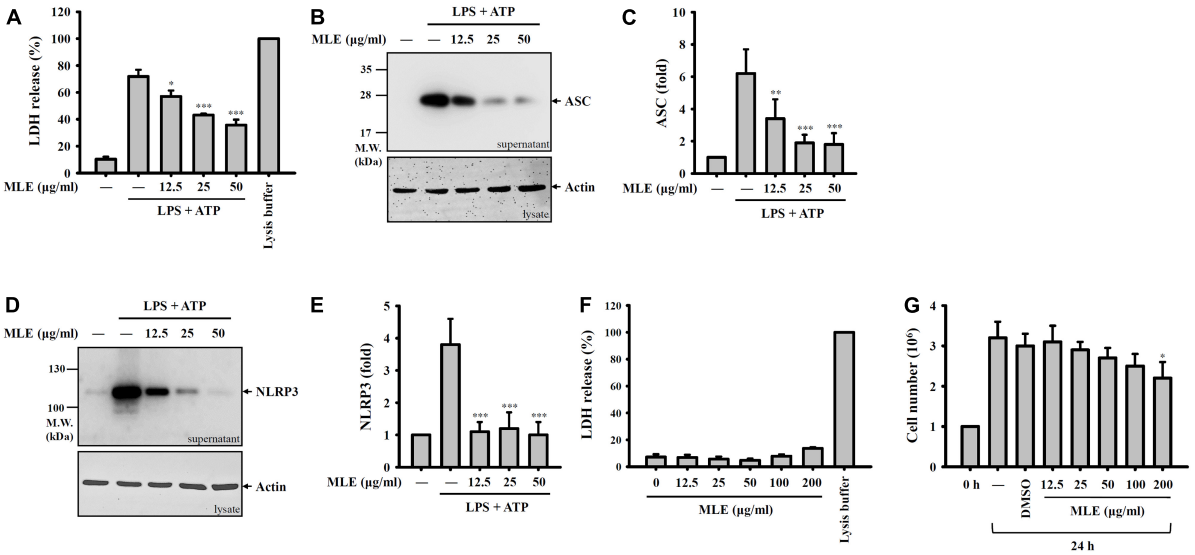

FIGURE 2
MLE inhibits pyroptosis. **(A–E)** LPS-primed J774A.1 macrophages were incubated with MEL for 0.5 h before ATP stimulation for an additional 0.5 h. The levels of LDH in the supernatants were analyzed by an LDH release kit **(A)**, and the levels of ASC in the supernatants were analyzed by western blot **(B)**. **(C)** The column diagram represents the fold change of ASC in **(B)** compared with the control group analyzed by ImageJ. **(D)** The levels of NLRP3 in the supernatants were analyzed by western blot. **(E)** The column diagram represents the fold change of NLRP3 in **(D)** compared with the control group analyzed by ImageJ. **(F)** J774A.1 macrophages were incubated with MEL for 24 h, and the levels of LDH in the supernatants were analyzed by an LDH release kit. **(G)** J774A.1 macrophages were incubated with MEL for 24 h, and the cell numbers were calculated by the Trypan Blue exclusion test of cell viability. The western blot images are representative of three different experiments. The LDH and cell counting data are expressed as the mean ± SD of three separate experiments. *$p < 0.05$, **$p < 0.01$, and ***$p < 0.001$ compared to the LPS + ATP group in **(A–E)** or compared to the vehicle-treated group in **(G)**.

4 h followed by incubation with MLE for 0.5 h. Mouse J774A.1 macrophages were then stimulated with ATP for an additional 0.5 h. The concentration of IL-1β in the culture medium was analyzed by ELISA. We found that MLE reduced ATP-mediated IL-1β expression in a dose-dependent manner (**Figure 1A**). The IL-1β inhibitory activity of MLE was confirmed by the detection of IL-1β in the culture medium using western blotting (**Figures 1B,C**). MLE also inhibited active caspase-1 (p10) expression in the culture medium, as analyzed by western blotting, indicating that MLE inhibited caspase-1 activation (**Figures 1D,E**). In addition, MLE not only reduced ATP-mediated IL-1β expression but also reduced IL-1β expression induced by other NLRP3 activators, including nigericin (**Figure 1F**) and MSU (**Figure 1G**). These results indicate that MLE inhibits the NLRP3 inflammasome in macrophages.

Makauy leaf ethanol extract inhibits pyroptosis

Pyroptosis is an inflammatory form of cell death caused by caspase-1-dependent plasma membrane pore formation, which leads to an increase in plasma membrane permeability and the release of inflammatory intracellular contents (21–23). We found that LDH was released from ATP-stimulated macrophages, and this effect was reduced by MLE (**Figure 2A**). NLRP3 inflammasome components released from pyroptotic macrophages serve as particulate danger signals that amplify the inflammatory response (24). We found that ATP induced ASC (**Figures 2B,C**) and NLRP3 (**Figures 2D,E**) release, and these effects were reduced by MLE. Importantly, MLE treatment for 24 h did not cause cytotoxicity to macrophages, as demonstrated by the LDH release assay (**Figure 2F**). Although MLE did not cause cytotoxicity to macrophages, at high concentrations, it slightly reduced cell growth (**Figure 2G**).

Makauy leaf ethanol extract did not inhibit the priming signals of the NLRP3 inflammasome

To investigate how MLE inhibits the NLRP3 inflammasome, the effect of MLE on the priming signals of the NLRP3 inflammasome was tested. Macrophages were incubated with MLE for 0.5 h followed by LPS stimulation for 6 h. The expression levels of proIL-1β and NLRP3 in the cell lysates were analyzed by western blot. We found that LPS increased the expression levels of proIL-1β (**Figures 3A,B**) and NLRP3 (**Figures 3C,D**); however, MLE did not affect proIL-1β and NLRP3 expression. In addition, MLE reduced the expression of

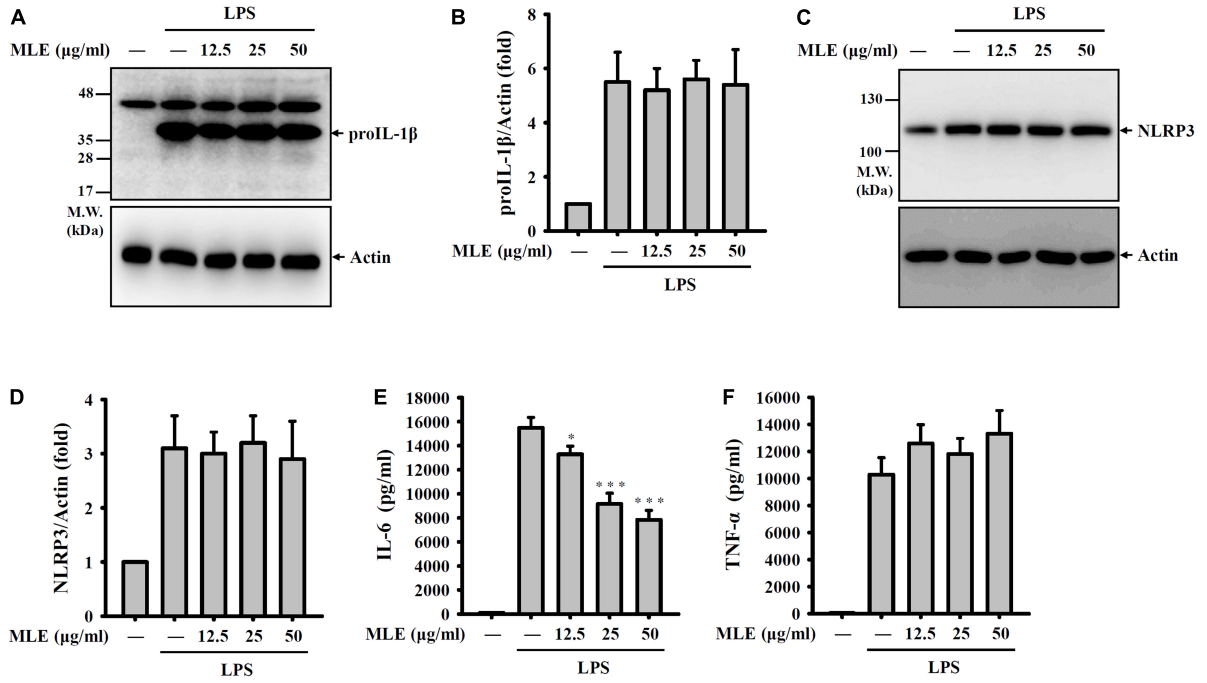

FIGURE 3
MLE did not inhibit the priming signals of the NLRP3 inflammasome. **(A–F)** J774A.1 macrophages were incubated with MEL for 0.5 h before LPS stimulation for an additional 6 h. **(A)** The levels of proIL-1β in the cell lysates were analyzed by western blot. **(B)** The column diagram represents the fold change of proIL-1β in **(A)** compared with the control group normalized to actin analyzed by ImageJ. **(C)** The levels of NLRP3 in the cell lysates were analyzed by western blot. **(D)** The column diagram represents the fold change of NLRP3 in **(C)** compared with the control group normalized to actin analyzed by ImageJ. The levels of IL-6 **(E)** and TNF-α **(F)** in the supernatants were analyzed by ELISA. The western blot images are representative of three different experiments. The ELISA data are expressed as the mean ± SD of three separate experiments. $^{*}p < 0.05$ and $^{***}p < 0.001$ compared to the LPS group.

IL-6 (Figure 3E) but not TNF-α (Figure 3F) in LPS-activated macrophages. These results indicate that MLE inhibited the NLRP3 inflammasome not through reducing the priming signals induced by LPS.

Makauy leaf ethanol extract inhibited NLRP3 inflammasome activation signals by reducing mitochondrial damage

NLRP3 activator stimulation leads to the release of reactive oxygen species (ROS) from mitochondria and is an important step for downstream caspase-1 activation. We found that MLE reduced mitochondrial ROS generation in ATP-stimulated macrophages, as analyzed by staining for the mitochondrial ROS indicator MitoSOX (Figures 4A,B). Mitochondrial ROS cause mitochondrial membrane damage, which induces mitochondrial DNA release into the cytosol. The released mitochondrial DNA binds to NLRP3 and activates caspase-1 (25). We demonstrated that MLE reduced mitochondrial membrane integrity loss in ATP-stimulated macrophages, as analyzed by the mitochondrial membrane potential indicator MitoTracker Deep Red and Green staining (Figures 4C,D). In addition, we found that the translocation of mtDNA into the cytosol was reduced by MLE (Figure 4E). These results indicated that MLE inhibits the NLRP3 inflammasome partially by preventing mitochondrial damage.

Makauy leaf ethanol extract ameliorates dextran sodium sulfate-induced colitis in a mouse model

It has been demonstrated that the NLRP3 inflammasome plays a crucial role in the pathogenesis of IBD (26). To investigate the *in vivo* inflammatory bowel disease inhibition potential of MLE, we tested the effect of MLE on a mouse model of DSS-induced colitis, characterized by significant NLRP3 inflammasome activation in colon tissue. We found that DSS caused significant diarrhea and bloody stool, and these effects were significantly improved by oral administration of 20–80 mg/kg MLE or 80 mg/kg 5-aminosalicylic acid (5-ASA), a clinical drug (Figure 5A). As DSS caused diarrhea, it induced significant body weight loss in mice, and oral administration of

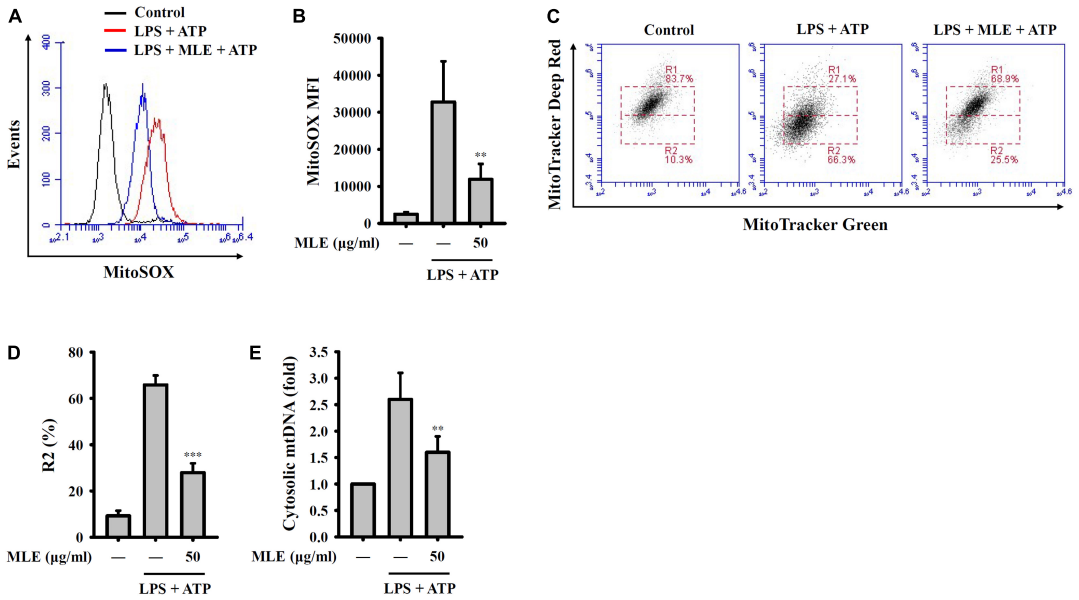

FIGURE 4
MLE inhibited activation signals of the NLRP3 inflammasome by reducing mitochondrial damage. **(A–E)** LPS-primed J774A.1 macrophages were incubated with MEL for 0.5 h before ATP stimulation for an additional 0.5 h. **(A)** Mitochondrial ROS production was analyzed by MitoSOX staining using flow cytometry. **(B)** The column diagram represents the mean fluorescence intensity of MitoSOX in **(A)**. **(C)** Mitochondrial membrane integrity was analyzed by MitoTracker Deep Red and Green staining using flow cytometry. **(D)** The column diagram represents the% of low MitoTracker Deep Red signal (R2) in **(C)**. **(E)** Mitochondrial DNA release into the cytosol was analyzed by the detection of cytochrome c oxidase I DNA in the cytosol. The data are expressed as the mean ± SD of three separate experiments. $^{**}p < 0.01$ and $^{***}p < 0.001$ compared to the LPS + ATP group.

MLE or 5-ASA attenuated the loss of body weight (Figure 5B). DSS also caused significant colonic shortening in mice, and MLE or 5-ASA significantly attenuated colonic shortening (Figures 5C,D). MLE improved the colonic damage analyzed by H&E staining (Figure 5E). In addition, DSS induced significant splenomegaly, indicating the elevated inflammatory status in mice, and MLE or 5-ASA significantly ameliorated the splenomegaly induced by DSS (Figures 5F,G). Furthermore, we found that DSS significantly increased the levels of IL-1β (Figure 5H) and IL-6 (Figure 5I) in colon tissue, and these effects were significantly reduced by MLE or 5-ASA, indicating that MLE ameliorates DSS-induced colonic inflammation.

Preliminary safety evaluation of mice exposed to makauy leaf ethanol extract

Oral administration of 1 or 2 g/kg MLE daily for 7 days did not cause body weight loss in mice, and no side effects were observed until 21 days after the first administration (Figures 6A,B). The organs were collected from the MLE-fed mice at 21 days after the first administration, and no pathological changes in the heart, liver, spleen, lung, or kidney were observed (Figure 6C). These results indicate that MLE was found to be safe for mice under this condition.

Identification of compounds from makauy leaf ethanol extract using gas chromatography-mass spectrometry Analysis

To identify the compounds that can be used for quality control, GC-MS analysis of MLE was performed (Figure 7), and the identified compounds in the MLE were summarized in Table 1. The top 10 major compounds of MLE were α-Terpinyl acetate (27.2%), 1,8-Cineole (17.7%), α-Terpineol (7.4%), Ethyl hexadecanoate (6.4%), Phytol (6.1%), Limonene (5.6%), β-Caryophyllene (4.9%), Ethyl 9,12,15-octadecatrienoate (4.2%), Linoleic acid ethyl ester (3.0%), and Terpinen-4-ol acetate (2.5%).

Discussion

Traditionally, the bacterial endotoxin LPS has been used as the stimulus to induce an inflammatory response in an inflammatory model system. Although this model is a commonly used anti-inflammatory drug screening platform, the disadvantage is that the inflammatory response induced by LPS cannot represent a specific disease condition. The NLRP3 inflammasome has become an important research topic, as

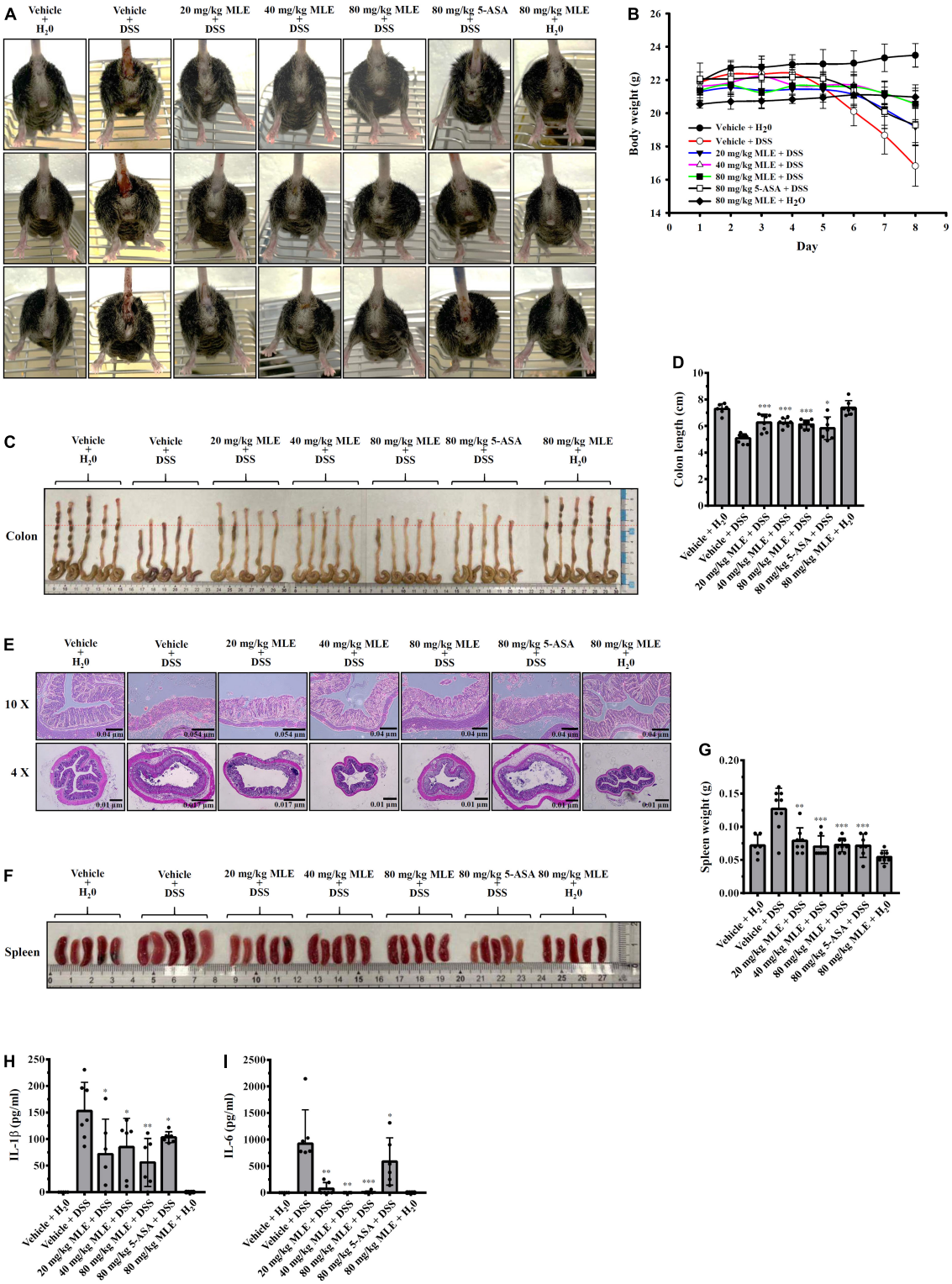

FIGURE 5
MLE ameliorates DSS-induced colitis in a mouse model. **(A)** Images of representative diarrhea and bloody stool from mice. **(B)** Effect of MLE on body weight loss. **(C)** Effect of MLE on colonic shortening. **(D)** The column diagram represents the colon length in **(C)**. **(E)** Effect of MLE on colonic damage analyzed by H&E staining. **(F)** Effect of MLE on splenomegaly. **(G)** The column diagram represents the spleen weight in **(F)**. **(H)** Effect of MLE on the levels of IL-1β in colon tissue. **(I)** Effect of MLE on the levels of IL-6 in colon tissue. The data are expressed as the mean ± SD. *, **, and *** indicate a significant difference at the level of $p < 0.05$, $p < 0.01$, and $p < 0.001$, respectively, compared to vehicle + DSS mice.

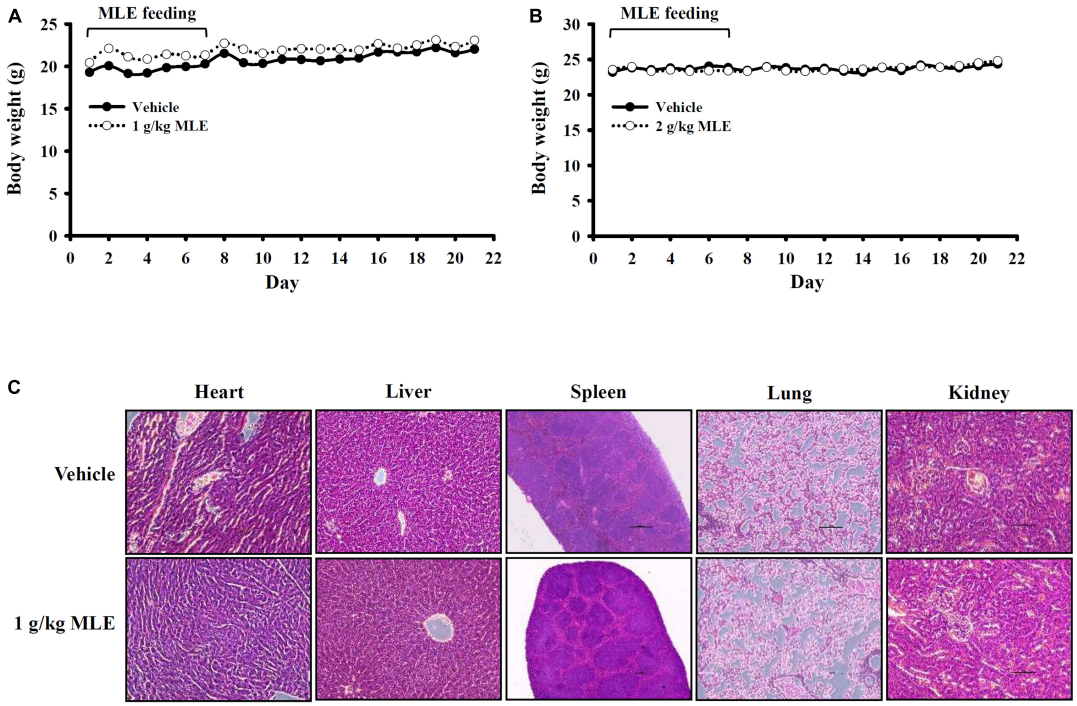

FIGURE 6
Preliminary safety evaluation of mice exposed to MLE. **(A,B)** Effect of MLE on body weight. **(C)** H&E staining of tissue sections from vehicle- or MLE-fed mice.

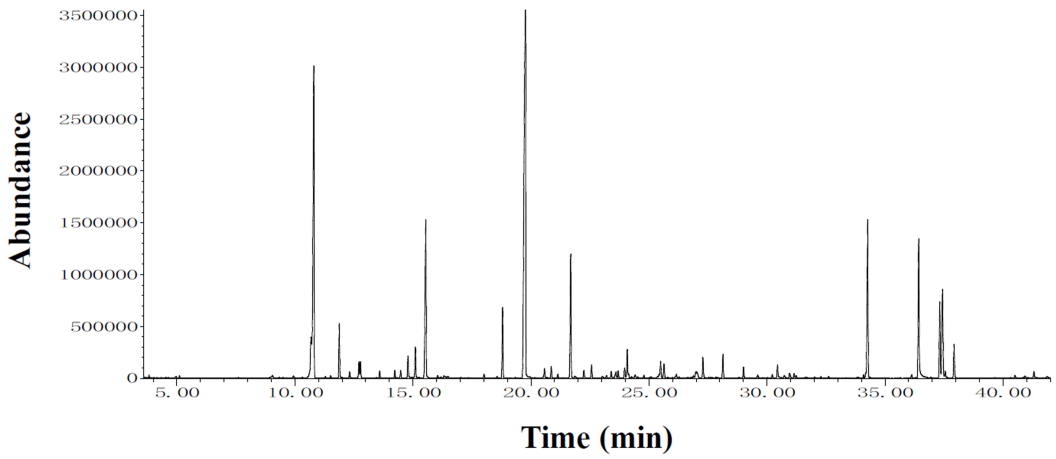

FIGURE 7
Chromatograms obtained from GC-MS screening of MLE.

it can be activated by particular medically relevant stimuli and is a promising target for drug discovery (4, 5). MCC950, a potent and selective small-molecule inhibitor of NLRP3, inhibited canonical and non-canonical NLRP3 activation and improved various NLRP3-associated diseases in animal models of inflammatory bowel disease, neurodegenerative diseases, cardiovascular diseases, rheumatoid arthritis, lung inflammation, asthma, stroke, liver disease, and many other inflammatory conditions (27, 28). However, the human trials of MCC950 were stopped as the blood levels of a liver enzyme were raised. Although no NLRP3 inflammasome inhibitor has been approved for marketing, the development of NLRP3 inflammasome inhibitors with few adverse drug reactions has attracted the interest of the pharmaceutical industry and academic researchers (4, 5).

Natural products are important sources for drug development because they have a wide range of diverse multidimensional chemical structures (29, 30). We

identified several natural products that inhibited the NLRP3 inflammasome *in vitro* and ameliorated NLRP3-associated disorders *in vivo*. We demonstrated that citral (3,7-dimethyl-2,6-octadienal) isolated from *L. cubeba* inhibited the production of nitric oxide (NO), TNF-α, and IL-6 by reducing NF-κB activation and ROS production in LPS-activated RAW264.7 macrophages and improved focal segmental glomerulosclerosis in mice (11). We further demonstrated that citral inhibited ATP-induced caspase-1 activation and IL-1β production in LPS-primed J774A.1 macrophages and alleviated lupus nephritis in mice (12). Autophagy is an important self-protective mechanism that can inhibit activation of the NLRP3 inflammasome by preserving mitochondrial integrity (31). We found that honokiol (32) from *Magnolia officinalis* and resveratrol in the skin of red grapes (19) inhibited the NLRP3 inflammasome in macrophages and alleviated renal inflammation in mice through autophagy induction. In this study, we demonstrated that MLE reduced mitochondrial ROS production and mitochondrial membrane integrity loss and inhibited the NLRP3 inflammasome in macrophages; however, the effect of MLE on autophagy needs further investigation.

TABLE 1 Chemical compositions of MLE analyzed by GC-MS.

Compound I.D.	LRI_{Exp} [a]	LRI_{Lit} [b]	Concentration (%)	Identification[c]
Sabinene	974	975	0.2	MS, LRI, CO-ST
p-Mentha-1(7),8-diene	1,002	1,004	0.1	MS, LRI
Limonene	1,029	1,029	5.6	MS, LRI, CO-ST
1,8-Cineole	1,033	1,031	17.7	MS, LRI, CO-ST
γ-Terpinene	1,057	1,059	0.1	MS, LRI, CO-ST
cis-Sabinene hydrate	1,069	1,070	1.8	MS, LRI
Terpinolene	1,086	1,088	0.2	MS, LRI, CO-ST
Linalool	1,094	1,096	0.6	MS, LRI, CO-ST
trans-Sabinene hydrate	1,096	1,098	0.6	MS, LRI
trans-p-Mentha-2,8-dien-1-ol	1,125	1,122	0.2	MS, LRI
Citronellal	1,150	1,153	0.3	MS, LRI, CO-ST
δ-Terpineol	1,166	1,166	0.9	MS, LRI
Terpinen-4-ol	1,176	1,177	1.2	MS, LRI, CO-ST
α-Terpineol	1,190	1,189	7.4	MS, LRI, CO-ST
Bornyl acetate	1,287	1,288	0.1	MS, LRI, CO-ST
Terpinen-4-ol acetate	1,301	1,299	2.5	MS, LRI
α-Terpinyl acetate	1,346	1,349	27.2	MS, LRI, CO-ST
β-Elemene	1,388	1,390	0.4	MS, LRI, CO-ST
β-Caryophyllene	1,416	1,419	4.9	MS, LRI, CO-ST
(*e*)-Isoeugenol	1,450	1,451	0.3	MS, LRI
α-Humulene	1,451	1,454	0.5	MS, LRI, CO-ST
cis-Muurola-4(14),5-diene	1,469	1,466	0.1	MS, LRI
γ-Muurolene	1,476	1,479	0.1	MS, LRI
β-Selinene	1,489	1,490	0.3	MS, LRI
α-Muurolene	1,499	1,500	0.4	MS, LRI, CO-ST
(e,e)-α-Farnesene	1,502	1,505	0.3	MS, LRI
γ-Cadinene	1,510	1,513	0.4	MS, LRI
δ-Cadinene	1,521	1,523	1.2	MS, LRI
Caryophyllene oxide	1,580	1,583	0.6	MS, LRI, CO-ST
t-Cadinol	1,638	1,640	0.2	MS, LRI, CO-ST
t-Muurolol	1,641	1,642	0.6	MS, LRI, CO-ST
α-Cadinol	1,652	1,654	0.8	MS, LRI, CO-ST
Ethyl hexadecanoate	1,990	1,993	6.4	MS, LRI
Ethyl heptadecanoate	2,086	2,089	0.1	MS, LRI
Phytol	2,097	2,110	6.1	MS, LRI, CO-ST
Linoleic acid ethyl ester	2,161	2,162	3.0	MS, LRI
Ethyl 9,12,15-octadecatrienoate	2,170	2,169	4.2	MS, LRI
Ethyl Oleate	2,173	2,174	0.3	MS, LRI
Octadecanoic acid, ethyl ester	2,192	2,193	1.3	MS, LRI
Eicosanoic acid, ethyl ester	2,392	2,395	0.3	MS, LRI

[a]LRI_{Exp} = Determined LRI relative to n-alkanes (C_8-C_{30}) on DB-5 capillary column. [b]LRI_{Lit} = LRI on DB-5 capillary column from reference 14. [c]Identification by MS = NIST 17 and Wiley 11 libraries spectra, and the literatures; LRI was same as references 14–16. CO-ST, co-injection and comparison with the l LRI and mass spectra of standards.

Although most of the studies focus on the fruits of *L. cubeba*, the roots, bark, wood, twigs, and leaves of *L. cubeba* also exert biological functions. *L. cubeba* root ethanol extract improved adjuvant arthritis in rats by reducing the levels of proinflammatory mediators and increasing the anti-inflammatory cytokine IL-10 in serum (33). The same group further identified 9,9′-O-di-(E)-fer-uloyl-meso-5,5′-dimethoxysecoisolariciresin, a pure compound isolated from *L. cubeba* root ethanol extract, that inhibited LPS-induced NO and TNF-α expression in macrophages (34) and reduced RANKL-induced osteoclast differentiation in mouse bone marrow macrophages (35). Boldine and rozuline isolated from *L. cubeba* root ethanol extract inhibited xylene-induced ear edema in mice and carrageenan-induced paw edema in rats (36). Furthermore, *L. cubeba* bark methanol extract inhibited NO and PGE_2 production in LPS-activated macrophages (37). Litebamine, a phenanthrene alkaloid from the wood of *L. cubeba*, exerts potential cardiovascular protective activity, as it inhibits rat smooth muscle cell adhesion and migration on collagen (38). A terpenoid ester glycoside isolated from *L. cubeba* twig ethanol extract induced cell death in human non-small-cell lung carcinoma A549 cells and human ileocecal adenocarcinoma HCT-8 cells (39). 1,8-Cineole- or linalool-containing *L. cubeba* leaf essential oil exerted antibacterial activity against *Escherichia coli* (40). In this study, we are the first to show that the ethanolic extract of *L. cubeba* leaves exerts NLRP3 inflammasome inhibitory activity in macrophages and ameliorates DSS-induced colitis in mice.

Although *L. cubeba* fruit and its essential oil have been used as seasonings for a long time, toxicity should be considered. The studies performed in Institute of Cancer Research mice and Sprague-Dawley rats showed that *L. cubeba* fruit essential oil is slightly toxic, as the oral 50% lethal dose is approximately 4,000 mg/kg of body weight. Importantly, no genetic toxicity was observed using standard genetic toxicity testing (41). *L. cubeba* leaves have also been used as seasonings or tea

for many years; however, there is no report evaluating the toxicity of *L. cubeba* leaves. Here, we provide preliminary results showing that there were no side effects observed in mice orally administered *L. cubeba* leaf ethanol extract at 1 or 2 g/kg body weight once daily for 7 continuous days. However, the detailed toxicity test, including the genetic toxicity of *L. cubeba* leaves, should be investigated before application in the food industry. It has been reported that α-terpinyl acetate, the major compound of MLE, reduced TNF-α and IL-6 in LPS-activated macrophages (42). In addition, 1,8-cineole, another major compound of MLE inhibited the NLRP3 inflammasome activation in macrophages (43). The limitation of this study is that although some compounds were identified, no active fractions or compounds with NLRP3 inflammasome inhibitory activity were identified. Activity-guided fractionation of MLE should be performed to isolate the active components in *L. cubeba* leaves in the future.

Data availability statement

The original contributions presented in this study are included in the article/supplementary material, further inquiries can be directed to the corresponding author.

Ethics statement

The animal study was reviewed and approved by the Institutional Animal Care and Use Committee of the National Ilan University.

Author contributions

C-FW was the guarantor of the article. W-TW and C-FW conceived and designed the study. W-TW, C-HW, L-HL, D-YH, and H-WC performed the experiments and analyzed the data. H-TH, C-LH, and OC assisted with some experiments. S-MC, S-PY, and K-FH contributed to critical revision of the manuscript. W-TW, C-HW, and C-FW wrote and finished the manuscript. All authors participated in revising the manuscript and approved the final version.

Funding

This work was supported by the Ministry of Science and Technology of Taiwan (MOST 111-2628-B-197-001-MY3, MOST 110-2923-B-197-001-MY3, MOST 111-2811-B-197-001, and MOST 111-2320-B-532-002) and Tri-Service General Hospital, National Defense Medical Center, Taipei, Taiwan (TSGH-D-109039 and TSGH-D-111048).

Conflict of interest

The authors declare that the research was conducted in the absence of any commercial or financial relationships that could be construed as a potential conflict of interest.

Publisher's note

References

1. Moretti J, Blander JM. Increasing complexity of NLRP3 inflammasome regulation. *J Leukoc Biol.* (2021) 109:561–71. doi: 10.1002/JLB.3MR0520-104RR

2. Sharma BR, Kanneganti TD. NLRP3 inflammasome in cancer and metabolic diseases. *Nat Immunol.* (2021) 22:550–9. doi: 10.1038/s41590-021-00886-5

3. Liao PC, Chao LK, Chou JC, Dong WC, Lin CN, Lin CY, et al. Lipopolysaccharide/adenosine triphosphate-mediated signal transduction in the regulation of NLRP3 protein expression and caspase-1-mediated interleukin-1β secretion. *Inflamm Res.* (2013) 62:89–96. doi: 10.1007/s00011-012-0555-2

4. Schwaid AG, Spencer KB. Strategies for targeting the NLRP3 inflammasome in the clinical and preclinical space. *J Med Chem.* (2021) 64:101–22. doi: 10.1021/acs.jmedchem.0c01307

5. Su M, Wang W, Liu F, Li H. Recent progress on the discovery of NLRP3 inhibitors and their therapeutic potential. *Curr Med Chem.* (2021) 28:569–82. doi: 10.2174/0929867327666200123093544

6. Yang Y, Chen Y, Zhang G, Sun J, Guo L, Jiang M, et al. Transcriptomic analysis of *Staphylococcus aureus* under the stress condition caused by *Litsea cubeba* L. Essential oil via RNA sequencing. *Front Microbiol.* (2020) 11:1693. doi: 10.3389/fmicb.2020.01693

7. Yang Y, Hao K, Jiang M, Memon FU, Guo L, Zhang G, et al. Transcriptomic analysis of drug-resistance *Acinetobacter baumannii* under the stress condition caused by *Litsea cubeba* L. Essential oil via RNA sequencing. *Genes.* (2021) 12:1003. doi: 10.3390/genes12071003

8. Chen HC, Chang WT, Hseu YC, Chen HY, Chuang CH, Lin CC, et al. Immunosuppressive effect of *Litsea cubeba* L. Essential oil on dendritic cell and contact hypersensitivity responses. *Int J Mol Sci.* (2016) 17:1319. doi: 10.3390/ijms17081319

9. Trisonthi P, Sato A, Nishiwaki H, Tamura H. A new diterpene from Litsea cubeba fruits: structure elucidation and capability to induce apoptosis in HeLa cells. *Molecules.* (2014) 19:6838–50. doi: 10.3390/molecules19056838

10. Zhang HJ, Zheng LH, Zhao K, Chen Y, Yi Z. Insecticidal activities of constituents of *Litsea cubeba* fruit extracts effective against the maize weevil (Coleoptera: Curculionidae). *J Insect Sci.* (2017) 17:103. doi: 10.1093/jisesa/iex079

11. Yang SM, Hua KF, Lin YC, Chen A, Chang JM, Kuoping Chao L, et al. Citral is renoprotective for focal segmental glomerulosclerosis by inhibiting oxidative stress and apoptosis and activating Nrf2 pathway in mice. *PLoS One.* (2013) 8:e74871. doi: 10.1371/journal.pone.0074871

12. Ka SM, Lin JC, Lin TJ, Liu FC, Chao LK, Ho CL, et al. Citral alleviates an accelerated and severe lupus nephritis model by inhibiting the activation signal of NLRP3 inflammasome and enhancing Nrf2 activation. *Arthritis Res Ther.* (2015) 17:331. doi: 10.1186/s13075-015-0844-6

13. Ho CL, Jie-Pinge O, Liu YC, Hung CP, Tsai MC, Liao PC, et al. Compositions and in vitro anticancer activities of the leaf and fruit oils of *Litsea cubeba* from Taiwan. *Nat Prod Commun.* (2010) 5:617–20.

14. Adams RP. *Identification of Essential Oil Components by Gas Chromatography/Mass Spectrometry*. 4th ed. Carol Stream, IL: Allured Publishing (2007).

15. Van den Dool H, Kratz PD. A generalization of the retention index system including linear temperature programmed gas liquid partition chromatography. *J Chromatogr A.* (1963) 11:463–71. doi: 10.1016/s0021-9673(01)80947-x

16. NIST. *NIST Chemistry WebBook: NIST Standard Reference Database Number 69*. Gaithersburg, ML: NIST (2022). Available online at: http://webbook.nist.gov/chemistry/

17. Chernikov OV, Chiu HW, Li LH, Kokoulin MS, Molchanova VI, Hsu HT, et al. Immunomodulatory properties of polysaccharides from the coral pseudopterogorgia americana in macrophages. *Cells.* (2021) 10:3531. doi: 10.3390/cells10123531

18. Zhai K, Duan H, Wang W, Zhao S, Khan GJ, Wang M, et al. Ginsenoside Rg1 ameliorates blood-brain barrier disruption and traumatic brain injury via attenuating macrophages derived exosomes miR-21 release. *Acta Pharm Sin B.* (2021) 11:3493–507. doi: 10.1016/j.apsb.2021.03.032

19. Chang YP, Ka SM, Hsu WH, Chen A, Chao LK, Lin CC, et al. Resveratrol inhibits NLRP3 inflammasome activation by preserving mitochondrial integrity and augmenting autophagy. *J Cell Physiol.* (2015) 230:1567–79. doi: 10.1002/jcp.24903

20. Zhai KF, Duan H, Cui CY, Cao YY, Si JL, Yang HJ, et al. Liquiritin from glycyrrhiza uralensis attenuating rheumatoid arthritis via reducing inflammation, suppressing angiogenesis, and inhibiting MAPK signaling pathway. *J Agric Food Chem.* (2019) 67:2856–64. doi: 10.1021/acs.jafc.9b00185

21. Bergsbaken T, Fink SL, Cookson BT. Pyroptosis: host cell death and inflammation. *Nat Rev Microbiol.* (2009) 7:99–109. doi: 10.1038/nrmicro2070

22. He WT, Wan H, Hu L, Chen P, Wang X, Huang Z, et al. Gasdermin D is an executor of pyroptosis and required for interleukin-1β secretion. *Cell Res.* (2015) 25:1285–98. doi: 10.1038/cr.2015.139

23. Shi J, Zhao Y, Wang K, Shi X, Wang Y, Huang H, et al. Cleavage of GSDMD by inflammatory caspases determines pyroptotic cell death. *Nature.* (2015) 526:660–5. doi: 10.1038/nature15514

24. Baroja-Mazo A, Martín-Sánchez F, Gomez AI, Martínez CM, Amores-Iniesta J, Compan V, et al. The NLRP3 inflammasome is released as a particulate danger signal that amplifies the inflammatory response. *Nat Immunol.* (2014) 15:738–48. doi: 10.1038/ni.2919

25. Kepp O, Galluzzi L, Kroemer G. Mitochondrial control of the NLRP3 inflammasome. *Nat Immunol.* (2011) 12:199–200. doi: 10.1038/ni0311-199

26. Kanneganti TD. Inflammatory bowel disease and the NLRP3 inflammasome. *N Engl J Med.* (2017) 377:694–6. doi: 10.1056/NEJMcibr1706536

27. Coll RC, Robertson AA, Chae JJ, Higgins SC, Muñoz-Planillo R, Inserra MC, et al. A small-molecule inhibitor of the NLRP3 inflammasome for the treatment of inflammatory diseases. *Nat Med.* (2015) 21:248–55. doi: 10.1038/nm.3806

28. Corcoran SE, Halai R, Cooper MA. Pharmacological inhibition of the nod-like receptor family pyrin domain containing 3 inflammasome with MCC950. *Pharmacol Rev.* (2021) 73:968–1000. doi: 10.1124/pharmrev.120.000171

29. Duan H, Khan GJ, Shang LJ, Peng H, Hu WC, Zhang JY, et al. Computational pharmacology and bioinformatics to explore the potential mechanism of Schisandra against atherosclerosis. *Food Chem Toxicol.* (2021) 150:112058. doi: 10.1016/j.fct.2021.112058

30. Zhai KF, Zheng JR, Tang YM, Li F, Lv YN, Zhang YY, et al. The saponin D39 blocks dissociation of non-muscular myosin heavy chain IIA from TNF receptor 2, suppressing tissue factor expression and venous thrombosis. *Br J Pharmacol.* (2017) 174:2818–31. doi: 10.1111/bph.13885

31. Biasizzo M, Kopitar-Jerala N. Interplay between NLRP3 inflammasome and autophagy. *Front Immunol.* (2020) 11:591803. doi: 10.3389/fimmu.2020.591803

32. Yang SR, Hsu WH, Wu CY, Shang HS, Liu FC, Chen A, et al. Accelerated, severe lupus nephritis benefits from treatment with honokiol by immunoregulation and differentially regulating NF-kappaB/NLRP3 inflammasome and sirtuin 1/autophagy axis. *FASEB J.* (2020) 34:13284–99. doi: 10.1096/fj.202001326R

33. Lin B, Zhang H, Zhao XX, Rahman K, Wang Y, Ma XQ, et al. Inhibitory effects of the root extract of *Litsea cubeba* (lour.) pers. on adjuvant arthritis in rats. *J Ethnopharmacol.* (2013) 147:327–34. doi: 10.1016/j.jep.2013.03.011

34. Lin B, Sun LN, Xin HL, Nian H, Song HT, Jiang YP, et al. Anti-inflammatory constituents from the root of *Litsea cubeba* in LPS-induced RAW 264.7 macrophages. *Pharm Biol.* (2016) 54:1741–7. doi: 10.3109/13880209.2015.1126619

35. Yu L, Jia D, Feng K, Sun X, Xu W, Ding L, et al. A natural compound (LCA) isolated from *Litsea cubeba* inhibits RANKL-induced osteoclast differentiation by suppressing Akt and MAPK pathways in mouse bone marrow macrophages. *J Ethnopharmacol.* (2020) 257:112873. doi: 10.1016/j.jep.2020.112873

36. Yang X, Gao X, Cao Y, Guo Q, Li S, Zhu Z, et al. Anti-inflammatory effects of boldine and reticuline isolated from *Litsea cubeba* through JAK2/STAT3 and NF-kappaB signaling pathways. *Planta Med.* (2018) 84:20–5. doi: 10.1055/s-0043-113447

37. Choi EM, Hwang JK. Effects of methanolic extract and fractions from *Litsea cubeba* bark on the production of inflammatory mediators in RAW264.7 cells. *Fitoterapia.* (2004) 75:141–8. doi: 10.1016/j.fitote.2003.11.003

38. Huang CH, Huang WJ, Wang SJ, Wu PH, Wu WB. Litebamine, a phenanthrene alkaloid from the wood of *Litsea cubeba*, inhibits rat smooth muscle cell adhesion and migration on collagen. *Eur J Pharmacol.* (2008) 596:25–31. doi: 10.1016/j.ejphar.2008.08.013

39. Wang LY, Tian Y, Qu YH, Wu YZ, Li YC, Li R, et al. Two new terpenoid ester glycosides from the twigs of *Litsea cubeba*. *J Asian Nat Prod Res.* (2018) 20:1129–36. doi: 10.1080/10286020.2018.1526789

40. Nguyen HV, Meile JC, Lebrun M, Caruso D, Chu-Ky S, Sarter S. *Litsea cubeba* leaf essential oil from Vietnam: chemical diversity and its impacts on antibacterial activity. *Lett Appl Microbiol.* (2018) 66:207–14. doi: 10.1111/lam.12837

41. Luo M, Jiang LK, Zou GL. Acute and genetic toxicity of essential oil extracted from *Litsea cubeba* (Lour.) Pers. *J Food Prot.* (2005) 68:581–8. doi: 10.4315/0362-028x-68.3.581

42. Cárdenas Garza GR, Elizondo Luévano JH, Bazaldúa Rodríguez AF, Chávez Montes A, Pérez Hernández RA, Martínez Delgado AJ, et al. Benefits of cardamom (*Elettaria cardamomum* (L.) Maton) and turmeric (*Curcuma longa* L.) extracts for their applications as natural anti-inflammatory adjuvants. *Plants.* (2021) 10:1908. doi: 10.3390/plants10091908

43. Lee EH, Shin JH, Kim SS, Lee H, Yang SR, Seo SR. *Laurus nobilis* leaf extract controls inflammation by suppressing NLRP3 inflammasome activation. *J Cell Physiol.* (2019) 234:6854–64. doi: 10.1002/jcp.27434

Advantages of publishing in Frontiers

OPEN ACCESS
Articles are free to read for greatest visibility and readership

FAST PUBLICATION
Around 90 days from submission to decision

HIGH QUALITY PEER-REVIEW
Rigorous, collaborative, and constructive peer-review

TRANSPARENT PEER-REVIEW
Editors and reviewers acknowledged by name on published articles

Frontiers
Avenue du Tribunal-Fédéral 34
1005 Lausanne | Switzerland

Visit us: www.frontiersin.org
Contact us: frontiersin.org/about/contact

REPRODUCIBILITY OF RESEARCH
Support open data and methods to enhance research reproducibility

DIGITAL PUBLISHING
Articles designed for optimal readership across devices

FOLLOW US
@frontiersin

IMPACT METRICS
Advanced article metrics track visibility across digital media

EXTENSIVE PROMOTION
Marketing and promotion of impactful research

LOOP RESEARCH NETWORK
Our network increases your article's readership